GEOCHEMICAL CHARACTERIZATION OF CENTRAL AMERICAN SUBDUCTION ZONE SYSTEM: SLAB INPUT, OUTPUT FROM THE VOLCANOES, AND SLAB-MANTLE INTERACTIONS

by

LINA CLAUDIA PATINO

A Dissertation submitted to the

Graduate School - New Brunswick

Rutgers, The State University of New Jersey

in partial fulfillment of the requirements

for the degree of

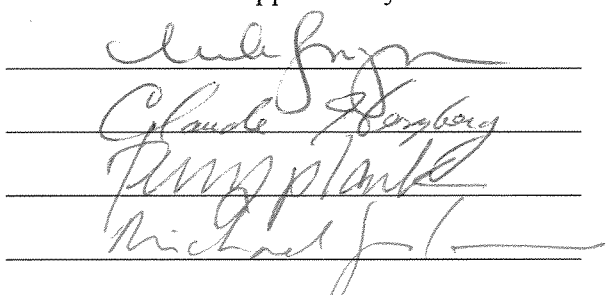
Doctor of Philosophy

Graduate Program in Geological Sciences

written under the direction of

Dr. Mark D. Feigenson

and approved by



New Brunswick, New Jersey

October, 1997

ABSTRACT OF THE DISSERTATION

Geochemical Characterization of Central American Subduction Zone System: Slab Input, Output from the Volcanoes, and Slab-Mantle Interactions

by LINA CLAUDIA PATINO

Dissertation Director:

Dr. Mark D. Feigenson

The geochemical characteristics of Central American lavas are controlled by the composition of the underlying mantle and of the Cocos Plate, and by the processes through which they interact. The DSDP 495 core, offshore Guatemala, reveals the geochemical variation of the subducting sediments with stratigraphy. The upper hemipelagic muds have higher U/La ratios than the carbonate oozes, but the carbonate sediments have higher Ba/Th ratios. However, there are ratios that remain almost constant through-out the sedimentation, such as Ba/La and U/Th.

The geochemical characteristics of lavas from Central America reveal both regional and local trends. The regional changes are produced by differences in the intensity of the flux from the subducting slab. The slab signal is strongest in Nicaragua and along the front. With increasing distance behind the volcanic front and north or south of Nicaragua, the slab signal decreases. The local trends depend on whether or not material derived from the hemipelagic sediments is involved in magmatism.

To better understand the interaction between the slab and the mantle two models are tested. First, partition coefficient data for mantle minerals are used to estimate the

composition of fluids and melts derived from the subducting slab. However, the compositions of the modeled fluids and melts are extremely sensitive to the inferred mineralogy, which is poorly constrained, and limited to the minerals for which partition coefficient data are available.

In the second model, element flux into the system is compared to element flux out of the system. K, B, Cs, and Rb are efficiently recycled from the subducted slab to the volcanoes. Sr, Ba, and U are returned to the surface with moderate efficiency, whereas all other elements may come entirely from the mantle wedge with no slab contribution required. The relative recycling order of incompatible elements suggests that a hydrous fluid is the process that transfers material from the slab to the mantle. Western Nicaragua has higher B flux than the rest of the arc, suggesting that in western Nicaragua the flux from the upper altered oceanic crust is greater there than in the other segments of the arc.

ACKNOWLEDGMENT

My education at Rutgers University has been enhanced by my interaction with a great number of people. First, my academic goals have been reached thanks to the guidance of the faculty from the Geological Sciences Department, especially my mentors Michael J. Carr and Mark D. Feigenson. Mike and Mark introduced me not only to analytical geochemistry, but also to research in general. To Mike and Mark, I will always be thankful for their teachings, and I look forward to the opportunity to collaborate with them in the future.

I would also like to thank Dr. Hewins and Dr. Herzberg for making my work as a Teaching Assistance a very memorable one. Through my interaction with the students from Mineralogy and Petrology, I have realized how much I enjoy teaching (so much that I decided to get my Ph.D.). Both Dr. Hewins and Dr. Herzberg always welcome my ideas and were willing to try new exercises in the labs.

The second group of people that I would like to acknowledge at the end of my studies at Rutgers is the staff and students from the International Faculty and Student Services, mainly the former director Gail Child-Szenes. Working with the international community of the university has allowed me to travel around the world without leaving New Brunswick. It has been a dream come true.

Lastly, I would like to thank my family, my parents and my sister, for all their support through out my studies. Without their understanding, encouragement, and support, I would have never gone as far as I have. Muchas gracias por su apoyo.

TABLE OF CONTENTS

ABSTRACT ii

ACKNOWLEDGEMENT iv

TABLE OF CONTENTS v

LIST OF TABLES viii

LIST OF FIGURES ix

I. INTRODUCTION 1

A. Arc Geochemistry 1

B. Special features of Central America 3

C. Synopsis of remaining chapters 5

II. METHODS 6

A. Sample preparation 6

B. ICP-MS parameters 8

III. INPUT: SIGNATURE OF THE SLAB AND MANTLE WEDGE 47

A. Introduction 47

B. Geochemical Stratigraphy of the subducting slab 47

1. Sediments from DSDP Site 495 47

a. Carbonate crash 48

b. Results 50

c. Biogenic component 52

d. Detrital component 54

e. Organic matter 56

2. Altered Oceanic crust (Site 504) 57

a. Volcanic rocks 59

b. Transition zone and Upper dikes 60

c. Lower dikes 61

d. Alteration 62
C. Constraints on the mantle wedge in Central America 63
D. Conclusions 65
IV. OUTPUT: INCOMPATIBLE ELEMENT VARIATIONS IN CENTRAL AMERICA 83
A. Introduction 83
B. Along arc variations 85
1. Regional variations 85
2. Local variations 88
C. Across arc variations 90
1. Similarities between volcanic front and back arc lavas 91
2. Differences between volcanic front and back arc lavas 92
D. Central America relative to other arcs 93
E. Conclusions 96
V. PROCESSES FOR SLAB INPUT 107
A. Introduction 107
B. Modeling hydrous fluids and melts 107
1. Hydrous fluids 107
2. Melts 109
3. Fluid-Melt models 111
a. Mineral variations 114
b. Fluids vs. melts 116
c. Different sections of the altered oceanic crust 117
C. Output/input flux calculations 120
1. Input flux 120
2. Output flux 121
3. Models 123

4. Residual oceanic crust 126

D. Conclusions 128

VI. REFERENCES 157

APPENDIX: ANALYSES OF BORON IN THE DCP-AES 166

A. Uses of boron in arc geochemistry 166

B. Sample preparation 167

1. Slurry 168

2. Acid digestion using mannitol 169

a. Sample preparation using mannitol 170

b. Cation exchange chromatography 172

c. DCP-AES settings 173

d. Results 174

VITA 182

LIST OF TABLES

Table 2-1	Standards for ICP-MS analyses	9
Table 2-2	Data set for selected lavas from Central America	14
Table 2-3	Geochemical composition of sediments from DSDP 495	37
Table 2-4	ICP-MS parameters	42
Table 2-5	Isotopes analyzed in the ICP-MS	43
Table 3-1	Compiled geochemical information for Site 504	67
Table 3-2	Composition of the subducting slab and mantle wedge	68
Table 5-1	Partition coefficients used in modeling fluids and melts from the subducting slab	131
Table 5-2	Mineral assemblages used in the modeling of fluids and melts from the subducting slab	132
Table 5-3	Results of the fluid and melt models	133
Table 5-4	Summary of fluid and melt models	135
Table 5-5	Percentages of the contributions from different units of the subducted slab	136
Table 5-6	Volume and arc length used in the mass flux models for different segments of Central American arc	137
Table 5-7	Results of the output/input modeling	138
Table A-1	Boron results using slurry solutions	176
Table A-2	Boron results using acid digestion and mannitol	177

LIST OF FIGURES

Figure 2-1	Comparison of results from DCP-AES and ICP-MS	44
Figure 3-1	Map of Central America and location of DSDP 495	69
Figure 3-2	Stratigraphic column of DSDP 495	70
Figure 3-3	Major element variations down core DSDP 495	71
Figure 3-4	Stratigraphic distribution of trace elements in DSDP 495	72
Figure 3-5	REE patterns for sediments from DSDP 495	73
Figure 3-6	Stratigraphic variations of cerium anomaly (a) and barium derived from non-biogenic sources (b)	74
Figure 3-7	Stratigraphic distributions of U/La (a) and Ba/Th (b) in DSDP 495	75
Figure 3-8	DSDP 495 sediments in La-Th-Sc space	76
Figure 3-9	Cerium anomaly vs. La_N	77
Figure 3-10	Stratigraphic distributions of Ba/La (a) and U/Th (b)	78
Figure 3-11	Location of Site 504	79
Figure 3-12	Summary information for Site 504	80
Figure 3-13	Variations in the composition of Site 504 down core	81
Figure 3-14	REE patterns for mean lavas from four segments in Central America	82
Figure 4-1	Map of Central American volcanic arc	98
Figure 4-2	U/Th vs. $^{143}Nd/^{144}Nd$	99
Figure 4-3	Regional geochemical variations in lavas from Central America	100
Figure 4-4	U/La vs. Cs/La	103
Figure 4-5	Local and regional variations in lavas from Central America	104
Figure 4-6	EMORB normalized diagrams for lavas from Central America	105
Figure 4-7	Ba/La vs. U/Th	106

Figure A-1	Elution curve for boron	178
Figure A-2	Background profile for boron in the DCP-AES	179
Figure A-3	Ba/La vs. B/La	180
Figure A-4	B/La vs. U/La	181

Figure 5-1	REE patterns for EMORB, Te-1 and Te-114	139
Figure 5-2	Models of fluids and melts from slab components with different mineral assemblages	140
Figure 5-3	Models for Te-114, carbonate rich end member, using different mineral assemblages	141
Figure 5-4	Models for Te-1, hemipelagic rich end member, using different mineral assemblages and a melt component	142
Figure 5-5	Differences in the compositions of fluids and melts from the altered oceanic crust and the hemipelagic sediments	143
Figure 5-6	Models for Te-1, hemipelagic rich end member, using different mineral assemblages and a fluid component	144
Figure 5-7	Fluids from different sections of the altered oceanic crust	145
Figure 5-8	Models for Te-114, carbonate rich end member, using different sections of the altered oceanic crust	146
Figure 5-9	Mixing lines between EMORB mantle and slab fluid and metasomatized mantle	147
Figure 5-10	Percentage input from the different units of the subducting slab	148
Figure 5-11	REE patterns for EMORB and mean lavas from different segments of Central American volcanic arc	149
Figure 5-12	EMORB normalized diagram for the mean lavas from different segments of Central American volcanic arc	150
Figure 5-13	Recycling efficiency plots for western Nicaragua (a) and eastern Nicaragua (b), El Salvador (c), and Guatemala (d)	151
Figure 5-14	Recycling efficiency plots for different segments of the Central American arc, using only the upper 500 m of the oceanic crust	153
Figure 5-15	Models of residual oceanic crust	155

I. Introduction

A. Arc Geochemistry

Subduction zones are one of the most active magmatic settings on earth. Along oceanic trenches old crust returns to the mantle, keeping balance with the new oceanic crust generated along mid-ocean ridges. The subducted lithosphere contributes material to the mantle, modifies the thermal structure of the mantle wedge in the subduction zone region and induces melting of the mantle (Peacock, 1991).

As the subducting slab enters the trench, material from the upper part of the oceanic crust may be scraped off forming an accretionary prism. At relatively shallow depths at least in some convergent margins, the oceanic crust dewaters forming serpentine bodies in fore arc regions, as in the Marianas (Woodhead, 1989). As subduction proceeds, the slab responds to new pressure and temperature conditions with changing mineral assemblages. At a depth of ~ 100-110 km, the breakdown of hydrous phases releases enough fluids to induce melting of the mantle. Amphibole has been assumed to be the hydrous phase that breaks down (Tatsumi et al., 1986), but recent experimental data show that other hydrous phases are also stable at the depths and estimated temperatures in subduction zones (Domanik and Holloway, 1996). Water lowers the solidus of the mantle wedge, and allows melting to occur (Peacok, 1991). The slab is not the primary source of melts, but instead triggers melting in the mantle wedge (e.g. Arculus, 1994). Even though the subducting slab does not contribute a large mass to the melt, its contribution is enough to make the composition of arc lavas unique.

Only a very small percentage of the subducted oceanic crust is used in the generation of arc magmas. Most of the subducted crust sinks into the mantle. Therefore, the subduction process is a major modifier of the composition of the mantle. The subducting slab can recycle continentally derived terrigenous sediments, as well as mantle products and marine sediments. The introduction of these materials creates

heterogeneities in the mantle, that may be observed later in lavas erupted far away from subduction zones (Weaver, 1991).

Subduction zone magmatism may contribute to the growth of continental crust, by adding volcanics at the surface and by emplacing large plutonic bodies (Brown, 1982). These plutonic bodies are more commonly exposed in old subduction zones, whereas in young subduction zones volcanic rocks are more common.

The chemical characteristics of lavas associated with subduction zones are clearly different from the lavas from other tectonic settings. Magmatism in divergent margins and within plates occurs because of adiabatic decompression of the mantle. However, in convergent margins magmatism is triggered by the interaction of subducted material with the mantle wedge. This interaction also modifies the mantle chemically.

Rocks that result from subduction zone magmatism are enriched in large ion lithophile elements (LILE) relative to light rare earth elements (LREE) and high field strength elements (HFSE). In addition, arc lavas display different systematics for several isotopic systems, e.g. ^{10}Be, $^{87}Sr/^{86}Sr$, $\delta^{11}B$, lead isotopes, and the uranium disequilibrium series (e.g. Morris, 1991; Condomines and Sigmarsson, 1993; Ishikawa and Nakamura, 1994; Reagan et al., 1994). The small contribution from subducted slab material is what makes the geochemical features of the arc lavas so unique.

Currently, the contribution of slab material to the magmas generated in subduction zones is less of an issue (e.g. Plank and Langmuir, 1993) than in the past. The problem of slab input is moving from the arena of whether or not it is present, to attempts to determine the contribution from different components of the subducting slab (Gill et al., 1993). In addition, much effort is being directed toward understanding the process(es) that transfer material from the subducting slab to the mantle wedge. To distinguish the contribution from different components of the slab, isotope systematics and trace element ratios can be used. If there are good constraints on the composition of the igneous and

sedimentary components of the subducting oceanic crust and the mantle wedge, then determining the contribution from the different parts of the slab should be possible.

The processes that transfer material from the slab to the mantle wedge are still controversial. The possibilities include bulk addition of the subducted material or addition of products derived from the slab, hydrous fluid and/or a siliceous melt (e.g. Ellam and Hawkesworth, 1988; Moran et al., 1992; Plank, 1993). Studies of several isotope systems in arc lavas indicate that both processes, fluids and melts, are important in the generation of arc magmas. Reagan et al. (1994) and Condomines and Sigmarsson (1993) suggest that melts derived from the slab metasomatize the mantle in the early stages of subduction. Subsequently, fluids produced by the dehydration of hydrous minerals trigger the melting of the metasomatized mantle.

B. Special features of Central America

The Central American volcanic arc results from the subduction of the Cocos Plate underneath the Caribbean Plate. The arc extends from the border of Mexico and Guatemala to central Costa Rica, a distance of about 1100 km (Carr and Stoiber, 1990). Magmatism along the present volcanic front has occurred throughout the Quaternary (Carr and Stoiber, 1990). The volcanic front consists of lines of stratovolcanoes, in eight distinct segments (Carr and Stoiber, 1977).

As in most arcs, there are two regions of magmatism, the volcanic front and back arc volcanism. Back arc volcanic fields coincide with breaks between some of the linear volcanic front segments (Carr and Stoiber, 1977). In most cases back arc magmatism is closely associated with extensional features. In Honduras the classical change on magma composition, increasing alkalic content of the lavas and decreasing slab input, with increasing distance from the trench is seen (Patino et al., in press).

The continental crust of southern Central America is relatively young and thin, compared to the crust of other continental margins . This thin and young crust is not as radiogenic as older continental crust; thus, the effects of crustal assimilation do not cause

drastic changes in the isotopic characteristics of the magmas. This does not imply that the lavas from Central America do not interact with crustal material. Although lavas from Guatemala, where the crust is thickest (>40 km), are affected by crustal assimilation (Carr et al., 1990; Walker et al., 1995), lavas from the southeast of Guatemala, El Salvador, and Nicaragua do not show geochemical characteristics of assimilation. The crust in these regions is thinner than in Guatemala, roughly 32-38 km in El Salvador and 32 km in Nicaragua (Carr, 1984).

Another geophysical parameter that changes along the arc is the angle of the subducting slab underneath the volcanoes. Seismological data suggest that the dip of the Cocos Plate underneath Nicaragua reaches a much steeper angle (65°, Carr et al. 1990; or 84°, Protti et al., 1995) than is found underneath the other segments of the arc (55° in El Salvador and 40° in Guatemala; Carr et al., 1990). In some arcs the rate of subduction also varies substantially along the arc. However, in Central America the NUVEL-1 convergence rate varies from 7.1 cm/yr in Guatemala to 9.0 cm/yr in Costa Rica (DeMets et al., 1990).

Davies and Stevenson (1992) show that geophysical parameters like crustal thickness, angle of subduction, and convergence rate contribute to the thermal structure of the subduction zone, which is a major control on the generation of magmas (e.g. Woodhead and Johnson, 1993). Therefore, the generation of magmas along Central America occurs under different thermal structures because of the differences along the arc in crustal thickness, subduction rate and the dip of the slab. These differences are likely to affect the geochemical characteristics of the lavas.

Two DSDP legs drilled close to the Middle American Trench, legs 69 and 170, give direct information on the nature of the subducting Cocos Plate (Coulbourn et al., 1982; Morris, personal communication). This information makes the geochemical study of the subduction zone system in Central America more comprehensive. Both legs show the absence of an accretionary prism in front of the Caribbean Plate, implying that most of

the sedimentary sequence of the Cocos Plate is carried down the subduction zone and can potentially be involved in the generation of the magmas. Furthermore, the geochemical composition of the subducting slab is complemented with information from Site 504, also in the eastern Pacific. The data from this hole, the deepest yet drilled into the oceanic crust (~2000 m), describe the state of alteration of the subducting oceanic crust (Alt et al., 1996).

C. Synopsis of remaining chapters

Chapter 2 contains the data tables and describes the methods used to obtain the data. The input to the subduction zone system is considered in chapter 3. The first part of the chapter describes the geochemical composition of the subducting slab, the sediments from DSDP Site 495 and the altered oceanic crust from Site 504. The last section of chapter 3 discusses the constraints on the composition of the mantle wedge in Central America.

Chapter 4 outlines the geochemical characteristics of the lavas from Central America volcanic arc. The approach in this chapter is to discuss the geochemical variations along-arc, at the regional and local scales, and across-arc. In Chapter 5, I try two different methods to understand the interaction between the subducting oceanic crust and the mantle wedge. First, I use partition coefficient data to estimate the composition of fluids and/or melts derived from different units of the subducting slab. In the second case, simple mass fluxes into and out of the subduction zones system are calculated to determine the efficiency with which material is mobilized from the slab to the mantle wedge.

II. METHODS

A. Sample preparation

The major and minor elements of volcanics from Central America and sediments from DSDP 495 were analyzed by DCP-AES following Feigenson and Carr (1985). The samples were prepared by fluxing with $LiBO_2$.

Trace elements (Rb, Nb, Y, Cs, Pb, Th, and U) and rare earth elements (REE, for some samples) for the lavas and sediments were analyzed by inductively coupled plasma mass spectrometry, using a VG Plasma Quad II Plus ICP-MS. The sample digestion used in this study follows Albrecht et al. (1992), except that open beaker digestion was used rather than bomb digestion. One hundred milligrams (0.1 g) of sample powder were treated with several different acids and evaporated to dryness after each (HF, $HF+HClO_4+HNO_3$, $HClO_4$, $HClO_4$, 20% HNO_3, 20% HNO_3). The sample was then taken up in 2.5 ml of 20% nitric acid and diluted to 5 ml to make a stock solution. The sample solution was diluted by a factor of 1500 with 5% HNO_3 to be run an the VG Plasma Quad II Plus ICP-MS. Recently, an equally effective sample preparation was tested with success; this new technique saves time and reagents (Plank, personal communication). This preparation only uses HF and HNO_3 acids to dissolve the rock in a beaker that can be tightly capped.

The analyses in the ICP-MS were done following Cheatham et al. (1993). A blank solution was run once at the beginning of the data acquisition and a drift control solution was analyzed repeatedly, after every four solutions. In each run at least three USGS rock standards with a matrix similar to the samples were run. The samples were introduced to the instrument via an autosampler and a peristaltic pump, using the autosampler parameters: 60 seconds for uptake, 60 seconds for acquisition (two replicates), and 90 seconds for rinse with 5% HNO_3.

The concentrations of the trace elements were determined by external standard calibration using the Excel macro sheet of Cheatham et al. (1993). This spread sheet is set

up to correct curvilinear drift as a function of time and mass. The method of Cheatham et al. (1993) was preferred because of the mass dependent drift observed in the ICP-MS. Another commonly used calibration for ICP-MS analyses uses internal standards (Kenison et al., 1995, Longerich et al., 1990). However, when analyzing isotopes over a wide range of masses, several internal standards would have to be added to each sample. The addition of many internal standards increases the possibilities of error and contamination.

Table 2-1 lists the average concentration for the standards used during the course of this study as well as the reference values for the elements analyzed. For BHVO-1, the Cs and Th reference values are from Cheatham et al. (1993) and not from Govindaraju (1994), as the other values are. The two sets of reference values are used because for some elements the BHVO-1 powders apparently are not homogenous. The concentrations of the standards obtained in this study match very well the reference values, with errors of $\leq 5\%$. When analyzing sediments from DSDP 495, USGS sediment standards SGR1 and Sco1 were used. Table 2-1 also has the new element concentrations for IZ, an in-house standard that was usually used as the drift correcting solution.

Table 2-2 contains a complete chemical data set for the lavas from Central America that were analyzed for this project and table 2-3 has the geochemical composition of the sediments from DSDP 495. The major and minor elements of most samples were determined prior to this study using a DCP-AES (direct current plasma atomic emission spectrometer) following Feigenson and Carr (1985). The REEs of several samples were also analyzed by DCP-AES. The sediments from DSDP 495 have very high Ba content, up to 7000 ppm. This high concentration of Ba increased the BaO (masses 151 and 153) formed in the ICP-MS and caused major interferences with Eu, making it impossible to measure. Figure 2-1 compares the results of DCP-AES and ICP-MS analyses for Rb, Y and Nb. In general, there is good agreement between the results from the two instruments. However, the ICP-MS results are consistently higher for most samples. The concentrations determined using the ICP-MS are preferred, and listed in table 2-2, over

those from the DCP-AES because the latter instrument has higher detection limits than the ICP-MS. High quality Nb data were especially difficult to obtain by DCP-AES (Bennet, 1990).

B. ICP-MS parameters

The operational settings for the ICP-MS are listed in table 2-4, and the isotopes that were analyzed are given in Table 2-5. Prior to any run in the instrument, the sampler and skimmer cones were cleaned with a stainless steel cleaner and polishing powder. The calibration procedure started 30 minutes after the instrument was turned on. The mass calibration was done with a solution that had 100 ppb of Co, Y, In, La, Yb, Bi, Th. After a satisfactory mass calibration was obtained, the lens settings were optimized on ^{139}La or ^{115}In using a solution that had the same matrix as the samples to be run, that is, a rock solution with the same dilution factor. The instrument response varied from 2-5 x 10^5 counts per second for a concentration of 50 ppb La or In. The instrument was run in a peak hopping mode with 5 points per peak and 6 DAC steps (digital to analog converter). The shapes of the peaks were examined on screen for symmetry, and if needed, new mass calibrations were done until the shape was satisfactory. The signals for Rb and U isotopes in the drift correcting solution were used to monitor drift. In most cases there was a drift of no more than 10% of the starting signal during the two hour runs. However, the drift pattern as documented by Cheatham et al. (1993) is complex and mass dependent. If the drift went higher than 20%, the samples were run again.

Table 2-1

	BHVO				
	Ref	Mean	%error*	Stdev	n
Rb	11.000	10.225	-7.05	0.91	14
Y	27.600	29.329	6.27	1.72	16
Nb	19.000	19.205	1.08	1.01	13
Cs[1]	.097	.097	-0.42	0.01	26
La	15.800	15.764	-0.23	2.43	12
Ce	39.000	38.887	-0.29	2.34	12
Nd	25.200	25.621	1.67	0.61	11
Sm	6.200	6.213	0.21	0.15	11
Eu	2.060	2.048	-0.61	0.04	11
Gd	6.400	6.348	-0.81	0.22	11
Dy	5.200	5.241	0.80	0.30	9
Er	2.400	2.460	2.51	0.16	6
Yb	2.020	2.023	0.13	0.11	9
Pb	2.600	2.735	5.20	0.39	15
Th[1]	1.249	1.243	-0.50	0.10	26
U	.420	.416	-1.00	0.05	26

* %error = (mean/ref -1)*100

[1] Ref values from Cheatham et al. (1993)

Ref values from Govindaraju (1994)

Table 2-1. Standards used during the analyses of the samples. For BHVO-1, Cs and Th reference values are from Cheatham et al. (1993). The other reference values for BHVO-1 and for the other standards are from Govindaraju (1994). The mean values, for BHVO-1, W2, W1, SGR1, and Sco1were obtained after calibrating with the reference values .

Table 2-1 cont.

	W2				
	Ref	Mean	%error*	Stdev	n
Rb	20.000	19.539	-2.31	2.73	15
Y	24.000	24.181	0.76	1.97	12
Nb	7.900	7.503	-5.02	1.14	14
Cs	.990	.911	-7.95	0.12	26
La	11.400	10.836	-4.94	0.17	4
Ce	24.000	23.274	-3.03	0.36	4
Nd	14.000	13.628	-2.66	0.03	2
Sm	3.250	3.266	0.50	0.00	2
Eu	1.100	1.091	-0.86	0.01	2
Gd	3.600	3.779	4.99	0.07	2
Dy	3.800	3.798	-0.06	0.03	2
Er	2.500	2.297	-8.11	0.01	2
Yb	2.050	2.059	0.43	0.06	2
Pb	9.300	9.033	-2.87	1.63	23
Th	2.200	2.230	1.35	0.35	26
U	.530	.514	-3.06	0.08	26

* %error = (mean/ref -1)*100

Ref values from Govindaraju

Table 2-1 cont.

	W1				
	Ref	Mean	%error*	Stdev	n
Rb	21.400	22.315	4.28	2.33	16
Y	26.000	24.105	-7.29	1.01	14
Nb	8.000	7.865	-1.68	0.39	13
Cs	.950	.994	4.64	0.08	27
La	10.900	10.899	-0.01	0.84	12
Ce	23.000	24.214	5.28	0.90	12
Nd	15.000	13.948	-7.02	0.72	11
Sm	3.500	3.438	-1.78	0.22	11
Eu	1.110	1.112	0.21	0.06	11
Gd	3.900	3.901	0.03	0.30	11
Dy	3.900	3.887	-0.32	0.31	10
Er	2.300	2.277	-0.99	0.16	6
Yb	2.120	2.111	-0.42	0.13	11
Pb	7.500	7.359	-1.88	0.95	27
Th	2.400	2.365	-1.47	0.09	27
U	.570	.569	-0.25	0.07	27

* %error = (mean/ref -1)*100

Ref values from Govindaraju

Table 2-1 cont.

	SGR1			Sco1		
	Ref	Mean	%error*	Ref	Mean	%error*
Rb	83.00	78.42	-5.51	112.00	114.73	2.44
Y	13.00	12.23	-5.94	26.00	25.10	-3.47
Nb	5.20	7.02	34.99	11.00	12.17	10.63
Cs	5.20	5.19	-0.20	7.80	7.83	0.45
La	20.30	19.12	-5.82	29.50	31.39	6.39
Ce	36.00	35.99	-0.03	62.00	62.08	0.13
Nd	15.50	14.60	-5.83	26.00	27.80	6.93
Sm	2.70	2.64	-2.28	5.30	5.49	3.56
Eu	0.56	0.53	-5.66	1.19	1.22	2.82
Gd	2.00	2.19	9.28	4.60	4.59	-0.30
Dy	1.90	1.98	4.40	4.20	4.19	-0.29
Er	1.11	1.18	6.38	2.50	2.49	-0.48
Yb	0.94	1.04	10.19	2.27	2.23	-1.67
Pb	38.00	39.89	4.98	31.00	30.00	-3.22
Th	4.78	4.64	-2.88	9.70	10.05	3.61
U	5.40	5.17	-4.23	3.00	3.05	1.59

* %error = (mean/ref -1)*100

Ref values from Govindaraju (1994)

Table 2-1 cont.

	IZ					
	Ref	Mean	%erro	Stdev	Median	n
Rb	49	49.05	0.10	3.75	47.98	6
Y	21.5	21.99	2.28	1.43	21.70	8
Nb	20.1	18.97	-5.64	1.31	19.38	5
Cs		0.79		0.06	0.80	9
Hf		4.33		0.21	4.29	7
Pb		6.88		0.57	6.86	8
Th		10.19		0.31	10.16	10
U		3.49		0.12	3.55	7

Table 2-2. Comprehensive geochemical data set for selected lavas from Central America.

Tabl 2-2

	TA-4C	SM126	AT-50	A-4	VF74-27	ACT-5	A-27-1	AC-30
SiO_2	58.31	51.4	51.69	56.19	48.67	53.11	52.39	55.05
TiO_2	0.76	0.95	1.03	0.77	1.09	1.16	0.97	0.86
Al_2O_3	18.9	18.69	19.37	19.54	17.97	20.34	18.91	19.21
Fe_2O_3	6.94	9.2	9.55	1.87	12.98	8.74	10.41	9.03
FeO				3.75				
MnO	0.154		0.13	0.134	0.18	0.15	0.17	0.16
MgO	2.08	5.2	4.56	1.69	6.27	2.59	3.73	2.22
CaO	7.34	9.35	9.28	7.41	9.39	8.52	8.84	8.23
Na_2O	3.12	3.6	3.24	4.42	2.68	4.23	3.48	3.84
K_2O	1.91	0.76	0.89	1.34	0.58	0.9	0.86	1.15
P_2O_5	0.23	0.22	0.22	0.267	0.14	0.17	0.2	0.21
B		12.8	15.2		12.9			
Be	1.27	0.86	0.91		0.6	0.78	0.87	0.94
Sc	12.86	24.96	23.25	14.2	25.83	29.5	22.13	16.76
V	125.1	217.7	226.8	133	279.3	294.8	207.6	187.7
Cr	2.33	26.89	101.1		18.51	21.7	6.81	1.01
Ni	2.77	19.01	40.97		39.95	12.91	14.43	7.81
Cu	12.18	63.69	66.88	71	71.65	75.12	57.36	54.89
Rb	46.85	13.22	20.27	27	8.52	14.53	15.86	21.56
Sr	568.9	630.5	589.5	605	518.2	572.8	544.7	595.5
Y	22.57	19.90	17.81	20	16.31	22.50	21.29	19.85
Zr	127.6	93.37	117.5	165	73.4	87.45	90.09	109.8
Nb	3.51	2.85	3.07		3.78	6.54	2.68	7.44
Ba	678.4	419.9	474.4	490	287.9	469.5	449.8	527.9
La	16.56	8.97	10.48	10.38	5.94	6.91	8.27	9.34
Ce	36.07	22.11	24.72	24.5	14.78	18.15	20.37	22.35
Nd	18.94	13.41	15.54	16	9.23	11.43	13.37	15.35
Sm	4.39	3.41	3.12	4.01	2.61	3.29	3.41	3.31
Eu	1.17	1.05	0.99	1.14	0.87	1.04	1.04	1.05
Gd	4	3.15	3.45	0	2.69	3.71	3.27	3.59
Dy	3.99	4.1	3.12	0	2.82	3.8	4.01	3.7
Er	2.18	1.87	1.49		1.64	2.08	1.73	1.72
Yb	1.77	1.47	1.4	2.12	1.32	1.94	1.63	1.6
Cs	1.825	0.697	0.75	1.08	0.377	0.38	0.644	0.899
Pb	12.28	4.53	7.77		3.21	5.05	5.53	5.23
Th	3.24	1.05	1.09	2.29	0.62	1.28	1.32	1.18
U	1.206	0.452	0.407	0.91	0.257	0.56	0.544	0.501
$^{87}Sr/^{86}Sr$	0.70457	0.70399	0.704		0.70388	0.70384		
$^{143}Nd/^{144}Nd$	0.51268	0.51282	0.51283		0.51291			
$^{206}Pb/^{204}Pb$	18.7004							
$^{207}Pb/^{204}Pb$	15.5929							
$^{208}Pb/^{204}Pb$	38.4725							
Latitude	15.13	14.76	14.58	14.58	14.48	14.50	14.50	14.50
Longitude	92.11	91.55	91.18	91.18	90.88	90.88	90.88	90.88
Distance	22.3	93.9	137.1	137.1	170.1	169.2	169.2	169.2

Table 2-2 cont.

	AG-8	E1	GUT102	GUM4	SALC1	SA22	SA204	IZ108
SiO_2	54.52	51.4	54.1	56.9	51.2	54.4	51.6	52.6
TiO_2	0.92	1.15	0.83	0.72	1.02	0.87	1.12	0.81
Al_2O_3	19.71	19.85	19	18.8	18.2	18.3	18.1	19.6
Fe_2O_3	8.32		2.47	3.8	3.1	1.36	3.74	1.13
FeO		8.9	5.51	3.2	7	7.26	6.05	7.16
MnO	0.15	0.16	0.18	0.12	0.18	0.16	0.17	0.15
MgO	2.85	3.5	4.82	2.58	4.67	3.75	4.23	4.31
CaO	8.24	9.89	9.42	7.7	9.4	8.5	8.93	9.49
Na_2O	3.76	3.57	3.47	3.9	3.38	3.51	3.38	3.54
K_2O	1.24	0.84	0.61	0.93	0.98	1.53	1.39	0.94
P_2O_5	0.23	0.27	0.15	0.14	0.2	0.27	0.25	0.14
B		8	0				15	18.8
Be	0.93	0.5	0.65	0.79	0.9	1.15	1.1	0.46
^{10}Be		3.5						6.9
Sc	21.64	24.55	29.15	20.22	31.46	23.14	32.61	25.16
V	199	266.5	234.6	191.4	308.5	225.4	321.5	276.3
Cr	13.73	22.69	35.19	4.52	17.45	7.62	2.55	11.74
Ni	14.98	16.09	21.08	9.17	20.21	12.65	9.1	15.74
Cu	56.6	83.38	58.15	55.86	132.6	129.8	147	114.4
Rb	27.12	13.53	8.02	18.49	19.01	44.06	32.8	21.21
Sr	555.3	622.9	435.9	443.4	460.5	502.2	440.8	491.4
Y	25.03	22.94	18.77	23.45	22.38	27.55	30.59	18.18
Zr	115.7	96.8	82.94	97.34	101.1	144.5	150.8	71.12
Nb	5.76	5.16	3.05	1.93	2.58	4.20	3.50	2.12
Ba	533.7	442.3	335.5	525.3	427.4	575.6	526.2	409.6
La	11.16	10.15	4.44	6.21	8.13	12.74	12.01	6.78
Ce	27.4	24.75	12.89	16.58	20.98	30.45	30.63	16.65
Nd	15.61	15.47	10.52	10.33	12.81	19.19	17.69	10.31
Sm	4.32	3.6	2.41	2.44	3.86	4.61	4.43	3.32
Eu	1.13	1.23	0.85	0.85	1.13	1.19	1.25	0.95
Gd	4.17	4.16	3	3.39	3.9	4.75	5.46	3.19
Dy	4.54	3.91	3.46	3.85	4.16	4.56	5.52	3.38
Er	2.12	2.17	1.8	1.91	2.15	2.5	3.13	1.94
Yb	1.93	1.77	1.44	1.71	1.84	1.91	2.7	1.6
Cs	0.925	0.582	0.271	0.832	0.72	2.202	0.67	1.047
Pb	5.48	5.51	2.90	4.12	3.00	6.70	5.29	5.75
Th	1.87	1.47	0.36	0.87	1.14	3.45	2.97	1.57
U	0.675	0.581	0.208	0.455	0.505	1.632	1.304	0.805
$^{87}Sr/^{86}Sr$	0.70386	0.70389	0.70365	0.70367			0.70369	0.70365
$^{143}Nd/^{144}Nd$		0.51293	0.51298	0.51304			0.51301	0.51301
$^{206}Pb/^{204}Pb$								18.629
$^{207}Pb/^{204}Pb$								15.516
$^{208}Pb/^{204}Pb$								38.269
Latitude	14.47	14.38	14.15	14.03	13.84	13.85	13.85	13.82
Longitude	90.75	90.60	90.42	90.10	89.80	89.63	89.63	89.63
Distance	183.2	201.6	231	266.5	304.5	319.4	319.4	321.2

Table 2-2 cont.

	B-6	B-21	SALC801	TE-4	US-2	SM-7	SM-8	CO-3
SiO_2	51.8	59	56.1	51.8	49.1	51.1	50.5	51.2
TiO_2	1	1.14	1.23	0.93	1.08	0.97	0.96	0.76
Al_2O_3	16.7	14.8	17.2	17.9	18.4	19.7	19.2	18.6
Fe_2O_3	4.57	2.59	3.79	5.34	3.39	2.45	3.38	2.95
FeO	5.75	7.09	5.99	4.6	7.9	6.57	6.62	7.25
MnO	0.19	0.22	0.22	0.14	0.19	0.18	0.17	0.15
MgO	4.41	2.05	2.64	4.53	5.1	3.38	4.78	5.53
CaO	9.47	5.54	7.47	9.32	10.41	10.31	10.97	10.35
Na_2O	2.98	4.42	3.77	3.14	2.89	2.93	2.89	2.53
K_2O	1.23	2.23	1.68	1.24	0.7	0.87	0.64	0.53
P_2O_5	0.18	0.4	0.31	0.2	0.17	0.23	0.17	0.16
B	12.7	37			9.8	20	11.8	7.7
Be	0.91	1.27	1.24	0.97	0.81	0.49	0.73	0.77
^{10}Be		14.4				7.5		
Sc	37.52	28.6	32.76	27.97	25.79	33.2	36.74	33.07
V	339.2	106.1	207	281.9	342.7	302.8	332.9	280.7
Cr	12.64	0.81	2.05	7.3	4.33	14.37	20.63	8.93
Ni	10.93	4.25	7.46	13.41	11.96	12.52	18.65	16.04
Cu	219.6	64.24	165.6	112.5	112.7	212.6	183	163.7
Rb	17.63	52.95	39.75	27.39	13.66	16.14	13.27	8.31
Sr	394.7	347.5	411.3	564	592.5	523.5	514.3	571.4
Y	31.09	59.114	42.25	26.07	26.41	23.86	23.35	14.91
Zr	123.3	212.3	171.7	97.41	69.25	81.69	68.74	53.03
Nb	2.85	8.94	5.19	3.10	2.57	2.79	2.20	1.58
Ba	546.3	931	765.8	567.5	378.8	526.3	410.7	497.5
La	8.79	16.87	12.95	8.51	5.52	8.61	6.05	6.41
Ce	22.52	42.24	32.87	21.33	15.57	20.93	14.85	14.96
Nd	14.23	27.98	21.77	14.52	9.56	14.6	10.06	10.04
Sm	4.14	7.13	6.1	3.58	2.95	3.98	2.86	2.73
Eu	1.07	1.84	1.61	1.11	1.02	1.15	0.96	0.85
Gd	4.65	8.33	6.89	4	3.6	4.55	3.43	2.79
Dy	4.99	8.37	7.1	4.17	3.47	4.66	3.4	2.76
Er	2.7	5.22	4.3	2.26	1.98	2.52	1.99	1.75
Yb	2.4	4.32	3.56	1.69	1.86	1.98	1.77	1.7
Cs	0.441	2.209	2.04	0.962	0.354	0.63	0.612	0.285
Pb	5.48	8.75	8.16	3.48	4.04	3.34	3.26	2.57
Th	1.65	3.27	2.62	1.25	0.75	0.71	0.73	1.20
U	0.8	1.58	1.28	0.69	0.464	0.438	0.492	0.695
$^{87}Sr/^{86}Sr$		0.70385			0.70387	0.70387		0.70396
$^{143}Nd/^{144}Nd$					0.51301			0.51302
$^{206}Pb/^{204}Pb$		18.594				18.587		
$^{207}Pb/^{204}Pb$		15.558				15.548		
$^{208}Pb/^{204}Pb$		38.297				38.268		
Latitude	13.73	13.73		13.50	13.42	13.43	13.43	13.28
Longitude	89.28	89.28		88.50	88.47	88.27	88.27	87.85
Distance	358	358	358	442.7	449.8	467.8	467.8	514.4

Table 2-2 cont.

	IC1	IM1	ZA1	ZA2	ZA3	ZA4B	ZA5	ZA6
SiO_2	50	54.6	63.03	53.23	52.26	52.1	58.43	49.71
TiO_2	0.78	0.75	0.62	0.87	0.97	0.95	1	0.78
Al_2O_3	18.9	18.1	16.5	18.23	18.88	19.12	17.08	22.54
Fe_2O_3	1.83	1.14						
FeO	7.76	6.69	5.51	8.51	9.18	9.02	7.6	7.26
MnO	0.21	0.13	0.15	0.17	0.17	0.17	0.2	0.14
MgO	4.9	4.11	1.13	5.44	4.18	4.97	2.37	2.85
CaO	10.61	8.62	4.2	8.88	8.95	9.22	6.32	11.1
Na_2O	2.36	3.34	5.13	3.34	3.28	3.16	4.16	2.88
K_2O	0.43	0.91	1.48	1.18	0.88	0.84	1.27	0.47
P_2O_5	0.13	0.2	0.35	0.32	0.31	0.29	0.33	0.17
Be	0.71	0.98						
Sc	31.74	25.92	9.88	25.78	25.83	24.81	21.64	22.1
V	293.2	201.8	21.92	214.4	224.7	257.5	108.6	192.6
Cr	14.42	25.25	5.57	104.8	25.21	39.77	8.25	11.08
Ni	15.8	18.72	3.67	78.94	22.69	54.64	6.26	5.52
Cu	146.9	61.57	10.91	101.2	104.4	340.5	48.88	89.33
Rb	10.63	16.11	22.3	18.7	14.1	9.16	17.4	5.9
Sr	562.1	489.3	501.9	514.5	552.4	547.2	528.3	701.5
Y	20.79	23.74	50.7	24.5	25.7	26.8	34.8	20.3
Zr	60.56	89.68	99.94	107.2	102.4	81.44	83.34	31.8
Nb	2.49	5.72	5.73	14.30	4.27	5.19	4.52	2.24
Ba	399.4	564.6	1011	624.9	535.7	682	700.5	336.3
La	5.37	9.04	17.784	14.344	11.525	11.499	11.336	5.866
Ce	12.22	19.53	31.468	28.78	25.656	24.749	25.415	11.635
Nd	9.05	11.81	26.236	17.185	17.226	16.812	18.814	9.709
Sm	2.53	3.18	6.079	3.815	4	3.897	4.708	2.49
Eu	0.88	0.98	2.047	1.319	1.367	1.382	1.691	1.051
Gd	3.06	3.63	6.719	4.093	4.165	4.241	5.105	2.896
Dy	2.73	3.68	6.448	3.607	3.696	3.663	4.842	2.661
Er	1.46	2.17	4.361	2.23	2.24	2.261	3.031	1.678
Yb	1.3	2.17	4.316	2.186	2.187	2.173	2.911	1.5
Cs	0.413	0.28	0.53	0.389	0.378	0.2	0.722	0.109
Pb	3.63	2.99	6.32	4.44	4.34	2.98	5.49	2.32
Th	0.61	0.93	1.41	1.52	0.70	0.71	1.07	0.32
U	0.48	0.56	1.051	0.533	0.407	0.34	0.689	0.2
$^{87}Sr/^{86}Sr$			0.70386	0.7037	0.70388	0.70386	0.70381	0.70378
$^{143}Nd/^{144}Nd$			0.51299	0.51296	0.51302	0.51297	0.51299	0.51292
Latitude	13.23	13.20						
Longitude	87.77	87.71						
Distance	524.9	531.8						

Table 2-2 cont.

	ZA7	ZA100	Am8	COS9A	Cos24-4	Cos18-1	SC2	SC3
SiO_2	51.83	51.57	51.1	58.9	52.9	53.3	48.44	51.45
TiO_2	0.88	0.901	0.932	0.71	0.8	0.77	0.82	0.92
Al_2O_3	19.53	19.67	18.63	18.5	18	18	18.79	20.13
FeO	9.17	8.5	10.16	7.13	9.33	9.14	10.26	9.68
MnO	0.18	0.169	0.187	0.16	0.185	0.19	0.19	0.2
MgO	3.63	4.3	5.36	2.2	4.29	4.25	5.86	3.27
CaO	9.71	10.19	10.82	7.6	9.2	8.96	11.37	10.5
Na_2O	3.18	3	2.43	3.88	2.93	3	2.4	3.1
K_2O	0.62	0.751	0.599	1.27	0.803	0.824	0.57	0.8
P_2O_5	0.19	0.238	0.159	0.22	0.18	0.156	0.17	0.22
B				46			7.4	9.6
Be				0.46			0.79	0.89
^{10}Be	7			14.5				
Sc	30.58	30.04	33.89	23.11			31.42	24.88
V	290.9	265.7	312.3	160.9	281	261	329	301.1
Cr	16.81	37.99	20.43	10.72	23	17	12.04	3.91
Ni	58.98	30.08	19.49	11.87	26	16	22.84	7.41
Cu	131.7	107.1	104.7	89.28			209.3	229.5
Rb	9.08	8.571	7.757	23.3	20.98	14.68	12.57	13.78
Sr	534.3	557.4	551.3	446.3	495	460	523.2	580.4
Y	26.5	30.168	19.824	30.43	29.14	23.69	23.03	25.28
Zr	49.38	82.71	58.67	108.7			58.24	70.12
Nb	2.92			9.50	3.67	1.81	3.50	4.96
Ba	484.2	614.3	438.8	879.3	596	561	456.5	589.9
La	7.761	10.488	5.85	8.61	6.049	5.591	5.03	6.73
Ce	14.803	21.052	12.828	21.86	13.757	12.713	13.17	17.1
Nd	12.384	15.276	10.192	15.01	10.996	10.573	9.42	11.32
Sm	3.188	3.63	2.724	4.5	3.091	2.936	2.8	3.23
Eu	1.247	1.214	0.955	1.2	1.026	0.984	0.91	1.13
Gd	3.72	4.093	3.03	5.25	3.398	3.309	3.18	4.21
Dy	3.473	3.832	3.019	5.56	3.616	3.563	3.39	3.98
Er	2.199	2.459	1.909	2.94	2.46	2.344	1.94	2.49
Yb	2.016	2.192	1.807	2.63	2.157	2.154	1.71	2.35
Cs	0.268	0.171	0.274	1.539	0.994	0.25	0.391	0.483
Pb	3.07	3.36	2.47	5.32	5.52	4.96	2.61	3.12
Th	0.49	0.65	0.50	1.34	0.96	0.87	0.54	0.74
U	0.361	0.352	0.309	1.182	0.775	0.638	0.461	0.64
$^{87}Sr/^{86}Sr$	0.70382			0.7039			0.70406	0.7039
$^{143}Nd/^{144}Nd$	0.51299			0.51311			0.51308	0.51309
$^{206}Pb/^{204}Pb$				18.5				
$^{207}Pb/^{204}Pb$				15.54				
$^{208}Pb/^{204}Pb$				38.2				
Latitude				12.98	12.98	12.98	12.70	12.70
Longitude				87.57	87.57	87.57	87.00	87.00
Distance				556.9	556.9	556.9	624.7	624.7

Table 2-2 cont.

	SC104	SC106	SC108	SC110	SC111	TE1	TE3	TE6
SiO_2	50.84	49.31	51.13	50.92	53.57	52.6	49.4	50.3
TiO_2	0.85	0.88	0.88	0.99	0.84	0.8	0.8	1.44
Al_2O_3	18.35	18.55	17.82	18.16	20.01	17.7	18.4	16.6
FeO	10.69	10.86	9.89	10.84	8.59	9.8	9.87	10.17
MnO	0.19	0.207	0.202	0.216	0.214	0.18	0.18	0.16
MgO	4.1	5.59	4.39	4.08	2.78	4.47	5.89	6.46
CaO	9.78	11.35	10.22	10.17	9.44	9.9	11.6	10.3
Na_2O	2.85	2.49	2.83	2.94	3.27	2.77	2.43	2.83
K_2O	0.919	0.602	1.13	0.834	0.7	1.34	0.94	0.88
P_2O_5	0.224	0.168	0.237	0.214	0.218	0.18	0.15	0.19
B						36	30	16
Be						0.39	0.79	0.61
^{10}Be						10.7		5.9
Sc	25.97	32.24	26.22	31.09	21	29.44	32.43	29.63
V	261.4	324.6	271.6	317.1	169.8	301.7	358.5	303.6
Cr	10.19	9.8	7.44	8.69	3.98	14.99	37.54	175.2
Ni	11.81	9.16	6.1	15.39	3.46	15.89	31.62	103.8
Cu	88.96	169	156.3	196.5	85.32	178.7	72.83	124.4
Rb	17.014	10.957	18.215	15.01	8.823	30.85	17.82	16.21
Sr	517.8	508.7	526.3	535.7	670	469.3	524	439.5
Y	25.623	23.424	25.634	26.824	22.116	25.96	18.93	23.55
Zr	78.82	46.49	76.21	61.41	44.78	93.07	66.02	109.6
Nb	3.47	4.64	4.17	1.39	3.14	2.87	3.50	12.06
Ba	635.4	428.3	668.8	587.7	548.9	817.7	577.7	439.1
La	7.321	5.309	6.869	6.174	5.636	7.02	5.89	6.21
Ce	16.532	12.339	15.494	14.144	12.551	17.72	14.54	16.73
Nd	14.71	10.405	14.24	13	12.31	11.97	10.28	11.67
Sm	4	2.825	3.86	3.73	3.59	2.64	2.46	3.37
Eu	1.195	1.05	1.15	1.16	1.3	0.92	0.92	1.22
Gd	4.14	3.01	4.06	3.91	3.85	3.83	3.37	4.18
Dy	4.56	3.23	4.32	4.34	4.23	3.73	3.29	3.89
Er	2.8	1.9	2.72	2.68	2.61	2.41	1.81	1.88
Yb	2.51	1.92	2.5	2.5	2.4	2.41	1.83	1.68
Cs	0.127	0.358	0.607	0.444	0.29	1.328	0.491	0.559
Pb	2.99	5.88	3.20	2.99	3.21	4.46	5.75	2.19
Th	1.01	0.54	0.94	0.69	0.48	1.43	0.80	0.85
U	0.841	0.473	0.832	0.587	0.388	1.302	0.627	0.627
$^{87}Sr/^{86}Sr$						0.70402	0.70408	0.70391
$^{143}Nd/^{144}Nd$						0.51309	0.51307	0.51303
$^{206}Pb/^{204}Pb$						18.5263		
$^{207}Pb/^{204}Pb$						15.5422		
$^{208}Pb/^{204}Pb$						38.1782		
Latitude	12.70	12.70	12.70	12.70	12.70	12.60	12.60	12.60
Longitude	87.00	87.00	87.00	87.00	87.00	86.85	86.85	86.85
Distance	624.7	624.7	624.7	624.7	624.7	644	644	644

Table 2-2 cont.

	TE111	TE112	TE114	TE115	TE116	TE117	TE123	TE124
SiO_2	51.53	51.32	51.34	52.62	50.11	49.49	51.34	50.53
TiO_2	0.85	0.85	0.87	0.75	0.86	0.89	1.16	1.47
Al_2O_3	21.1	21.66	20.45	19.25	19	19.13	18.08	17
FeO	8.9	8.35	9.31	8.96	10.91	10.4	9.16	9.94
MnO	0.203	0.196	0.203	0.175	0.21	0.207	0.162	0.164
MgO	3.43	3.05	3.78	4.09	4.98	4.83	5.15	6.25
CaO	10.27	10.63	10.37	10.22	11.82	10.72	10.42	10.38
Na_2O	3.25	3.12	3.09	2.45	2.37	2.61	2.73	2.74
K_2O	0.613	0.623	0.656	1.13	0.603	0.751	1.13	0.872
P_2O_5	0.155	0.147	0.161	0.138	0.12	0.165	0.177	0.174
Sc	20.65	20.66	22.47	26.9	30.81	28.53	27.28	28.48
V	222.4	208.6	249.7	276.2	359.6	322.3	250.2	242.5
Cr	5	10.13	4.26	31.52	6.32	7.68	59.54	128.4
Ni	3.94	7.3	3.15	63.04	17.25	9.42	38.82	111.9
Cu	114.8	217.2	175.7	216.4	198.2	132.9	128.8	121.4
Rb	7.35	7.243	7.729	23.976	10.71	10.53	22.264	16.411
Sr	754	788.7	736	479.6	495.5	544.3	462.8	430
Y	22.002	21.329	23.181	22.051	20.934	21.036	24.594	23.425
Zr	45.53	45.72	41.39	77.02	47.67	52.6	94.6	96.98
Nb	1.08	2.52	2.44	1.84	3.90	0.99	10.00	10.59
Ba	595.8	562.1	546.7	728	538.3	561.8	599.5	423.8
La	5.354	4.881	5.137	6.365	4.018	5.152	7.198	6.668
Ce	12.189	11.46	11.701	14.26	9.284	11.895	16.343	15.457
Nd	11.835	9.9	10.91	10.7	7.87	9.86	13.415	12.755
Sm	3.295	2.76	3.06	2.84	2.37	2.735	3.865	3.87
Eu	1.25	1.135	1.205	0.96	0.93	1.085	1.245	1.35
Gd	3.43	2.73	3.16	3.04	2.55	2.9	4.33	4.21
Dy	3.67	2.87	3.38	3.27	2.93	3.04	4.33	4.15
Er	2.2	1.65	1.97	2.02	1.81	1.8	2.5	2.21
Yb	2.13	1.725	1.98	2.045	1.81	1.84	2.36	2.045
Cs	0.157	0.345	0.342	1.143	0.462	0.385	0.901	0.631
Pb	2.34	3.88	7.36	4.82	4.38	4.47	3.74	2.94
Th	0.35	0.29	0.29	1.43	0.44	0.66	1.13	1.06
U	0.321	0.276	0.256	1.16	0.397	0.583	0.85	0.838
$^{87}Sr/^{86}Sr$			0.70391		0.704104		0.703923	0.703787
$^{143}Nd/^{144}Nd$					0.513052		0.513056	0.513028
Latitude	12.60	12.60	12.60	12.60	12.60	12.60	12.60	12.60
Longitude	86.85	86.85	86.85	86.85	86.85	86.85	86.85	86.85
Distance	644	644	644	644	644	644	644	644

Table 2-2 cont.

	TE125	TE127	TE128	RO1	RO2	RO4	RO5	LP1
SiO_2	48.68	52.28	51.69	47.92	53.52	53.64	50.54	53.6
TiO_2	0.78	0.83	0.87	0.8	0.71	0.77	0.77	1.67
Al_2O_3	21.24	18.64	19.1	21.38	17.92	19.07	19.82	16
FeO	9.4	9.46	9.47	9.68	8.79	8.23	9.25	9.8
MnO	0.18	0.198	0.192	0.189	0.183	0.175	0.174	0.18
MgO	3.98	4.38	3.87	3.83	4.18	2.8	4.75	4.75
CaO	12.16	10.16	10.04	11.96	9.18	8.94	11.4	8.7
Na_2O	2.38	2.74	3.09	2.35	3.13	3.4	2.26	3.03
K_2O	0.515	0.832	0.804	0.433	1.06	1.22	0.712	0.85
P_2O_5	0.13	0.173	0.182	0.134	0.162	0.215	0.117	0.22
Be								1.15
Sc	27.26	30.3	28.57	27.26	22.54	21.9	29.68	27.5
V	331.1	276.5	294.9	317.1	244.7	216.2	307.1	254
Cr	11.36	20.01	7.52	13.09	12.31	16.58	31.78	128.6
Ni	29.37	28.44	4.57	153.5	490.8	62.69	41.46	67.02
Cu	215.3	146.3	208.9	126.7	105.6	165.1	189.6	166.5
Rb	8.052	15.21	12.66	5.41	18.279	21.983	13.069	15.59
Sr	573	550.8	570.1	621.5	600.2	598.4	502.5	392.5
Y	17.878	23.097	22.363	19.575	22.006	31.884	18.394	28.65
Zr	46.53	63.64	59.64	45.43	68.54	66.36	54.4	138.1
Nb	2.23	2.57	1.28	3.97	1.75	1.94	3.76	10.51
Ba	474.9	729.2	649.4	514.7	724.7	903.6	509.2	528.3
La	4.181	6.483	5.775	4.651	7.142	9.852	4.575	7.07
Ce	9.475	14.307	13.133	10.46	14.943	20.873	9.452	21.65
Nd	7.915	12.87	9.695	7.91	12.855	15.615	7.715	15.79
Sm	2.275	3.565	2.705	2.235	3.245	4.095	2.1	4.66
Eu	0.88	1.25	0.99	0.89	1.2	1.47	0.845	1.45
Gd	2.45	4	2.2	2.3	3.61	4.34	2.19	4.97
Dy	2.77	4.1	2.86	2.62	3.67	4.44	2.46	4.87
Er	1.67	2.47	1.8	1.54	2.22	2.72	1.49	2.54
Yb	1.647	2.46	1.72	1.59	2.029	2.75	1.52	2.02
Cs	0.322	0.568	0.337	0.211	0.636	0.719	0.452	0.644
Pb	3.02	3.52	2.84	3.25	3.61	4.81	2.87	2.95
Th	0.49	0.75	0.57	0.88	1.03	1.07	0.68	0.92
U	0.428	0.657	0.461	0.636	0.806	0.829	0.451	0.654
$^{87}Sr/^{86}Sr$		0.703957						
Latitude	12.60	12.60	12.60	12.55	12.55	12.55	12.55	12.50
Longitude	86.85	86.85	86.85	86.75	86.75	86.75	86.75	86.68
Distance	644	644	644	655	655	655	655	664.9

Table 2-2 cont.

	LP2	LP101	LP102	LP103	LP107	LP108	AS1	AS2
SiO_2	50	53.08	53.61	52.71	51.62	52.45	54.2	54.2
TiO_2	0.76	0.86	1.59	1.52	0.87	0.92	1.49	1.55
Al_2O_3	17.3	16.67	16.19	15.95	16.4	16.98	15.4	15.6
FeO	9.4	9.26	9.84	9.69	9.48	9.62	9.4	10
MnO	0.18	0.184	0.175	0.17	0.183	0.186	0.14	0.18
MgO	6.27	5.61	5.65	5.8	6.4	5.48	5.29	5.12
CaO	12.2	10.91	9.17	9.04	11.3	11.05	8.4	8.8
Na_2O	2.14	2.6	2.94	2.9	2.47	2.56	2.91	2.8
K_2O	0.63	0.908	0.924	0.853	0.728	0.812	0.8	0.89
P_2O_5	0.16	0.196	0.233	0.224	0.171	0.184	0.23	0.2
B								19.4
Be	0.78						1.05	0.73
^{10}Be								6.2
Sc	38.55	33.03	26.98	27.17	34.47	32.67	27.38	25.7
V	295.3	253.6	224.6	229.5	259.8	246.6	259.8	238.9
Cr	140.2	75.68	128.9	144.6	108.3	35.09	136.2	144.8
Ni	46.01	28.24	118.4	79.65	32.99	25.06	69.88	68.33
Cu	136.9	125.6	117.6	135.6	115.8	134.7	152.9	145.8
Rb	12.30	21.635	17.033	16.585	14.4	16.382	19.04	18.23
Sr	501.9	458.8	406.4	408.3	430.6	453.8	391.5	405.5
Y	18.69	30.769	28.822	28.088	23.516	24.963	30.04	29.28
Zr	69.69	83.79	120.2	116.6	76.22	81.24	126.8	117.8
Nb	3.17	7.01	11.88	14.03	6.35	3.51	12.25	13.07
Ba	387.1	571.8	484	465.9	438.4	504.6	549.9	486.7
La	6.02	8.56	8.345	8.102	6.374	7.025	7.4	7.06
Ce	13.24	19.426	20.317	19.855	14.699	16.07	20.38	20.99
Nd	10.24	12.05	16.735	15.495	11.695	10.335	14.35	14.31
Sm	2.91	3.22	4.65	4.23	3.225	2.81	4.19	4.19
Eu	0.86	0.985	1.54	1.445	1.105	0.975	1.4	1.35
Gd	3.43	3.46	4.79	4.27	3.67	3	5.02	4.88
Dy	3.49	3.8	4.85	4.18	3.83	3.21	5.23	4.64
Er	1.75	2.34	2.57	2.23	2.2	1.86	2.36	2.34
Yb	1.42	2.155	2.38	2.077	2.22	1.895	2.1	1.85
Cs	0.437	0.864	0.658	0.646	0.558	0.664	0.829	0.793
Pb	2.33	4.41	3.16	3.33	2.63	3.70	3.54	3.53
Th	0.61	1.65	0.97	1.04	0.55	0.74	0.98	1.19
U	0.488	1.516	0.65	0.745	0.372	0.533	0.712	0.714
Latitude	12.50	12.50	12.50	12.50	12.50	12.50	12.50	12.50
Longitude	86.68	86.68	86.68	86.68	86.68	86.68	86.68	86.68
Distance	664.9	664.9	664.9	664.9	664.9	664.9	664.9	664.9

Table 2-2 cont.

	AS4	CN1	CN10	MT8	MT101	MT201	NE201	NE202
SiO_2	55.9	50.8	49.4	52.2	54.4	49.83	47.9	47.5
TiO_2	0.96	0.77	0.73	0.82	0.73	0.92	0.93	1.2
Al_2O_3	15.7	19.5	18.8	18	16.9	17.27	15.3	15.4
FeO	10.6	9.7	10.4	9.5	9.1	11.48	11.32	11.28
MnO	0.2	0.18	0.19	0.19	0.18	0.213	0.19	0.19
MgO	3.77	4.73	6	4.98	4.47	5.55	9.95	9.51
CaO	8.3	11.5	11.9	10.2	9.2	11.44	11	10.7
Na_2O	2.84	2.2	2	2.65	2.89	2.48	2.3	2.51
K_2O	1.31	0.46	0.37	0.72	0.91	0.915	0.19	0.24
P_2O_5	0.2	0.12	0.11	0.14	0.15	0.196	0.1	0.11
B	0	13.3	11	19.5	25			2.9
Be	0.93	0.33	0.7	0.76	0.39			0.39
^{10}Be		7.2			10.8			2.4
Sc	31.09	31.69	35.96	31.21	29.69	32.54		34.58
V	297.5	332.3	341.8	321.4	304.8	380.7	256	251
Cr	12.7	21.18	39.95	16.78	14.69	8.37	303	333.9
Ni	13.11	17.81	28.37	15.01	13.58	22.34	140	145.2
Cu	226.1	162.9	168.9	110.6	127.8	176.6		134.3
Rb	23.98	7.9	7.2	11.84	15.98	18.101	10	3.1
Sr	419.5	480.8	455.3	481.5	480.1	446.3	360	308.7
Y	28.86	16.63	14.76	18.81	22.66	25.963	20.8	20.22
Zr	108.5	47.85	47.17	68.05	77.58	75.3	54.28	70.68
Nb	8.16	2.40	2.50	1.93	4.34	4.70	6.54	6.10
Ba	851.6	406.6	339.9	550.4	693.3	454	115	143.7
La	7.41	3.6	3.18	5.59	6.03	7.467		3.31
Ce	19.65	9.15	7.78	13.3	14.77	16.45		9.75
Nd	13.89	7.1	6	9.61	10.08	12.705		7.81
Sm	3.94	1.95	1.69	2.49	3.13	3.52		2.27
Eu	1.11	0.77	0.69	0.9	0.94	1.19		0.93
Gd	4.48	2.53	2.34	3.27	3.61	3.88		3.22
Dy	4.6	2.95	2.39	3.26	3.86	4.16		3.19
Er	2.9	1.73	1.44	1.83	2.22	2.39		2.07
Yb	2.88	1.62	1.42	1.5	1.84	2.37		1.76
Cs	1.248	0.487	0.407	0.337	0.692	0.499	0.077	0.079
Pb	4.62	2.90	2.68	2.44	4.50	5.05	1.54	1.23
Th	1.31	0.41	0.29	0.59	0.81	0.82	0.25	0.26
U	1.053	0.38	0.262	0.513	0.733	0.703	0.175	0.124
$^{87}Sr/^{86}Sr$		0.70397	0.70392		0.70405		0.70375	0.70376
$^{143}Nd/^{144}Nd$		0.51311	0.51309				0.51302	0.51308
$^{206}Pb/^{204}Pb$		18.5492	18.5577		18.6			18.6378
$^{207}Pb/^{204}Pb$		15.5367	15.5246		15.55			15.5293
$^{208}Pb/^{204}Pb$		38.1817	38.1867		38.31			38.1917
Latitude	12.50	12.50	12.50	12.42	12.42	12.42	12.11	12.11
Longitude	86.68	86.70	86.70	86.53	86.53	86.53	86.32	86.32
Distance	664.9	663.3	663.3	683.3	683.3	683.3	720	720

Table 2-2 cont.

	NE203	NE3	NE5	NE6	CDP12	MS4	AP3	AP5
SiO_2	47.4	50.3	48	47.2	48.2	50.9	48	48.8
TiO_2	1.13	0.89	0.81	0.7	1.18	1.14	0.99	0.74
Al_2O_3	14.9	18.1	16.3	14.8	17.13	14.8	15.6	20.4
FeO	11.53	9.5	9.6	10.3	11.17	11.9	9.9	9.1
MnO	0.18	0.19	0.19	0.18	0.19	0.23	0.18	0.19
MgO	11.02	5.54	8.02	8.68	7.5	5.26	8.59	4.15
CaO	10.8	11	12.4	13.3	12	9.9	13.5	11.8
Na_2O	2.19	2.55	2.22	1.58	2.35	2.82	2.07	2.36
K_2O	0.14	0.62	0.41	0.4	0.16	1.16	0.3	0.59
P_2O_5	0.1	0.15	0.17	0.13	0.13	0.27	0.12	0.14
B	3.2	6.8	3.6	4.3		24.5		
Be	0.33	0.87	0.79	0.79	0.78	0.74	0.86	0.9
^{10}Be	1.4					24		
Sc	35.18	34.33	36.88	43.22	37.99	38.42	44.41	28.51
V	292.1	325.8	320.7	316.9	323.2	439.9	319.7	342.7
Cr	440.8	23.25	198.4	275.1	255	46.94	224.7	14.67
Ni	198.7	26.59	78.98	80.19	99.71	31.18	83.78	19.46
Cu	136.1	134.4	139.2	132.7	106.4	258.6	108.3	163.3
Rb	2.3	14.15	9.89	8.65	4.46	22.99	12.2	11.69
Sr	282.5	439	368.4	386.1	310.3	433.2	297.6	511.5
Y	19.01	18.00	19.06	16.73	24.75	28.06	17.35	18.07
Zr	59.04	80.03	59.83	53.7	67.06	105.1	65.15	60.49
Nb	7.30	5.40	5.20	1.71	3.25	3.66	2.90	2.94
Ba	81.81	447.7	353.4	337.9	88	893.2	204.8	470
La	2.87	6.17	6.64	5	3.28	10.32	4.64	5.95
Ce	8.41	14.71	14.93	12.07	10.02	23.67	11.86	13.7
Nd	6.96	9.29	10.18	8.19	8.47	16.87	8.62	9.43
Sm	2.02	2.34	2.8	2	2.66	4.24	2.63	2.46
Eu	0.9	0.9	0.93	0.77	0.99	1.29	0.94	0.86
Gd	3.34	2.98	3.22	2.8	3.74	4.71	2.83	2.59
Dy	3.45	3.12	3.05	2.7	3.94	4.93	3.1	2.92
Er	1.83	1.59	1.81	1.64	2.03	2.57	1.56	1.53
Yb	1.52	1.6	1.63	1.43	1.71	2.14	1.44	1.39
Cs	0.019	0.357	0.204	0.32	0.054	0.87	0.045	0.17
Pb	1.34	2.21	2.91	2.54	4.38	4.82	1.53	2.97
Th	0.20	0.80	0.90	0.64	0.25	1.81	0.33	0.96
U	0.109	0.654	0.621	0.584	0.149	1.49	0.214	0.658
$^{87}Sr/^{86}Sr$	0.70362	0.70393	0.70407	0.70405		0.70419	0.70388	0.70406
$^{143}Nd/^{144}Nd$	0.51299	0.51305	0.51307	0.51307	0.51286		0.51301	0.51305
$^{206}Pb/^{204}Pb$	18.61	18.5852	18.5298	18.5548		18.605		
$^{207}Pb/^{204}Pb$	15.54	15.521	15.4878	15.5067		15.5656		
$^{208}Pb/^{204}Pb$	38.24	38.2071	38.1708	38.1481		38.315		
Latitude	12.11	12.11	12.11	12.11	12.11	11.98	11.93	11.93
Longitude	86.32	86.32	86.32	86.32	86.32	86.15	86.05	86.05
Distance	720	720	720	720	720	742.7	754.8	754.8

Table 2-2 cont.

	GR3	GR5	GR101	MB101	N101	N146	N148	N77
SiO_2	48.6	48.1	46.9	51	54.8	55.96	51.9	
TiO_2	1.26	1.15	0.55	1.19	0.93	1.14	1.13	
Al_2O_3	16.4	16.1	15.9	18.6	18.03	17.66	19.03	
Fe_2O_3					4	2.25	3.85	
FeO	11.2	10.4	10.03	10.18	4.47	5.73	5.36	
MnO	0.18	0.17	0.18	0.18	0.19	0.17	0.16	
MgO	6.96	7.97	8.72	3.87	4.09	2.9	3.94	
CaO	12.1	12.4	14.4	9.9	8.55	6.88	9.02	
Na_2O	2.4	2.19	1.46	3.06	3.42	4.06	2.88	
K_2O	0.14	0.1	0.3	0.6	1.31	1.65	1.2	
P_2O_5	0.12	0.12	0.11	0.21	0.21	0.58	0.37	
B	3.4	2.1	4.8					
Be	0.6	0.67	0.5	0.91	0.96	1.41	1.22	
Sc	38.48	40.66	49.67	29.7	26.74	20.43	27.21	
V	307.3	289.8	335.9	325.6	174.1	130.4	229.5	
Cr	167.4	332.6	173.3	8.34	12.85	15.96	15.59	
Ni	74.03	94.82	52.82	12.04	13.31	12.04	12.34	
Cu	168.6	137.5	145.9	139.7	95.03	32.63	91.07	
Rb	5.27	4.04	6.46	9.9	28.1	35.5	26.5	37.158
Sr	282.9	305.3	472.1	448.4	402.5	607.3	577.9	
Y	22.72	19.91	15.38	27.3	28.81	40.21	28.99	37.158
Zr	72.28	71.23	44.8	126.4	126.5	159.1	136.2	
Nb	3.90	4.50	1.74	7.60	5.70	10.70	10.30	
Ba	117	117.2	211.6	584	708.4	986.6	789.4	
La	2.83	3.44	5.24	10.58	13.23	27.04	22.05	17.344
Ce	9.41	10.12	11.82	25.82	28.32	56.17	44.68	31.261
Nd	8.64	8.02	7.83	16.41	16.6	34.83	26.45	26.382
Sm	2.58	2.76	2.46	4.67	4.37	7.35	5.73	6.101
Eu	1.01	0.98	0.74	1.38	1.22	2.26	1.69	1.895
Gd	3.7	3.56	2.64	4.95	4.47	7.56	5.71	6.208
Dy	3.92	3.4	2.85	5.21	4.97	6.45	5.14	5.532
Er	2.04	2.08	1.39	2.59	2.48	3.57	2.69	3.299
Yb	1.48	1.58	1.18	2.39	2.48	3.69	2.33	3.134
Cs	0.067	0.09	0.129	0.48	0.721	0.822	0.69	0.666
Pb	1.23	0.94	1.37	4.01	3.24	4.48	3.98	5.00
Th	0.20	0.23	0.39	1.80	2.16	2.48	2.16	1.41
U	0.134	0.15	0.29	1.09	1.497	1.835	1.497	0.769
$^{87}Sr/^{86}Sr$	0.70384	0.70388	0.70403					0.703804
$^{143}Nd/^{144}Nd$	0.51301	0.51302	0.51307					
$^{206}Pb/^{204}Pb$	18.649						18.54	18.524
$^{207}Pb/^{204}Pb$	15.531						15.54	15.557
$^{208}Pb/^{204}Pb$	38.275						38.34	38.216
Latitude	11.88	11.88	11.88	11.83	11.73	11.53	11.53	
Longitude	86.00	86.00	86.00	85.98	85.82	85.62	85.62	
Distance	762.2	762.2	762.2	766.4	785	816.9	816.9	

Table 2-2 cont.

	N83	N87	C922	G921	RV1	RV-203	TE1	TE9
SiO_2			58.75	49.83	56.59	54.27	57.06	53.56
TiO_2			0.71	0.6	0.69	0.71	0.61	0.77
Al_2O_3			16.58	19.65	16.9	17.8	17.24	18.97
Fe_2O_3								
FeO			8	9.21	7.13	8.84	7.26	8.78
MnO			0.17	0.16	0.16	0.17	0.15	0.17
MgO			3.72	5.67	4.46	5.52	4.04	4.75
CaO			7.11	10.26	8.29	9.19	7.91	9.02
Na_2O			3.17	2.31	3.01	2.7	2.94	2.94
K_2O			1.7	0.61	1.37	1.07	1.35	0.76
P_2O_5			0.23	0.15	0.18	0.18	0.17	0.16
B			14.4		12	0	6.8	5.3
Be			1.59		0.99	0.85	0.82	0.8
^{10}Be			18.8					
Sc			23.51	29.15	25.83	27.52	26.68	32.06
V			237	279.3	216	231.9	155.1	275.3
Cr			20.4	118	65.78	27.57	28.37	20.28
Ni			18.6	46.1	23.5	26.51	14.88	15.57
Cu			84.4	150.8	115.4	88.69	48.71	93.13
Rb	29.314	30.316	51.336	3.5	24.8	27.09	22.32	9.6
Sr			589.1	599.6	554.6	569.7	631.9	530.3
Y	29.314	30.316	44.158		27.66	30.56	24.82	27.10
Zr			119.8	42.2	109.6	85.6	92.83	67.75
Nb		4.74	30.06	0.00	1.60	4.76	4.50	4.24
Ba			990.3	318.8	752.9	612.7	839	515.1
La	9.762	7.23		7.204	18.28	13.38	21.06	11.19
Ce	17.885	16.823		14.27	37.31	28.67	41.42	22.3
Nd	15.887	13.933		10.642	21.6	16.42	25.6	17.13
Sm	3.981	3.862		2.633	4.99	3.77	4.96	4.08
Eu	1.298	1.288		0.926	1.34	1.12	1.38	1.34
Gd	4.594	4.459		2.542	5	3.95	4.52	4.66
Dy	4.339	4.626		2.314	4.77	4.04	4.03	4.59
Er	2.698	2.89		1.445	2.34	1.94	2.23	2.14
Yb	2.54	2.744		1.267	2.32	1.99	1.75	1.83
Cs	0.313	0.068	0.952	0.161	0.73	0.435	0.23	0.35
Pb	3.99	4.96	5.84	4.88	5.67	5.03	4.34	2.39
Th	0.87	0.64	3.68	0.79	2.51	1.83	2.93	1.02
U	0.359	0.288	2.354	0.279	1.248	0.86	1.047	0.572
$^{87}Sr/^{86}Sr$	0.70372	0.703586			0.70391			0.70379
$^{143}Nd/^{144}Nd$					0.51304			0.51302
$^{206}Pb/^{204}Pb$	18.512	18.464						
$^{207}Pb/^{204}Pb$	15.532	15.494						
$^{208}Pb/^{204}Pb$	38.061	38.032						
Latitude			11.53	10.98	10.83	10.83	10.67	10.67
Longitude			85.62	85.47	85.33	85.33	85.02	85.02
Distance			816.9	861.5	882.3	882.3	920.4	920.4

Table 2-2 cont.

	G924	AR82	PP3	PLA-68	PP7	PP8	PP9	PP11
SiO_2	49.12	54.64	52.34	49.12	44.8	47.11	49.7	49.76
TiO_2	0.84	0.61	0.88	0.78	0.77	1.58	1.25	0.85
Al_2O_3	17.1	19.04	18.63	18.87	13.56	14.99	17.03	18.8
Fe_2O_3								
FeO	10.49	7.19	8.81	9.81	8.77	9.75	8.79	9.26
MnO	0.18	0.15	0.16	0.18	0.16	0.17	0.15	0.16
MgO	7.78	4.76	4.36	5.98	14.06	10.21	8.82	4.58
CaO	11.01	9.04	8.92	9.83	12.43	11.47	10.05	9.15
Na_2O	2.27	3.08	2.86	2.2	1.06	2.23	2.81	2.83
K_2O	0.66	0.64	1.69	0.97	1.18	1.32	0.81	2.81
P_2O_5	0.25	0.17	0.28	0.17	0.36	0.52	0.38	0.58
B		11.5	7.9			2.4	2.7	6.3
Be		0.63	1.22	0.85		1.38	1.18	2
^{10}Be		0.6			0.8			
Sc	31.7	22.75	26.1	37.3	38.7	32.21	26.88	24.18
V	278.8	190.5	215.5	331.5	233.5	266.1	262.3	298.9
Cr	180.3	47.97	5.58	46.48	785.3	479	337.6	6.71
Ni	77.7	41.69	13.03	28.54	439.6	207.5	201.1	15.52
Cu	77.7	106.3	106.1	193.9	104.7	116.6	117.8	173.8
Rb	13.7	9.50	38.72	21.57	19.87	32.13	15.86	51.94
Sr	798.4	748.4	646.5	589.6	2770.9	816.7	916.8	1582
Y		13.22	29.02	23.10	14.02	29.18	19.18	32.56
Zr	67.7	61.75	131.4	88.75	92.4	179.8	116.8	169.5
Nb		7.91	15.52	7.43	7.83	21.47	16.00	22.28
Ba	416.9	577.7	877.4	558.7	2863.4	645.9	562.2	1944
La	14.392	13.16	37.4	23.47	64.39	59.9	33.4	103
Ce	28.778	26.63	73.04	37.85	125.1	118.9	66.6	186.9
Nd	17.558	13.13	33.17	21.8	59.57	57.5	32.3	82.5
Sm	2.863	2.88	6.84	4.73	7.526	10.8	6.1	14.2
Eu	1.221	0.99	1.69	1.3	2.162	2.9	1.8	3.7
Gd	3.506	2.97	5.8	4.31	5.192	8.6	5.1	10.3
Dy	3.105	2.82	4.95	3.73	3.428	6.1	3.6	6.3
Er	1.83	1.55	2.4	1.84	1.893	3.2	2	3.2
Yb	1.554	1.49	2.14	1.38	1.666	2.7	1.5	2.7
Cs	0.112	0.173	0.388	0.273	0.667	0.33	0.221	0.398
Pb	3.29	4.31	8.77	4.25	6.36	3.79	4.71	7.41
Th	1.62	0.94	8.80	3.38	5.41	5.81	3.21	19.61
U	0.612	0.35	3.036	1.181	0.912	2.04	1.085	5.038
$^{87}Sr/^{86}Sr$		0.70389	0.70373	0.70374	0.70356	0.70376	0.70362	0.70375
$^{143}Nd/^{144}Nd$		0.51302	0.51295	0.51291	0.51293	0.51294		0.51291
Latitude		10.47	10.30	10.30	10.30	10.30	10.30	10.30
Longitude		84.73	84.37	84.37	84.37	84.37	84.37	84.37
Distance	939	958.3	1003.8	1003.8	1003.8	1003.8	1003.8	1003.8

Table 2-2 cont.

	PO2	PO4	B7	B8	IZ84-1	IZ-63A	D2	GUC201
SiO_2	51.13	54.21	51.08	50.66	55.19	55.29	50.39	49.8
TiO_2	0.75	0.79	1.57	1.68	0.9	0.94	1.02	1.27
Al_2O_3	19.64	19.35	16.39	17.83	17.8	17.34	15.84	17.2
Fe_2O_3								4.9
FeO	8.99	7.71	8.51	9.42	6.6	6.84	7.96	3.9
MnO	0.18	0.16	0.15	0.16	0.11	0.12	0.14	0.15
MgO	5.55	3.84	6.39	6.12	4.27	5.7	8.99	6.88
CaO	9.61	8.61	9.57	9.44	7.63	8.15	9.1	10.4
Na_2O	2.89	3.09	3	2.95	3.49	3.46	2.73	3.3
K_2O	0.75	1.06	2.32	0.94	1.75	1.98	1.56	0.91
P_2O_5	0.15	0.19	0.48	0.33	0.33	0.35	0.41	0.29
B	4.7					14.5	6	
Be	0.8	0.88	1.62	1.26	1.27	1.4	1.36	
^{10}Be						1.3		
Sc	26.4	22.21	27.62	31.87	20.96	23	27.28	
V	230	167	236.6	259.1	152	195	231	155
Cr	23.52	4.9	197.9	89.29	58.36	208	419.5	16
Ni	25.05	10.26	73	44.36	41.66	96	151.6	8
Cu	92.19	147.3	88.85	134.4	123.2	134	107.5	
Rb	14.73	20.2	35	15.6	39	48.60	18.30	34
Sr	618	687.6	859.9	795.2	884.7	805	770.4	456
Y	18.64	20.63	22.55	24.81	15.81	21.28	22.18	26.63
Zr	78.02	84.84	218.1	160.5	148	175	144.3	
Nb	7.80	7.20	24.86	16.37	22.02	18.10	14.21	
Ba	374	636.8	737.9	534	757.3	806	669.2	581
La	10.71	19.71	52.95	35.64	31.84	40.61	41.44	13.3
Ce	23.95	36.82	105.3	61.76	62.4	79.29	83.24	29.37
Nd	13.05	18.13	49.24	34.4	28.25	35.5	39.31	17.46
Sm	2.71	4.14	8.13	7.04	5.43	6.45	7.12	4.19
Eu	1.02	1.15	2.4	2.27	1.43	1.64	1.88	1.36
Gd	3.18	3.59	7.02	6.63	4.33	4.99	5.31	4.47
Dy	3.58	3.6	5.58	5.18	3.9	3.99	4.62	4.46
Er	1.65	1.94	2.71	2.37	1.79	2.33	2	2.3
Yb	1.46	1.38	2.01	1.76	1.64	1.89	1.62	2.22
Cs	0.283	0.31	0.58	0.21	0.68	0.921	0.17	0.53
Pb	5.27	6.54	5.26	3.16	5.85	6.60	4.31	5.17
Th	1.43	2.89	7.70	3.51	5.88	10.75	5.06	1.25
U	0.596	1.028	2.57	1.191	2.098	3.613	1.804	0.53
$^{87}Sr/^{86}Sr$	0.70375		0.70358			0.70366		0.70359
$^{143}Nd/^{144}Nd$	0		0.51299			0.51296		0.51299
$^{206}Pb/^{204}Pb$						19.062		
$^{207}Pb/^{204}Pb$						15.602		
$^{208}Pb/^{204}Pb$						38.829		
Latitude	10.20	10.20	10.13	10.13	9.98	9.98	9.98	
Longitude	84.22	84.22	84.08	84.08	83.85	83.85	83.85	
Distance	1021	1021	1037.2	1037.2	1037.2	1037.2	1037.2	

Table 2-2 cont.

	Guc1009s	Guc1008s	Guc1007s	Guc1006s	Guc1006	Guc1005s	uc1005bo	Guc1004s
SiO_2	50.95	48.25	50.05	51.95	52.31	50.25	50.45	51.8
TiO_2	1.285	1.125	1.265	1.775	1.713	1.31	1.315	1.19
Al_2O_3	17.6	17.9	16.7	17	17.175	17.4	17.45	18.4
FeO	8.99	9.64	8.855	10.3	9.979	8.8	8.725	9.02
MnO	0.155	0.174	0.16	0.191	0.188	0.159	0.155	0.156
MgO	6.36	6.62	7.1	3.985	3.978	6.485	6.465	4.595
CaO	9.005	10.4	9.26	7.925	7.769	8.9	9.055	8.215
Na_2O	3.15	2.69	2.815	3.61	4.23	3.145	3.45	3.325
K_2O	0.94	0.754	1.43	1.175	1.206	1.245	1.295	1.08
P_2O_5	0.349	0.306	0.349	0.349	0.393	0.393	0.393	0.262
Sc	27.28	28.58	27.71	28.44	28.805	25.95	26.33	22.94
V	217.8	236.1	227.35	233.15	233.35	203.97	206.35	235.5
Cr	187.3	46.2	247.1	4.37	9.008	163.23	150.55	18.28
Ni	80.73	28.38	81.68	4.58	9.477	86.87	60.52	
Cu	56.93	52.17	50.05	24.43	14.635	50.48	37.44	50.3
Rb	15.251	15.23	25.142	22.994	26.982	24.634	22.801	16.681
Sr	543.55	629.05	636.85	584.2	596.7	606.43	615.75	607.8
Y	29.795	25.187	27.154	40.156	47.743	30.828	31.436	30.231
Zr	165.65	130.2	145.7	173.8	191.5	163.23	167.55	135.8
Nb	8.41	4.62	9.50	10.63	12.33	12.75	13.28	7.12
Ba	444.103	357.405	471.356	535.122	515.98	482.927	460.63	519.413
La	16.27	12.997	17.096	17.331	16.919	17.431	17.767	14.28
Ce	35.197	29.702	35.787	39.981	39.503	38.473	38.712	31.353
Nd	21.891	18.955	23.254	25.484	25.625	22.901	23.245	19.555
Sm	4.775	4.267	5.219	6.119	5.955	4.953	5.195	4.511
Eu	1.575	1.349	1.692	1.98	1.911	1.638	1.698	1.432
Gd	5.06	4.453	5.554	6.373	6.245	5.116	5.401	4.794
Dy	4.541	3.91	4.632	5.699	5.647	4.41	4.605	4.212
Er	2.639	2.311	2.702	3.436	3.365	2.483	2.631	2.439
Yb	2.451	2.191	2.506	3.192	3.024	2.333	2.477	2.247
Cs	0.435	0.397	0.831	0.637		0.607	0.634	0.522
Pb	5.41	5.50	6.22	7.46	8.67	8.54	6.13	9.11
Th	1.30	0.77	1.68	1.74	1.99	1.15	1.55	1.58
U	0.463	0.345	0.651	0.588	0.812	0.537	0.677	0.598

Table 2-2 cont.

	Guc1004b	Guc1004a	Guc1003s	Guc1002s	Guc1001s	HONC107	HONC109	HONC111
SiO_2	52.65	53.2	52	50.53	48.85	53.25	50.89	50.39
TiO_2	1.325	1.225	1.165	1.207	0.962	1.03	0.88	0.99
Al_2O_3	18.5	19.35	18.3	17.62	21.45	17.2	20.42	17.72
FeO	9.765	9.055	9.645	8.623	8.22	8.82	8.54	9.22
MnO	0.17	0.159	0.186	0.157	0.137	0.16	0.15	0.18
MgO	4.905	4.52	4.78	7.344	4.76	5.04	4.8	5.15
CaO	8.59	8.895	8.38	9.299	11.85	8.67	9.71	8.97
Na_2O	3.66	3.54	3.21	3.136	2.465	2.79	3.02	3.01
K_2O	0.996	1.14	0.894	1.017	0.828	1.6	0.8	1.17
P_2O_5	0.262	0.262	0.393	0.306	0.218	0.4	0.18	0.32
Sc	24.85	22.44	24.24	27.05	25.4	24.9	24.29	29.43
V	235.15	232.65	201.9	198.4	254.8	219.5	235.8	250.5
Cr	22.58	19.63	46.45	228.35	65.43	99.09	21.69	86.15
Ni	5.7	5.35	64.62	145.55	12.05	63.53	35.53	46.99
Cu	34.43	27.42	37.95	58.63	68.63	79.46	55.05	80.53
Rb	14.578	16.854	15.397	16.301	24.561	28.7	13.85	14.3
Sr	619.9	622.35	598.55	554.05	684.35	599.3	596.3	580.5
Y	27.352	29.502	39.131	27.287	22.545	28.1	27.079	37.102
Zr	138.35	135.9	118.15	134.7	86.05	153.6	79.91	122.3
Nb	5.92	6.70	6.30	9.14	3.62	7.05	3.02	6.23
Ba	508.36	514.897	494.99	385.517	328.944	730.9	406	752.4
La	14.212	14.595	12.652	12.175	8.818	20.766	10.746	19.936
Ce	31.055	31.034	28.391	27.077	19.618	43.5	19.633	34.971
Nd	20.141	19.506	20.609	17.02	13.465	25.749	17.128	24.54
Sm	4.62	4.479	4.888	3.959	3.206	5.308	4.122	5.311
Eu	1.517	1.429	1.676	1.308	1.115	1.61	1.413	1.705
Gd	4.977	4.726	5.29	4.302	3.505	5.323	4.528	5.925
Dy	4.328	4.121	4.87	3.889	3.034	4.164	4.176	5.052
Er	2.604	2.436	2.951	2.355	1.779	2.41	2.568	3.174
Yb	2.324	2.239	2.776	2.166	1.571	2.196	2.32	2.833
Cs	0.47	0.485				0.631	0.154	0.248
Pb	7.43	7.97	7.70	6.08	5.20	8.56	3.94	5.63
Th	1.35	1.19	1.68	1.45	1.28	1.43	0.70	1.32
U	0.525	0.396	0.737	0.616	0.611	0.589	0.236	0.447
$^{87}Sr/^{86}Sr$						0.70396		0.70394
$^{143}Nd/^{144}Nd$						0.51286		0.51288

Table 2-2 cont.

	HONC112	HONC113	HONC114	HONC118	HONC119	HONC121	HONC122	HONC125
SiO_2	51.07	51.73	54.46	53.54	52.25	51.45	51.3	51.18
TiO_2	0.99	1.11	1.21	0.87	1.31	1.04	1.02	1.01
Al_2O_3	17.98	17.58	16.77	17.38	17.24	17.08	17.53	17.58
FeO	9.18	9.21	9.18	8.68	9.1	8.91	9.56	8.75
MnO	0.19	0.17	0.17	0.2	0.16	0.12	0.14	0.15
MgO	5.17	5.41	3.27	5.98	5.52	4.78	4.77	4.94
CaO	8.76	8.72	7.4	9.38	9.03	8.57	8.94	9.72
Na_2O	3.11	2.99	3.31	2.72	3.08	2.88	2.93	3.14
K_2O	1.26	1.21	1.65	2.05	1.41	1.41	1.04	1.33
P_2O_5	0.33	0.44	0.33	0.34	0.46	0.35	0.3	0.43
Sc	29.36	27.73	27.98	29.1	26.26	27.83	28.96	26.7
V	250	226.3	254.9	252.2	223.5	235.1	245.6	228.8
Cr	91.58	115.1	13.92	124.9	107.7	130.5	107.1	73.97
Ni	45.1	50.25	17.17	57.87	50.15	70.98	49.57	34.78
Cu	82.79	54.63	10.15	74.44	76.23	90.15	56.16	68.77
Rb	21.9	18.2	42.2	54.1	26.3	27	14.3	18.6
Sr	587.9	574.6	550.2	659.7	577.7	555.7	544	611.5
Y	54.2	46.877	71.9	53.9	37.4	98.1	98.8	31.5
Zr	123.8	163.3	134.6	119.4	185.9	147.5	125.7	212.2
Nb	6.66	9.79	9.70	3.89	12.90	8.08	6.20	10.50
Ba	912.4	639.1	877.5	942.3	653.6	698.1	796.1	816.1
La	34.474	24.653	41.219	24.496	30.861	54.059	57.561	22.859
Ce	75.768	45.491	76.512	40.31	52.469	57.167	68.677	48.33
Nd	43.98	32.461	48.74	27.922	39.113	55.295	67.766	27.988
Sm	9.672	6.867	10.566	6.243	8.195	11.945	14.791	5.635
Eu	2.881	2.201	3.116	2.006	2.378	3.104	4.386	1.696
Gd	10.036	7.375	11.243	7.331	7.753	13.68	17.036	5.68
Dy	8.506	6.344	9.549	5.791	6.101	11.542	14.395	4.322
Er	4.84	3.925	5.488	3.569	3.288	7.015	7.956	2.513
Yb	4.49	3.435	4.786	2.889	2.906	6.058	6.662	2.308
Cs	0.692	0.536	1.168	0.773	0.664	1.298	0.554	2.358
Pb	6.14	6.95	9.03	6.66	10.70	6.59	5.98	7.94
Th	1.46	1.17	3.50	2.07	1.35	1.61	1.08	1.56
U	0.57	0.443	1.064	0.94	0.519	0.607	0.421	0.581
$^{87}Sr/^{86}Sr$	0.70396	0.70402	0.70451	0.70408	0.70394	0.70406		0.70403
$^{143}Nd/^{144}Nd$	0.51292	0.51283	0.5128	0.51289	0.51283			0.51283

Table 2-2 cont.

	YO1	YO2	YO3	YO5	YO6	YO7	YO9	YO10
SiO_2	47.99	48.41	49.13	48.68	48.81	47.96	48.45	48.99
TiO_2	1.93	1.94	1.77	2.54	2.53	2.52	2.61	2.55
Al_2O_3	17.26	17.32	16.88	17.57	18.31	17.29	17.39	17.06
FeO	8.74	8.87	8.84	10.67	9.92	10.56	10.78	10.51
MnO	0.15	0.15	0.16	0.18	0.18	0.18	0.18	0.18
MgO	6.86	7	6.84	4.75	4.15	4.62	4.77	5.58
CaO	8.48	8.7	8.53	8.44	9.07	8.33	8.77	8.81
Na_2O	3.86	3.64	3.91	3.54	4.19	3.66	3.67	3.78
K_2O	1.66	1.65	1.53	1.8	1.7	1.79	1.77	1.7
P_2O_5	0.51	0.52	0.52	0.54	0.76	0.55	0.55	0.57
^{10}Be								2
Sc	24.99	25.08	25.68	26.91	24.91	26.4	27.83	28.24
V	197.7	205.1	204.5	279.3	224.7	272.4	273.5	260.3
Cr	173.4	187.8	197.2	43.89	29.04	37.04	45.25	84.03
Ni	89.42	120.8	120.6	22.25	16.86	23.94	39.25	87.45
Cu	42.13	42.79	50.71	28.28	26.58	27.4	23.74	35.89
Rb	14.9	13.7	15	15	20	17.6	18.5	18.8
Sr	611.7	767.9	563.2	555.7	621.7	527.9	576.4	506.8
Y	55.9	40.7	38.5	45.1	41	37.8	37.3	37.4
Zr	225.5	242.3	257.7	271.5	236.7	260.7	263.8	263.6
Nb	39.30	44.70	28.60	38.40	52.70	47.70	51.00	49.50
Ba	246.3	277.6	348.7	244.1	327	244	245.2	279.9
La	29.1	23.238	22.385	25.7	26.141	25.4	25.511	25.067
Ce	47.5	46.329	45.19	53.8	54.89	50.1	53.443	52.812
Nd	27.5	24.899	24.941	29.4	29.666	28.1	29.187	29.784
Sm	5.14	5.286	5.397	6.83	6.512	7.7	6.45	6.667
Eu	2.01	1.815	1.786	2.33	2.143	1.62	2.063	2.117
Gd	6.37	5.777	5.762	6.88	6.728	6.97	6.638	6.892
Dy	7.54	5.146	5.123	7.04	5.973	6.21	5.947	6.105
Er	5.04	3.202	3.095	4.41	3.483	3.05	3.402	3.531
Yb	3.36	2.739	2.682	3.83	3.104	3.54	3.046	3.143
Cs	0.143	0.082	0.107	0.156	0.269	0.115	0.143	0.2
Pb	2.94	3.02	3.67	2.51	3.41	3.51	3.34	4.01
Th	1.86	2.06	1.94	2.00	2.83	3.28	2.77	2.51
U	0.796	0.741	0.564	0.79	0.984	1.255	0.931	0.894
$^{87}Sr/^{86}Sr$	0.70288	0.70291	0.70321	0.70295	0.70308	0.70312	0.70319	0.70316
$^{143}Nd/^{144}Nd$	0.51304	0	0.51299	0.51303	0.51299	0.51301	0.51302	0.51298
$^{206}Pb/^{204}Pb$	18.646	18.659	18.646	18.5837	18.632	18.65		
$^{207}Pb/^{204}Pb$	15.58	15.582	15.542	15.5015	15.5269	15.546		
$^{208}Pb/^{204}Pb$	38.306	38.325	38.219	38.0551	38.1953	38.25		

Table 2-2 cont.

	YO11	YO13	Ut1	M1	M2	M3	G1	G2
SiO_2	48.42	49.29	48	61.19	81.19	79.12	70.84	59.65
TiO_2	1.91	1.85	1.71	1.59	1.04	1.02	0.26	0.96
Al_2O_3	19.56	20.04	17.69	22.34	11.74	11.92	13.37	15.74
FeO	8.43	8.28	9.2	1.43	0.39	0.39	1.75	6.84
MnO	0.16	0.15	0.245	0.01			0.01	0.14
MgO	3.96	4.09	6.27	0.75	0.3	0.29	0.14	3.33
CaO	9.87	10.14	8.63	0.18	0.16	0.14	0.49	6.04
Na_2O	3.92	4.04	4.07	0.32	0.13	0.14	4.66	2.93
K_2O	1.49	1.46	2.05	6.03	2.59	2.66	3.94	1.6
P_2O_5	0.56	0.52	0.508	0.05	0.03	0.03	0.04	0.19
Sc	21.28	20.86	22.55	25.49	11.52	12.33	5.99	23.43
V	157.1	167.4	188.9	213.1	73.7	73.6	2.01	173
Cr	36.27	34.21	178.2	121.5	46.16	49.74	5.55	51.76
Ni	20.09	8.33	90.32	10.73	30.94	33.69	3.87	20.83
Cu	23.74	25.46	56.28	7.24	3.97	5.26	15.18	41.95
Rb	15.1	14.6	33.576					
Sr	659.4	667.9	537.4	95.61	37.02	38.02	101.6	236.8
Y	33.6	28.9	30.971	69.6	30.5	29.65	32.87	38.82
Zr	217.7	196.2	199.4	225.8	426	456.9	274.7	268.3
Nb	39.70	35.00		27.65	15.89	16.50	15.40	9.39
Ba	298.4	275.2	382.6	2950	1377	1441	862.8	511.6
La	21.6	20.581	30.479	74.98	34.1	33.08	23.53	19.34
Ce	45.9	43.951	55.466	151.7	78.2	78.13	48.94	49.06
Nd	25.4	24.517	25.606	81.5	30.5	28.68	22.81	24.17
Sm	6.6	5.441	5.267	15.1	5.86	5.92	5.2	6.14
Eu	2.22	2.139	1.711	3.08	1.12	1.15	0.91	1.31
Gd	6.21	5.597	5.325	13.3	4.92	5.01	4.61	6.23
Dy	5.54	4.876	4.823	12.14	5.18	5.01	4.81	6.1
Er	2.96	2.753	2.846	6.56	3.72	3.69	3.78	4.04
Yb	2.66	2.416	2.628	6.22	3.04	2.86	3.21	3.27
Cs	0.14	0.187	0.303	9.696	5.612	6.441	1.561	1.568
Pb	2.85	2.20	2.22	16.89	5.76	5.47	9.46	15.54
Th	2.07	1.92	4.25	20.31	6.78	6.69	10.73	7.50
U	0.727	0.701	0.997	4.003	1.773	2.288	3.548	1.242
$^{87}Sr/^{86}Sr$	0.70294	0.70295		0.73908	0.74277	0.7433	0.70596	0.7066
$^{143}Nd/^{144}Nd$	0.51304	0.51302		0.51213	0.5121	0.51209	0.51274	0.51263
$^{206}Pb/^{204}Pb$				19.128	19.3244	19.2947	18.691	18.7874
$^{207}Pb/^{204}Pb$				15.691	15.6366	15.6821	15.553	15.6052
$^{208}Pb/^{204}Pb$				39.648	39.6937	39.6439	38.518	38.5962

Table 2-2 cont.

	G3	SOII1	SOII2	SOII3	SOII4	SOP1	SOP2	SOP3
SiO_2	74.94	77.32	51.74	62.955	53.45	72.055	72.25	72.515
TiO_2	0.2	0.097	0.931	0.556	0.818	0.167	0.173	0.181
Al_2O_3	12.46	11.39	19.615	16.56	18.995	12.395	12.545	12.865
FeO	1.37	0.923	8.828	4.693	7.278	1.041	1.077	1.142
MnO	0.04	0.018	0.156	0.126	0.134	0.047	0.048	0.048
MgO	0.16	0.162	4.873	2.237	4.081	0.268	0.29	0.288
CaO	0.58	0.638	9.84	5.342	8.115	1.26	1.279	1.311
Na_2O	3.89	3.372	3.317	4.035	3.434	3.376	3.369	3.412
K_2O	4.61	4.237	0.835	1.738	1.331	3.836	3.889	3.788
P_2O_5	0.03	0.029	0.246	0.166	0.208	0.037	0.044	0.045
Sc	3.59	2.409	23.245	9.172	19.14	2.334	2.124	2.086
V	6.07	3.171	210.85	93.415	193.2	10.264	13.251	9.342
Cr	3.65	7.43	12.6	13.335	14.51	9.192	5.159	11.805
Ni	6.82	8.928	18	12.96	12.785	31.45	14.595	29.965
Cu	3.13	4.208	32	21.9	13.55	4.118	3.477	3.998
Rb		162.436	19.75	95.057	35.513			
Sr	38.25	52.985	652.75	416.85	547.4	154.2	155.85	153.8
Y	18.13	23.051	21.459	15.781	18.064			
Zr	181.5	65.31	65.72	123.15	98.39	81.34	75.305	73.23
Nb	14.71	7.59	2.94	4.75	3.14			
Ba	494.9	376.1	334.6	543.5	442	905	913.85	913.3
La	22.06	31.605	10.49	14.857	10.184			
Ce	46.61	39.062	22.059	23.473	19.34			
Nd	17.25	29.569	18.101	16.441	15.073			
Sm	3.82	5.686	4.302	3.416	3.466			
Eu	0.33	0.588	1.119	0.851	0.938			
Gd	3	5.113	4.312	3.178	3.429			
Dy	2.79	3.956	3.862	2.666	3.032			
Er	2.15	2.057	2.189	1.464	1.775			
Yb	1.63	2.298	2.379	1.573	1.889			
Cs	2.911	4.523	0.74	1.765	1.105			
Pb	13.03	17.49	3.77	4.32	5.15			
Th	14.54	16.33	1.42	2.18	1.52			
U	2.136	3.289	0.495	0.685	0.6			
$^{87}Sr/^{86}Sr$	0.70769							
$^{143}Nd/^{144}Nd$	0.51276							
$^{206}Pb/^{204}Pb$	18.7679							
$^{207}Pb/^{204}Pb$	15.6172							
$^{208}Pb/^{204}Pb$	38.6174							

Table 2-2 cont.

	CHO1	CHO2	CHO3	BONIS
SiO_2	76.22	72.1	72.635	58.265
TiO_2	0.067	0.094	0.185	0.761
Al_2O_3	11.2	11.795	12.31	17.4
FeO	0.604	0.628	1.167	5.173
MnO	0.009	0.062	0.05	0.102
MgO	0.106	0.119	0.35	2.591
CaO	0.292	0.686	1.318	5.787
Na_2O	3.677	3.59	3.737	3.301
K_2O	3.855	4.138	2.835	2.955
P_2O_5	0.021	0.021	0.043	0.227
Sc	3.562	2.517	2.758	15.09
V	3.421	4.343	14.31	140.65
Cr	9.699	14.89	5.167	35.655
Ni	15.47	44.615	6.499	17.35
Cu	2.612	2.59	6.116	21.51
Rb	118.974			
Sr	6.316	75.555	188.8	481.55
Y	19.104			
Zr	41.265	36.51	82.955	164.05
Nb	16.70			
Ba	418.2	930.3	893.05	845.55
La	16.199			
Ce	33.66			
Nd	19.539			
Sm	4.421			
Eu	0.282			
Gd	3.922			
Dy	3.45			
Er	1.892			
Yb	1.952			
Cs	2.587			
Pb	14.64			
Th	10.01			
U	1.924			

Table 2-3. Geochemical composition of the sediments from DSDP Site 495. Europium is not listed because inaccurate results due to mass interferences with BaO in the ICP-MS.

Table 2-3

	s3-5-76	s6-4-33	s9-5-41	s12-5-62	s15-6-102	s18-7-60
Depth	25.800	52.300	82.400	111.100	141.500	171.100
Age	0.800	1.700	2.900	4.000	5.300	10.700
SiO_2	51.700	54.300	58.600	56.000	54.400	59.700
TiO_2	0.710	0.740	0.480	0.500	0.530	0.530
Al_2O_3	13.300	14.000	11.000	12.300	11.200	9.100
Fe_2O_3	7.240	7.200	5.490	5.460	5.670	6.440
MnO	0.100	0.080	0.180	0.170	0.200	0.100
MgO	2.290	2.290	2.110	2.340	2.260	1.880
CaO	4.440	1.980	2.800	2.480	3.260	1.250
Na_2O	2.100	2.300	2.010	2.120	1.970	2.000
K_2O	1.630	1.800	1.700	2.240	1.730	1.930
P_2O_5	0.139	0.117	0.105	0.107	0.162	0.105
Sc	20.919	19.292	0.000	16.291	17.398	11.469
V	133.211	169.752	0.000	170.708	113.416	148.018
Cr	45.812	50.307	0.000	41.317	38.052	48.740
Ni	74.158	147.834	0.000	374.882	306.088	119.626
Cu	115.322	155.423	0.000	240.629	250.089	552.980
Rb	36.246	36.535	34.500	52.264	39.053	46.111
Sr	304.591	287.969	315.000	351.459	399.341	358.574
Y	20.401	23.723	23.600	31.143	39.563	47.945
Zr	91.580	101.800	86.180	94.710	103.700	152.700
Nb	4.267	5.491	0.000	5.701	4.149	5.548
Ba	1588.720	3066.850	3182.000	4487.200	4395.130	6929.040
La	9.810	11.856	16.100	20.518	19.656	29.845
Ce	21.071	24.322	25.000	34.297	28.910	34.715
Nd	10.899	12.907	14.100	20.789	20.590	27.333
Sm	2.674	3.132	2.800	4.809	4.857	6.019
Gd	2.602	3.259	3.320	4.524	4.855	6.240
Dy	3.149	3.616	3.620	4.901	5.568	7.485
Er	2.058	2.376	0.000	2.952	3.577	4.997
Yb	1.922	2.227	2.320	2.657	3.101	4.451
Cs	2.563	2.419	1.425	2.790	2.057	1.794
Pb	5.863	8.606	9.687	11.236	9.755	12.380
Th	2.154	2.727	3.030	4.295	2.510	3.254
U	5.874	7.355	5.496	4.461	4.179	1.970
$^{87}Sr/^{86}Sr$			0.70763			
$^{143}Nd/^{144}Nd$			0.51274			
$^{206}Pb/^{204}Pb$			18.783			
$^{207}Pb/^{204}Pb$			15.631			
$^{208}Pb/^{204}Pb$			38.673			

Table 2-3 cont.

	s21-7-29	s24-7-19	s27-5-113	s30-2-40	s33-5-41	s36-4-49
Depth	199.300	227.700	254.100	277.400	310.400	337.500
Age	14.200	16.800	17.600	18.200	19.200	19.900
SiO_2	7.950	13.600	17.600	13.000	7.110	7.020
TiO_2	0.050	0.030	0.050	0.030	0.005	0.010
Al_2O_3	0.850	0.880	0.950	0.620	0.200	0.140
Fe_2O_3	1.840	3.140	2.900	2.500	0.820	0.600
MnO	0.450	0.610	0.470	0.300	0.180	0.170
MgO	0.570	0.980	0.910	0.830	0.370	0.330
CaO	52.400	41.300	39.700	45.500	51.400	53.000
Na_2O	0.330	0.430	0.400	0.370	0.130	0.120
K_2O	0.170	0.260	0.260	0.270	0.080	0.080
P_2O_5	0.136	0.153	0.122	0.141	0.084	0.088
Sc	2.924	3.672	4.155	3.265	1.940	2.040
V	45.328	74.504	51.430	40.521	47.873	40.977
Cr	12.084	11.488	15.775	19.356	12.946	11.668
Ni	31.547	39.940	33.947	34.696	16.176	13.191
Cu	85.331	139.372	140.714	78.930	41.871	41.268
Rb	4.140	6.402	5.844	4.509	2.099	1.372
Sr	1725.800	1289.730	1450.080	1367.010	1568.340	1530.800
Y	25.423	27.050	20.778	21.177	13.710	9.490
Zr		0.000	29.970	0.000	10.350	0.000
Nb	0.580	0.878	1.079	0.704	0.150	0.208
Ba	1954.780	2784.840	3072.520	2745.000	1715.980	1949.720
La	11.493	14.056	11.542	11.652	6.081	4.834
Ce	4.180	5.320	4.440	3.282	1.110	0.965
Nd	8.450	11.752	10.827	9.982	4.225	3.470
Sm	1.807	2.532	2.392	2.151	0.895	0.755
Gd	2.072	2.842	2.517	2.343	1.085	0.853
Dy	2.567	3.347	2.837	2.735	1.331	1.020
Er	1.835	2.225	1.818	1.869	0.955	0.734
Yb	1.587	1.837	1.499	1.589	0.810	0.630
Cs	0.154	0.257	0.231	0.145	0.055	0.047
Pb	3.255	5.845	6.134	4.468	1.549	1.452
Th	0.222	0.381	0.438	0.245	0.080	0.064
U	0.164	0.159	0.127	0.100	0.125	0.133
$^{87}Sr/^{86}Sr$			0.70862		0.70854	
$^{143}Nd/^{144}Nd$			0.51243		0.51240	
$^{206}Pb/^{204}Pb$			18.496		18.468	
$^{207}Pb/^{204}Pb$			15.578		15.534	
$^{208}Pb/^{204}Pb$			38.299		38.144	

Table 2-3 cont.

	s39-3-106	s41-6-53	s42-3-50	s43-5-24	s44-6-111	s45-41-25
Depth	365.100	388.000	393.000	405.200	417.100	424.400
Age	20.700	21.400	21.500	21.900	22.200	22.400
SiO_2	3.680	3.640	2.330	4.410	4.840	6.390
TiO_2	0.010	0.005	0.010	0.010	0.010	0.030
Al_2O_3	0.240	0.210	0.140	0.040	0.001	0.210
Fe_2O_3	1.700	1.560	1.000	2.290	2.010	3.250
MnO	0.190	0.240	0.230	0.230	0.130	0.370
MgO	0.530	1.020	0.400	0.720	0.870	1.060
CaO	54.000	56.100	48.100	52.000	52.900	48.100
Na_2O	0.170	0.130	0.130	0.170	0.190	0.310
K_2O	0.190	0.220	0.090	0.140	0.140	0.210
P_2O_5	0.122	0.159	0.107	0.107	0.114	0.140
Sc	2.972	2.164	1.839	2.061	1.956	0.000
V	48.421	55.769	44.276	44.781	50.268	0.000
Cr	18.068	22.023	12.836	15.861	18.629	0.000
Ni	23.596	29.303	20.232	29.255	28.087	0.000
Cu	51.158	53.910	72.874	76.367	55.415	0.000
Rb	4.800	7.544	3.534	3.320	3.489	0.000
Sr	1650.210	1454.850	1585.210	1595.150	1328.160	0.000
Y	18.989	15.466	12.413	15.592	14.447	0.100
Zr	0.000	0.000	0.000	0.000	0.000	0.000
Nb	0.242	0.229	0.281	0.318	0.174	0.000
Ba	2347.700	1645.640	1734.820	2436.970	1212.260	0.000
La	9.166	7.169	6.331	7.624	6.636	0.000
Ce	1.786	1.426	1.254	1.636	1.033	0.000
Nd	6.699	4.655	4.035	5.980	4.576	0.000
Sm	1.388	0.951	0.838	1.284	0.921	0.000
Gd	1.658	1.191	1.008	1.448	1.157	0.000
Dy	2.045	1.520	1.257	1.769	1.438	0.000
Er	1.468	1.166	0.956	1.295	1.059	0.000
Yb	1.252	0.997	0.789	1.105	0.873	0.000
Cs	0.072	0.178	0.113	0.102	0.150	0.317
Pb	7.568	1.126	2.009	2.200	0.451	8.320
Th	0.009	0.090	0.083	0.094	0.060	0.190
U	0.079	0.196	0.166	0.078	0.133	0.363
$^{87}Sr/^{86}Sr$						
$^{143}Nd/^{144}Nd$						
$^{206}Pb/^{204}Pb$						18.237
$^{207}Pb/^{204}Pb$						15.443
$^{208}Pb/^{204}Pb$						37.820

Table 2-3 cont.

	46-1-85		Mean Hem.	Mean Carb.	Mean Sed.
Depth	428.400		97.367	340.585	220.000
Age	22.500		4.233	19.885	0.000
SiO_2	4.470		55.783	7.388	31.586
TiO_2	0.070		0.582	0.025	0.303
Al_2O_3	0.280		11.817	0.366	6.091
Fe_2O_3	2.000		6.250	1.970	4.110
MnO	0.220		0.138	0.292	0.215
MgO	0.870		2.195	0.728	1.461
CaO	54.200		2.702	49.900	26.301
Na_2O	0.270		2.083	0.242	1.163
K_2O	0.190		1.838	0.177	1.008
P_2O_5	0.160		0.123	0.126	0.124
Sc	0.000		17.074	2.635	9.854
V	0.000		147.021	49.468	98.244
Cr	0.000		44.845	15.521	30.183
Ni	0.000		204.517	27.270	115.894
Cu	0.000		262.888	76.110	169.499
Rb	0.000		40.785	4.278	22.531
Sr	0.000		336.156	1504.120	920.138
Y	0.000		31.063	17.694	24.378
Zr	0.000		105.112	20.000	60.000
Nb	0.000		5.031	0.440	2.736
Ba	0.000		3941.490	2145.480	3043.480
La	0.000		17.964	8.780	13.372
Ce	0.000		28.053	2.403	15.228
Nd	0.000		17.770	6.786	12.278
Sm	0.000		4.049	1.447	2.748
Gd	0.000		4.133	1.652	2.893
Dy	0.000		4.723	1.988	3.355
Er	0.000		3.192	1.398	2.295
Yb	0.000		2.780	1.179	1.979
Cs	0.000		2.175	0.152	1.163
Pb	0.000		9.588	3.698	6.643
Th	0.000		2.995	0.163	1.579
U	0.000		4.889	0.152	2.521
$^{87}Sr/^{86}Sr$			0.70800	0.70858	0.7083
$^{143}Nd/^{144}Nd$			0.51300	0.51242	0.5127
$^{206}Pb/^{204}Pb$	18.053		18.783	18.314	18.548
$^{207}Pb/^{204}Pb$	15.298		15.631	15.463	15.547
$^{208}Pb/^{204}Pb$	37.497		38.673	37.940	38.306

Table 2-4

ICP-MS Operational Parameters	
Extraction	0.2
Collector	8.65
L1	7.54
L2	2
L3	6.27
L4	0.75
Pole Bias	4.8
Resolution	5.6
D Mass	3
HT 1	4.92
HT 2	1.82
Pump (rpm)	26
Nebulizer gas flow	0.828 L min-1
Auxiliary gas flow	1 L min-1
Coolant gas flow	12 L min-1
ICP	
Power	1350 W
Reflect	<5 W
Cones	
Sampler	VG Nikel, 1 mm
Skimmer	VG Nikel, 0.7 mm
Nebulizer	Meinhard Tr-30-C3

Table 2-4. Operational parameters for the ICP-MS.

Table 2-5

Isotopes Analyzed	
Rb	85
Y	89
Nb	93
Cs	133
La	139
Ce	140
Nd	143
Nd	146
Sm	147
Sm	149
Eu	151
Eu	153
Gd	157
Dy	162
Dy	163
Er	166
Er	168
Yb	172
Yb	174
Pb	206
Pb	207
Pb	208
Th	232
U	238

Table 2-5. List of the isotopes analyzed in the ICP-MS to determine the composition of the samples

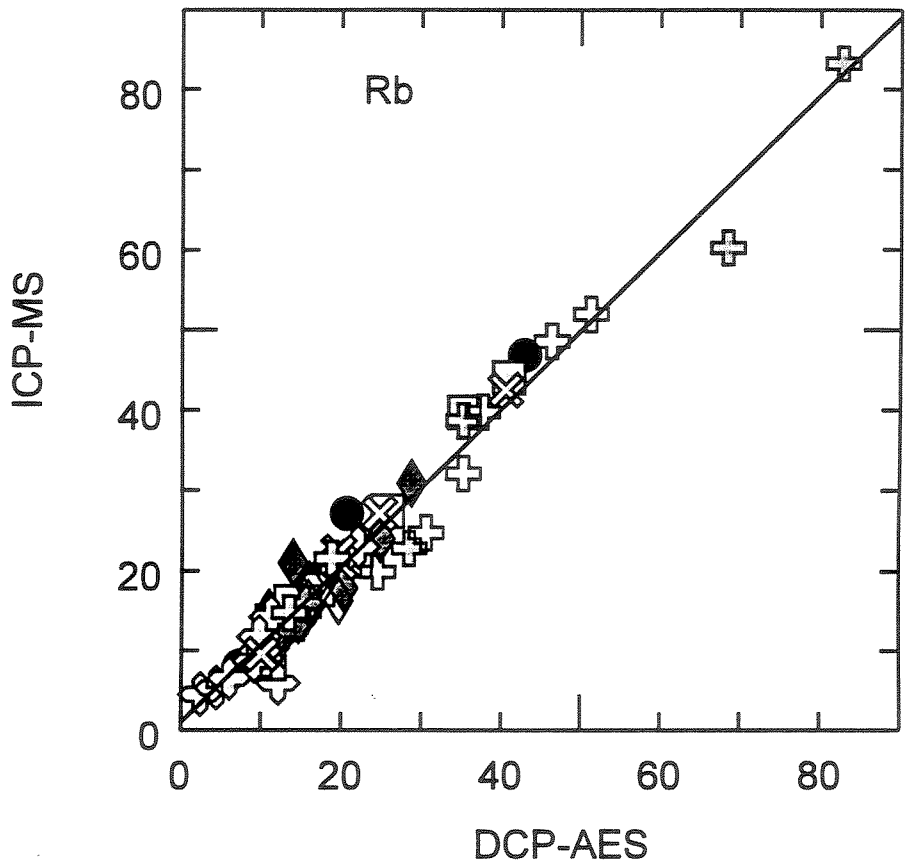


Figure 2-1. Comparison of the concentrations of Rb, Y, and Nb in the DCP-AES and the ICP-MS. For Rb, the correlation coefficient between the two data sets is 0.982. Most of the ICP-MS concentrations are higher than the DCP-AES. However, not all the samples show this pattern.

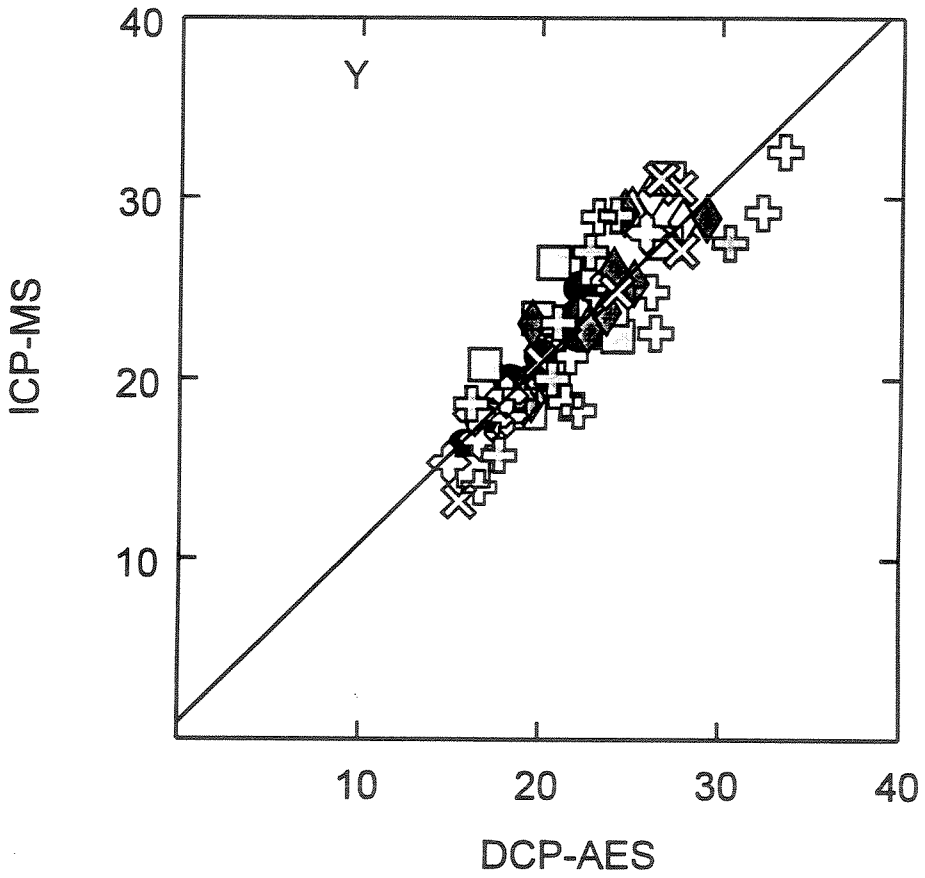


Figure 2-1 cont. Comparison of Y concentrations in the DCP-AES vs. ICP-MS. The regression coefficient for these two data sets is 0.879. Most of the ICP-MS concentrations are higher than those obtained in the DCP-AES.

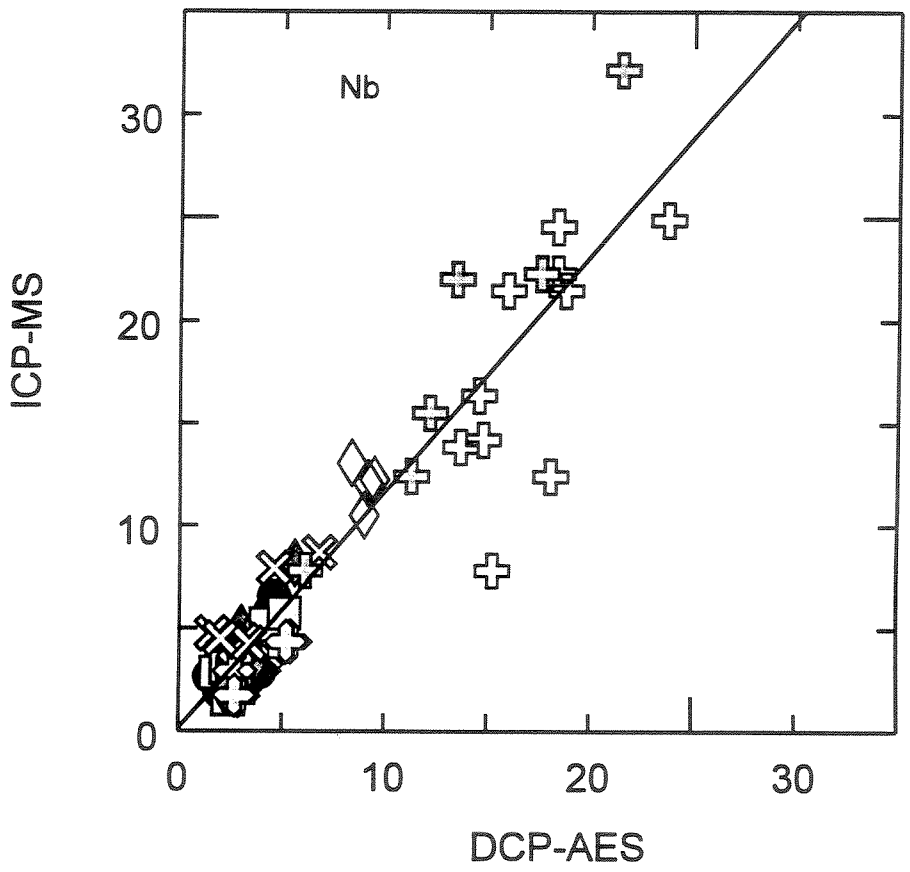


Figure 2-1 cont. Comparison of Nb concentrations in the DCP-AES vs. ICP-MS. Despite the large scatter for the samples with high Nb content, the correlation coefficient for the two data sets is high, 0.94.

III. INPUT: SIGNATURE OF THE SLAB AND MANTLE WEDGE

A. Introduction

In order to understand the geochemical characteristics of a subduction zone system, it is indispensable to know the composition of the subducting oceanic crust. It is also important to have some constraints on the composition of the mantle from which the magmas originate. In this chapter, the geochemical characteristics of the subducting Cocos Plate will be explored, as well as the composition of the mantle underneath the Central American volcanic arc.

The subducting oceanic Cocos Plate has three stratigraphic units, an upper sequence of hemipelagic muds, a middle sequence of carbonate oozes, and finally the basaltic oceanic crust. The chemical characteristics of these units will be described in the first part of the chapter, including the geochemical tracers that can be used to identify the slab flux in the erupted lavas. The last section in the chapter discusses the inferred composition of the mantle wedge.

B. Geochemical Stratigraphy of the Cocos Plate

1. Sediments from DSDP 495

Marine sediments are active recorders not only of their own history, but also of the history of the oceanic plate on which they are deposited. Stratigraphic sections from marine cores allow the study of temporal changes in the environmental conditions under which the sediments were deposited. These environmental changes may then be related to global climate, changes in the water circulation patterns, and/or changes in the tectonic characteristics of the oceanic plate on which the sediments are deposited.

Deep Sea Drilling Project (DSDP) leg 67 sampled several sites in the Guatemalan Basin, proximal to the Central American continental margin and the Middle America Trench (Fig. 3-1). Sediments from the different sites indicate the presence of continental turbidite deposits on the Caribbean Plate and of pelagic sediments on the Cocos Plate. Site 495 is located on a horst 22 km seaward from the Middle America Trench, on the

Cocos Plate, at a water depth of 4140 m (Coulbourn et al., 1982). The recovered material from Site 495 includes a sedimentary column ~428 meters thick overlying the basaltic oceanic crust (Coulbourn et al., 1982). Von Huene et al. (1982) describe the upper part of the sedimentary column (177m) as Quaternary to upper Miocene hemipelagic diatomaceous mud and middle Miocene brown abyssal clay (Fig. 3-2). The lower half of the sedimentary column consists of middle-lower Miocene chalky carbonate ooze and manganiferous chalk and chert (von Huene et al., 1982; Fig. 3-2). This stratigraphic distribution is a classic sequence that records the passage of DSDP Site 495 from the East Pacific Rise to depths greater than the carbonate compensation depth (CCD), to a place close to a terrigenous source (von Huene et al., 1982). In addition, Coulbourn et al. (1982) describe three sedimentation rates that are associated with the different types of sediments. The carbonate-rich units have a sedimentation rate of 50 m/my. The Cocos Plate then moved northward away from the high productivity area near the equator. This period is represented by the deposition of brown abyssal clay, reflecting a drastically lower sedimentation rate (9 m/my). The uppermost sediments were deposited closer to the Central American land mass, and the contributions from volcanic material helped increase the sedimentation rate to 41 m/my. The significant differences in the biogenic and mineral content of sediments from DSDP Site 495, hemipelagic diatomaceous mud vs. chalky carbonate ooze, produce different geochemical units down the core. The following sections will describe the differences in the geochemical characteristics of sediments from DSDP Site 495.

a. Carbonate Crash

The transition from a carbonate-rich sedimentary sequence to a section depleted in calcareous material in DSDP 495 core has been attributed to the thermal subsidence of the Cocos Plate as it moved away from the East Pacific Rise and/or to the shallowing of the CCD in the Pacific (von Huene et al., 1982 and Lyle et al., 1995, respectively).

Berger (1970) classifies marine basins into two major groups: a saline lagoon and an estuarine model. In the saline lagoon model, deep water replaces upper water, evaporation exceeds precipitation, and biogenous sedimentation is dominated by calcareous oozes (e.g. Atlantic Ocean). In the estuarine model, upper fresh water is exchanged for deep saltier water, the sediments are poor in carbonates and proportionally enriched in siliceous oozes (e.g. Pacific Ocean). The carbonate supply to both types of ocean basins may be similar, but the Atlantic type basin has higher carbonate sedimentation rates because dissolution is greater in the Pacific type basin due to a shallower lisocline. Farrell et al. (1995) indicate that in the Guatemalan Basin, the $CaCO_3$ concentrations were greater than 70% around 11.2 Ma, implying that in the early to middle Miocene Atlantic type basin conditions prevailed in the area of deposition. However, the percentage of $CaCO_3$ and its flux declined to near zero around 9.5 Ma; the conditions of deposition in the Guatemalan Basin changed to those similar to the Pacific type basin, where the carbonate sediments are poorly preserved.

Lyle et al. (1995) indicate that the CCD in the Guatemalan Basin shallows by 800 meters at 10 Ma. This time coincides with the transition from carbonate-rich sediment with low dissolution to carbonate depleted sediments affected by strong dissolution. Lyle et al. (1995) argue that this change occurred because of the beginning of the closure of the isthmus of Panama, modifying the deep water circulation in the basin and restricting the flow of deep water rich in carbonate from the Atlantic. However, there is evidence that a "carbonate crash" also occurred in other basins far from the east Pacific, as for example in the Indian Ocean and in other regions of the Pacific ocean (Peterson et al., 1992; Farrell et al., 1995), implying that the cause of the carbonate crash was not localized as argued by Lyle et al. (1995). Only events at a global scale could cause similar effects in areas so distant from each other. Examples of such global phenomena may be: the rearrangement of deep water circulation caused by the formation of the North Atlantic Deep Water in the middle Miocene (Wright et al. 1992) and the closure of sea gateways (Kennett, 1987). In

the eastern Pacific, synchronous events (thermal subsidence, the slow closure of the isthmus of Panama, and the rearrangement of deep water circulation) probably contributed to the carbonate crash and raised the CCD to its present level, about 3600 meter below sea level.

b. Results

The stratigraphic geochemical variations of the sediments from DSDP Site 495 are a clear reflection of the different nature of the two major units present, hemipelagic vs. carbonate sediments. Major elements in marine sediments are mostly affected by the input of terrigenous material, with the exception of elements like silica and calcium that are greatly influenced by the biogenic content of the sediments. The carbonate sediments from the deeper part of the core have more than four times the content of CaO than the hemipelagic sediments (Fig. 3-3a). The upper hemipelagic sediments have higher concentrations of SiO_2 than the older carbonate sediments, reflecting the dominance of siliceous fossils and detrital material in these sediments (Fig. 3-3b). The SiO_2 content of the hemipelagic sediments varies with age, the silica content increases with increasing age. The hemipelagic sediments are also enriched in the elements normally associated with a detrital component, e.g. Al, Ti, Fe, compared to the carbonate oozes (Fig. 3-3c). The stratigraphic distribution of elements associated with detrital input in the hemipelagic sediments is opposite to that of SiO_2, i.e. the younger sediments have higher concentrations of Al, Ti, and Fe.

Aluminum concentrations are markedly distinct between the two sediment types. The Al_2O_3 content of the hemipelagic sediments is ≥ 9 wt. %, whereas that of the carbonate sediments is ≤ 1 wt. %. The aluminum content of the sediments decreases with increasing age, in both the carbonate and the hemipelagic sections, with a large jump down the core corresponding to the transition between hemipelagic and carbonate sediments (Fig. 3-3c). The low content of aluminum oxide in the carbonates (<1 wt. %) correlates with the mineralogy, which indicates the near absence of detrital clays in these oozes (von

Huene et al., 1982). This relationship is the opposite to that in the upper sediments of DSDP Site 495. The mineral content of the hemipelagic section indicate abundant layers of volcanic glass and detrital clays, such as kaolinite and illite. The presence of nonbiogenic components increases the aluminum content of the hemipelagic sediments significantly compared to the deeper biogenic sediments. The stratigraphic distribution of the elements associated with the detrital component, decreasing content with increasing depth, suggest that the older sediments have lower contents of terrigenous material. However, the composition of the detrital material does not seem to change with time; the hemipelagic sediments have a constant ratio of MgO/Al_2O_3 of ~0.2 (Fig. 3-3d).

In general, the hemipelagic sediments have higher or similar concentrations of trace elements compared to the carbonates, with Sr being the only exception. As expected, the strontium concentration is higher in the carbonate sediments, as much as one order of magnitude (Fig. 3-4a). Some trace elements in the hemipelagic sediments correlate with SiO_2, i.e. increasing with depth. The stratigraphic distribution of these elements in the hemipelagic sediments, e.g. Ba (Fig. 3-4b), indicates that a significant percentage of these trace elements is of biogenic or hydrogenic origin. The highest concentrations of these elements are found in the abyssal brown clay (sedimentation rate 9 m/my); with the uppermost hemipelagic sediments having concentrations similar to the deeper carbonate sediments. Only Sc and U show an inverse correlation with SiO_2, and a positive correlation with the indicator of input of terrestrial material, Al_2O_3 (Fig. 3-4c). A third group of trace elements (e.g. Rb, Cs, Th) shows great differences in concentration between the carbonates and hemipelagic sediments, with the hemipelagic sediments having significantly greater abundances (Fig. 3-4d). This implies that the detrital component increases the content of this group of elements.

The two distinctive sedimentary units from DSDP Site 495 display very different rare earth element patterns (Fig. 3-5). All the sediments are enriched in the light rare earth elements, with the hemipelagic sediments having higher concentrations. The calcareous

and siliceous tests take the elemental composition of the seawater in which they form; therefore, the fossils have similar REE patterns to that of seawater (Toyoda et al., 1990). The REE pattern of the carbonate sediments shows the well known pronounced negative cerium anomaly of sea water; whereas the hemipelagic sediments have a much smaller Ce depletion. The magnitude of the small Ce anomaly in the hemipelagic sediments is not uniform, as the anomaly is greater in the deeper hemipelagic sediments. The stratigraphic distribution of the Ce anomaly is parallel to the distribution of Al_2O_3, implying that the input of terrigenous material dilutes the inherited hydrogenous Ce anomaly (Fig. 3-6a).

The geochemical characteristics of the two major groups of sediments from DSDP Site 495 (hemipelagic vs. carbonate oozes) are drastically different; the geochemical composition is mainly controlled by the presence or absence of two end members: a carbonate-rich biogenic component and detrital material. These two end members are not coeval. The carbonate-rich component clearly dominates the geochemistry of the lower part of the sedimentary column, whereas the detrital input occurs in the upper sediments, diluting to great extent the signal from the siliceous biogenic end member of this section. The transition from carbonate-rich to carbonate poor sediments and from detrital poor to detrital-rich sediments is contemporaneous, producing the contrasting geochemistry. However, the events may not have a cause/effect relationship. More likely the processes that affect the geochemistry of the sediments are related to plate tectonics and/or changes in ocean circulation.

c. Biogenic component

The biogenic component tends to dilute most elements that are enriched by the detrital material (e.g. Th, Rb, Cs, REE; Plank and Ludden, 1992; Figs. 3-4 and 3-7). However, the concentration of other elements is increased by the input of biogenic/hydrogenic material. Barium-rich sediments have been found below high biological productivity zones (Puchelt, 1972; Plank and Ludden, 1992). Sediments from the continental margin off the coast of the Sea of Japan and from upwelling areas off Peru

have high abundances of siliceous fossils and also have high Ba contents (10,000 ppm Ba; Masazawa et al., 1992; von Breymann et al., 1990). Bishop (1988) explained the association between Ba enrichment and productivity zones by suggesting that barium is incorporated into the skeleton of marine plankton. By normalizing the barium content of sediments to the Ba content of a detrital component, it is possible to determine the contribution to the Ba budget from biogenic/hydrogenic origin relative to the percentage originating from detrital input (von Breymann et al., 1992). The stratigraphic distribution of excess barium (Ba not from terrigenous material) down the Site 495 core shows how biogenic material dominates the composition of the deeper sediments (Fig. 3-6b). There is very little change in the barium excess in the carbonate-rich section of the sedimentary column. During the 8 million year duration of the carbonate-rich sedimentation, almost all of the barium is of biogenic origin (i.e. 100% Ba excess). Most likely these sediments were deposited near the equator beneath a high productivity area. The excess barium decreases upward in the core. The younger hemipelagic sediments have a greater percentage of their Ba derived from detrital material. The youngest sediments in the uppermost part of the core have about 25% Ba of detrital origin and 75% of biogenic origin. Even though the uppermost sediments were deposited near a continental margin with high biogenic productivity, as seen by the high content of organic matter in these sediments (see below), the barium content is not maximum here because the detrital material dilutes the biogenic barium. Similar observations have been made in other areas, such as the Peru upwelling area (von Breymann et al. 1990).

The chemical composition of calcareous and siliceous tests are greatly influenced by the chemical characteristics of the sea water where they grow, e.g. the pattern of the rare earth elements. As discussed earlier, the sediments from DSDP 495 can be separated into two major groups according to their REE patterns: those with large negative Ce anomalies and those with significantly smaller Ce anomalies. This separation coincides with the already mentioned compositional differences of the sediments. The carbonate

sediments display the larger Ce anomaly, whereas the hemipelagic sediments have a much smaller negative anomaly (Figs. 3-5 and 3-6a). The relationship between Ba excess (used as an indicator of biogenic component) and the negative Ce anomaly of the carbonate sediments indicates that these sediments are mostly derived from biogenic material, with very little material, if any, derived from other sources (Fig. 3-6a and 3-6b).

d. Detrital component

Coulbourn et al. (1982) indicated that the sedimentary column of Site 495 is a record of the trajectory of the Cocos Plate from its origins at the East Pacific Rise to its subduction along the Middle American Trench. The oldest sediments (22 m.y.) were deposited far away from sources of detrital material (<1 wt. % Al_2O_3; Fig. 3-3c), where biogenic and hydrogenic components were the most important sources for the sediments. As the Cocos Plate moved away from the ridge and closer to the trench, the biogenic and hydrogenic components were mixed with detrital material. In the sediments from DSDP 495, the enrichment of the detrital component is clearly seen in the stratigraphic distribution of Al_2O_3, which increases content with decreasing age, with the greatest percentage of terrigenous material in the upper part of the stratigraphic column (9.1 to 14 wt. % Al_2O_3; Fig . 3-3c).

If detrital aluminosilicates were the only source of the detrital component, then we would expect to see positive correlations between Al_2O_3 and the trace elements like Sc, REE, Th, Pb, Rb, and Cs. However, this is not the case, as only Sc displays a positive correlation with alumina. Therefore, there must be another detrital source for the other elements. The small variation in the MgO/Al_2O_3 ratio of the hemipelagic sediments indicates that the composition of this material did not change significantly with time (Fig. 3-3d). In addition, the smooth stratigraphic variations of the trace elements can be explained by changing the amount of detrital input, without invoking significant changes in the composition of the detrital material. McLennan et al. (1990) used a triangular plot of La-Th-Sc to infer the source of detrital material in turbidites . Figure 3-8 shows that in

the La-Th-Sc space the hemipelagic sediments from DSDP Site 495 are distributed along the continental arc related field of McLennan et al. (1990), with the content of Sc increasing and that of La decreasing as the sediments become younger and are deposited closer to the Central American volcanic arc. Volcanism in Central America started in the Oligocene-early Miocene, and volcanoes in the region have remained active since then (Donnelly et al. 1990). Therefore, the most likely source for the detrital component in the hemipelagic sediments from DSDP Site 495 is material derived from the Central American volcanic arc. Despite the fact that Site 495 was at a considerable distance from the Central American arc at the time of hemipelagic sediment deposition, fine-grained tephra from the Central American volcanoes could have reached the site. Moreover, ubiquitous volcanic glass layers were identified by the ship board scientists during the leg 67 cruise (Coulbourn et al., 1982). In the hemipelagic section, some layers have up to 85% volcanic glass, while the highest amount of clay minerals is 75% and that of biogenic siliceous material is 55%.

One of the most distinctive fingerprints of the detrital material in the sediments from site DSDP 495 is the dilution of the negative cerium anomaly (Fig. 3-6a). Present day deep-sea water always shows a negative Ce anomaly (Elderfield, 1988), causing marine biogenic or hydrogenic material to be relatively depleted in cerium (Lin, 1992; Toyoda et al., 1990; Othman et al., 1989; Hole et al., 1984). The deeper sediments from DSDP 495 that are mostly of biogenic origin display a pronounced negative Ce anomaly (Fig. 3-6a). The reduced Ce anomaly in the uppermost hemipelagic sediments could be caused by the absence of carbonate sediments in the upper 177 meters of the core. However, Karl et al. (1992) studied biogenic siliceous sediments from the Pacific and found that when the detrital component is low, the siliceous biogenic material displays cerium anomalies similar to that displayed by the biogenic carbonate-rich material from DSDP Site 495. Therefore, the negative Ce anomaly of the biogenic/hydrogenic components of the hemipelagic sediments is diluted by the input of detrital material that

lack a cerium anomaly. The detrital component from the upper part of the hemipelagic sediments is dominated by feldspars, volcanic glass, detrital clay minerals, and quartz (Coulbourn et al., 1982 and Shipboard Scientific Party, 1982); these components do not have significant negative Ce anomalies. Non biogenic/hydrogenic material, like volcanic glass layers, becomes very abundant in the Pleistocene, contributing to the increase of the sedimentation rate from 9 m/my to 41 m/my (Coulbourn et al., 1982).

Rare earth elements (REEs) in marine sediments are commonly associated with the input of detrital material or with adsorption from sea water (Othman et al., 1989; Toyoda et al., 1990; Murray et al., 1992; Plank and Ludden, 1992; Minai et al., 1992). In the hemipelagic sediments from DSDP 495, REEs concentrations vary inversely with the inferred amount of detrital material (Fig 3-9); i.e. the highest concentrations of La are observed in the samples with the lowest detrital input ($Ce/Ce^* >> 1$). The sediments with the highest concentration of REEs were deposited at a rate of 9 m/my, allowing the abyssal clays to incorporate significant amounts of rare earth elements from the sea water. Furthermore, volcanic detrital material is not significantly enriched in REEs (as it is demonstrated by the Aleutian turbidite in Fig. 3-9) and can dilute any possible enrichment produced by the pelagic component of these hemipelagic sediments.

e. Organic Matter

Uranium behaves differently than other trace elements in the hemipelagic sediments. The down core distribution of U is such that the highest concentration is observed in the uppermost sediments, and concentration then decreases with depth (Fig. 3-4c and 3-7), similar to the stratigraphic distribution of Al_2O_3 . This distribution is opposite to the distribution of elements like Th or Ba (Fig. 3-4b and 3-4d). The reverse trend seems to indicate that the detrital material is rich in uranium. However, volcanic detrital material is not significantly enriched in uranium relative to other trace elements like thorium (McLennan et al., 1990).

Masuzawa et al (1992) and Klinkhammer and Palmer (1991) showed a close association in the amount of total organic carbon and the concentration of uranium in sediments from the northern Sea of Japan and from the shelf and slope off central California, respectively. Harrison et al. (1982) reported that the upper 100 meters of DSDP Site 495 are enriched in organic carbon (up to 2.4%) and that the concentration of organic carbon in the carbonate-rich sediments from Site 495 is significantly lower than that in the hemipelagic sediments. The authors explained this decrease with depth as a consequence of the change in sedimentation rate from 9 m/my in the lower Miocene to 41 m/my in the Quaternary. Therefore, the enrichment of uranium in the younger hemipelagic sediments from DSDP Site 495 is better explained by the increasing content of organic material in the younger, more rapidly buried sediments.

2. Altered oceanic crust (Site 504)

Several authors have argued for the involvement of altered basaltic oceanic crust (AOC) in the generation of arc lavas (e.g. Shibata and Nakamura, 1997; Plank and Langmuir, 1993; and Carr et al., 1990). One of the most ubiquitous indicators of AOC is the strontium isotope signature of arc lavas. Strontium isotopes in the basaltic oceanic crust depend on the degree of alteration (Staudigel et al., 1995), caused by the interaction with sea water. In a study of basalts from DSDP 417, 417A and 418, Staudigel et al. (1995) found that the ratio of $^{87}Sr/^{86}Sr$ decreases with depth towards values closer to non-altered MORB. The authors indicated that the high values of $^{87}Sr/^{86}Sr$ in the upper part of the basaltic sequence are the result of continuous interaction of the rocks with sea water.

Because no basaltic material from DSDP 495 has been analyzed, it is necessary to use geochemical data from the literature. Site 504 was selected because it is one of the deepest holes drilled, 2111 mbsf (meters below sea floor), giving a comprehensive picture of the geochemical composition of the basaltic oceanic crust (table 3-1). Site 504 is located in the eastern Pacific south of the Costa Rica Rift (Fig. 3-11), and the age of the

uppermost igneous rock is 6 m.y. A relatively fast sedimentation rate, 50 m/my, has sealed the igneous rocks from extensive direct contact with sea water (Alt et al., 1996). Because DSDP 495 has a similar sedimentation rate, there is a strong possibility that sites 495 and 504 were altered under similar conditions. Most of the information below has been taken from the comprehensive summary by Alt et al. (1996) on Site 504. Figure 3-12, from Batch et al. (1996), gives leg information, as well as lithology and alteration characteristics of Site 504.

The extensive sampling of the basaltic oceanic crust in Site 504 shows two different types of alteration that are depth dependent. The variation in the style of alteration correlates with physical changes down the core. In Site 504, the inferred alteration temperature increases with depth from 60°C in the upper volcanic rocks to 160°C in the sheeted dikes (Mitchell and Terrell, 1985), whereas the porosity decreases with depth (Alt et al., 1996). In addition, the nature of the fluids that altered the rocks changes down the core. The lower sheeted dike section did not interact significantly with sea water, whereas the upper part of the core had sea water freely circulating throughout (Alt et al., 1996). The poor penetration of sea water to the lower part of Site 504 is related to the lower porosity of the rocks. Therefore, changes with depth in temperature and porosity are important factors affecting the nature of alteration of basaltic oceanic crust.

Alt et al. (1996) summarize the stratigraphy from DSDP 504 as follows: 274.5 m of sediments (siliceous oozes, chert, limestone, and chalk), and 1831 meters of basaltic oceanic crust. The basaltic oceanic crust is divided into three major sections: an upper volcanic section (571.5 meters thick), mainly of pillow and sheet lavas, and breccias, with low extents of alteration, 5-15%. A transition zone (209 m) with pillow basalts and dikes. The background alteration in this part is a little greater that in the upper volcanics, 20-30%, but at the local scale the recrystallization can be more extensive (50-75%). The lower sequence consist of sheeted dikes, with a wide range of recrystallization, some parts

Figure 3-13 shows the significant difference in the concentration of K and B between the volcanic rocks and the other sections of Site 504; the upper crust that interacts more with sea water has the highest and more variable contents of boron and alkali elements. With increasing depth the interaction of the rocks with sea water decreases significantly, creating a suboxic to anoxic alteration. Staudigel et al. (1995) indicate that the concentration of uranium in altered oceanic basalts depends on the type of alteration. Oxidizing alteration does not increase the concentration of uranium as much as reducing alteration; reducing alteration can take the concentration of U from 0.4 ppm to 0.9 ppm. Unfortunately, there are no data that record the uranium variations in the upper 1350 m of Site 504 where the alteration style changed from oxidizing to reducing.

b. Transition Zone (846 - 1055 mbsf) and Upper Dikes (1055 - 1500 mbsf)

The porosity and permeability of the rocks from the transition zone decrease greatly relative to the volcanic zone (Alt et al., 1996). The transition zone (209 ms) is characterized by very fractured, hydrothermally altered and brecciated pillows and dikes. The upper part of the transition zone displays alteration similar to that of the volcanic section, and the transition to the hydrothermally altered rocks is abrupt at 898 mbsf (Alt et al., 1996). The fluids that interact with the rocks from the transition zone are less oxidizing than those interacting with rocks in the upper part of the core; pyrite substitution of silicates is frequently observed (Alt et al., 1996). The transition zone is heavily mineralized by the rising hydrothermal fluids, with the lower part, the upper sheeted dikes, being the most extensively hydrothermally altered.

Overall, the temperature of alteration increases downward as well as the intensity of fluid-rock interaction. The alteration of the transition zone and the upper part of the sheeted dikes is divided into four parts by Alt et al. (1996). The first stage formed during axial hydrothermal alteration by sea water hydrothermal fluids (temperatures between 200° to 300°C). The second stage of alteration occurred at higher temperatures, 250° to 380°C, by highly reacted, evolved hydrothermal fluids. Extensive mineralization of this

zone was the product of the interaction of upwelling hydrothermal fluids with cooler seawater circulating through the more permeable volcanic rocks. As the oceanic crust moved off-axis, fracturing and faulting allowed penetration of seawater into the warm rock. The last stage of alteration took place along fractures further away from the spreading center and it was caused by more evolved hydrothermal fluids. The temperatures of alteration for the last stage are assumed to be slightly lower, <250°C.

The chemical effects of hydrothermal alteration in the transition zone and upper dikes make the rocks drastically different from those in the upper and lower sections of Site 504. The chemical characteristics of these rocks are a direct manifestation of the high temperatures and fluid composition that interacted with the rock. Copper, Zn, Mn and S are markedly enriched in the transition zone (910 mbsf), due to the formation of sulfide minerals (Fig. 3-13; Alt et al., 1996). In contrast to the volcanic rocks, alkali elements, like K and Rb, decrease with depth because of the leaching of these elements from the rocks at higher temperatures.

c. Lower Dikes (1500 - 2111 mbsf)

The rocks from the lower dikes display some hydrothermal alteration (Alt et al., 1996). The extent of alteration is mostly controlled by fracturing that permits the circulation of very evolved hydrothermal fluids and seawater recharge. The lower dikes went through alteration at the highest temperature, ≥400°C, and it preceded the alteration of the upper sheeted dikes. The two most important stages of alteration in the lower dikes are summarized by Alt et al. (1996). The initial stages of alteration occurred at temperatures higher than 400°C, with extensive interaction between the fluids and the rocks. The later stages of alteration occurred at lower temperatures, 250°C, by continued circulation of evolved off-axis hydrothermal fluids.

The geochemical effects of the hydrothermal alteration of the lower dikes are the loss of Cu, Zn and S (Alt et al., 1996). These elements are lost due to the breakdown of titanomagnetite and sulfides by the high temperature hydrothermal fluids. The lost of

these elements in the lower dike section is equaled by their enrichment of elements like Cu, Zn and S in the mineralized transition zone. Another consequence of the high temperatures of alteration is the loss of alkali elements, such as K (Fig. 3-13).

d. Alteration

The occurrence of two types of alteration in the basalts from Site 504 affects the stratigraphic distribution of elements of interest in subduction zone magmatism (Fig. 3-13). The alteration observed in the upper part of the basaltic oceanic crust is caused mostly by the interaction of the igneous rocks with sea water. This type of alteration is manifested by higher concentrations of alkali elements (e.g. K, B, Rb, Cs). Mitchell and Terrell (1985) indicate that the maximum concentration of K is at about 500 mbsf, more or less in the middle of the volcanic section. The deeper part of the core was altered by hydrothermal fluids that were created as sea water was heated up by the magma chamber. The high temperature fluids leach elements from the surrounding rock that are later deposited in the transition zone.

It is known that the basaltic oceanic crust plays an important role in the generation of arc related lavas, along with the sedimentary component of the oceanic crust. There is much information on the nature of sedimentary sequences subducting along trenches, but relatively little is known about the composition of the basaltic oceanic crust. Due to the little information available on the composition of the basaltic component, researchers commonly use ophiolites as analogs to the basaltic component of subducting slabs. However, Alt et al. (1996) indicate that such comparisons must be done carefully because ophiolites do not seem to have the same types of alteration as the basalts from Site 504. In general, both ophiolites and Site 504 show evidence of a steep temperature gradient with depth. However, the degree of recrystallization in Site 504 is not similar to that of ophiolite complexes (Alt et al., 1996). The volcanic sequences of ophiolites seem to be more recrystallized and altered at higher grades than the Site 504 volcanic section.

Moreover, the sheeted dikes of ophiolite sequences also display higher degrees of crystallization than those from Site 504.

Unfortunately, there is not a comprehensive geochemical data set for the upper volcanic section nor for the transition zone of Site 504. Therefore, in order to compile the composition of the basaltic component of the subducting slab, the data from Site 504 was supplemented by data from other sites (Sites 417, 417A, and 418; Plank, 1993). Table 3-2 gives the composition of the different units of the subducting slab that were used in the modeling of lavas from Central America.

C. Constraints on the mantle in Central America

Feigenson and Carr (1993) studied the composition of the mantle underneath the Central American volcanic arc using the rare earth element (REE) composition of mafic lavas. The authors indicated that there are two types of mantle in Central America: one has a composition similar to the source of depleted mid ocean ridge basalts (D-MORB) and the other one has a more enriched composition, similar to E-MORB source. Feigenson and Carr (1993) used the REE to understand the mineralogy of the mantle source from which the lavas originated because of the uniform behavior of these elements during melting. In addition, only clinopyroxene and garnet in the mantle have a significant effect on the behavior of the REEs. Thus, the results of the inverse modeling by Feigenson and Carr (1993) give the ratio of garnet to clinopyroxene present at the mantle source of the lavas.

The REE have distinctive patterns in the different segments of the arc (Fig. 3-14). In Nicaragua, the REE pattern is the least enriched in light REE. In El Salvador and Guatemala, the lavas display similar enrichment of the light rare earth elements, but those from Guatemala are more depleted in the heavy REE. Lavas from Costa Rica have steeper REE patterns than the other segments of the arc; the light REE are more enriched and the heavy REE are more depleted. The variation in the REE patterns for the lavas from Central America are explained by Feigenson and Carr (1993) as the result of

variation in the ratio of garnet to clinopyroxene in the source. They estimate that in Guatemala the ratio is between 0.3 to 0.7, in El Salvador and Nicaragua between 0 to 0.1. In northern Costa Rica the garnet/clinopyroxene ratio is similar to that of Guatemala, 0.3 to 1; and the highest amount of garnet is inferred to be in central Costa Rica, where the garnet/clinopyroxene ratio is between 0.5 to 1.5. The above ratios indicate that the mantle sources for Guatemala and Costa Rica must have garnet present, while in El Salvador and Nicaragua the presence of garnet is not essential.

According to Carr et al. (1990) The type of mantle that melts to create the arc lavas is not controlled directly by the mantle composition, but by the structure of the subduction zone. In Nicaragua where the dip of the subducting slab is steepest, the flux from the slab modifies a small volume of mantle and causes extensive melting of the more refractory mantle. The process is different in central Costa Rica, where the dip of the subducting slab is much shallower. In this case the flux from the slab interacts with a larger volume of mantle, melting mostly the enriched component to a small extent.

More recent studies (Patino et al., in press; Feigenson et al., in review; and Abratis and Wörner, 1997) of lavas from Central America suggest a complementary characterization of the mantle underneath the arc. These studies indicate that the mantle underneath Central American does not have a uniform composition along the entire arc. The arc can be divided into two regions depending on the type of mantle. One type of mantle is present along most of the arc from Guatemala to the border between Nicaragua and Costa Rica (the precise location of the southern boundary is being defined). This mantle is thought to be similar to the source of enriched MORB, based on the isotopic composition and the distribution of REEs in the lavas. The most clear evidence is from alkalic lavas from Lake Yojoa in Honduras. These lavas display Nd-Sr isotopic systematics that places their source in the MORB field. The other type of mantle is inferred to be present underneath Costa Rica (Feigenson et al., in review) based on lead isotopic composition of the lavas. The $^{206}Pb/^{204}Pb$ ratio of the lavas from Costa Rica is

higher than for those from other sections of the arc, pointing towards a HIMU component. The authors inferred that the HIMU component represents remnants of the Galapagos hot spot.

D. Conclusions

The stratigraphic units of the subducting Cocos Plate have significantly different geochemical characteristics that can be used to trace their input into the magma generation process in Central America. DSDP 495 reveals that the Cocos Plate has three stratigraphic units: the upper 177 m. are hemipelagic sediments with an abundant detrital component, the lower 233 m. are dominated by biogenic carbonate-rich sediments, and the altered oceanic crust.

The biogenic component clearly dominates the barium content in the carbonate and hemipelagic sequences. The proportion of biogenic/hydrogenic components also dominates the magnitude of the negative Ce anomaly. The increasing input of detrital material in the upper hemipelagic sediments dilutes the biogenic/hydrogenic signature, decreasing the magnitude of the negative Ce anomaly.

The volcanic detrital material in the hemipelagic muds increases the content of trace elements like Rb, Th, Cs, Pb, and the REEs compared to the carbonate sediments. Furthermore, the hemipelagic sediments are enriched in organic matter, increasing the content of uranium in this set of sediments.

The two sedimentary sequences have such different geochemical characteristics that it should be possible to distinguish their input into the magma generation process along the Central American volcanic arc. For example, a possible signature for the carbonate-rich sediments can be a significant negative Ce anomaly in the lavas, and the input from the hemipelagic sediments can be distinguished by relative uranium enrichments in the lavas. In addition, ratios of elements that have differ within the stratigraphy can be used (Fig. 3-7); for example, ratios that have hemipelagic enriched elements in the

denominator (like Ba/Th or Sr/U) will be high for the carbonate-rich input and low for the material derived from the hemipelagic sediments.

To characterize the whole sedimentary sequence, elements with similar distribution down core DSDP 495 can be used. For example, the carbonate and hemipelagic sediments have similar concentrations of Ba and La; thus, Ba/La is a ratio that can identify the overall sediment input (Fig. 3-10). Another set of elements that can be used to trace the flux from the sediments into the magma generation process is U-Th. The concentrations of these elements in the two sedimentary units is different, U and Th are more abundant in the hemipelagic muds than in the carbonate oozes. However, the U/Th ratio is not significantly different in the sedimentary units (Fig. 3-10). Therefore, U/Th can be used as an indicator of the input from the sediments to the mantle melts.

Site 504 gives information on the chemical composition of the altered oceanic crust. The results from this site indicate that the oceanic crust undergoes two types of alteration. The upper volcanic rocks are altered under low temperature conditions. This section of the oceanic crust can be geochemically identified by the enrichment of elements such as B, K, Rb, and Cs. The other type of alteration in the deeper section of the oceanic crust is of hydrothermal origin, and its geochemical signature is the enrichment of Pb, Cu, Zn, Mn and S.

Table 3-1

	Leg 69	Leg 70	Leg 83	Leg 111	Leg 137	Leg 140	Leg 148
mbsf	280-500	500-820	820-1350	1350-1520	1520-1610	1610-2000	2000-2111
K_2O	0.2	0.2	0.02	0.015	0.011	0.011	0.015
Rb	3.85	3.85	0.65	0.2	0.104	0.225	0.103
Cs	1.042	1.042					
B	11.84	0.885	0.618	0.284	0.193		
Sr	67.5	67.5	54.5	55.05	47	54	38
Ba	32.5	32.5		15.396	11.7	11.7	
Pb	2.5	2.5			5	5	
Cu	152	152	214.5				
La	7	1.99	1.7	1.127	0.924	0.924	1.035
Yb	2.469	2.469	2.675	2.66	2.13	2.13	2.12
Th	0.82	0.18	0.113		1.692	1.692	0.022
U				15	0.013	0.013	0.005

Table 3-1. Compiled geochemical information for Site 504.

Table 3-2

	Mean Hemipelagic DSDP 495	Mean Carbonate DSDP 495	Mean Sediment DSDP 495	Alt. Upper MORB Site 504	Alt. Lower MORB Site 504	NMORB S & McD 1989	EMORB S & McD 1989
Thicness (km)	0.2	0.2		0.5	1.5		
Density	1.3	1.75		2.75	2.75		
K_2O	1.84	0.18	1.01	0.20	0.02	0.07	0.25
K (ppm)	15272	1494	8383	1660	166.00	581	2100
B	70.0	10.0	40.0	5.0	0.6	0.3	0.6
Be	0.90	0.34	0.62	0.45	0.45	0.37	0.45
^{10}Be	1400	0	700	0	0	0	0
Cu	262.89	76.11	169.50	150.00	50.00	50	50
Rb	40.78	4.28	22.53	3.85	0.20	0.56	5.04
Sr	336.16	1504.12	920.14	68.00	55.00	90	155
Nb	5.03	0.44	2.74	0.55	0.90	2.33	8.3
Ba	3941.49	2145.48	3043.49	33.00	12.00	6.3	57
La	17.96	8.78	13.37	4.50	1.20	2.5	6.3
Yb	2.78	1.18	1.98	2.50	2.10	3.05	2.37
Cs	2.17	0.15	1.16	0.06	0.01	0.01	0.063
Pb	9.59	3.70	6.65	2.50	5.00	0.3	0.6
Th	3.00	0.16	1.58	0.50	0.80	0.12	0.6
U	4.89	0.15	2.52	0.10	0.05	0.05	0.18

Table 3-2. Geochemical composition for the subducting slab and mantle wedge. Data for DSDP Site 495 is from this study, for Site 504 is mostly from Alt et al. (1996) and references therein. NMOB and EMORB composition is from Sun and McDonough (1989).

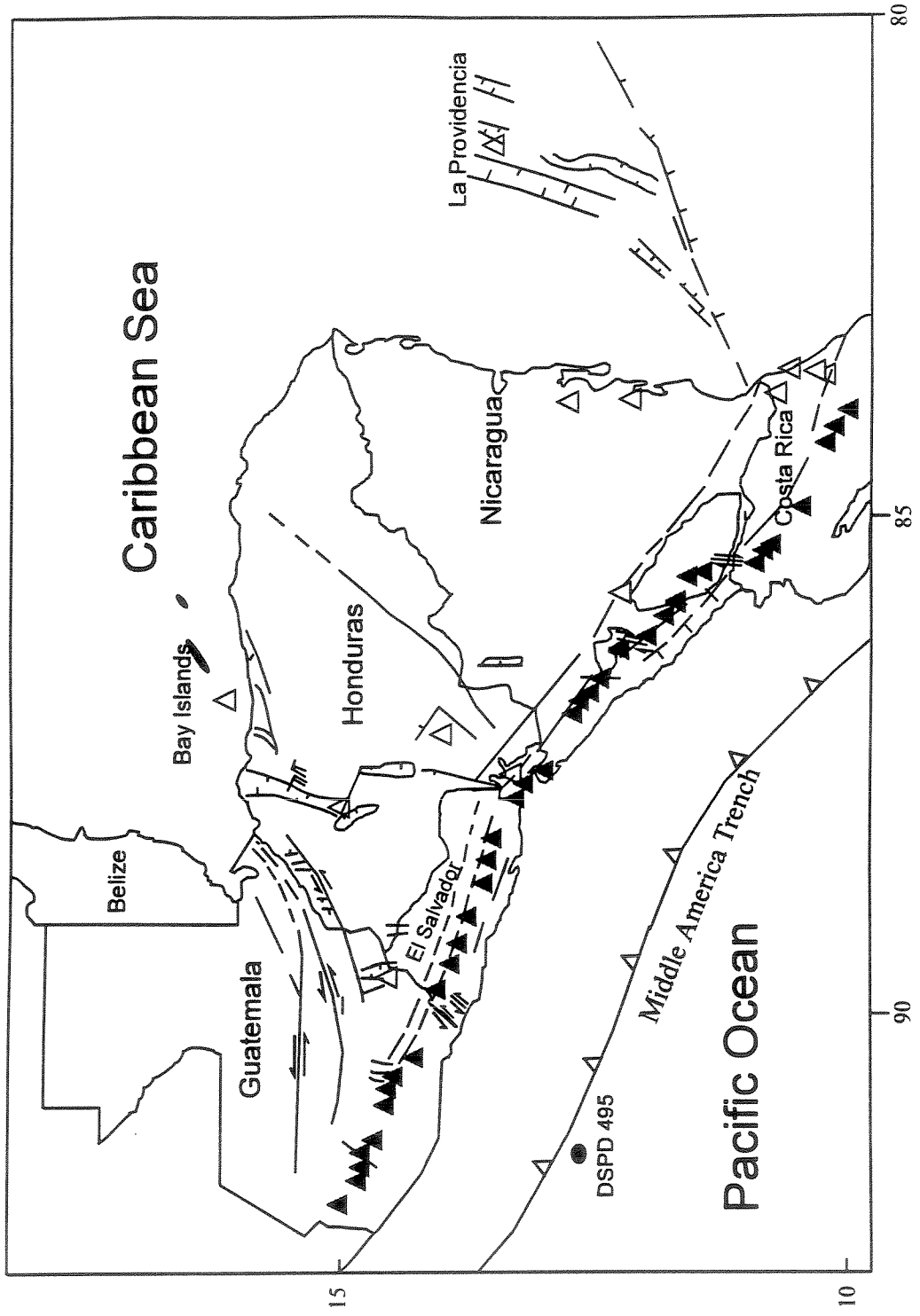


Figure 3-1. Location of DSDP Site 495 relative to Central American volcanic arc. Filled triangles represent volcanoes from the front. Empty triangles indicate areas of back-arc volcanism.

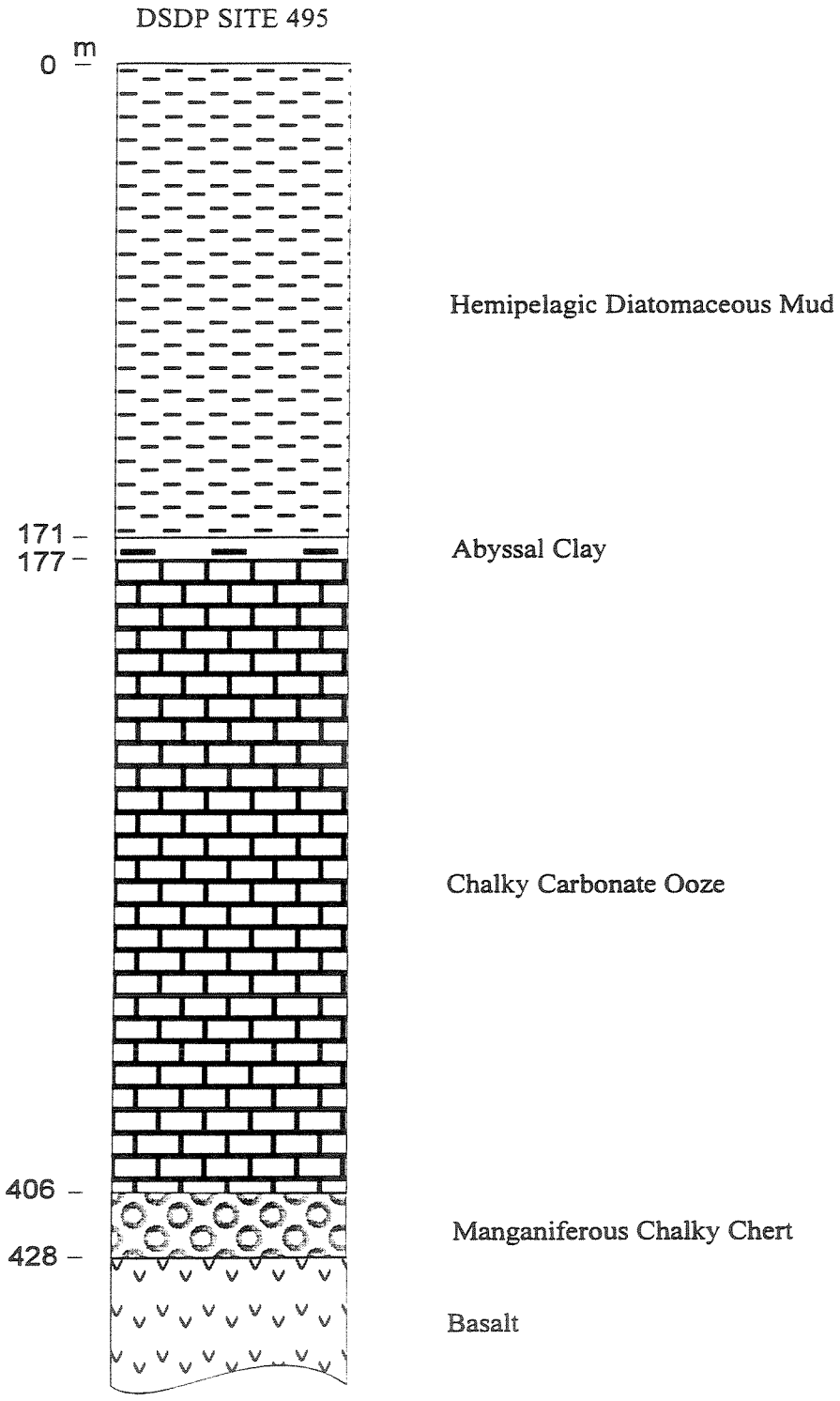


Figure 3-2. Stratigraphic column of DSDP Site 495 off the coast of Guatemala. These deposits are representative of the material being subducted underneath the Caribbean Plate. The three largest components are hemipelagic mud, carbonate oozes, and basaltic oceanic crust. Depth is in meters below seafloor (mbsf).

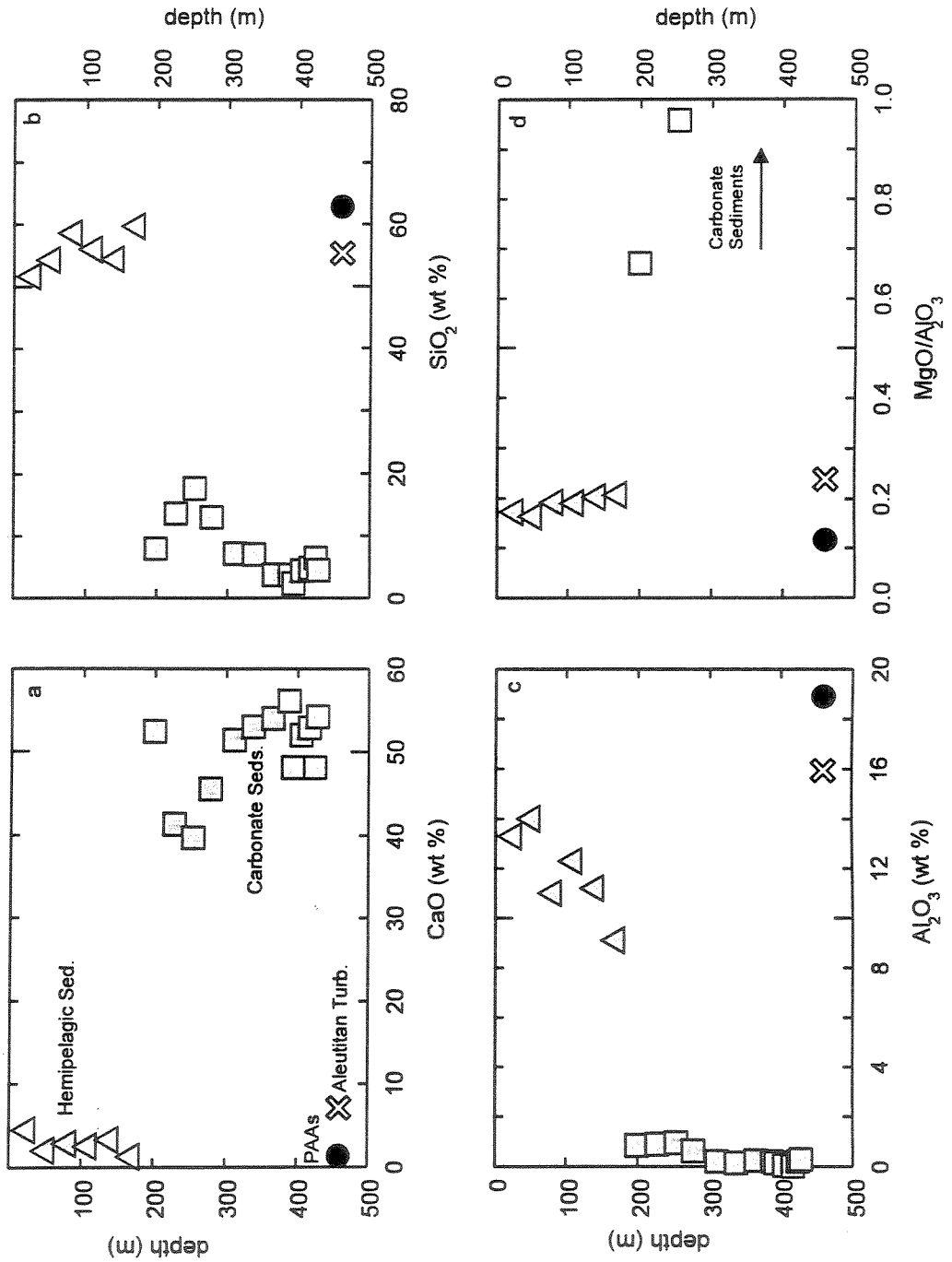


Figure 3-3. Major element variation down core DSDP Site 495. The triangles represent the hemipelagic sediments and squares indicate carbonate oozes. Other sedimentary material is also plotted for reference: post-Archean average Australian shale (circle; Taylor and McLennan, 1985) and Aleutian turbidite (cross; McLennan et al., 1990).

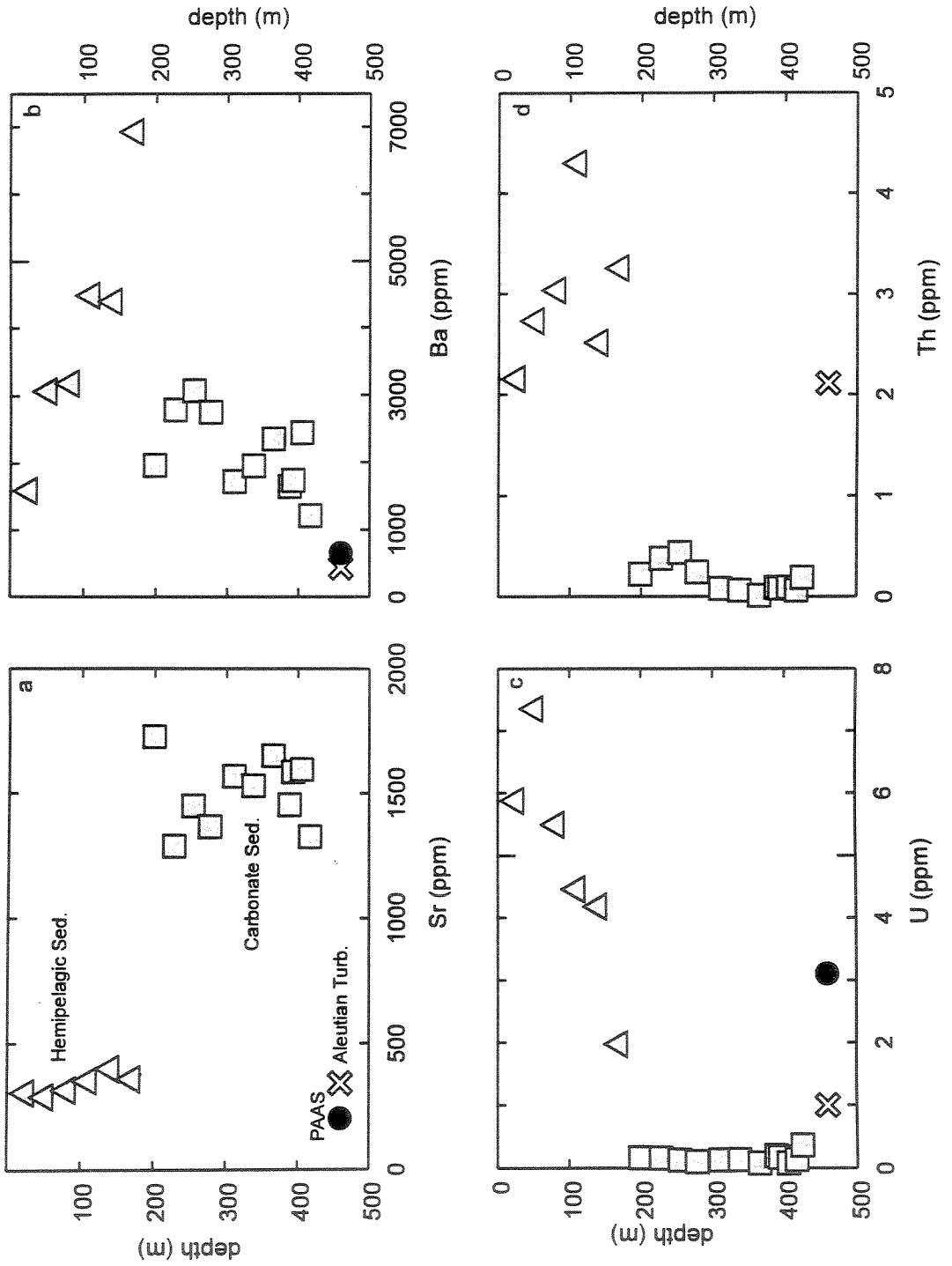


Figure 3-4. Trace element variation down core DSDP Site 495. The hemipelagic sediments (triangles) are enriched in U and Th, the carbonates oozes (squares) have higher Sr. The two sedimentary units have similar Ba. PAAS (circle) and Aleutian turbidite (cross) are plotted for reference.

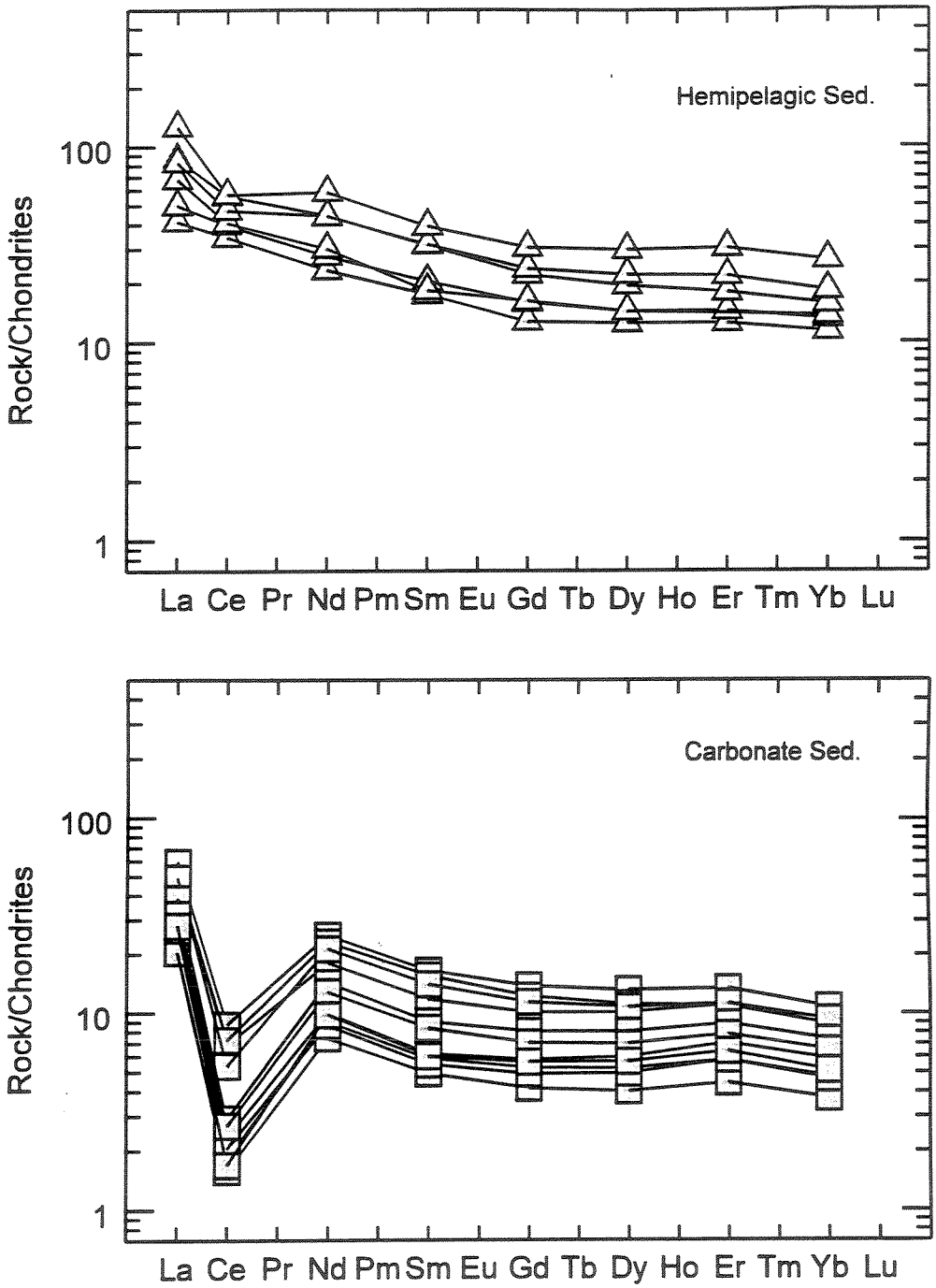


Figure 3-5. REE patterns for the two sedimentary units from DSDP Site 495. The Hemipelagic sediments (triangles) have higher concentrations of REEs than the carbonates (squares). The carbonates are display a large negative Ce anomaly. Normalization factors from Sun and McDonough (1989).

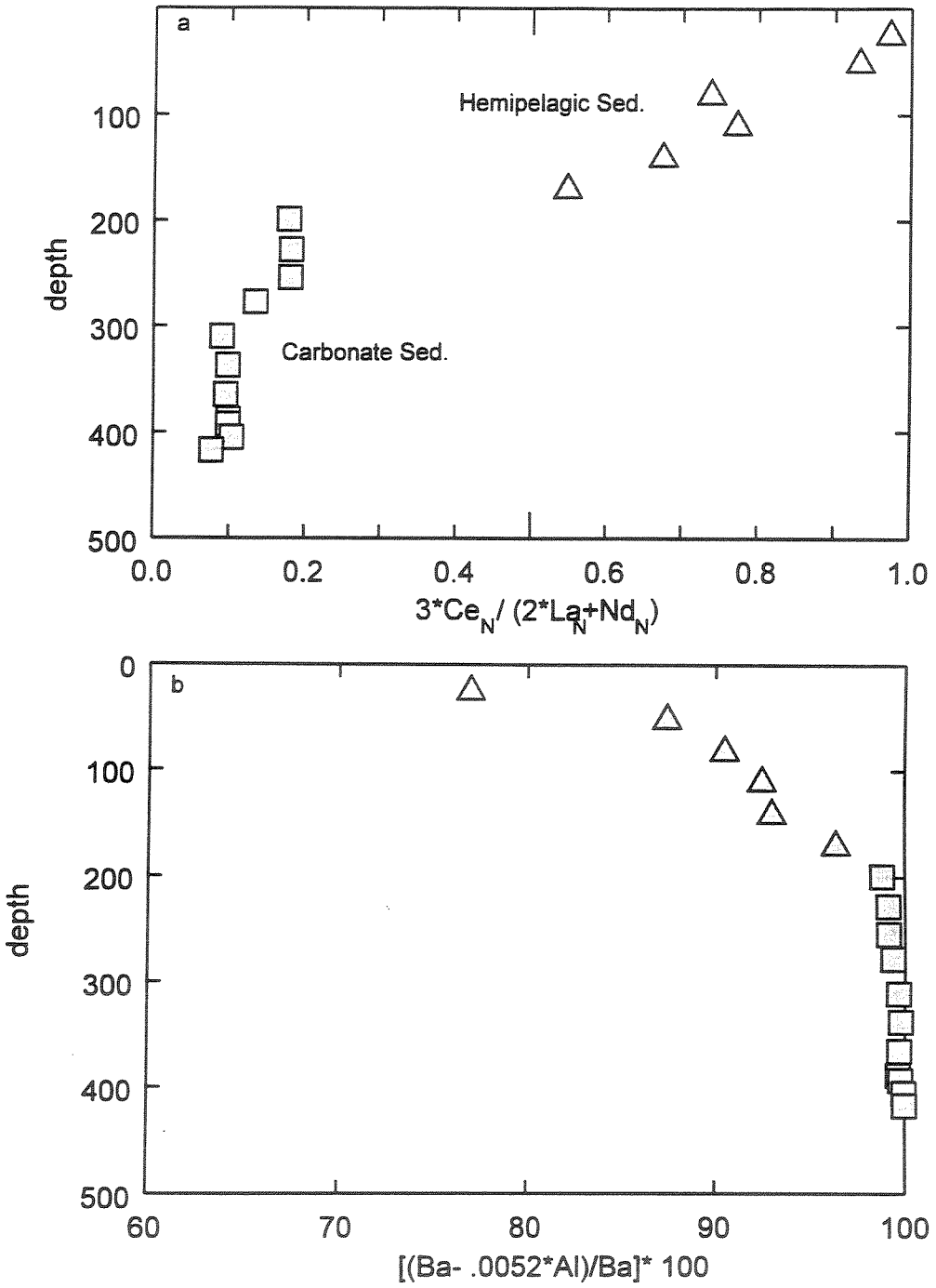


Figure 3-6. a. Variations with depth of cerium anomaly for sediments from DSDP Site 495. The smaller the value is the greater the negative cerium anomaly (squares = carbonate sediments). b. Variation with depth of the percentage of Ba derived from biogenic sources (von Breymann et al., 1992). The carbonate sediments derive their Ba mostly from biogenic material; whereas the upper hemipelagic sediments have a greater percentage of their Ba coming from detrital sources.

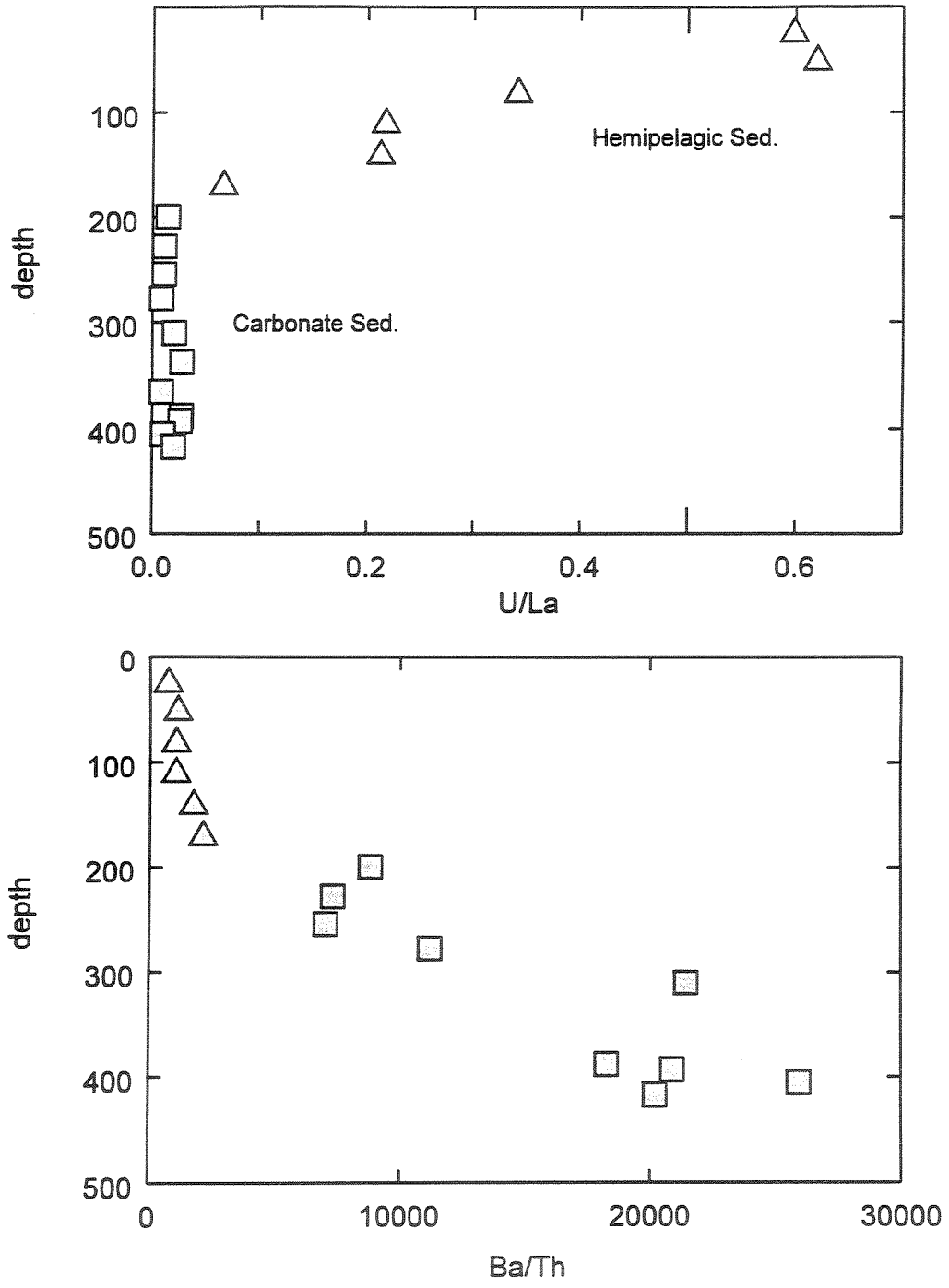


Figure 3-7. Variation of trace element ratios down core for sediments from DSDP Site 495. If the ratios are constructed with elements enriched in the hemipelagic muds in the numerator, the hemipelagic sediments will have higher ratios than the carbonate sediments, and vice-versa.

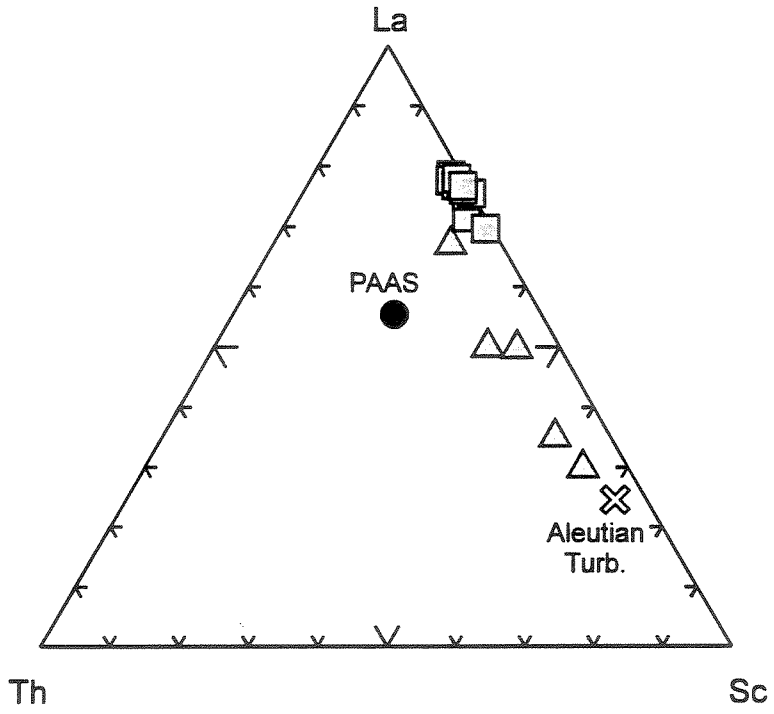


Figure 3-8. Triangular plot of La-Th-Sc used to determine provenance of hemipelagic sediments. The carbonate oozes cluster (squares) in the line between La and Sc. The hemipelagic sediments (triangles) spread from an area close to the carbonate sediments towards the Sc corner, approaching a turbidite from the Aleutians (cross). The sediments from DSDP Site 495 have lower Th concentrations than PAAS (circle).

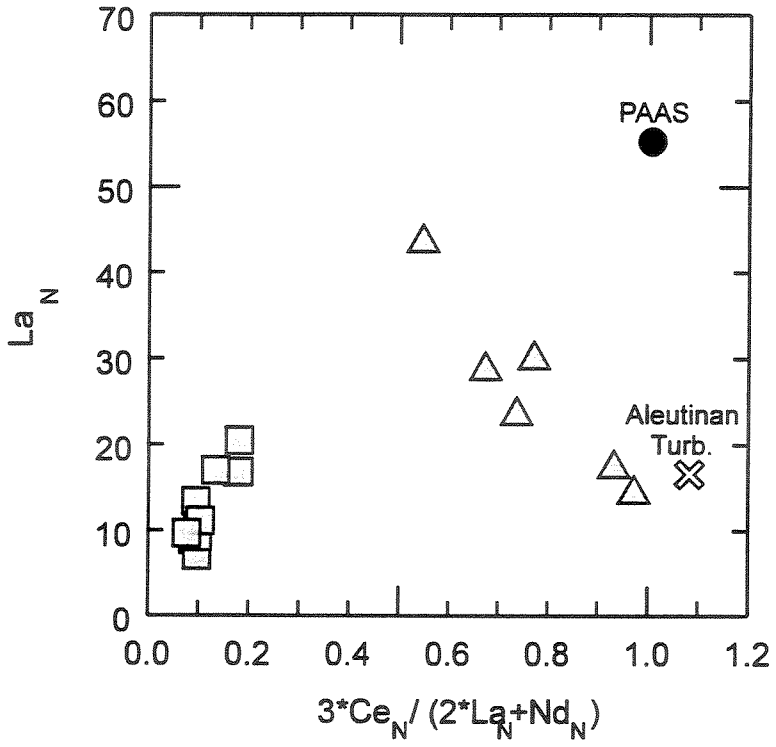


Figure 3-9. Cerium anomaly vs. La_N. The hemipelagic sediments from DSDP Site 495 (triangles) have a greater hydrogenic component than PAAS (circle) or turbidites from the Aleutians (cross). The large negative Ce anomaly of the carbonates oozes (squares) is the result of the biogenic nature of these sediments.

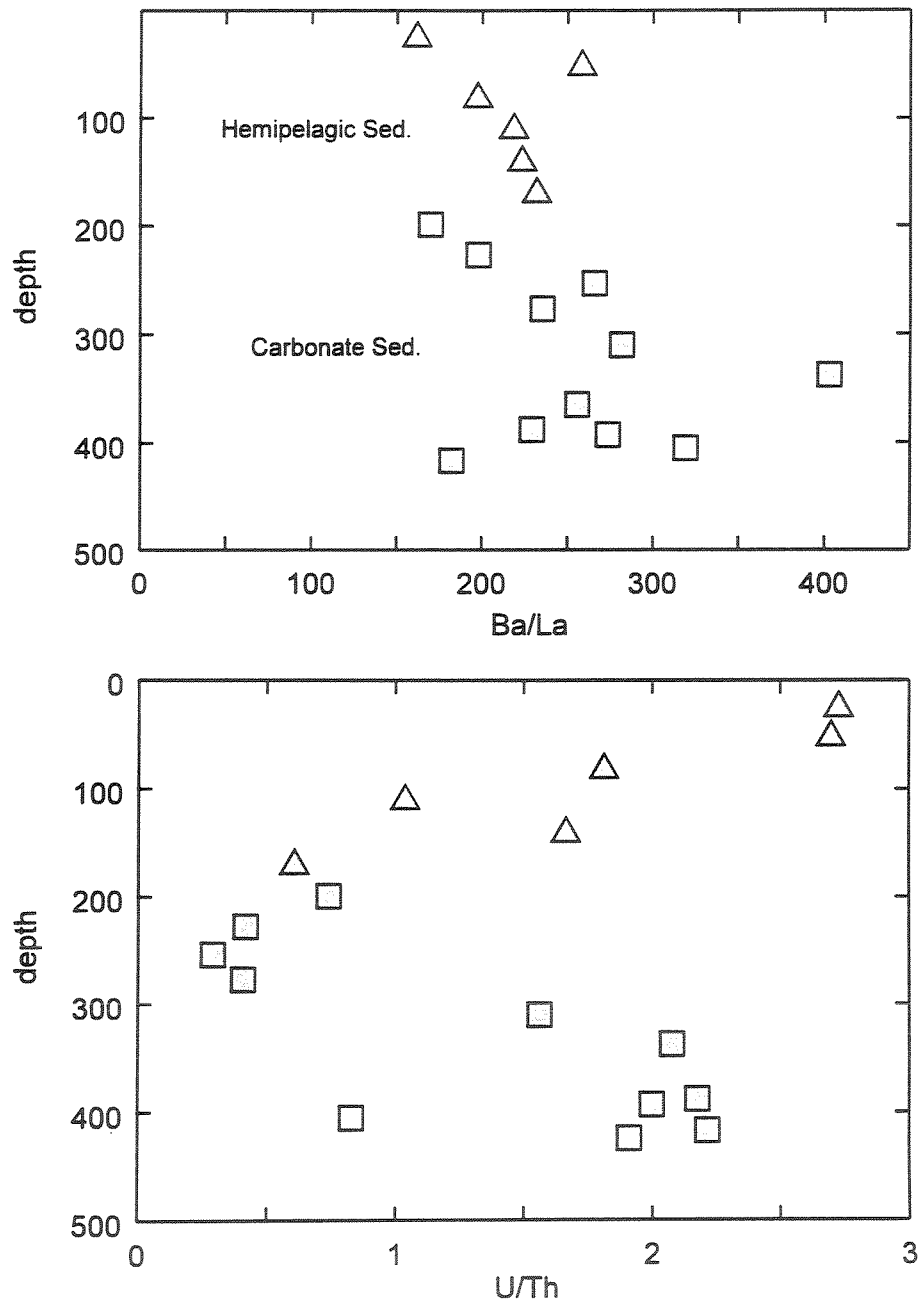


Figure 3-10. Trace element ratios that can be used to identify the overall sediment input. The ratio of Ba/La or U/Th does not change significantly down the core.

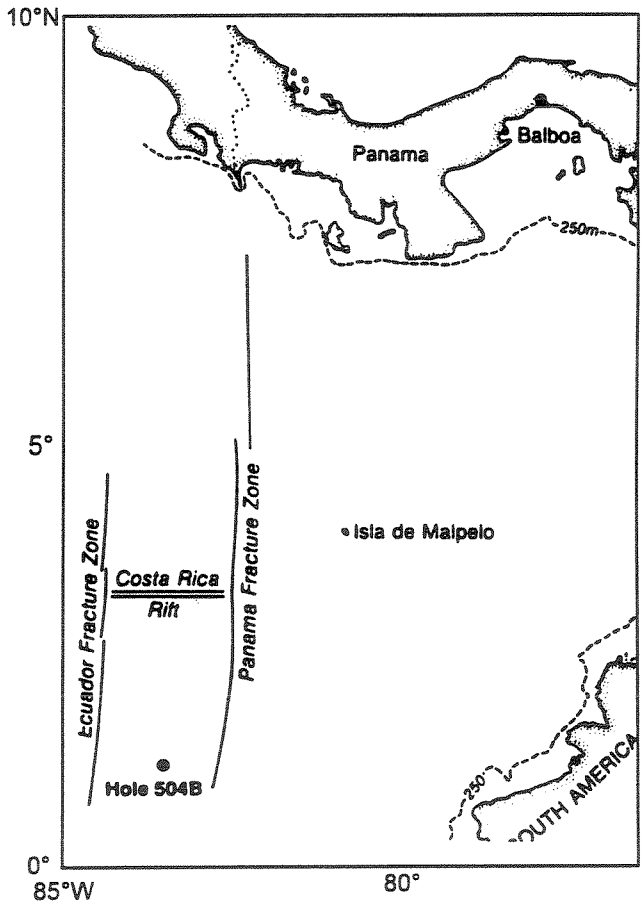


Figure 3-11. Location of Site 504 in the Eastern Pacific, south of the Costa Rica rift (Alt. et al. 1996).

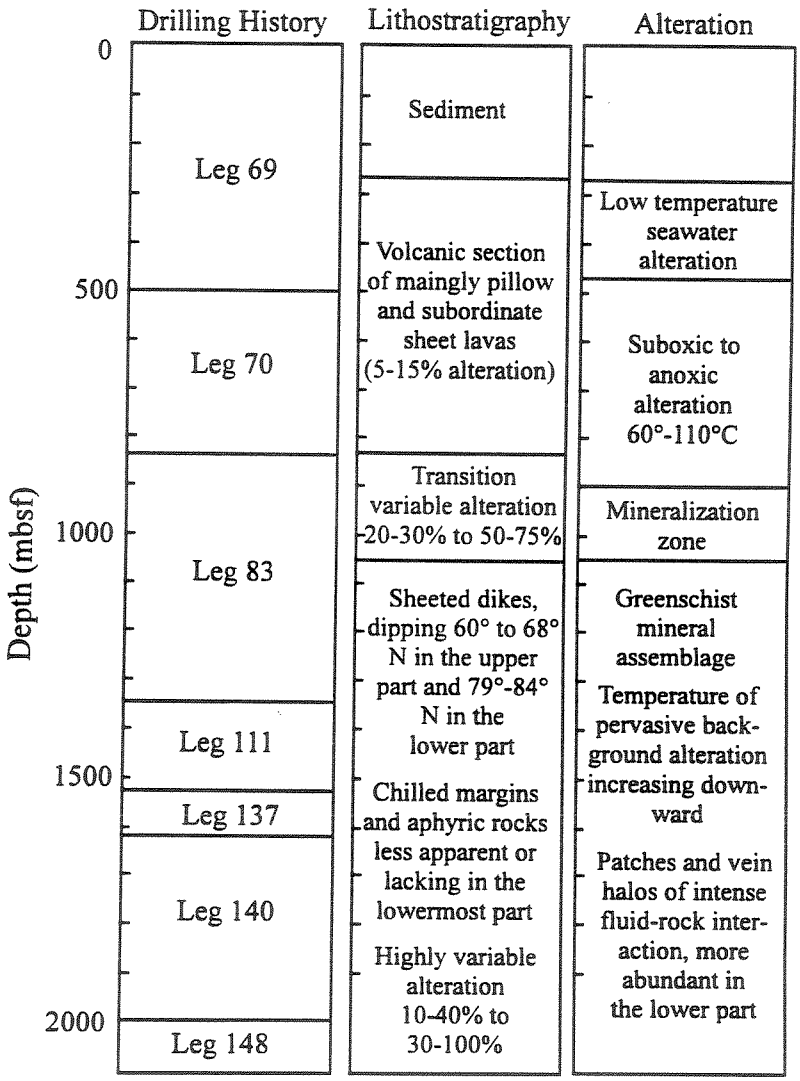


Figure 3-12. From Bach et al. (1996), summary of the lithology and nature of alteration of Site 504.

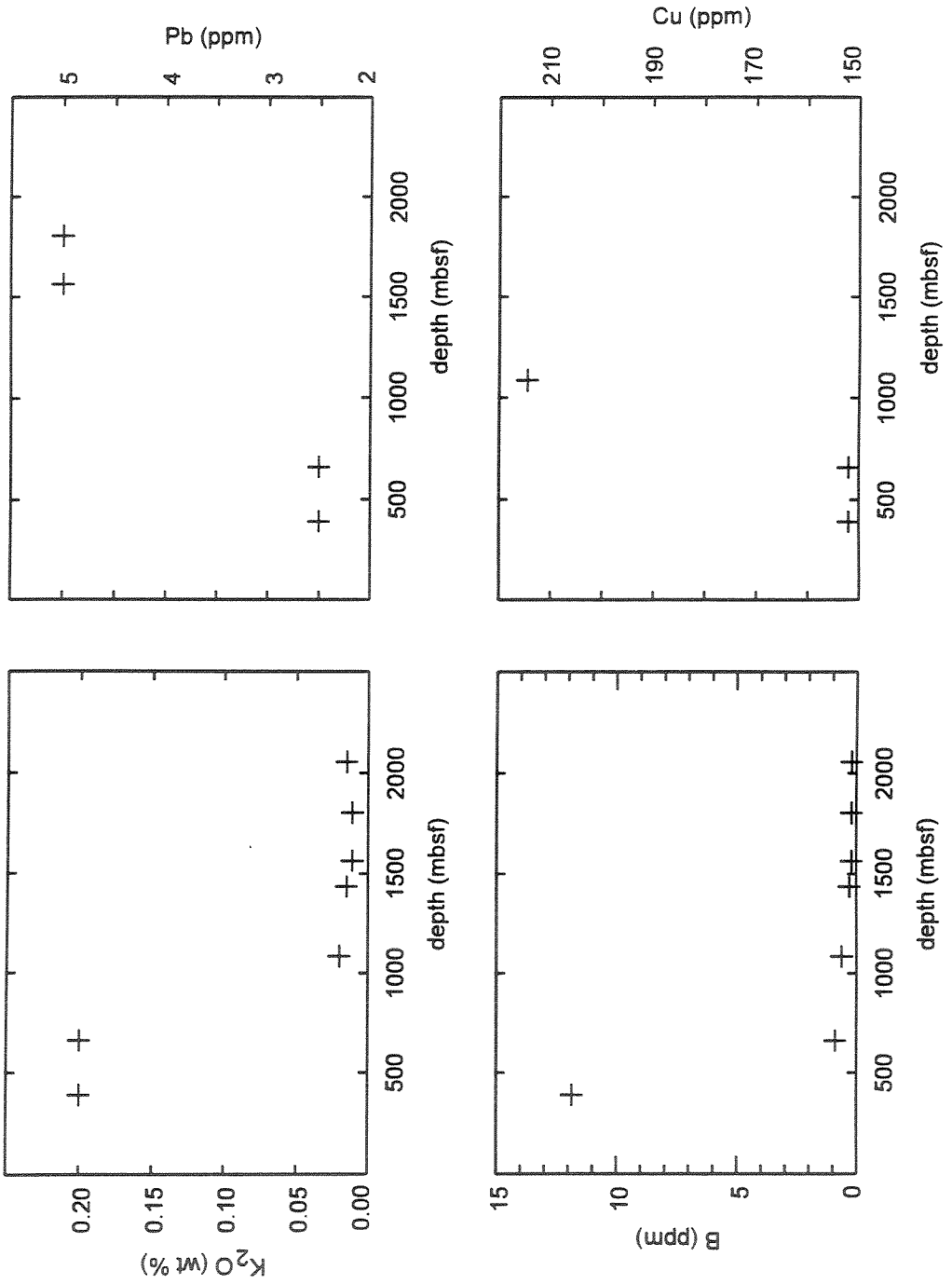


Figure 3-13. Compiled geochemical characteristics of Site 504. Boron and alkali elements are enriched in the upper volcanic rocks by low temperature alteration. Hydrothermal alteration in the lower part of the core produces higher concentrations of elements like Pb and Cu.

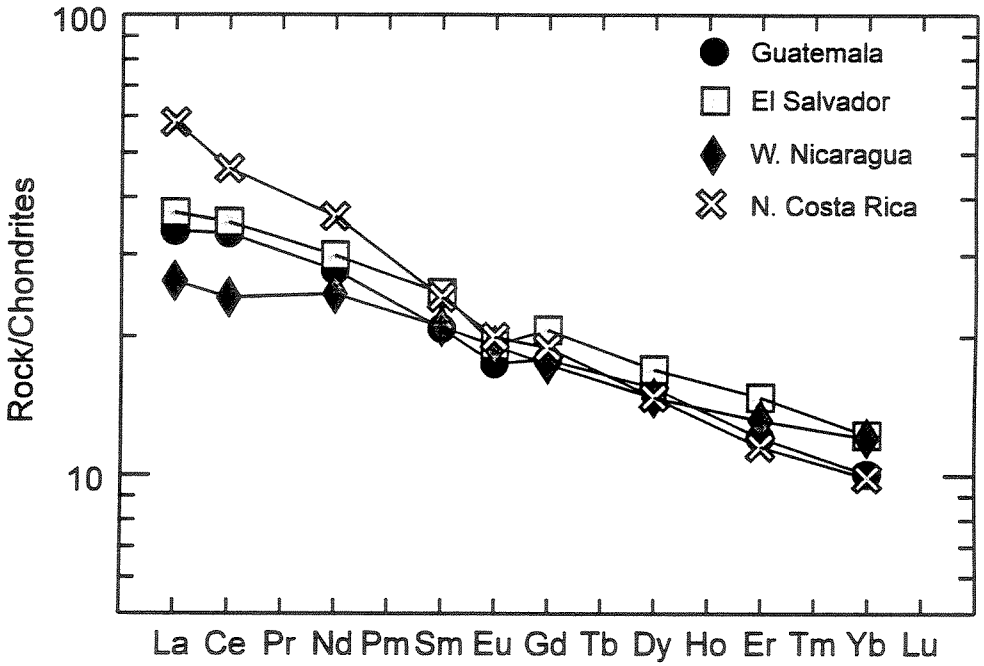


Figure 3-14. REE patterns for mean lavas from Guatemala, El Salvador, western Nicaragua, and northern Costa Rica. The lavas from Nicaragua have the lowest La/Yb ratios and those from Costa Rica have the highest ratio.

IV. OUTPUT: INCOMPATIBLE ELEMENT VARIATIONS IN CENTRAL AMERICA

A. Introduction

The central American volcanic arc has two major regions of volcanism, a linear volcanic front and dispersed back arc volcanic fields (Fig. 4-1). This geographical distribution of volcanism allows the study of chemical variations not only along the arc but also with increasing distance from the trench, adding an extra dimension to regional geochemical studies. Back arc magmatism in Central America is closely associated with extensional features, with the greatest abundance of volcanic fields found in southeast Guatemala and Honduras (Williams and McBirney, 1969). Magmatism in the back arc commonly occurs as cinder cones and shield volcanoes; stratovolcanoes that are common along the volcanic front are scarce behind the volcanic front. Carr et al. (1990) studied the geochemistry of lavas from the front to infer the relationship between the volcanic front rocks and subducted material. The geochemical characteristics of lavas from back arc volcanoes have been summarized by Walker et al. (1995) and Patino et al. (in press).

In Central America, there are geophysical changes along the arc that affect the interaction between the subducting oceanic crust and the mantle wedge (Carr, 1984). One such parameter is crustal thickness. The crust is thinnest in Nicaragua (32 km) but increases to more than 40 km in Guatemala and Costa Rica. Another geophysical parameter that changes along the arc is the dip of the subducting Cocos Plate, and it has a similar geographic distribution along the arc as crustal thickness. The dip appears steepest in Nicaragua (65°-75°), and it gets shallower towards Guatemala (40°) and central Costa Rica (35°). Changes in the geochemical characteristics of arc lavas are sometimes associated with changes in the rate of subduction (Davies and Stevenson, 1992). However, the rate of subduction of the Cocos Plate underneath the Caribbean Plate does not change significantly along the Central American arc; the subduction rate is about 8 cm/y along the arc.

Lavas from Costa Rica will be excluded from the following discussion of the geochemical characteristics Central American rocks. Even though Costa Rican volcanoes are a geographic continuation of the arc, there are geophysical and petrological features that make volcanism in Costa Rica different from the rest of the arc. The subduction of the aseismic Cocos Ridge underneath central Costa Rica makes the angle of subduction very shallow (Protti et al., 1995). There is not a clear transition from the volcanic front to back arc magmatism in this region, and Costa Rica is the only segment of the volcanic front where alkalic lavas erupt close to calc-alkaline volcanoes (Carr and Stoiber, 1990). Moreover, there are significant differences in the rare earth element (REE) and Pb isotopic composition of the rocks (Feigenson and Carr, 1993; Feigenson et al., in review). The lavas from Costa Rica have significantly higher La_N/Yb_N ratios (>5) compared to the rest of the arc (<5). Feigenson and Carr (1993) explain the steep REE patterns as a manifestation of the more enriched mantle source in the area. The authors indicate that the mantle source from which the lavas originate has a different mineralogical composition, having a greater garnet/clinopyroxe (≥ 1) ratio compared to the rest of the arc. The lead isotopic composition of the lavas from Central America is relatively uniform, except for $^{206}Pb/^{204}Pb$. This lead isotope ratio is higher for samples from Costa Rica (>18.8), where the ratios are similar to those from La Providencia, a late Miocene alkalic volcanic center in the Caribbean Sea. Feigenson et al. (in review) interpret the high $^{206}Pb/^{204}Pb$ of these samples as a signature of remnants of the Galapagos hot spot. Abratis and Wörner (1997) reached a similar conclusion when studying samples from Costa Rica that represent volcanism before and after the collision of the Cocos Ridge.

Even though the Central American arc is a continental margin, the effects of crustal contamination are not pronounced along the arc. Walker et al. (1995) and Patino et al. (in press) suggest that low Nd isotope ratios are good indicators of crustal contamination for Central American lavas. The range in $^{143}Nd/^{144}Nd$ varies little along the arc, except for samples from western Guatemala that have significantly lower isotope

ratios (Fig. 4-2). The low $^{143}Nd/^{144}Nd$ ratios of the samples from western Guatemala could be produced by the input from subducted sediments into the magma genesis. However, to produce the low Nd isotope ratios, unrealistically large amounts of sediment, up to 10%, would have to be added to the mantle wedge. Furthermore, other geochemical indicators of sediment input do not support the hypothesis that the low Nd isotope ratios in lavas from NW Guatemala are produced by higher slab flux. Instead, the low $^{143}Nd/^{144}Nd$ ratios for rocks from this section of the arc are the result of crustal assimilation.

Incompatible element ratios are widely used to characterize lavas in arc settings. The ratios can be used as tracers of the components (the subducting slab and the mantle wedge) from which the magmas originate (e.g. Ellam and Hawkesworth, 1988), and/or they can be used to infer the process(es) that transfer material from the slab to the mantle wedge (e.g. Gill et al., 1993). I will describe the variation of several trace element ratios along and across the Central American arc to determine changes in the input from the different components of the subducting slab.

B. Along-arc variations

1. Regional Variations

Along-arc geochemical variations in lavas from Central America have been described by Carr et al. (1990), Leeman et al. (1994), and Morris et al., (1990). The authors point out that Ba/La, B/La and $^{10}Be/^{9}Be$ ratios are highest in Nicaragua and decrease to the northwest and southeast. Other trace element ratios that display similar distributions along the arc are U/Th, Pb/La, Ba/Th, U/La, Ba/ Nb (Fig. 4-3). In Central America, most of the ratios that display a regional variation are ratios of highly mobile (non-conservative) to less mobile or immobile (moderate non-conservative elements or non-conservative) elements. These ratios can also be considered from another perspective, their distribution down core at DSDP Site 495. Ratios like U/Th and Ba/La

do not change significantly down core, whereas U/La is higher in the hemipelagic sediments, and high Ba/Th characterizes the carbonate sediments.

The variability of the trace element ratios that change along the arc is not uniform (Fig. 4-3). Some of the trace element ratios have smaller ranges along the arc and within segments of the arc, whereas other ratios exhibit more variations. The range of U/Th, as well as that of Ba/La, is very small within segments of the arc; no one segment has a range wide enough to include all the values found along arc. The U/Th ratios varies from about 1 to 0.35 along the arc, and the arc segment with the widest range in western Nicaragua, where U/Th varies from about 1 to 0.6. Moreover, there is a smooth transition in U/Th from one segment of the arc to the next. In contrast, most of the other ratios have wider ranges within segments of the arc. For example, Ba/Th varies between about 2000 to 150 along the arc, and the ratios in lavas from western Nicaragua vary almost as much, from 2000 to 350. In addition, the transition from one segment of the arc to the next is not as smooth as that of U/Th. The most dramatic transition is the one for the western Nicaraguan segment. The highest Ba/Th ratio in western Nicaragua is two and three times greater than the highest ratios in the lavas from the adjacent segments. It is clear from figure 4-3 that the variability of a trace element ratio is independent of the scale of the ratio because Ba/Th and U/Th differ greatly in magnitude. Despite the different behavior of incompatible element ratios along the arc, the most extreme values are consistently found in Nicaragua, more precisely in western Nicaragua. The only exception is described by Morris et al. (1990), who show that the highest $^{10}Be/^{9}Be$ ratio of any arc lava is found in Masaya, which is located in eastern Nicaragua.

It is unlikely that the regional variations are due to fractionation processes during melting because the elements that make up the ratios behave similarly during mantle melting; the elements are incompatible in most mantle minerals. Nor are the variations likely to be the result of shallower processes. Figure 4-2 shows the lack of correlation between U/Th and $^{143}Nd/^{144}Nd$ (an analog for crustal contamination). This is especially

true if each segment is separately examined. Therefore, the U/Th variation along the arc is independent of crustal contamination.

Hochstaedter et al. (1996) indicate that U, Cs and B behave congruently in lavas from the Mexican volcanic belt. The lavas from Central America follow a similar trend. Most of the samples from the arc display a linear relationship between Cs and U (Fig. 4-4). However, the slope defined by the lavas from eastern Nicaragua is steeper than the trend of the samples from the rest of the arc. As stated earlier, of the element ratios studied previously along Central America only $^{10}Be/^{9}Be$ has a maximum value in eastern Nicaragua, rather than in western Nicaragua. $^{10}Be/^{9}Be$ is an unambiguous indicator of the presence of material derived from the uppermost hemipelagic sediments during magma genesis (Tera et al., 1986). Thus, the geographic distribution of $^{10}Be/^{9}Be$ along Central America implies that the highest hemipelagic input is observed in lavas from eastern Nicaragua. The high hemipelagic input in eastern Nicaragua also explains the excess uranium of the lavas, because the hemipelagic sediments from the Cocos Plate have unusually high uranium contents (chapter 3).

Along arc variations have also been observed in other arcs, e.g. Japan and Kamchatka (Shibata and Nakamura, 1997 and Kepezhinskas et al. 1997). In both cases, the variations along the arc are thought to be the result of changes of geophysical parameters. The variations in Kamchatka are attributed to differences in the age of the subducting oceanic plate. In the southern part of the arc, older oceanic crust is subducting and contributing hydrous fluids to the mantle wedge; whereas, in the northern part of the arc much younger crust is being subducted and melted (Kepezhinskas et al., 1997). The regional variations in Japan are related to differences in the amount of sediment involved in the magma generation process. Shibata and Nakamura (1997) report that the sediment involvement is higher in the northeast of Japan compared to the Izu arc, further south. The authors imply that this regional variation is caused by geophysical differences along the arc, e.g. changes in the dip of subduction and subduction rate. These geophysical

parameters, age and dip of the subducting slab, as well as convergence rate affect the thermal structure of subduction zones (Davies and Stevenson, 1992).

In Central America there are no large variations of the convergence rate along the arc. However, changes in the dip of the subducting slab have been proposed (Carr, 1984) and documented in Costa Rica (Protti et al., 1995). The geochemical variations along the arc coincide with variations in the dip of the subducting slab (Carr et al., 1990). Figure 4-3 shows this relationship for trace element ratios associated with slab signature. The highest values are observed in western Nicaragua, and values decrease towards Guatemala and Costa Rica. The dip of the slab is steepest in Nicaragua (65°-75°) and it becomes shallower towards the northeast and southwest. Carr et al., (1990) concluded that the slab material is better utilized in Nicaragua were the steeper dip of subduction induces intensive metasomatism and melting of a smaller volume of mantle. A relatively small amount of high degree melt is produced. Here the melt generated in the mantle is heavily imprinted with a subduction signature. In the other segments of the arc, where the dip of the subducting slab is shallower, a larger volume of the mantle is modified and then melted to a low to moderate degree, producing a larger volume of melt and the slab signature is diluted. The new variations reported in figure 4-3 are in agreement with Carr et al. (1990) because these ratios are similar indicators of slab input. However, this scenario does not explain the local variations that will be discussed next.

2. Local Variations

Trace element ratios that vary on a local scale in Central America are better seen when plotting two ratios against each other. The ratios that best display the local variations have drastically different values for the carbonate and the hemipelagic sediments from DSDP 495 (chapter 3). The carbonate sediments are depleted in most trace elements, and the hemipelagic sediments in general have higher concentrations of trace elements. Therefore, if we take Ba (of similar concentration in both sedimentary units) and Th (extremely depleted in the carbonate sediments) to make Ba/Th ratio, a carbonate

component will have very high values of the ratio. In a similar manner, U (enriched in the hemipelagic sediments) and La (of similar concentrations down core DSDP 495) can be combined and thus high U/La ratios will be indicative of the input from the hemipelagic sediments. The local geochemical variations in Central America seem to be first order manifestations of the ratio of carbonate to hemipelagic sediment input to the magma generation process.

Figure 4-5 shows the local variations of the lavas from Central America. For each segment of the arc there are lavas that have higher Ba/Th and lower U/La, and vice-versa. Similar local variations are observed in all the arc segments, but their scale is dependent of the amount of slab input. The local variations are observed in Nicaragua as well as in Guatemala, and in even in some back arc regions, like Honduras, however, the lavas from Nicaragua plot furthest away from MORB or mantle values and those from back arc regions in Guatemala and Honduras plot closer to MORB or mantle compositions. The distance from the mantle corner is a function of the quantity of the slab input.

In Telica, a volcano from western Nicaragua, the local variations are temporally controlled. The older lavas have higher Ba/Th and lower U/La ratios, implying that the magmas originated from a carbonate-rich component that had little input from the hemipelagic sediments. The younger lavas, on the other hand, appear to have significant input from the hemipelagic sediment, because of the higher U/La ratio and lower Ba/Th. Balzer et al. (1996) observed stratigraphic differences when comparing Quaternary to Miocene lavas from several volcanic edifices in Nicaragua. The older rocks have lower U/Th for a given Ba/La ratio compare to the younger samples. The lower U/Th implies that older lavas lack the input of uranium-rich hemipelagic sediments (Balzer et al., 1996). However, it seems that stratigraphic variations, at least in a short time scale, are not a common feature in other segments of the arc. Samuels (personal communication) did a chemostratigraphic study of lavas from Tecuamburro and Moyuta in Guatemala; she did

not find age-related variations that imply different ratios of carbonate to hemipelagic sediment during magma genesis.

The local variations (changes in the carbonate to hemipelagic ratio) can be explained by the presence or absence of sediment traps created in the fracture zones. There are small scale roughness variations on the surface of the subducting Cocos Plate (Aubouin et al., 1982); for example, DSDP Site 495 is located on a horst. Small scale structural features, like horsts or grabens, create sediment traps. When a horst subducts the upper part of the hemipelagic unit may be scraped off or underplated. If the hemipelagic sediments do not take part in the metasomatism of the mantle, the slab component will have higher carbonate/hemipelagic ratio. The effect on the composition of the lavas will be higher Ba/Th and lower U/La. On the other hand, when grabens are subducted, few or no hemipelagic muds are underplated, and most of the sedimentary sequence is involved in the generation of magmas. The slab component in this case will have a lower carbonate/hemipelagic sediment ratio, and the lavas will have higher U/La and lower Ba/Th.

C. Across arc variations

Lavas from back arc regions usually have less slab input that those from the volcanic front, most likely due to progressive loss of volatiles as subduction continues (e.g. Price et al., 1992; Woodhead and Johnson, 1993; Gill et al., 1993; Ryan et al., 1995; Shibata and Nakamura, 1997; Patino et al., in press). Therefore, back arc lavas tend to have geochemical features closer to MORB than volcanic front samples, but are still significantly different from mid-ocean ridge and ocean island basalts (e.g. Ryan and Langmuir, 1993).

Due to a smaller and more patchy slab signature, it is easier to alter the geochemical signature of back arc magmas on their way to the surface. This modification is variable in Central America. Walker et al. (1995) show some large effects that even small amounts of crustal assimilation have on the isotope geochemistry of most of the

back arc lavas from southeast Guatemala. Patino et al. (in press) show that crustal contamination is not as ubiquitous in back arc basalts from Honduras as it is in Guatemala. Some geochemical tracers are more readily affected by crustal contamination than others. For example, in Honduras Nd isotope ratios are easily modified by crustal assimilation, but Ba/La is not. The differences in the extent of crustal contamination between the back arc lavas from southeast Guatemala and Honduras may be caused by slight differences in their tectonic settings. Both back arc volcanic regions are closely associated with extensional features, but the back arc volcanic fields in Guatemala are closely spaced, with almost continuous volcanism from the volcanic front to the Jocotán fault. In Honduras, on the other hand, there are two back arc volcanic fields, Zacate Grande and Tegucigalpa (17 km and 102 km from the volcanic front, respectively), that are widely space and do not overlap. Moreover, Zacate Grande and Cerro de Hule (near Tegucigalpa) in Honduras are large volcanic centers whose later lavas may have come through a well established plumbing system with less contact with crustal rocks. The volcanic edifices in SE Guatemala are all small cinder cones whose magmas may have been in more contact with the crust.

1. Similarities between volcanic front and back arc lavas

In an EMORB-normalized plot all the lavas along and across the Central American arc show similar patterns (Fig. 4-6). All the lavas display large differences between Ba and Th and between U and Nb; these similarities between lavas from the front and rear volcanoes are also common in other arcs, e.g. northeastern Japan (Shibata and Nakamura, 1997). However, the peaks and troughs of the samples from the back arc are smaller compared to the volcanic front lavas.

In Honduras, Patino et al. (in press) show that slab material contributes to the magma generation process for volcanoes as far as 102 km from the front and that Zacate Grande, a volcanic complex just 17 km behind the volcanic front, has a slab signature as strong as that of the volcanic front. These results are confirmed by the ^{10}Be content of

one sample from Zacate Grande (Za7). This sample has 7.03 x 10^6 atm/gm of ^{10}Be, a value similar to that of other volcanic front lavas from Central America and other arcs (Morris et al, 1990). Another back arc lava from El Salvador, SALC502 also has a relatively high ^{10}Be (4.7 x 10^6 atm/g) content, implying that the subducting slab contributed material to the magma generation process. These results are in contrast to those from Walker et al. (1995), who found the slab signature to be absent in a center 20 km from the front in SE Guatemala. The presence of a slab signature in back-arc volcanoes has been observed in other arcs, e.g. the Kuriles and Japan (Ryan et al., 1995 and Shibata and Nakamura, 1997, respectively). In both cases, the authors indicate that water and slab components can reach depths greater than 150 km, allowing back arc magmatism to be influenced by the subducting slab.

Figure 4-5 shows that back arc lavas from Zacate Grande and Tegucigalpa in Honduras have significantly high Ba/Th, even higher than some lavas from the volcanic front. Although back arc lavas generally have less input from the subducting lithosphere, the composition of the slab component may be similar to the one that generated the volcanic front lavas. In Central America, the back arc lavas from Honduras represent the most extreme examples of the carbonate-rich end member found in the arc, with the exception of lavas from western Nicaragua.

2. Differences with the front lavas

Some differences in geochemistry and petrogenesis between the volcanic front and back arc lavas may shed light on details on magma generation in arcs. Ba/La and U/Th have been used as indicators of slab input, and more specifically, sediment input to the generation of magmas (Carr et al., 1990 and previous section). The lavas from behind the volcanic front in Central America show lower Ba/La ratios than those from the volcanic front (Fig. 4-7; Walker et al., 1995 and Patino et al., in press). However, the ratios in some samples from behind-the-front are similar, if not higher, to ratios from volcanic front lavas in other arcs, e.g. northeast Japan (e.g. Shibata and Nakamura, 1997). Even though

the back arc lavas from Central America have significantly less slab material, the extremely high Ba/La of the subducting sediments on the Cocos Plate makes it possible to observe a relatively clear slab signature in these back arc lavas. Another geochemical difference across the arc is the U/Th in back-arc lavas, which have ratios that are similar to mantle values and thus lack the prominent U enrichment (Figs. 4-5 and 4-7). The lower uranium ratios in the back arc lavas, as in the older Nicaraguan lavas, implies that the input from the hemipelagic-rich component to the magmas is relatively small. The lower hemipelagic contribution to the generation of back arc magmas can be explained in two ways. It could be argued that because the hemipelagic sediments are the upper unit of the subducting slab, these sediments can potentially be accreted or underplated in the early stages of subduction. This scenario is unlikely because the geochemical characteristics, mainly the $^{10}Be/^{9}Be$ ratios, of lavas from the volcanic front and the back arc indicate that the hemipelagic sediments are involved in the magma genesis. The second possibility, and the most likely, is that the amount of hemipelagic material available to interact with the mantle at greater depths is depleted by the metasomatic events that generated the volcanic front magmas.

D. Central America relative to other arcs

Central American lavas, like other arc lavas, are the product of the interaction of the subducting plate with the mantle wedge. Therefore, the geochemical features commonly associated with this process are seen in samples from Central America. In an EMORB normalized diagram the lavas from Central America display the common enrichment of LILE relative to REE and HFSE (Fig. 4-6). However, the geochemical characteristics of the subducting Cocos Plate (chapter 3), mainly that of the sediments, give Central American lavas a special flavor that sets them apart from other arc related magmas.

Of the eight sedimentary sequences associated with arc lavas studied by Plank and Langmuir (1993), DSDP 495 off the coast of Guatemala is the only one that is dominated

by biogenic components. The uncommon composition of the subducting sedimentary sequence of the Cocos Plate allows it to be easily traced. In most arcs it is difficult to associate sediment component with original sedimentary units. The sedimentary column in front of some arcs may consist of only one unit, or the thicknesses of different sedimentary units are small and the units blend into one upon subduction. Moreover, volcaniclastic material is a common component of trench sedimentary sequences, making the chemical composition of the lavas and the sediments very similar. In contrast, Central America has two distinct sedimentary units.

The signature of the sediments from the Cocos Plate can be seen in the lavas from Central America because of the uncommon composition of the sediments (chapter 3). Even though the hemipelagic sediments contain much volcaniclastic material, these sediments are distinguished by their high $^{10}Be/^{9}Be$ ratio (Morris et al., 1990), as well as by their high uranium content. The carbonate sediments are depleted in elements like Th. Therefore, the carbonate input can be traced by using ratios like Ba/Th.

The unusual composition of the sedimentary units on the Cocos Plate makes the direct comparison of lavas from Central America with lavas from other arcs difficult. For example, Hawkesworth et al. (1997) studied U and Th systematics in several arcs: the Marianas, South Sandwich, Tonga-Kermadecs, Vanuatu, Aeolian Islands, Indonesia, the Philippines, Japan-Kamchatka, and the Lesser Antilles. But the geochemical features of lavas from Central America can not be explained by their model because the lavas from Central America are unusually enriched in uranium due to the contribution of the hemipelagic elements that have high organic matter content. The range of U/La along Central America (0.04 to 0.19) is higher than along other arcs like southern Kamchatka (0.02-0.05; Kepezhinskas et al., 1997), northeastern Japan (0.03-0.11; Shibata and Nakamura, 1997) and the Marianas (0.04-0.07; Elliott et al., in press).

The thick carbonate sequence contributes material that is depleted in elements like Th, a feature that is inherited by the lavas. Reflecting the biogenic nature of the entire

sedimentary sequence from DSDP Site 495, the lavas from Central America have some of the higher Ba/Th ratios (up to nearly 2000) of arc related lavas. Lavas from the southern part of Kamchatka have Ba/Th ratios that vary from 171 to 842 (Kepezhinskas et al., 1997), those from northeast Japan range from 113 to 311 (Shibata and Nakamura, 1997) and the Ba/Th for samples from the Marianas varies from 184 to 664 (Elliott et al., in press).

It is becoming apparent that the composition of the subducting component that takes part in the generation of arc magmas is not homogenous (Ryan et al., 1995; Thirlwall et al., 1996; Hochestaedter et al., 1996; Hoogewerff et al., 1997; Elliott et al., in press), and the magmas from Central America are no exception. Several authors have proposed that variations along (Thirlwall et al., 1996; Hochestaedter et al., 1996) and across (e.g. Ryan et al., 1995 and Hoogewerff et al., 1997) different arcs are produced by a heterogeneous slab component. Some argue that the slab input is comprised of two components: a hydrous fluid (mostly from the altered oceanic crust) and a melt (mainly derived from the sediments, e.g. Plank and Johnson, 1997). Presumably, the geochemical variations in arc related lavas are produced by changing the ratio of fluid/melt that modifies the mantle to generate the magmas (Ryan et al., 1995; Thirlwall et al., 1996; Hochestaedter et al., 1996; Hoogewerff et al., 1997; Elliott et al., in press).

Most of these models determine the composition of the fluids and the melts using partition coefficient data (e.g. Brenan et al., 1995) for minerals like clinopyroxene, amphibole, and garnet, in fluids and/or melts. In addition, most of these models assume that amphibole is the hydrous phase that triggers mantle melting in subduction zones. However, recent experiments suggest that other hydrous phases (e.g. lawsonite, chloritoid, phengite) may be as important, or even more important, than amphibole in the generation of arc magmas (e.g. Holloway, 1997 and Domanik and Holloway, 1996). Therefore, the models that explain heterogeneities in the slab component based on the

fluid/melt ratio will have to be re-evaluated as new partition coefficient data become available.

In Central America the models that explain the heterogeneity of the slab component do not depend on partition coefficient data. The local variations, seen within segments along and across the arc, even within individual volcanic centers, are produced by heterogeneities in the slab component, mainly variations on the content of hemipelagic sediments in the metasomatic agent, not by the process(es) that transfer material from the slab to the mantle wedge (Fig 4-5).

Shibata and Nakamura (1997) indicated that the composition of the subduction component in northeast Japan is uniform and that the slab component is less abundant towards the back arc. Back arc lavas from Central America, as well as those associated with other arcs, show smaller input from subducted material. However, the Ba/La ratios of lavas from back arc regions in Central America are similar to, or even higher than those observed in some volcanic front lavas, like northeast Japan. In Central America the composition of the slab component is heterogeneous in both the volcanic front and in back arc regions. The lavas from behind the volcanic front have a carbonate-rich end member similar to the one present in the volcanic front, but the contribution of this component to the magmatism in the back arc is significantly less (Fig. 4-5). However, the back arc lavas have lower uranium content than those from the front. This conclusion partially agrees with Hoogewerff et al. (1997) and Ryan et al. (1995) who inferred different composition of the slab component for the front and the behind the front lavas from East Sunda and the Kuriles arcs.

E. Conclusions

Heterogeneities in the composition of arc lavas are common, and are likely produced by variations in the composition of the slab component. The composition of the metasomatic agent can change because of differences in the processes that mobilize material from the slab to the mantle or because different slab units participate in the

generation of the magmas. In Central America, there are heterogeneities in the lava compositions along arc, across arc, within segments of the arc, and even in one volcano. The nature of the heterogeneities is two fold. There are variations in the intensity of the slab signature and there are differences in the composition of the slab input, both of which can be produced by physical features, like fracture zones or grabens in the subducting oceanic crust.

The data from Central America indicate that the greatest slab flux is observed in Nicaragua, where the dip of the subducting slab is also greatest. During subduction the oceanic crust bends as it sinks. As the dip angle increases, the flexure of the subducting slab will increase, and may cause or reactivate more fractures in the oceanic crust. The regional variations in the slab flux might be produced because as subduction proceeds more fluids will be released from the more highly fractured oceanic crust where the dip is steepest. These variations in flux then create the along-arc variation in trace element ratios like Ba/La and U/Th.

Subducted fracture zones, besides being areas where large amounts of slab fluids might be released, can also act as sediment traps (Miller et al., 1992). These traps can control the composition of the subducting sedimentary sequence that metasomatizes the mantle, producing the local variations observed in the lavas. In sediment traps most of the sedimentary sequence would be preserved, enhancing the possibility that both hemipelagic and carbonate sediments would be involved in the generation of arc magmas. On the other hand a horst could lead to off-scraping of the upper hemipelagic sediments. Thus, the magmas produced from slab fluxes originating from horsts would have a greater carbonate to hemipelagic ratio with larger Ba/Th ratios. Moreover, the back arc lavas from Central America seem to be the product of the interaction of the mantle with a carbonate-rich slab flux. The input from the hemipelagic sediments to the generation of back arc magmas is smaller than that for the front magmas.

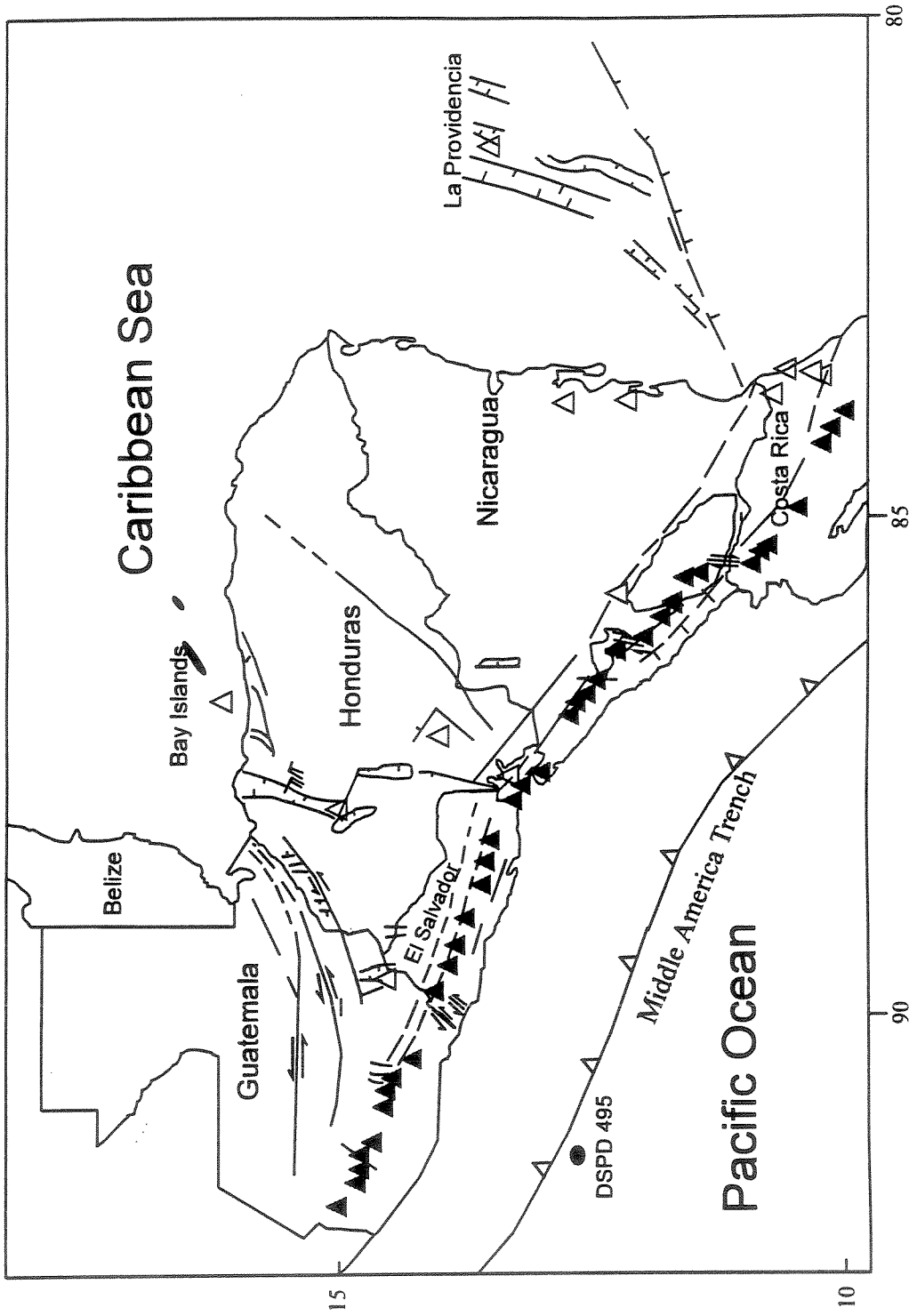


Figure 4-1. Map of Central American volcanic arc. Filled triangles represent volcanoes from the front. Back arc volcanoes are represented by empty triangles. Notice the close association of back arc magmatism to extensional tectonic features. The location of DSDP Site 495 is also indicated.

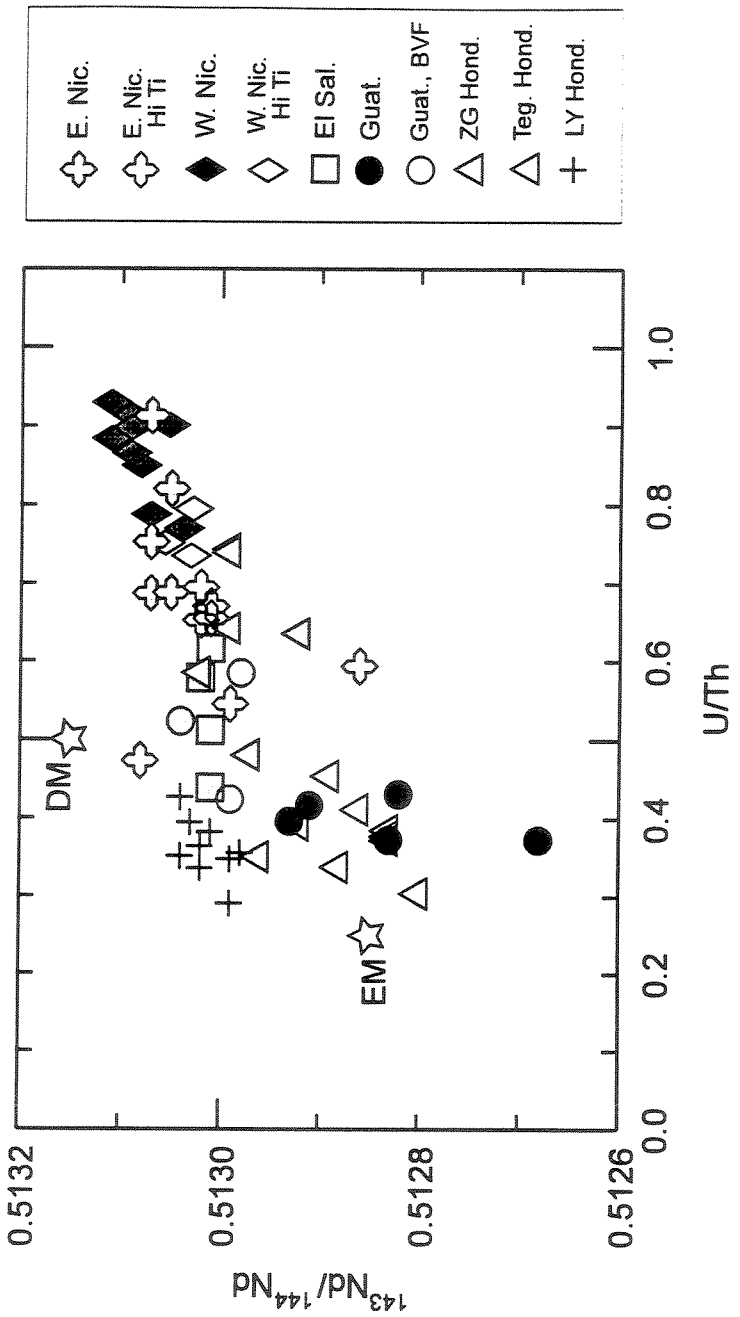


Figure 4-2. U/Th vs. $^{143}Nd/^{144}Nd$. The variations in U/Th is independent of Nd isotopes. The lavas from Guatemala have a large range of $^{143}Nd/^{144}Nd$, produced by crustal assimilation. In the legend the following abbreviations are used: Eastern Nicaragua (E. Nic.), Western Nicaragua (W. Nic.), El Salvador (El Sal.), Guatemala (Guat.), behind the front in Guatemala (Guat., BVF), Zacate Grande - behind the front in Honduras (ZG Hond.), Tegucigalpa - behind the front in Honduras (Teg. Hond.), Lake Yojoa - behind the front in Honduras (LY Hond.).

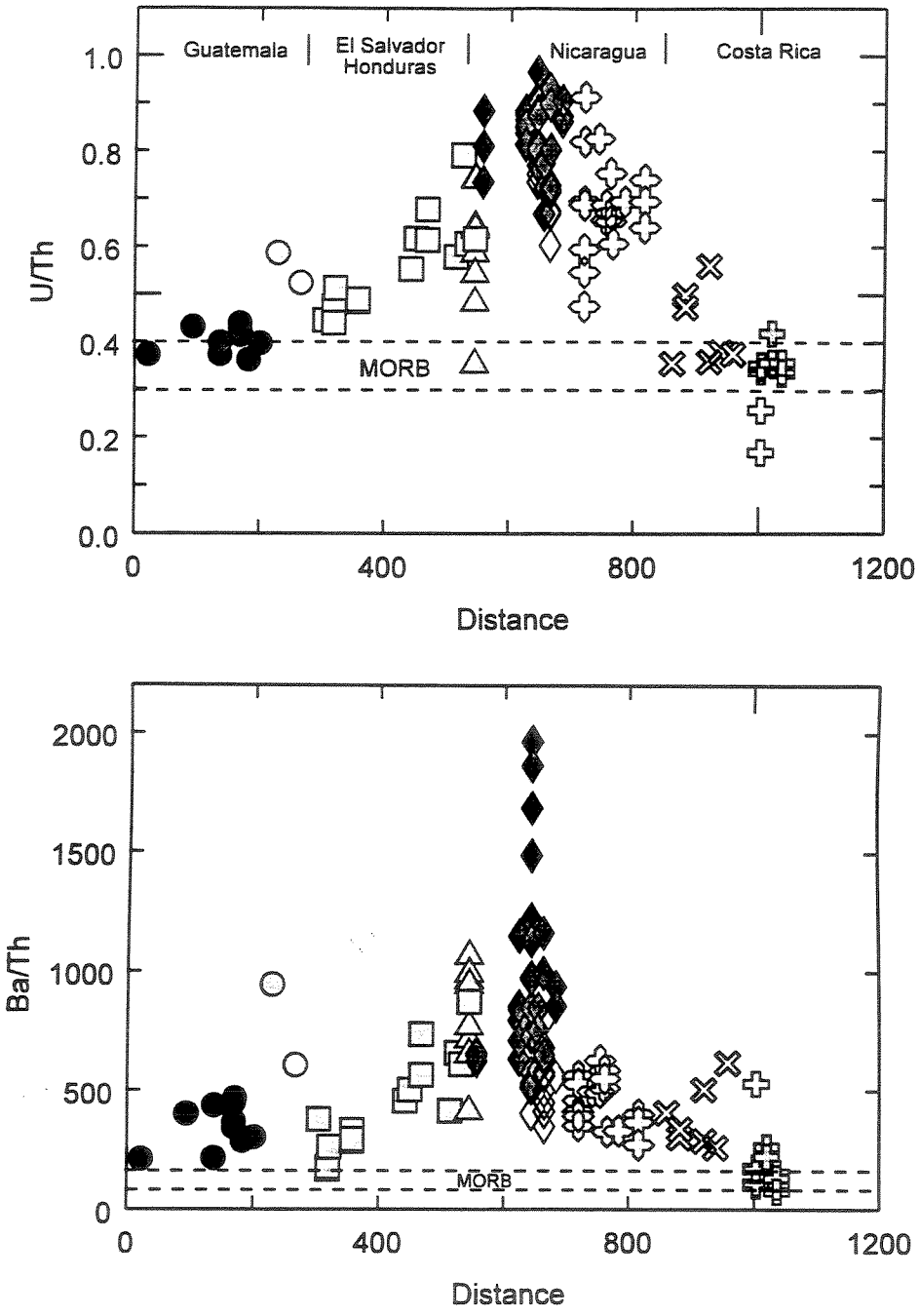


Figure 4-3. Regional variations of U/Th and Ba/Th. U/Th range along the arc is relatively small, the transition from one segment to the next is smooth. Ba/Th has a wider range along the arc, and the transitions from segment to segment are abrupt. Samples from western Nicaragua have the highest ratios U/Th and Ba/Th.

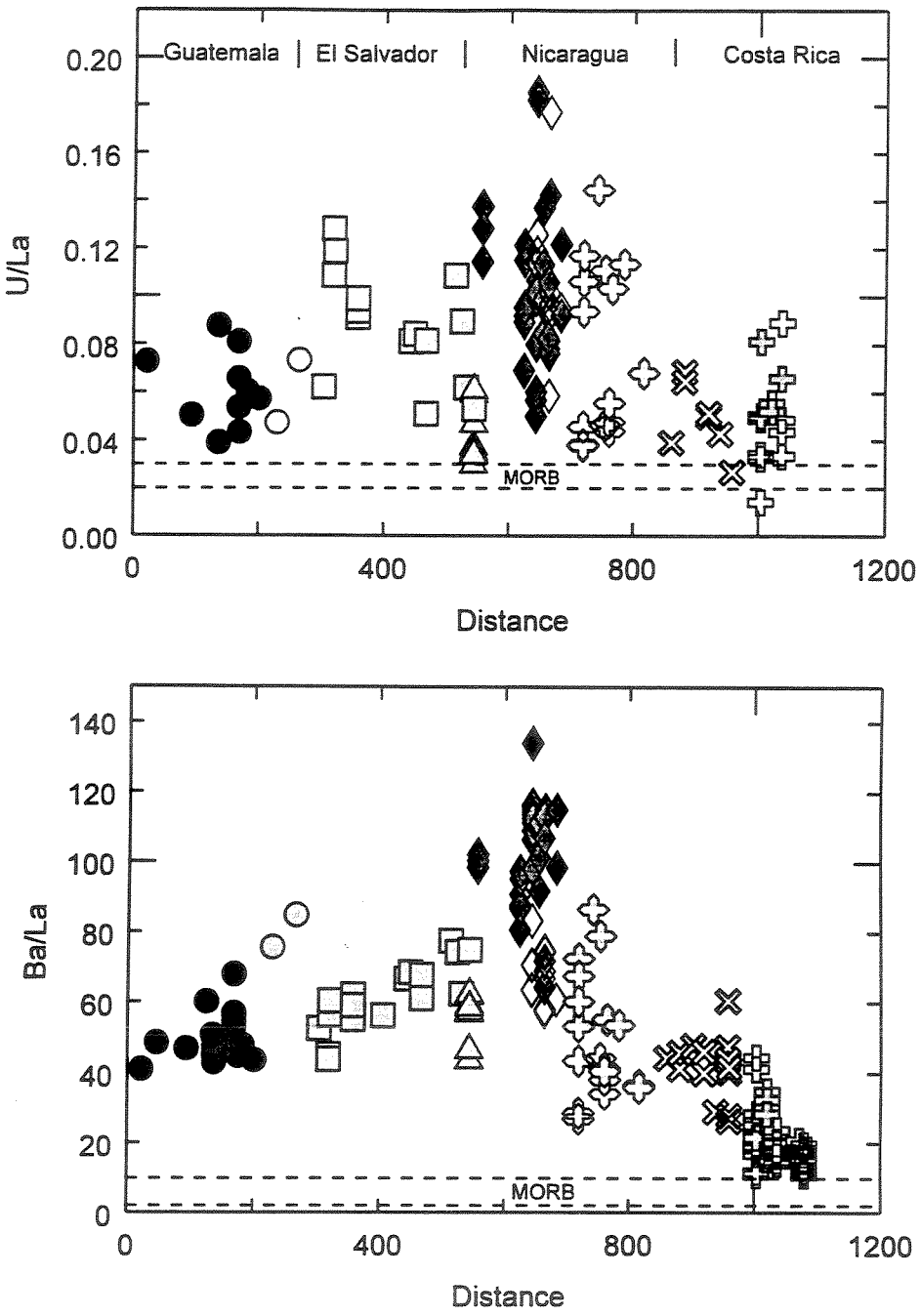


Figure 4-3 cont. Regional variations of U/La and Ba/La. The U/La ratio is more scattered than the Ba/La, mainly in El Salvador and eastern Nicaragua. Both ratios have higher values in western Nicaragua.

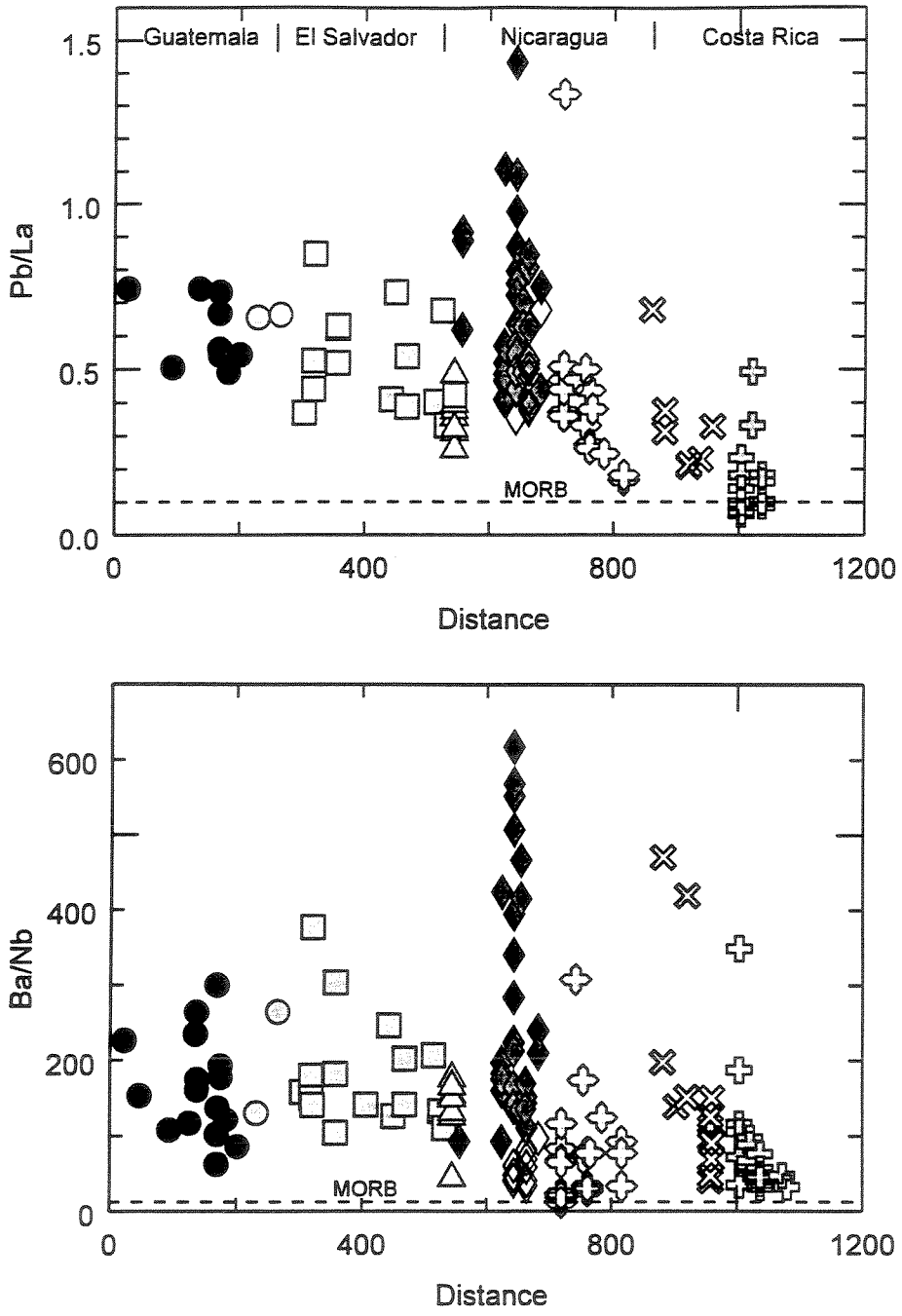


Figure 4-3 cont. Regional variations of Pb/La and Ba/Nb . As in the previous plots, the lavas from western Nicaragua have the highest ratios. These two ratios have less clear to negligible regional variations.

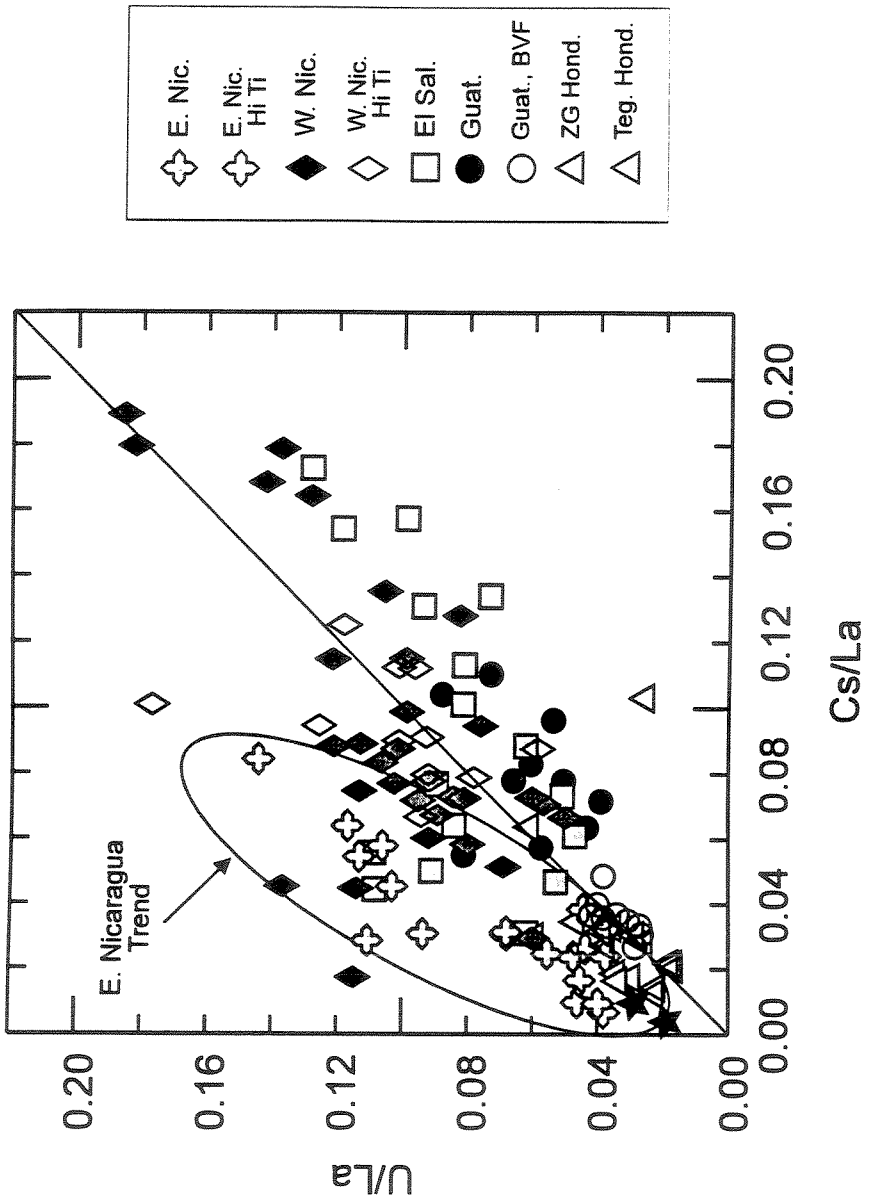


Figure 4-4. U/La vs. Cs/La. Most of the lavas from Central America plot close to the line with slope of one. However, the samples from eastern Nicaragua define a trend that has a steeper slope. The black stars represent E-MORB and N-MORB from Sun and McDonough (1989).

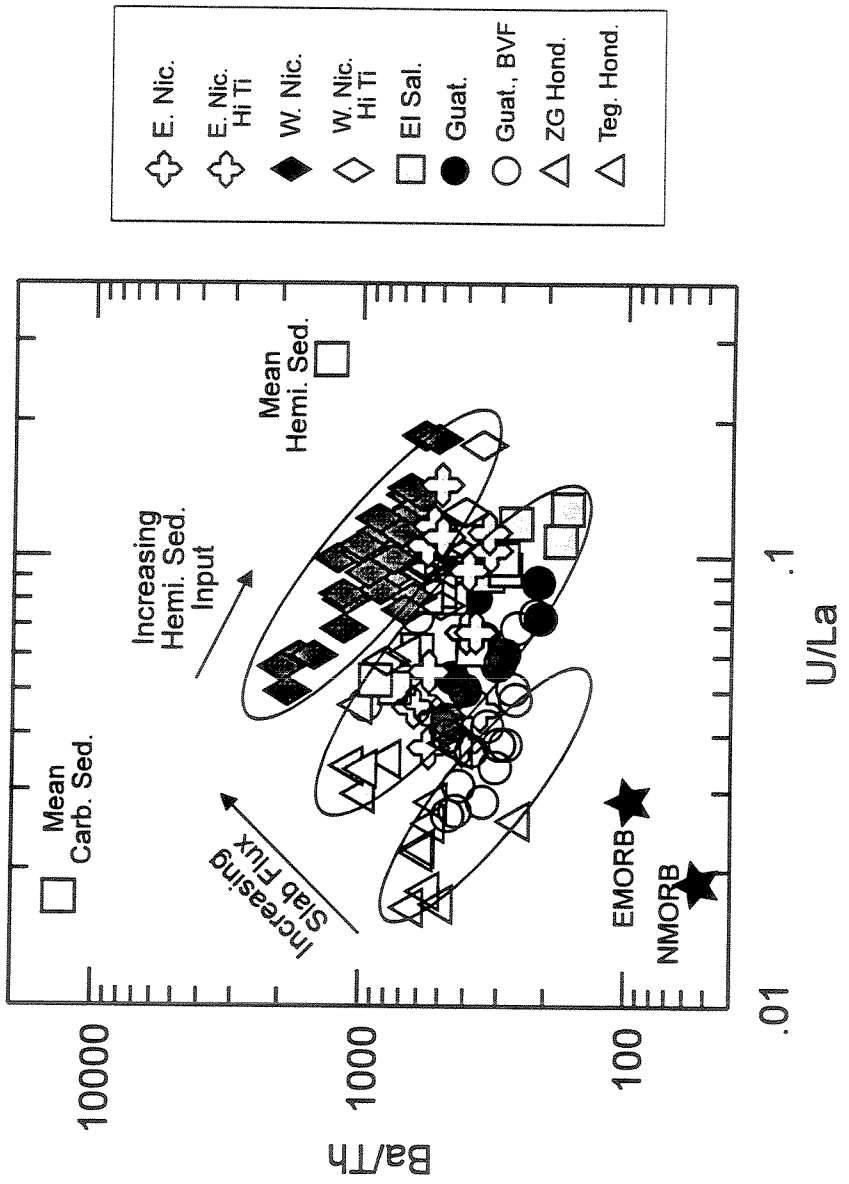


Figure 4-5. Local and regional variations in lavas from Central America. Local variations are produced by varying the ratio of carbonate to hemipelagic sediment in the slab component during magma genesis. With increasing hemipelagic sediment involvement, Ba/Th decreases and U/La increases. The regional variations in the amount of slab flux are also observed. Samples from western Nicaragua plot the furthest from MORB and the lavas from back arc regions plot closest to MORB.

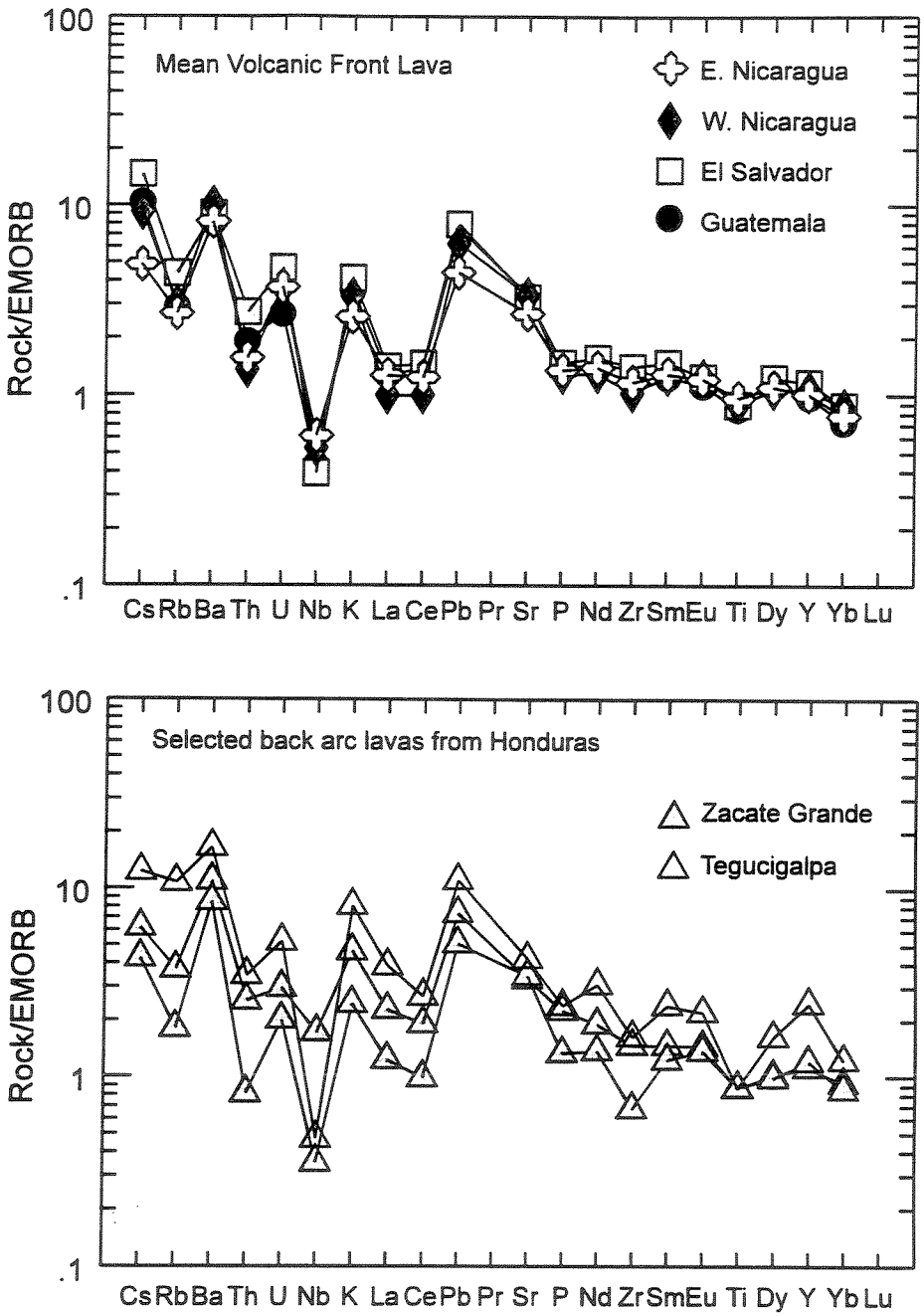


Figure 4-6. EMORB normalized diagrams for mean lavas from different segments of the volcanic front and for selected samples from back arc regions in Honduras. These samples display the arc related enrichment of LILE relative to REE and HFSE.

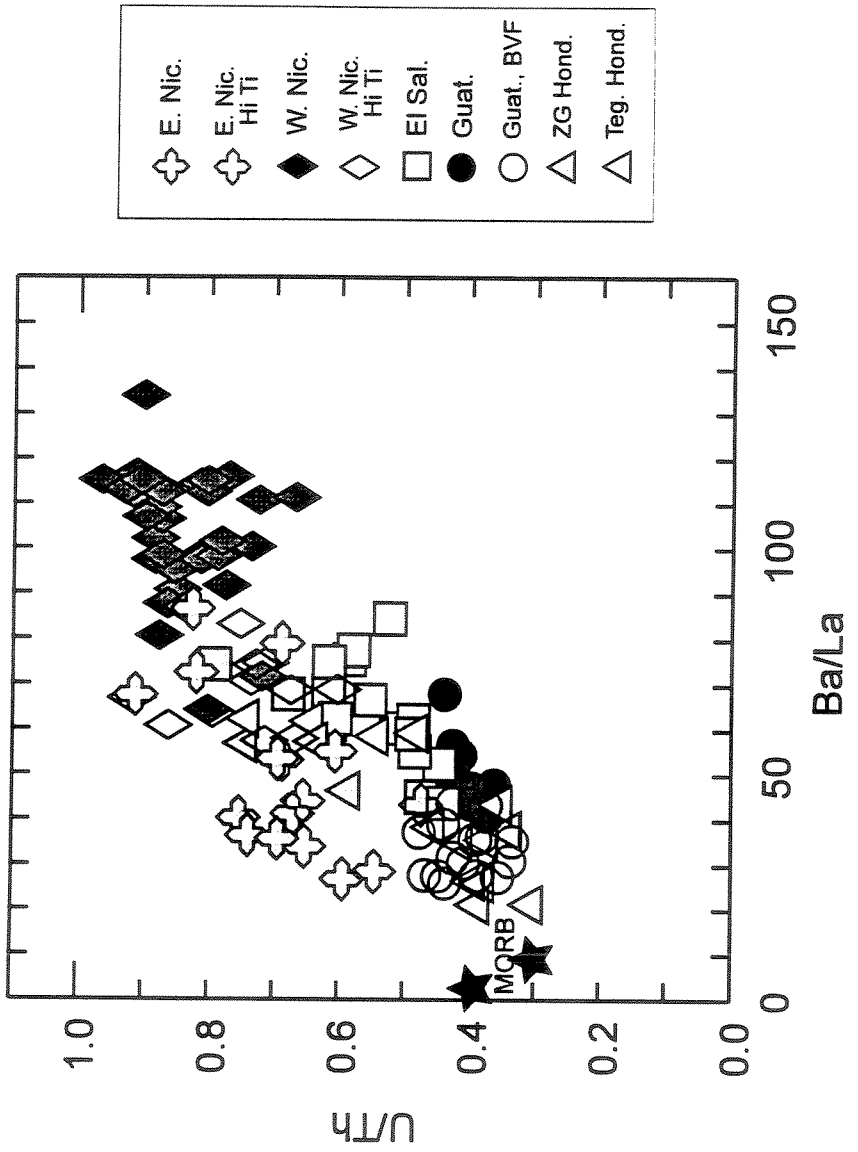


Figure 4-7. Ba/La vs. U/Th for lavas from Central America. The samples from behind the volcanic front have lower Ba/La than the samples from the front, but higher than E-MORB and N-MORB. The U/Th of most of the back arc lavas is similar to that of MORB.

V. PROCESSES FOR SLAB INPUT

A. Introduction

There is little controversy over the involvement of the subducted slab in the generation of arc magmas (e.g. Tera et al., 1986; Plank and Langmuir, 1993; Ishikawa and Nakamura, 1994). However, the processes that move elements in the subduction zone system are poorly understood and subject to debate; the most accepted transfer agents are hydrous fluids and siliceous melts (e.g. Plank, 1993; Hoogewerff et al., 1997). In many instances, heterogeneities in the chemical composition of arc lavas are explained by variation in the ratio of the two processes (e.g. Ryan et al., 1995). Models of the process(es) that mobilize material from the slab to the mantle wedge are limited by lack of knowledge of the mineral assemblage of the subducted oceanic crust and by poorly constrained partition coefficient data (Langmuir, 1994). Another way to understand the subduction zone system is to estimate the mass fluxes into and out of the system and try to determine the efficiency with which the entire magma production process returns material from the subducting slab. In the sections below I will apply both the modeling and mass balance approach to Central America.

B. Modeling hydrous fluids and melts

1. Hydrous Fluids

Arc lavas are commonly enriched in some elements relative to MORB and/or subducted sediments. This enrichment has been explained as a consequence of metasomatism of the mantle by hydrous fluids, because fluids selectively fractionate elements from the subducting slab (Arculus, 1994 and references therein). The bulk addition of subducted material to the mantle or the addition of a melt derived from the subducted slab does not produce the selective enrichment of incompatible elements observed in arc lavas (Pearce and Peate, 1995). The presence and importance of hydrous fluids in the generation of arc related magmas is inferred from data derived from different types of materials associated with subduction zones: veins in metamorphic rocks, mantle

xenoliths, water content in back arc lavas, and arc lava geochemistry (Bebout et al., 1992; Maury et al., 1992; Stolper and Newman, 1994; Shibata and Nakamura, 1997).

Bebout et al. (1992) studied rocks from the Catalina Schist Complex, California, associated with high pressure - low temperature metamorphism, indicative of a subduction zone setting. The authors found veins and reaction zones, evidence of fluid transport, and they suggest that the hydrous fluids were produced as the subducting slab lost volatiles. These veins have higher concentrations of elements highly mobilized by fluids, such as B, than the host metamorphic rocks. Maury et al. (1992) noticed that xenoliths from the Philippines are depleted in Si, Na, Al, Eu and enriched in large ion lithophile elements (LILE). This geochemical composition led them to conclude that the xenoliths originated from a hydrous fluid and not from a siliceous melt. Stolper and Newman (1994) found a direct relationship in back arc lavas from the Marianas Through between H_2O content of glasses and concentration of LILEs. Shibata and Nakamura (1997) inferred the presence of hydrous fluids in the generation of arc lavas by comparing elements that are mobilized by hydrous fluids (like Sr and Pb) to those that are not easily mobilized by hydrous fluids (like rare earth elements, REEs). Their main observation, that the ratios of Sr/Nd and Pb/Nd in the slab component decrease with increasing depth, but Sr/Pb remains almost constant, is most easily explained by the high mobility of Sr and Pb and low mobility of the REEs in a fluid.

The most accepted origin for the hydrous fluid in subduction zones is the dehydration of the altered oceanic crust (e.g. Tatsumi et al., 1986; Ellam and Hawkesworth, 1988; Shibata and Nakamura, 1997). In the subduction zone the altered igneous rocks are metamorphosed, and hydrous fluids are produced by the breakdown of minerals as pressure and temperature conditions change (Arculus, 1994). For a long time, it has been assumed that the hydrous fluid is most likely produced by the dehydration of amphiboles (Tatsumi et al., 1986). However, recent experiments indicate that other hydrous minerals, such as lawsonite, can also generate hydrous fluids at relevant depths

(e.g. Domanik and Holloway, 1996). In any event, the hydrous fluid is likely to trigger the melting event that produces arc magmas (e.g. Arculus, 1994 and references there in).

There are several scenarios for hydrous fluid interaction with the mantle wedge. Hydrous fluids can create gravitational instabilities and upwelling in the mantle, and/or the fluids can lower the solidus temperature of the mantle (Plank and Langmuir, 1988; McCullock and Gamble, 1991; Arculus, 1994; Davies and Stevenson, 1992). Furthermore, hydrous fluids act as transporting agents of selected elements from the subducting slab or from the mantle wedge (Arculus, 1994; Hawkesworth et al., 1994; Plank, 1993; McCullock and Gamble, 1991; Ellam and Hawkesworth, 1988).

The composition of the hydrous fluid is inferred from the enrichment of arc lavas relative to igneous rocks from other tectonic settings. Bebout et al. (1992) assumed that the composition of the hydrous fluid is homogenous along subduction zones, but that the composition and quantity of the fluid is inferred to change during progressive metamorphism of the slab (e.g. Ryan et al., 1995). The composition of the hydrous fluids derived from the dehydration of the altered oceanic crust is inferred to be enriched in hydrophilic elements like B, Cs, Rb, Ba, K, Sr, Pb, Sb (Maury et al., 1992; Woodhead and Johnson, 1993; Edwards et al., 1993; Leeman et al., 1994; Ishikawa and Nakamura, 1994; Hawkesworth et al., 1994; Ryan et al., 1995; Pearce and Peate, 1995; Noll et al., 1996; Thirlwall et al., 1996; Shibata and Nakamura, 1997; Elliott et al., in press). Even though uranium is not a hydrophilic element, the high oxygen fugacity of the hydrous fluids enhances the mobility of this element (Bailey and Ragnardottir; 1994 and Hawkesworth et al., 1997).

2. Melts

Melts from different units of the subducted slab may have taken part in the generation of some arc magmas (e.g. Ellam and Hawkesworth, 1988 and Plank, 1993). Lavas associated with the subduction of young oceanic crust have different geochemical characteristics from those associated with older oceanic crust; the most striking

differences are the common occurrence of high Nb basalts and high Mg andesites (e.g. Stolz et al., 1996 and Yogodzinski et al., 1995). Another line of evidence for the involvement of a melt phase in arc magma genesis comes from the systematics of elements, like Th, that are not easily mobilized by a hydrous fluid (Reagan et al., 1994). Furthermore, Kepezhinskas et al. (1996) found xenoliths associated with high Nb lavas from the northern part of the Kamchatka arc, that contain inclusions rich in Si, Al, and Na, providing direct evidence for a siliceous melt.

Melts derived from the subducted slab can originate from siliceous sediments or from the basaltic oceanic crust depending on the conditions of subduction (Stern and Wyllie, 1973 and Stolz et al., 1996). Stern and Wyllie (1973) demonstrated that red clays from the Atlantic start melting at 30 kbar and 680°C in the presence of 7.8 wt.% H_2O. In a similar set of experiments, Plank and Johnson (1997) concluded that mobilization of LREE, Th, Be and Nb from sediments increases when temperatures exceed the wet solidus of red clay (>700°C) at 20 kbar.

Moran et al. (1992) suggested that melting of subducted oceanic crust is not likely because the boron content of arc lavas is relatively high, restricting sub-arc temperatures to less than 900°C. However, Schiano et al. (1995) found evidence of low degrees of melting of subducted oceanic crust in mantle xenoliths from the Luzon arc. The melts, preserved as glass inclusions in the xenoliths, are enriched in water, silica and LILE and depleted in HFSE (high field strength elements). In addition, the thermal structure of subduction zones where the oceanic crust is young and more buoyant is such that the wet basalt solidus is shallower (Davies and Stevenson, 1992). Therefore, the young oceanic crust will melt, rather than dehydrate, and carry a different geochemical signature from that produced by dehydration of mature oceanic crust (Yogodzinski et al., 1995). The composition of slab melts will depend on the composition of the starting material, subducted siliceous sediments or basaltic oceanic crust. In any event, slab melts are likely

to mobilize Th, LREE, HFSE, and Be (Pearce and Peate, 1995; Plank and Johnson, 1997; Hawkesworth et al., 1997; Elliott et al., in press).

Ryan et al. (1995) described the distribution of several elements across the Kuriles Islands and classify the elements into two groups. The first group of elements are those that drastically decrease from the volcanic front to the back arc (B, Cs, and Sb). The other set of elements are those that remain almost constant across the arc (K, Ba, La, Be). They concluded that these two trends are produced because elements are being mobilized by two different processes. Boron, Cs and Sb are transported in a hydrous fluid, whose abundance decreases as the slab loses volatiles. The other elements (K, Ba, La, Be) are mobilized by a melt, and the melt production does not change significantly as subduction proceeds (Ryan et al., 1995). The conclusions of Ryan et al. (1995) are in agreement with Schiano et al. (1995), who found that melts associated with the Luzon arc are enriched in water, silica and LIL and depleted in HFS elements.

3. Fluid-Melt Models

In order to reproduce the composition of fluids and melts derived from the subducted slab, several parameters must be known: the chemical composition of the slab (chapter 3), the mineral assemblage that results from the progressive metamorphism of the slab units, and the partition coefficient of elements of interest between the mineral phases present and the fluids and/or melts. Of these three factors, only the chemical composition of the sedimentary layers of the Cocos Plate are well constrained.

The composition of slab derived melts or fluids depends on the mineral assemblages and on the partitioning behavior of elements. Brenan, in collaboration with other scientists (e.g. Brenan et al., 1995), has determined partition coefficients for elements in mantle minerals (olivine, clinopyroxene, garnet, and amphibole). However, additional minerals are being recognized as important in metamorphosed subducting slabs (e.g. Nelson, 1995). The partition coefficients also vary according to the volatile content

of the fluids and melts. The volatile composition of the fluid/melt can restrict or enhance the mobilization of some elements, such as uranium.

Understanding the systematics of uranium in subduction zones is of more general interest because U subducted into the mantle of arcs may be the source of the HIMU component in the mantle. However, uranium is an element that is difficult to model. Uranium may be mobilized by a melt from mantle minerals or by hydrous fluids. If the process transferring U is a fluid, the mobility of U depends on the fO_2 of the fluid (Keppler and Wyllie, 1990; Bailey and Ragnarsdottir, 1994).

The partition coefficients used in models that generate fluids and/or melts from the different components of the subducting Cocos Plate are listed in table 5-1. The element concentrations in the fluids and melts are calculated using the equilibrium batch melting equation of Shaw (1970):

$$C_{liq}^{\ i} = \frac{C_o^{\ i}}{D_i^{\ o} + F\,(1\text{-}P_i)}$$

This equation gives the concentration of element *i* in a fluid or melt (depending on the partition coefficients selected) from a source with a concentration $C_o^{\ i}$. F is the fluid or melt fraction. $D_i^{\ o}$ is the bulk solid-liquid partition coefficient at F = 0 (initial bulk solid-liquid partition coefficient), and P_i is the partition coefficient for the fluid (or melt) norm relative to the source minerals (i.e. the partition coefficient for the mineral proportions entering the fluid or melt). The absence of a particular mineral from the assumed assemblage implies that the mineral is no longer relevant because it has been consumed by melting. The mineral assemblages used for the different models are listed in table 5-2 and selected results from the different calculations are listed in table 5-3.

Because of all the uncertainties previously stated, several parameters were varied in trying to reproduce the chemical characteristics of lavas from Central America. In Central America, there are regional variations in the intensity of the slab flux as well as

local variations that are controlled by the carbonate/hemipelagic sediment ratio involved in magma genesis. The lavas used in the models, Te-1 and Te-114, represent the end-member lavas, richest in hemipelagic and carbonate components, respectively. These samples from Telica were chosen for two reasons. Telica is located in western Nicaragua, where the maximum slab flux is observed. Thus, the samples show clear and strong slab signatures. In addition, the REEs pattern of the lavas are very similar to EMORB (Fig. 5-1). Even though these lavas represent different local end members, their similar REE patterns indicate that they originated from similar mantle sources and by similar degrees of melting because the REE are not easily mobilized by slab fluids.

The arc magmas are mostly produced by melting of the mantle with fluid or melt contributions of a few percent at most. The composition of the magma source is assumed to be similar to the EMORB source of Sun and McDonough (1989). Table 5-2 describes the parameters used to calculate the source composition. In terms of mass, the slab component is dominated by the input from the altered basaltic oceanic crust. Similar fluid compositions have also been inferred for other arcs, like northeastern Japan and Java (Shibata and Nakamura, 1997; Edwards et al., 1993).

To reproduce the composition of the carbonate-rich endmember (Te-114) the slab contribution consists of a mixed fluid (FAOC + FCS), with 80% of hydrous fluid from the altered oceanic crust (AOC) and 20% hydrous fluid from the carbonate sediments (CS). To model the hemipelagic-rich endmember (Te-1) a new component must be added to the previous mixed fluid (FAOC + FCS); this component can be either a hydrous fluid (FHS) or a melt (MHS) derived from the hemipelagic sediments. The slab components were mixed with the EMORB source mantle in the following proportions: 98% EMORB mantle plus 2% mixed fluid (FAOC + FCS) to model Te-114, the carbonate-rich endmember. In addition, 99.5% EMORB mantle plus 0.35% mixed fluid (FAOC + FCS) plus 0.15% hemipelagic fluid (FHS) or melt (MHS) was used to reproduce the composition of Te-1, the hemipelagic-rich end member.

Several variants of the two basic models described above allow one to consider the effects of changing the mineralogical composition of the residue (with or without amphibole; Figs. 5-2 to 5-4), the effect of using a hemipelagic fluid or hemipelagic melt (Figs. 5-5 and 5-3 vs. 5-6), and the effects of using different sections of the altered oceanic crust (Figs. 5-7 and 5-8). Table 5-2 list the mineral assemblages used for the different models and table 5-4 summarizes the different models.

a. Mineral variations

Mineral assemblage and partition coefficient data on subduction zones are poorly known, producing large uncertainties in the results of these forward models. For a long time it has been assumed that melting in subduction zones occurs because of the breakdown of amphibole at a given pressure (Tatsumi et al., 1986). There is no doubt that amphiboles are important minerals in subduction zones, but by no means they are the only hydrous phase stable at the pressure and temperature conditions of interest for arc magmatism (Domanik and Holloway, 1996 and Schmidt, 1996). For example, Schmidt (1996) proposes that phengite is an important phase in the recycling of potassium in subduction zones. He suggested that at depths less than 110 km, fluids are produced by the dehydration of relatively K-poor phases like chlorite, epidote, zoesite, lawsonite, amphiboles, and chloritoid. But at depths greater than 110 km, fluids are produced by the dehydration of phengite. Domanik and Holloway (1996) also show that amphiboles are not the only hydrous phase in subducting slabs. They indicated that phengite, lawsonite, topaz-OH, and Mg-pumpellyite are stable beyond the pressure and temperature conditions of arc magma genesis.

The subducting Cocos Plate consists of three units, all of which must undergo progressive metamorphism in the subduction zone. There are few data on what happens to carbonate sediments after subduction. Therefore, to model the carbonate sediments the mineral composition of the residue and the melt were assumed to be 100% olivine. This mineral composition arbitrarily allows most elements of interest (but not REEs) to be

transferred by the fluid. The mineral assemblage of the source and residue for the hemipelagic sediments and the altered oceanic crust are more variable and will be discussed in more detail (tables 5-2 and 5-4).

The metamorphic mineral assemblage of the subducted hemipelagic sediments is assumed to change from aluminum-rich clay minerals to a more complex assemblage that may include mica-quartz-amphibole-garnet-ilmenite-clinopyroxene-kyanite-cordierite, among others. However, as explained earlier, there are few data on the behavior of elements of interest in the presence of phases like mica. Therefore, the mineral composition of the models involving the hemipelagic elements will be restricted to clinopyroxene, garnet and amphiboles, for which partition coefficients are known. Due to progressive metamorphism in the subduction zone, the MOR basalts and gabbros are likely to transform into amphibole eclogites. Thus, the mineral assemblage of the oceanic crust is also represented by clinopyroxene, garnet and amphibole.

Figure 5-2 shows the effects of different mineral assemblages on the compositions of the modeled fluids and melts. By increasing the amount of amphibole dehydrating, U/La decreases and Ba/Th increases. Unfortunately, this study of the effects of varying mineral proportions had to be restricted to changing the amount of amphibole present because there are no partition coefficient data on other minerals that have recently been recognized in metamorphosed oceanic crust associated with subduction zones.

Changing the residual mineralogy (during fluid/melt generation) by allowing all of the amphibole to break down does not significantly affect the fit of the model that attempts to reproduce the composition of Te-114 (carbonate-rich end member). Figure 5-3 compares a model in which some amphibole (Fig. 5-3a) remains in the residue with one for which all of the amphibole is consumed to trigger melting (Fig. 5-3b). As expected, the K and Pb melt concentrations in the model without residual amphibole are slightly higher than in those generated in equilibrium with residual amphibole. The other elements are not significantly changed.

If an amphibole eclogite mineral assemblage is assumed for both residue and the melt of hemipelagic sediments, the composition of Te-1 is to some extent reproduced, with the exception of K which is too low in the model (Fig. 5-4a). Allowing all of the amphibole to break-down will increase the concentration of most elements in the melt, including K (Fig. 5-4b). Thus, a model with hemipelagic melt with a residue that has low amounts of amphibole best reproduces the composition of lavas like Te-1.

b. Fluids vs. Melts:

Figure 5-5 shows the differences in the element ratios generated in fluids vs. melts from the hemipelagic sediments and altered oceanic crust. In both cases, the compositions of the melts are closer to the compositions of the starting materials (hemipelagic sediments or altered oceanic crust, respectively). This is not surprising, because moderate to high degree melts are not efficient in selectively mobilizing incompatible elements from the starting compositions (Pearce and Peate, 1995). Furthermore, in both cases, the Ba/Th and U/La of the fluids are higher than those of the melts or the bulk compositions.

In Central America, the subducting altered oceanic crust is assumed to generate hydrous fluid instead of melt because of the oceanic crust is not young enough to be a likely candidate for slab melting. However, there is no consensus on the process(es) that transfer material from the hemipelagic sediments to the mantle wedge (Reagan et al., 1994). For this reason, two models for Te-1 (hemipelagic-rich endmember) are presented, one which assumes that a melt is the mobilizing agent (Fig. 5-4), and the other which assumes it is a hydrous fluid (Fig. 5-6). Figure 5-4b (a melt model) best reproduces the chemical composition of Te-1. The 20% mantle melt model matches the Cs, Rb, K, and Pb concentrations of the lava relatively well. The major discrepancies are for Ba, Th, and U, where the model concentrations are higher than the lava. The discrepancies most likely reflect the poorly constrained mineral assemblage and the poorly known partition coefficient data.

Fluids, in general, are better than melts at selectively leaching elements from different materials. If we assume that a hydrous fluid is the agent that transfers material from the hemipelagic sediments to the mantle wedge, uranium is greatly affected (Fig. 5-6). The uranium and thorium concentrations in the melt model are higher than the U and Th concentrations of the lavas (Fig. 5-4b). However, when a hydrous fluid is assumed, the model produces lower concentrations than in the lava (Fig. 5-6). This result, that U is more readily mobilized by a melt, does not agree U-Th disequilibrium studies of arc lavas (Hawkesworth et al., 1997; Gill et al., 1993; Reagan et al., 1994); these models typically assume that uranium is more easily mobilized by a hydrous fluid than a melt in arc settings. However, more partition coefficient data for U under different conditions may bring light to this paradox.

c. Different sections of the altered oceanic crust:

The altered oceanic crust is assumed to be composed of two major units (chapter 3) based on the Site 504. The upper volcanic part (0.5 km) underwent low temperature alteration and is enriched in elements like B, K and Rb (Alt et al., 1996), and the lower section (1.5 km) corresponds to the upper dikes. This lower section, closer to the magma chamber, was extensively altered by hydrothermal fluids (Alt et al., 1996). The hydrothermal fluids leach elements from the lower part, and deposit them in the upper section of the dikes. The models thus far have assumed that the full 2 km thickness of the altered oceanic crust is involved in magma genesis. The basis for this assumption is the water content of the samples from Site 504, which remains almost constant (~1%) throughout the section (Alt et al., 1996).

Figure 5-7 shows fluids derived from different sections of the altered oceanic crust. The upper volcanic section produces fluids that are significantly enriched in Ba/Th relative to its bulk composition and to the fluids produced by the lower section of the oceanic crust. The U/La of the fluids from the upper and lower sections of the oceanic crust are

similar to each other, but the U/La ratios of the hydrous fluids are significantly higher than their bulk compositions.

Figure 5-8 shows the effects of varying the section of altered oceanic crust used. The composite altered oceanic crust (0.5 km upper section + 1.5 km lower section) is dominated by the lower section. Therefore, there are no significant differences in the models when the entire section is used or when only the lower section is used (Fig. 5-3b vs. 5-8a). Barium, Th, U and Sr seem to be independent of the composition of the altered oceanic crust, implying the these elements are mostly contributed by the subducted sediments. On the other hand, elements like Pb, and to a lesser extent Rb, K and Cs, are controlled by the composition of the altered oceanic crust. If only the upper volcanic section of the oceanic crust (Fig. 5-8b), along with the carbonate oozes, is involved in the generation of lavas like Te-114, Pb is lower and Cs, K, and Rb are higher than if the lower section or the entire section take part in magma genesis. These results closely reflect the geochemical composition of the different sections of the altered oceanic crust (Alt et al., 1996).

The models that best reproduce the chemical characteristics of Te-114 and Te-1, the carbonate- and hemipelagic-rich endmembers respectively, are those presented in figures 5-3b and 5-4b. In both cases it is assumed that all the amphibole breaks down. If these models are valid, they should be able to describe the chemical characteristics of the other lavas from Central America. Figure 5-9 shows mixing lines between the mantle and fluids derived from the subducting Cocos Plate. The composition of the carbonate-rich lavas is easily reproduced by metasomatizing the mantle with a mixed fluid (line A). This mixed fluid is 80% fluid derived from the altered oceanic crust (where all the amphibole dehydrates to produce the fluid) and 20% fluid derived from the carbonate sediments. The variations in the chemical characteristics of the carbonate-rich lavas from Central America are produced by changing the ratio of EMORB source mantle to this mixed fluid. The

lavas from western Nicaragua will have a lower mantle/fluid ratio relative to lavas from other segments of the arc.

The modeling of the hemipelagic-rich lavas is more troublesome than the modeling of the carbonate-rich lavas. Figure 5-4b shows the model that best approximates the composition of the hemipelagic-rich lava Te-1. This model was created by melting metasomatized EMORB mantle, where the metasomatizing agent is a mixture of fluid (80% fluid from the altered oceanic crust and 20% fluid from the carbonate sediments) and melt derived from the hemipelagic sediments, with no amphibole left in the residue. It is evident from figure 5-4b that the model lavas are too high in most elements (especially Ba), but the overall trace element pattern of Te-1 is reproduced. The high barium content in this model is clearly displayed in figure 5-9. Mixing line B, defined by EMORB source mantle and the fluid-melt mixture described above has Ba/Th ratios that are too high to reproduce several low Ba/Th lavas Telica. A better mixing line for Ba, Th, U and La is case C. In this case the mantle has been modified by fluids and melts that form in the presence of some residual amphibole in the oceanic crust. However, the spider diagram for this metasomatized mantle shows that the model lavas have lower K content than Te-1 (Fig. 5-4a).

The models presented (Figs 5-2 to 5-9) clearly show the current limitations on forward modeling to reproduce the chemical characteristics of lavas related to subduction zones. This modeling, using weakly constrained mineralogical data and poorly known partition coefficients, produces weak results. However, the models provide a general idea of what is geochemically happening along Central American volcanic arc. Because none of these models exactly reproduce the chemical composition of the lavas, the models presented in this section should be revised as new partition coefficient data become available.

C. Output/Input Flux Calculations

In light of the uncertainties in forward modeling, a different approach was tried. In this case, there are no attempts to separate out the processes that mobilize material from the subducting slab to the mantle wedge. Instead, this approach just compares the contribution from the subducted slab with the composition of the erupted lavas.

1. Input Flux

The output/input flux ratios for Central America are relatively well constrained because there are few uncertainties in the calculation of the input flux. The calculations of the slab flux are based on a comprehensive geochemical data set for the sediments and altered oceanic crust involved in the generation of arc magmas. Chapter 3 describes in detail the composition of the sediments from DSDP Site 495 off the coast of Guatemala, and also has information regarding the geochemical characteristics of altered oceanic crust from Site 504. This site was selected to represent the composition of the igneous part of the oceanic crust because it is the deepest hole yet drilled, giving the most complete geochemical composition of the subducting igneous rocks.

The flux into the system was calculated using the following equation:

$$\text{Input flux (gm cm}^{-1}\text{yr}^{-1}) = \text{convergence rate} * \Sigma\, \text{ppm}_i * \text{density}_i * \text{thickness}_i$$

where i = Slab units (hemipelagic sediments, carbonate sediments, and altered oceanic crust).

The convergence rate for Central American arc varies from 7.1 cm/y to 9 cm/yr. In the input flux calculation the convergence rate in Nicaragua was used (8.1 cm/yr); ppm is the concentration of different elements in the different slab units (chapter 3); the biggest uncertainty in the calculation of the flux into the system is the composition of the altered oceanic crust. There are no recent geochemical data on the volcanic section of Site 504, and the concentrations of important elements like Ba, Cs, U, Th, and Pb are poorly constrained. The densities used are 1.3 gm/cc, 1.7 gm/cc, and 2.75 gm/cc for the

hemipelagic sediments, the carbonate oozes, and the altered oceanic crust respectively. The thicknesses of the hemipelagic sediments and the carbonate oozes were approximated at 0.2 km each. As discussed by Alt et al. (1996), Site 504 can be divided into two units depending on the type of alteration. The upper 0.5 km shows characteristics of low temperature alteration, whereas the lower 1.5 km of rock was altered by hydrothermal fluids. Plank (1993) did similar input flux calculations for eight trenches. The only difference between her equation and the one presented here is that she took into account the water content of the sediments to compensate the masses of sedimentary units that have vastly different thicknesses.

Table 5-5 and figure 5-10 show the percentage of the input flux from the different slab units. The hemipelagic sediments contribute most of the B, Cs, Rb, U, K, and some of the Ba. The carbonate oozes contribute most of the Sr, and significant quantities of Ba. The upper section of the altered oceanic crust also contributes B, Rb, Cs, and K. Lead is mostly supplied by the hydrothermally altered oceanic crust.

2. Output Flux

The flux out of the system has more uncertainties than the input flux, with the greatest uncertainties being related to the production of magma in the arc. The output flux was calculated using the following equation:

$$\text{Output flux (gm cm}^{-1}\text{yr}^{-1}\text{)} = (\text{rock} * \text{density} * \text{volume}) / (\text{arc length} * \text{time})$$

Rock represents the chemical composition of the mantle corrected average lava from a segment of the arc, and the density of the lava is 2.65 gm/cc. Volume is the measured volume of the volcanoes (Carr, 1984). This introduces a significant error because it represents only a portion of the total magma volume. It ignores the volume of distal tephras, intrusive rocks, back arc lavas, and it does not take into account the volume of lava that has been removed by erosion since eruption. Because of this uncertainty, the

calculated output flux represents a minimum value. Arc length corresponds to the length of each arc segment, Guatemala, El Salvador, western Nicaragua, and eastern Nicaragua. Table 5-6 lists the volumes and arc lengths for each segment of the arc. Another factor that is not well constrained is the duration of magma production. The time used in the output flux calculation is 100,000 years. This number is based on tephrachronology of two extensive units from Central America (Ledbetter, 1985); in Guatemala all the active volcanoes appear to sit on the Los Chochoyos tephra dated 84,000 yr B.P. In Nicaragua the wide- spread Las Sierras tephras appear to be from proto Masaya. Their distinctive Fe-rich mafic composition allows them to be correlated with layer J1 of Ledbetter (1985) with an estimated age of 135,000 yr. All the active Nicaraguan volcanism appear to sit on this unit. Unfortunately, the lack of mapping and age dating for the younger volcanic rocks in Central America prevents us from selecting an age that will clearly allow a minimum flux estimate. If the measured volumes include units much older than 100,000 years, then this value will provide an over estimate of the flux.

Another factor complicating output fluxes is the contribution from the mantle to the magmas. In order to correct for the mantle contribution, the REEs were used as guide lines. The REEs in lavas from Central America have been used to infer the type of mantle and the extent of melting that generated these magmas (Feigenson and Carr, 1993). The REE pattern for the mean lava from western Nicaragua is very similar to the EMORB described by Sun and McDonough (1989; Fig. 5-11). Therefore, for western Nicaragua, the composition of EMORB was used to correct for the mantle contribution. For the other segments of the arc (eastern Nicaragua, El Salvador and Guatemala) the mantle corrections were not as straightforward. The REE patterns of the mean lavas from eastern Nicaragua, El Salvador, and Guatemala are not as similar to EMORB (Fig. 5-11). However, all the mantle corrections use a mantle that has the composition of the EMORB source assuming 15% melting. This composition was directly used for the mantle correction in western Nicaragua. The differences of the mantle corrections involve

variations in the degree of melting of the EMORB source. For eastern Nicaragua, it is assumed that the EMORB source melted 12.5%. A 10% melt was assumed for El Salvador and Guatemala.

As stated previously, the output flux is based on the composition and volume of the erupted lavas. Figure 5-12 shows an EMORB normalized diagram of the mean lavas from the different arc segments. The similarities in the compositions of the mean lavas are remarkable. All of the samples display enrichment of the same elements relative to EMORB, and the relative order of enrichment is approximately the same for all of the mean lavas (B > Cs = Ba = Pb > Rb = U = K = Sr). Thorium is slightly enriched relative to EMORB, but not as much as the other elements. Most of the other elements are very similar in the Central American lavas and EMORB. Niobium and to a lesser extend Ti are depleted, which suggest that a minor phase is holding these elements.

3. Models

The similarities in the compositions of the mean lavas could suggest that the ratio of output to input flux will be the same for the different segments of the arc. However, this is not the case: figure 5-13 and table 5-5 show the output/input ratio for the four segments of the arc expressed as a percentage. It is clear from these diagrams that the relationships between the output to the input flux are not uniform across Central America.

The scale of the output/input flux ratio is not well defined, as the pattern for El Salvador segment demonstrates. The actual percentage of the output/input flux ratio is greatly affected by uncertainties discussed earlier (e.g. magma volume). The values of the ratios calculated are plausible minima for Guatemala and Nicaragua, where there is some age control. This is clearly not the case for El Salvador. The ratio of output/input flux for Cs is greater than 100%, and for other elements like K and Rb the flux ratios are greater than 80%. These high percentages do not allow the other magmatic products to be taken into account and suggest that the volume estimate is too high or the time estimate is too short. Even though the scale of the output/input flux model is not well constrained, the

models give valuable information if we compare the relative order of enrichment of the elements within the segments.

The relative arrangement of the elements indicates the efficiency of the system in recycling elements from the slab through the volcanoes (table 5-5 and Fig. 5-13). Taking the results from western Nicaragua as the reference model (Fig. 5-13a), the elements can be classified into three groups depending on how efficiently they are recycled through the system. Cs, Rb, B and K are efficiently recycled; Sr, U, and Ba intermediate; and Pb, Th and ^{10}Be are weakly recycled through the system. The elements that are efficiently recycled in Central America also have large ionic radii (Cs^+, Rb^+, and K^+ have ionic radii greater than 1.5 Å). Tatsumi et al. (1986) experimentally found that elements with large ionic radii are easily mobilized by a hydrous fluid. Therefore, the order in which elements are recycled through Central America indicates that the mobilizing agent is a hydrous fluid. The only element that is efficiently recycled, but has a small ionic radii (0.25 Å) is B. However, the behavior of boron during prograde metamorphism has led petrologists to conclude that it can also be easily mobilized by a hydrous fluid (Moran et al., 1992 and Bebout et al., 1992).

Many researchers have suggested that Pb behaves similarly to Sr and Ba in arc magmatism (e.g. Shibata and Nakamura, 1997). However, the results of the output/input flux model indicate otherwise. Figure 5-10 shows that the reservoir for Ba and Sr is the sedimentary component of the subducting Cocos Plate. Lead, on the other hand, is hosted by the hydrothermally altered oceanic crust. The low efficiency in the recycling of Pb in Central America could be related to having a different reservoir in this subduction zone system. The poor efficiency in Pb recycling suggests that the lower part of the altered oceanic crust is not significantly involved in the generation of the hydrous fluids that metasomatize the mantle wedge beneath Central America. Therefore, the output/input flux model indicates that the hydrous fluid that triggers melting in Central America is mostly derived from the sedimentary units and the upper altered oceanic crust. The

efficiency of Pb, and to a lesser extent Th and Be, increase, if only the upper 0.5 km of altered oceanic crust is considered in the input flux (Fig. 5-14). The output/input ratio for Pb becomes similar to that of Sr. Other LILE and U are not affected by changing the input composition because these elements are mostly coming from the upper section of altered oceanic crust and the sediments.

Even though a sample from Masaya volcano in eastern Nicaragua has the highest ^{10}Be content of any arc lava (Morris et al., 1990), the output/input flux model indicates that relatively little of the subducted ^{10}Be is recycled through the system. The poor efficiency in the recycling of beryllium, along with Th, is a likely consequence of the process that transfers material from the slab to the mantle wedge. Several researchers have suggested that Be and Th, along with LREE and HFSE, are more easily mobilized by a melt than by a hydrous fluid (e.g. Reagan et al., 1993; Plank and Johnson, 1997; Hawkesworth et al., 1997). However, the relative arrangement of the elements in figure 5-13 indicates that a hydrous fluid is the dominant mobilizing process in Central America.

The classification of elements based on the efficiency of recycling (Fig. 5-13) can be applied to all the segments studied with the exception of one element. Boron is the only element that behaves differently in western Nicaragua relative to the other three segments. In western Nicaragua, boron is efficiently recycled through the system, but in the other segments the recycling efficiency of boron is only intermediate. The different behavior of boron in western Nicaragua could be due to sampling bias. Western Nicaragua is the most extensively sampled segment, and the mean lava is an average of 53 samples. For the other segments fewer samples were considered when calculating the mean lava composition (24 for eastern Nicaragua, 16 for El Salvador and 4 for Guatemala). However, none of the segments have complete data sets for boron analyses. In western and eastern Nicaragua, only 9 samples from each segment have been analyzed for boron. In Guatemala only one sample has been analyzed for B. The segment with the greatest number of boron analyses is El Salvador which has 11 samples for which B has

been analyzed. Guatemala should be excluded, but El Salvador and eastern Nicaragua segments of the arc appear much less efficient in recycling boron than western Nicaragua (Fig. 5-13).

In western Nicaragua, the boron efficiency is similar to that of Cs and K, whereas in other segments of the arc, the efficiency of boron is closer to that of U and Ba. For Central American lavas, the possible sources of boron are the subducted hemipelagic sediments and the low temperature altered oceanic crust (Fig. 5-10). The difference in the efficiency of recycling boron in Central America could be explained if the sources of boron are different for western Nicaragua and the other arc segments. Figure 5-10 shows that the hemipelagic sediments are the major source of U, Ba, Rb, Cs, B, and K; with the upper altered oceanic crust being the next most important source of B, Cs, Rb, and K. The altered oceanic crust contributes almost no U or Ba to the subduction zone system. The close association of boron with Cs, K, and Rb in western Nicaragua implies that the most likely source of B in western Nicaragua is the low temperature altered oceanic crust. However, in the other segments of the arc the hemipelagic sediments contribute most of the boron. This conclusion implies that the hydrous fluid that is involved in the generation of western Nicaraguan magmas is relatively enriched in material from the upper 0.5 km of the altered oceanic crust. The higher flux from the upper altered oceanic crust might explain the regional variations described in chapter 4.

4. Residual oceanic crust

There is evidence that some of the geochemical characteristics of the source of ocean island basalts (OIB) could be inherited from residual subducted slabs (Weaver, 1991). The output/input flux models in arcs can be taken a step further to calculate the residual oceanic crust after the generation of arc lavas (e.g. Elliott and Plank, 1997 and White et al., 1997).

The residual oceanic crust for the western Nicaraguan segment was calculated as follows:

$$\text{Residual oceanic crust (ton cm}^{-1}\text{yr}^{-1}\text{)} = [\text{input} - 2 * \text{output}]$$

The output was multiplied by two to compensate for the low volume that was used in the output flux calculations. The multiplication factor was obtained by assuming that Cs (50% efficiency in western Nicaragua) was completely recycled through the generation of the arc the magmas. The flux of residual oceanic crust into the mantle was calculated in ton $cm^{-1}yr^{-1}$ in order to have the residual flux in a similar scale to Sun and McDonough (1989) OIB composition.

Figure 5-15 is an EMORB normalized diagram of melts from modified N-MORB mantle and a HIMU-OIB from St. Helena (Sun and McDonough, 1989). The N-MORB mantle (assuming that 15% melts form the N-MORB) was mixed with the residual oceanic crust in a ratio 97:3 and then melted in an attempt to reproduce and the composition of the OIB lava. The first conclusion that can be drawn from figure 5-14 is that the patterns of the calculated lavas tend to follow the pattern for the lava from St. Helena except for Ba and Pb. In addition, the composition range of low degree melts (1 to 5%) includes the composition of the HIMU-OIB for most elements, with the exception of Ba and Pb. Slightly increasing the degree of melting would decrease the concentration of Ba close to the value of OIB, but Pb remains high unless the extent of melting is increased to 20%. Such a high degree melt would produce lavas that are too depleted in all the other elements. The behavior of Ba might be explained in light of the high content of this element in the subducting biogenic sediments, which are unusually enriched in this element (Plank and Langmuir, 1993). Furthermore, the lavas from western Nicaragua are not highly efficient in recycling barium (Fig. 5-13). Thus, the residual oceanic crust can carry significant amounts of Ba deeper into the mantle beneath Central America.

The source of HIMU OIBs has been depleted in Pb relative to U and Th, producing basalts that have high U/Pb. The enrichment of U and Th over Pb may result from the poor mobility of U and Th relative to Pb in hydrous fluids from subduction zones

(e.g. Weaver, 1991). Lead is supposed to be more efficiently mobilized by the hydrous fluid and so the residual oceanic crust will be depleted in Pb. However, the results from the output/input flux model from western Nicaragua do not support this explanation for the origin of HIMU-OIBs. Elliott and Plank (1997) also find that residual oceanic crust in the Marianas is not an appropriate mantle modifier to originate OIBs. The residual oceanic crust in Central America is enriched in Pb, primarily because the lower part of the altered oceanic crust, which is enriched in Pb, appears not to be significantly involved in the generation of the arc magmas. In fact, the models indicate that U was mobilized more efficiently than Pb, when both the upper and lower altered oceanic crust are considered in the output/input modeling (Figs 5-13a vs. 5-14a). However, Pb is efficiently removed from the subducting oceanic crust if only the upper part of the altered oceanic crust is involved in the generation of magmas (Fig. 5-14). In any event, the information from Site 504 indicates that large quantity of Pb is being added to the mantle in subduction zones. The results from this model agree with Bailey and Ragnarsdottir (1994) who suggest that uranium can be efficiently mobilized by a hydrous fluid and that residual oceanic crust is not completely responsible for the geochemical characteristics of the HIMU OIB source.

D. Conclusions

The forward modeling of lavas from Central America is limited by the poorly constrained metamorphic mineral assemblages and partition coefficient data available. However, the models give an idea of what is happening in this subduction zone system. Models of slab fluids and melts were created to reproduce the geochemical characteristics of lavas like Te-1 (hemipelagic end member) and Te-114 (carbonate end member).

The carbonate-rich endmember lavas, like Te-114, are relatively easy to reproduce by metasomatizing the mantle with a fluid that is a mixture of fluids derived from the altered oceanic crust (FAOC) and from the carbonate sediments (FCS). The presence or absence of amphibole in the residual altered oceanic crust after the generation of the fluid affects the composition of the fluid. However, the composition of the modeled lavas does

not seem to be significantly affected by the residual mineralogy of the altered oceanic crust. In the forward modeling of the carbonate-rich lavas, 20% melts of the metasomatized mantle reproduced the lava composition (Fig. 5-3b). However, the modeled lava is depleted in Cs and K and has excess Ba and Th. Lower degrees of melting will improve the fit of Cs and K, but at the same time it will increase the excess Ba and Th. To improve the Ba and Th fits, it is likely that other mineral phases should be included in the modeling of the slab fluids.

The modeling of the hemipelagic-rich endmember lavas is more complex because there is little partition coefficient data on the metamorphic minerals that could be present. The composition of the hemipelagic-rich lava, Te-1, is reproduced by melting metasomatized EMORB mantle source to 20% (Fig. 5-4b). The metasomatic agent is a small volume of the mixed fluid (FAOC + FCS) and a melt derived from the hemipelagic sediments (MHS; Fig. 5-4b). However, the modeled melt has excess Ba, Th and U, but is deficient in Sr relative to the sample. The excess Ba and Th can be reduced if some amphibole (Fig. 5-4a) is allowed in the residue of the slab after the generation of the fluid and melt. The Sr concentration of the model can be increased by having lower degrees of melting.

From the forward modeling, a melt is the preferred process to transfer material from the hemipelagic sediments to the mantle, even though the trace element patterns produced by a melt and a fluid are not drastically different. The major discrepancy is in the behavior of U. The modeled lavas have excess U when a melt is assumed to be the transporting agent (Fig. 5-4b), and U too low when a fluid is assumed (Fig. 5-6b). However, there is evidence that a fluid with a special composition, for example enriched in Cl or with high fO_2, could mobilize U more efficiently than a melt (Bailey and Ragnardottir, 1994).

Output/input mass balance calculations are a better approach to the understanding of geochemical recycling in subduction zones because these models do not depend on

partition coefficient data. For Central America, the efficiency with which elements are recycled (Fig. 5-13) suggests that a hydrous fluid is the dominant process that transfers material from the slab to the mantle wedge. However, the composition of this fluid does not seem to be uniform along the arc. This conclusion is based on the difference with which boron is recycled in the different segments of the arc. Boron is most efficiently recycled in western Nicaragua where it has an efficiency similar to that of K and Cs. In the other segments of the arc the efficiency of boron is more like that of Sr, Ba and U. Thus, the fluid involved in the generation of lavas from western Nicaragua seems to have a larger proportion of material derived from the upper part of the altered oceanic crust; whereas for the other segments of the arc, the percentage of altered oceanic crust involved in magmatism seems to be smaller relative to the input from the sediments.

Ocean island basalts have some geochemical characteristics that resemble those from residual oceanic crust (Weaver, 1991). However, the residual oceanic crust from western Nicaragua is not an appropriate contributor to the generation of HIMU-OIB. The models indicate that the magmatic process in Central America does not recycle Pb efficiently, mainly because of the large input from the hydrothermally altered oceanic crust.

Table 5-1

Mineral-Fluid Partition Coefficients (Brenan et al., 1995) used to model fluids from subducted components				
	Clinopyroxene	Garnet	Olivine	Amphibole
Ba	0.00048	0.000059	0.000023	0.51
Sr	0.48	0.00076	0.000064	1.7
Pb	0.02	0.0034	0.0012	0.081
Nb	0.04	0.09	0.25	1.1
U	0.29	0.72	0.0077	0.35
Th	1.03	0.13	0.0072	0.93
La	25	0.4	1	100
Nd	75	14	1	225
Yb	100	146	1	250

Mineral-Melt Partition Coefficients used to model melts					
	Clinopyroxene	Garnet	Olivine	Orthopyroxene	Amphibole
Cs	0.001	0.001	0.001	0.001	0.07
Rb	0.001	0.001	0.001	0.001	0.14
K	0.001	0.001	0.001	0.001	0.25
Ba	0.0005	0.00001	0.001	0.001	0.12
Sr	0.1	0.0006	0.001	0.001	0.28
Pb	0.01	0.00001	0.001	0.001	0.12
Nb	0.01	0.01	0.001	0.001	0.2
U	0.0009	0.011	0.001	0.001	0.008
Th	0.0013	0.0015	0.001	0.001	0.017
La	0.02	0.01	0.001	0.001	0.15
Ce	0.09	0.02	0.001	0.006	0.22
Nd	0.22	0.09	0.001	0.01	0.62
Sm	0.4	0.22	0.001	0.012	0.66
Eu	0.48	0.33	0.001	0.015	0.8
Dy	0.6	1.06	0.001	0.025	1
Y	0.5	4	0.001	0.05	1.25
Yb	0.5	4	0.001	0.05	1.25

Table 5-1. Partition coefficients used in the modeling of fluids and melts from the slab.

Table 5-2

	Clinopyroxene	Garnet	Amphibole	Olivine
Amphibole left in the residue (Figs. 5-3a, 5-4a, 5-6a)				
D_m	33	33	33	
P_m	5	5	90	
All the amphibole breaks down (Figs. 5-3b, 5-4b, 5-6a,5-8)				
D_m	45	45		10
P_m	45	45		10

To calculate EMORB source			
	Clinopyroxene	Olivine	Orthopyroxene
D_m	20	70	10
P_m	40	30	30

Table 5-2. Mineral assemblages of the molten source (D_m^o) and of the liquid norm relative to the molten source minerals (P_m) used to calculate the D_i^o and P_i respectively in the batch melting equation of Shaw (1970). When a mineral is not included, it implies that this mineral has melted completely.

Table 5-3

	Model Fluids and Melts							
	TE-1	TE-114	EMORB SOURCE	F-CS 5%btch	F-AOC 5%btch Amph. residue	F-AOC 5%btch No Amph res.	F-UAOC 5%btch No Amph res.	F-LAOC 5%btch No Amph res.
Cs	1.328	0.342	0.010	2.550	0.277	0.379	1.167	0.194
Rb	28.800	7.729	0.760	71.892	12.325	21.635	74.873	3.890
Ba	817.700	546.700	8.594	42909.50	88.21	343.24	656.63	238.78
Th	1.427	0.293	0.091	2.868	1.043	1.326	0.915	1.464
U	1.302	0.256	0.027	2.651	0.130	0.130	0.207	0.104
Nb	2.400	2.440	1.263	1.531	2.001	6.283	4.253	6.959
K_2O	1.340	0.656	0.038	2.973	0.194	1.264	3.890	0.389
La	7.020	5.137	0.967	45.612	0.077	0.458	1.017	0.271
Ce	17.720	11.701	2.454	10.012	0.134	0.492	1.007	0.320
Pb	4.457	7.358	0.091	72.313	54.372	72.774	41.585	83.170
Sr	469.300	736.000	25.530	30025.35	84.18	227.94	266.09	215.22
Nd	11.970	10.910	1.638	20.258	0.080	0.163	0.180	0.157
Sm	2.640	3.060	0.539	2.756	0.019	0.028	0.028	0.028
Eu	0.920	1.205	0.199	1.143	0.006	0.009	0.009	0.009
Dy	3.730	3.380	0.838	1.348	0.022	0.032	0.032	0.032
Y	24.070	23.181	4.915	5.243	0.132	0.194	0.194	0.194
Yb	2.410	1.980	0.529	0.306	0.013	0.019	0.022	0.018

F-CS = Fluid from carbonate sediment
F-AOC = Fluid from altered oceanic crust
F-UAOC = Fluid from upper altered oceanic crust
F-LAOC = Fluid from lower altered oceanic crust

Table 5-3. Results of the fluid and melt models using partition coefficients.

Table 5-3 cont.

Model Fluids and Melts			
	M-HS 1%btch Amph. residue	M-HS 1%btch No Amph res.	F-HS 1%btch No Amph res
Cs	65.642	197.877	189.430
Rb	733.553	3711.085	3552.670
Ba	80953.96	381697.80	383887.70
Th	182.849	263.960	5.678
U	296.510	317.469	10.612
Nb	62.275	264.675	54.295
K_2O	20.222	167.273	160.133
La	264.043	765.606	3.932
Ce	240.042	474.630	2.473
Pb	185.028	658.575	466.709
Sr	2526.96	6121.23	1499.31
Nd	57.107	119.900	0.383
Sm	9.500	14.140	0.041
Eu	3.376	4.857	0.017
Dy	5.380	6.301	0.041
Y	16.400	15.417	0.262
Yb	1.468	1.380	0.023

M-HS = Melt from hemipelagic sediments
F-HS = Fluid from hemipelagic sediments

Table 5-4

	Te-114 Carb. end member 98% EMORB mantle 2% Slab Fluid (80% F-AOC + 20% F-CS)	Te-1 Hemip. end member 99.5% EMORB mantle 0.5% Slab material (70% Slab Fluid [80% F-AOC + 20% CS] 30% Hemipelagic Sed. Melt)
Mineral variations		
Amphibole in residue	Fig. 5-3a	Fig. 5-4a
No Amphibole in residue	Fig. 5-3b higher K compared to Fig. 5-3a	Fig. 5-4b higher Cs, Rb, Ba, Th, and K compared to Fig. 5-4a
Melts vs. Fluids		
Melt from Hemipelagic sed		Fig. 5-4
Fluid from Hemipelagic sed		Fig. 5-6 lower U, Th, LREE relative to Fig. 5-4
Different sections of AOC		
Lower AOC	Fig. 5-8a similar to Fig 5-3b	
Upper AOC	Fig. 5-8b higher K, Cs, Rb and lower Pb compared to Figs. 5-3b and 5-8a	

Table 5-4. Summary of the fluid and melt models.

Table 5-5

Percentage of Individual Slab Unit contributions to the Input Flux					
	Altered Oceanic Crust	Lower Altered Oceanic Crust	Upper Altered Oceanic Crust	Carbonate Sediments	Hemipelagic Sediments
B	30.1	8.0	22.1	11.3	58.6
Cs	14.8	3.4	11.4	7.3	77.9
Rb	33.6	4.5	29.1	8.2	58.2
Ba	5.1	2.6	2.4	40.1	54.8
Th	82.7	68.4	14.3	1.2	16.2
U	20.6	12.4	8.2	3.1	76.2
Nb	75.4	62.6	12.8	2.6	22.1
K	39.8	9.2	30.6	7	53.2
La	59	26.2	32.8	16.3	24.7
Ce	78.4	38.3	40.1	2.2	19.3
Pb	86.4	74.1	12.3	4.6	9
Sr	34.3	24.3	10	56.4	9.4
P	90.9	68.2	22.7	5.4	3.7
Nd	85.1	61.6	23.5	5.1	9.9
Be	87.5	65.6	21.9	4.2	8.3
^{10}Be	0	0	0	0	100
Zr	93.7	70.3	23.4	0.8	5.5
Sm	90.2	67.6	22.5	3.2	6.6
Eu	86.9	65.2	21.7	5	8.1
Dy	91	68.3	22.8	3.2	5.7
Y	89.5	67.1	22.4	4.6	6
Yb	91.4	65.4	26	3.1	5.5

Table 5-5. Percentages of the contributions from different units of the subducted slab.

Table 5-6

	Volume km^3	Arc Length km
Eastern Nicaragua	214	96.7
Western Nicaragua	257	127
El Salvador	927	284
Guatemala	134	100

Table 5-6. Volume and arc length for the different segments of Central American volcanic arc that were used to calculate the flux out of the volcanoes.

Table 5-7

Output/Input Flux Ratios				
	W. Nic.	E. Nic.	El Salvad.	Guatemala
Cs	48.2	29.3	123.9	34.5
B	44.5	16.0	51.2	10.2
K	44.0	36.3	81.3	26.9
Rb	37.5	38.4	87.9	17.9
Sr	26.2	23.1	33.8	14.6
U	19.3	24.9	37.7	6.0
Ba	18.5	19.4	25.1	9.0
Pb	7.6	6.3	15.1	5.8
Th	3.3	4.6	17.5	2.6
^{10}Be	4.2	5.8	7.1	1.1
Nb	-39.6	-66.7	-154.7	-61.2
La	0.9	3.6	-0.4	-2.0
Ce	1.0	3.9	4.1	0.3
P	3.6	3.8	3.5	0.9
Nd	4.3	5.1	5.9	1.5
Be	3.6	9.7	11.9	2.3
Zr	0.8	1.5	3.6	1.2
Sm	3.2	3.2	4.8	0.3
Eu	2.9	2.2	1.1	-0.3
Dy	1.2	0.9	1.6	-0.1
Yb	-1.0	-4.3	-5.3	-3.4
Y	1.2	-0.6	0.0	-1.3

Table 5-7. Results of the output/input modeling. The input flux for these results are calculated using 2 km for the thickness of the altered oceanic crust. The negative ratios for Nb indicate that this element is being retained in the mantle. And the negative ratios for La, Yb, and Y are an artifact of the mantle correction.

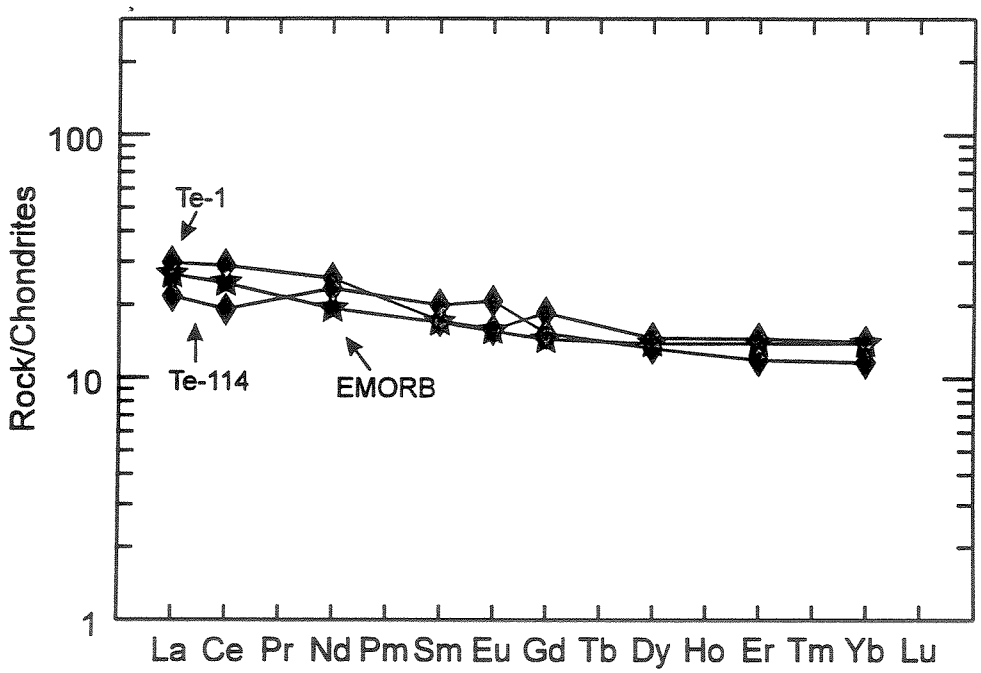


Figure 5-1 REE pattern distribution for EMORB, Te-1, and Te-114. The similarity in the patterns suggests that the lavas originated from a mantle source similar to the one for EMORB. The normalization factors from Sun and McDonough (1989).

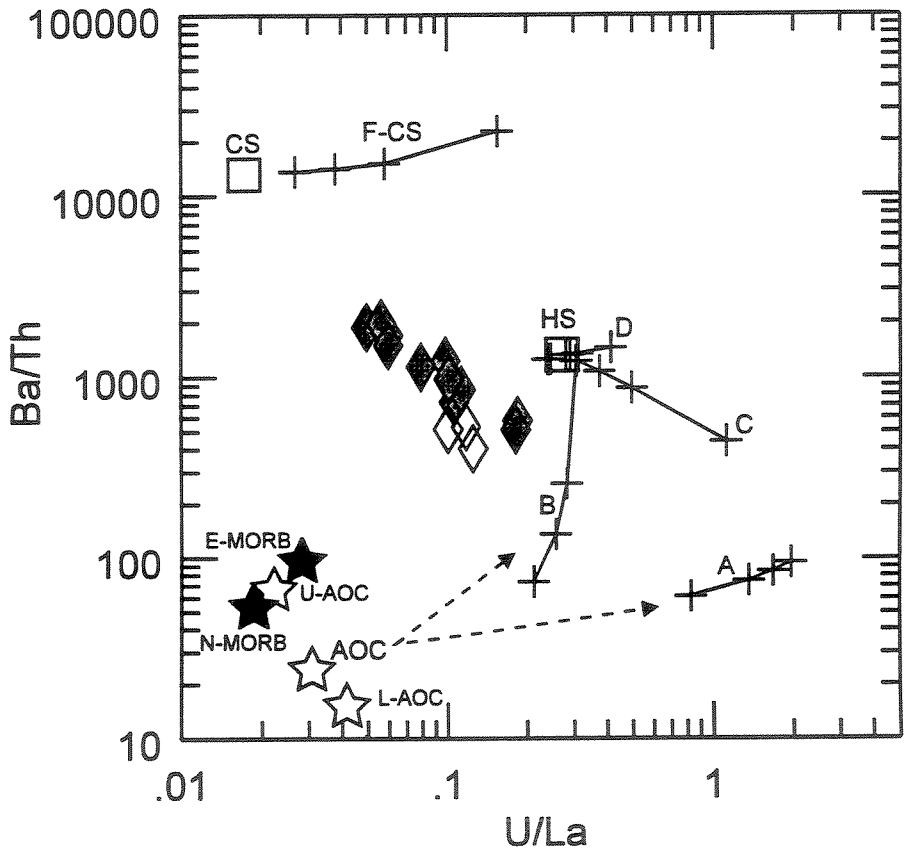


Figure 5-2 U/La vs. Ba/Th showing the fluids and melts produced from the slab components. CS = Carbonate Sediment, F-CS = Fluid derived from the Carbonate Sediments. AOC = Altered Oceanic Crust. HS = Hemipelagic Sediments. The crosses represent the extend of fluid/melt production from the different slab units (1,5,10, and 20%). Lines A and B represent fluids derived from the AOC, and lines C and D are melts from the hemipelagic sediments. When creating lines A and C some amphibole was allowed in the residue. For lines B and D no amphibole was allowed in the residue. Decreasing the amount of amphibole in the residue creates fluids and/or melts that have higher Ba/Th and lower U/La. The filled stars are EMORB and NMORB. The lavas from western Nicaragua are plotted for reference.

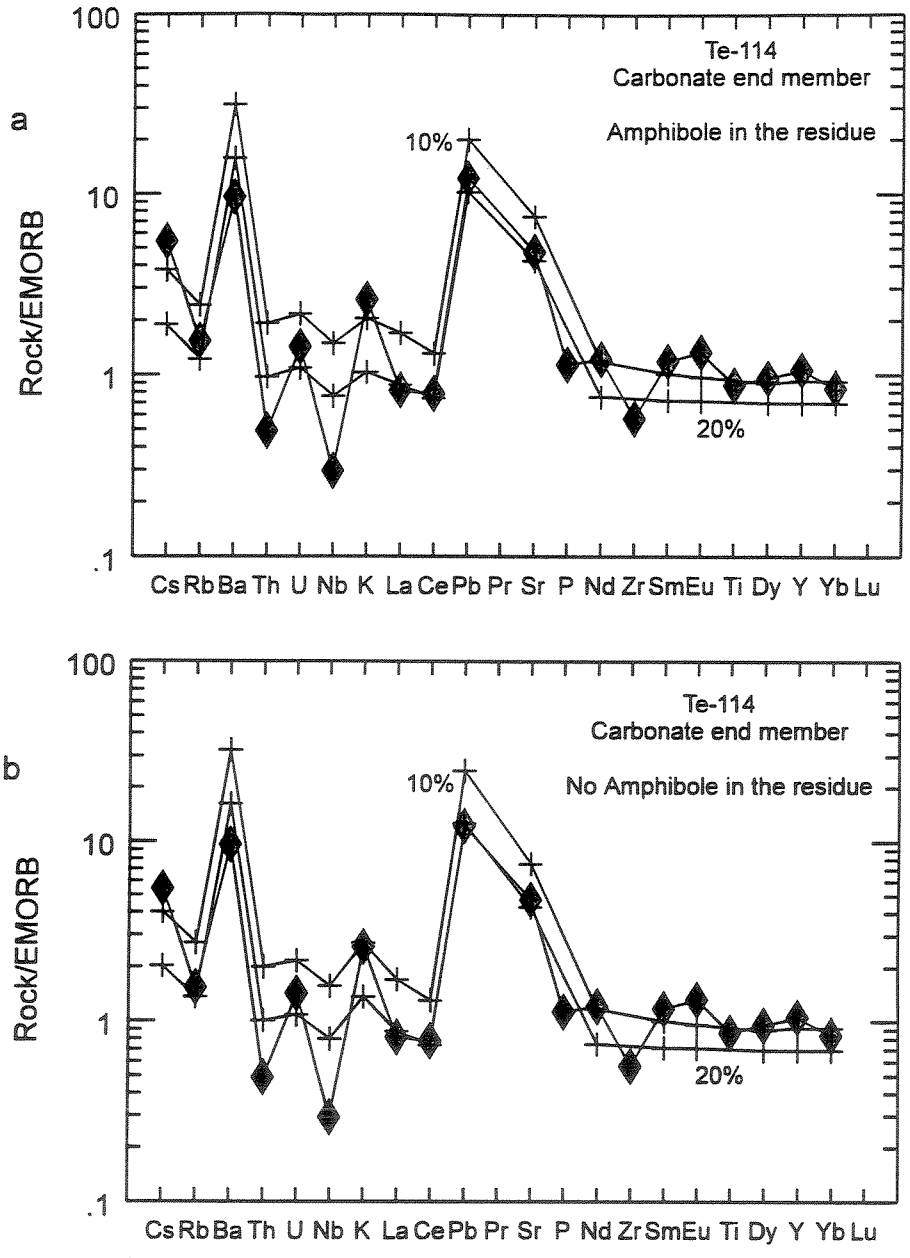


Figure 5-3 EMORB normalized diagrams of Te-114 (diamonds) and the model generated lavas (crosses; metasomatized mantle melts). The modeled lavas are melts of EMORB source mantle (98%) that was metasomatized with 2% of a mixed fluid (80% Fluid from the Altered Oceanic Crust and 20% Fluid from the Carbonate Sediments). For the modeled lavas in figure a, some amphibole was allowed in the residue after creating the fluid from the altered oceanic crust. In figure b, no amphibole was allowed in the residue. The significant differences between the diagrams are the higher K and Pb concentrations when no amphibole was allowed. Normalization factors from Sun and McDonough (1989).

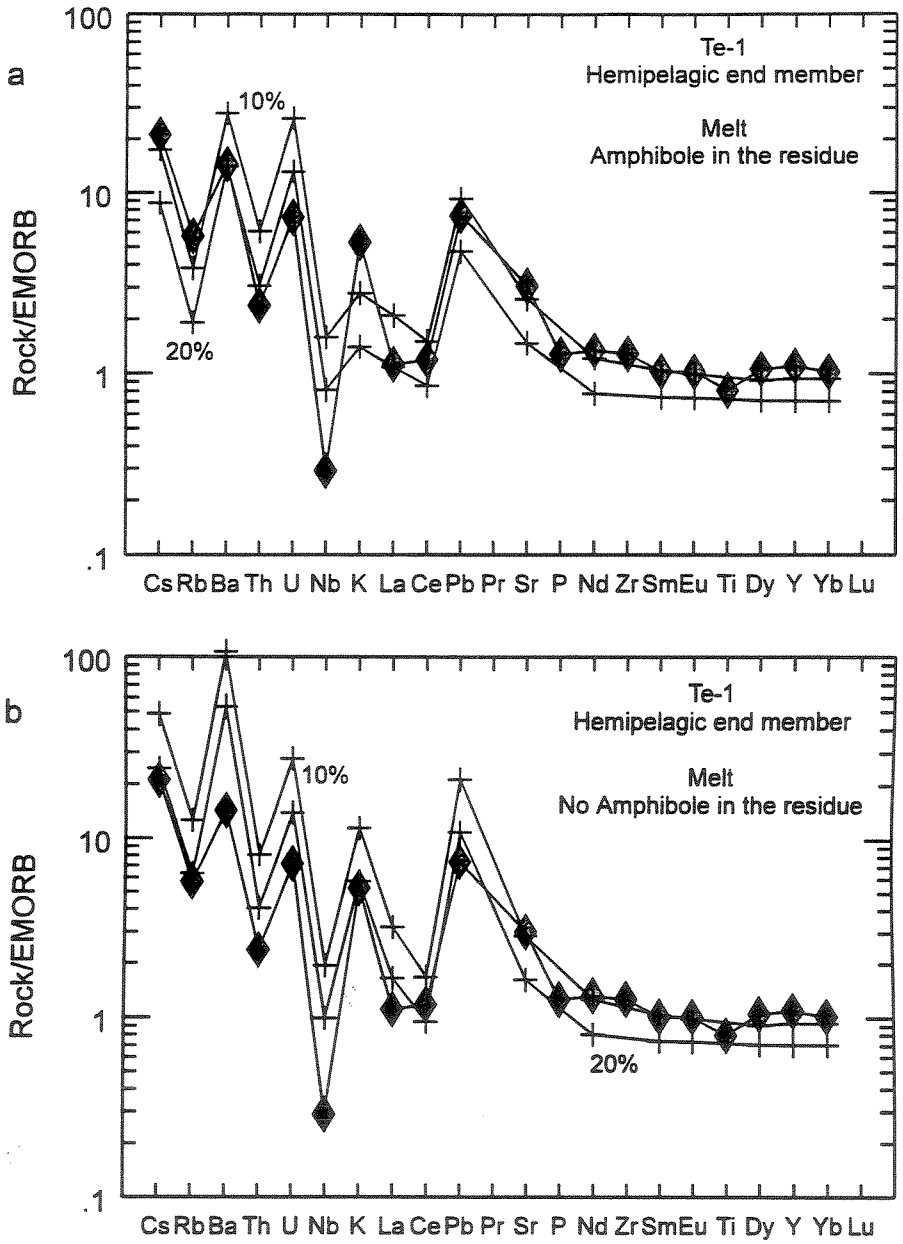


Figure 5-4 EMORB normalized diagrams of Te-1 (diamonds) and model generated lavas (crosses). The modeled lavas are melts of EMORB source mantle (99.5%) metasomatized with 0.35% of a mixed fluid (80% fluid from altered oceanic crust and 20% fluid from carbonate sediments) and 0.15% melt from the hemipelagic sediments. In figure a, the modeled lavas roughly (ignoring Nb) match the composition of Te-1, except for K. In this model some amphibole was allowed after the generation of fluids from the altered oceanic crust and after the generation of melts from the hemipelagic sediments. The concentration of most elements is higher in the modeled lavas in figure b, including K. In figure b, no amphibole was allowed in any residue.

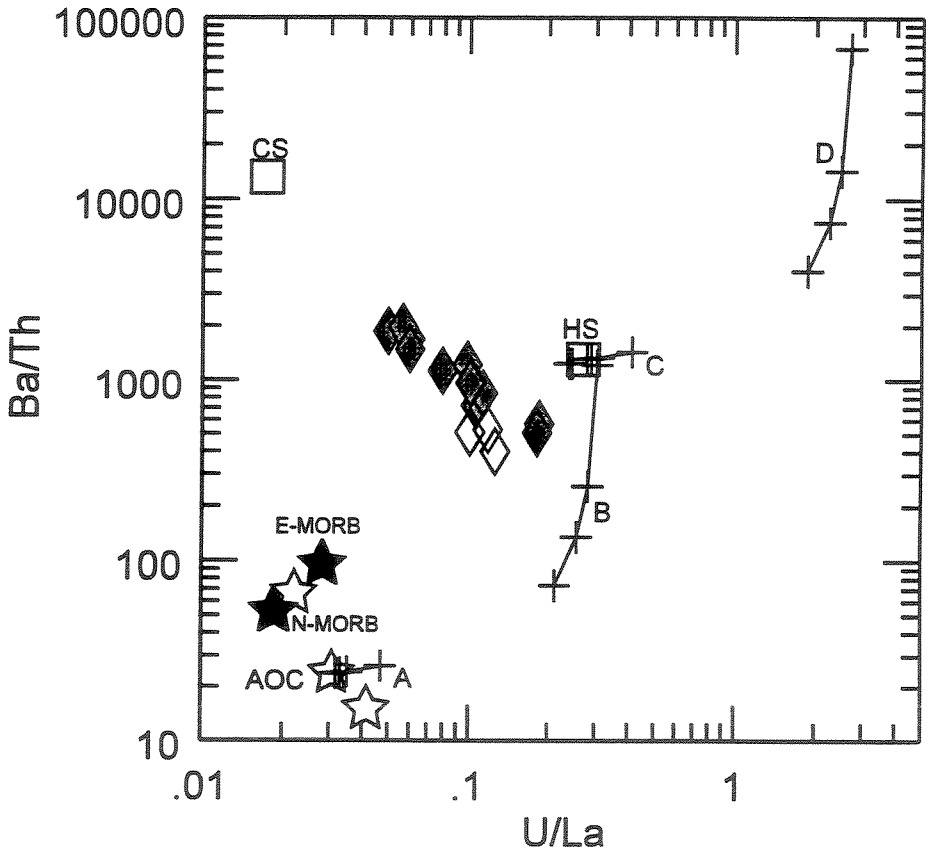


Figure 5-5 U/La vs. Ba/Th variations in fluids and melts from the altered oceanic crust (AOC) and the hemipelagic sediments (HS), no amphibole was allowed in the residue. Lines A and C represent melts from AOC and HS respectively. Lines B and D indicate fluids from AOC and HS respectively. The composition of the melts is closer to the composition of the starting material. Fluids from the AOC and the HS display much higher ratios than the bulk compositions.

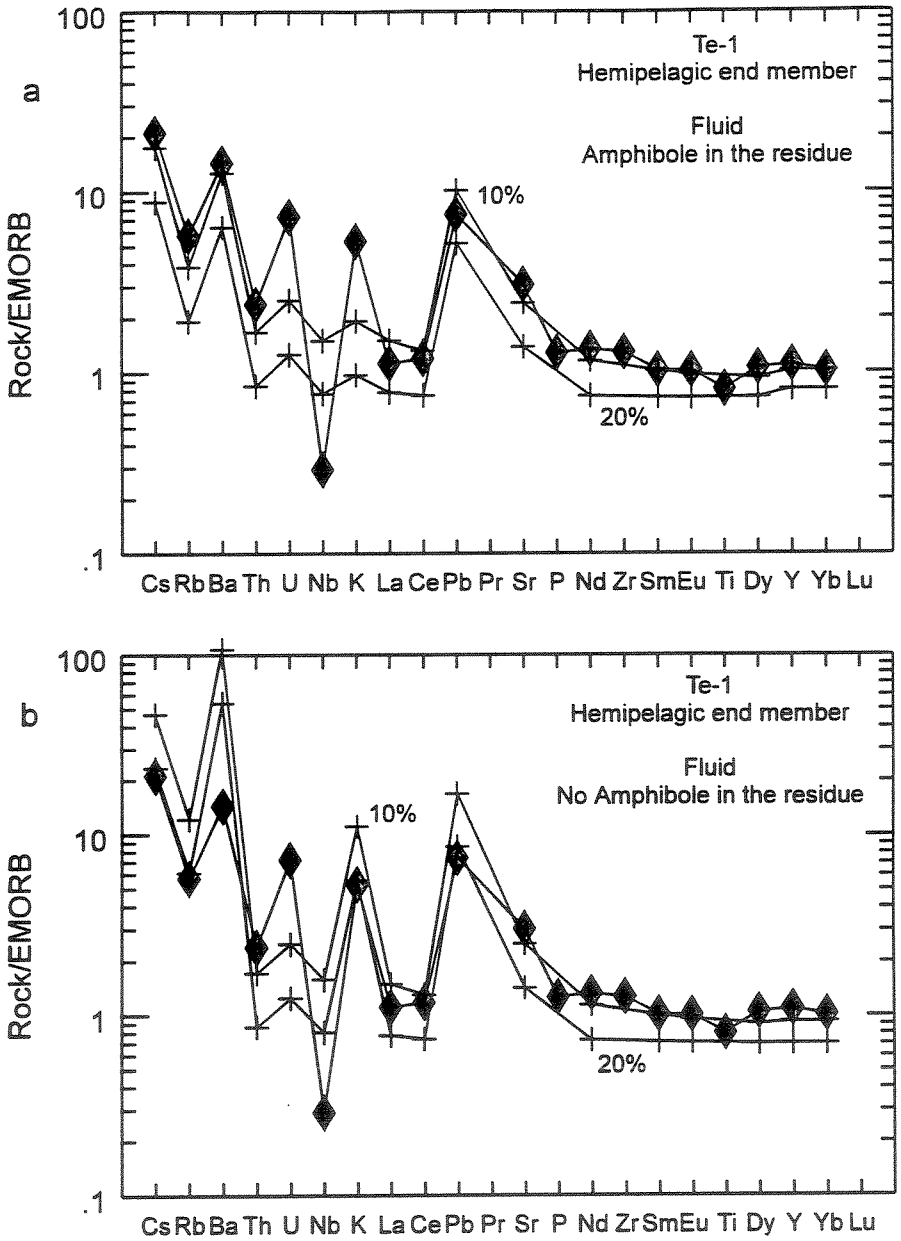


Figure 5-6 EMORB normalized diagram of Te-1 (diamond) and modeled lavas (crosses). The modeled lavas were produced in a similar way to those from figure 5-4. The only difference is that the product from the hemipelagic sediments is a fluid instead of a melt. Notice that the compositions of the modeled lavas are very similar in both diagrams. However, the concentration of uranium is significantly lower in the modeled lavas for which the hemipelagic component is a fluid.

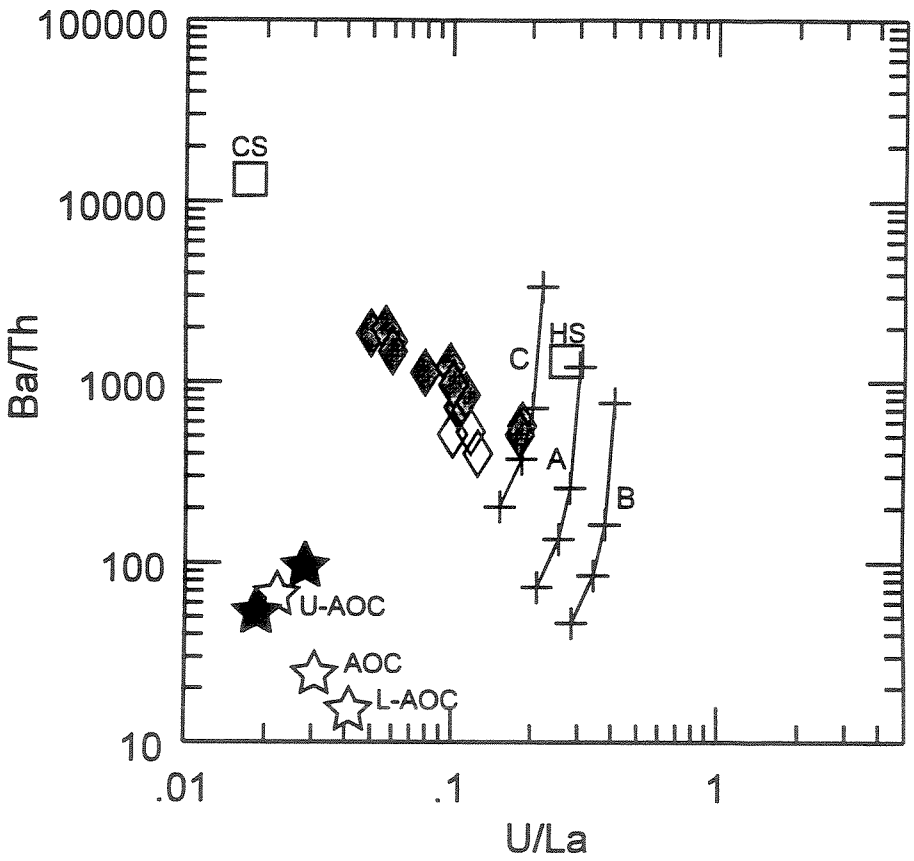


Figure 5-7 U/La vs. Ba/Th showing the variability in the fluids generated by using different sections of the altered oceanic crust. AOC = altered oceanic crust. L-AOC = lower hydrothermally altered oceanic crust. U-AOC = upper low temperature altered oceanic crust. Line A represents fluids generated AOC. Line B indicates fluids that originated from the dehydration of L-AOC, and line C represents fluids from U-AOC. In all of the models, no amphibole was allowed in the residue after the generation of the fluids.

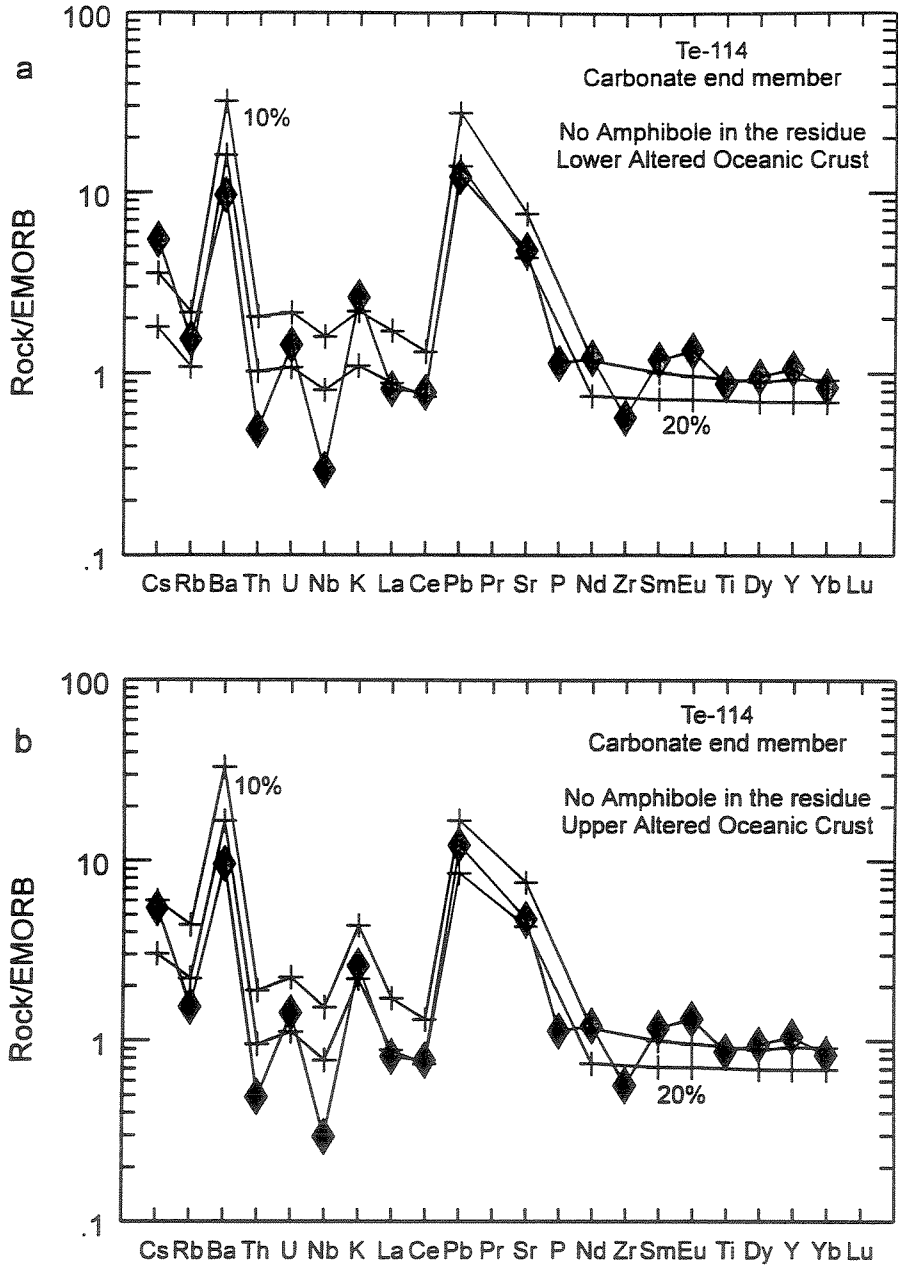


Figure 5-8 Carbonate end member, showing effect of changing AOC input. EMORB normalized diagram of Te-114 (diamonds) and modeled lavas (crosses) that were created as those from figure 5-3b. The difference is that the modeled lavas from figure 5-8 were created using different sections of the altered oceanic crust. Figure 5-8a is very similar to figure 5-3b. However, the composition of the modeled lavas in figure 5-8b have higher K, Cs, Rb and lower Pb than those in the other diagrams, and thus more realistically bracket the lava composition.

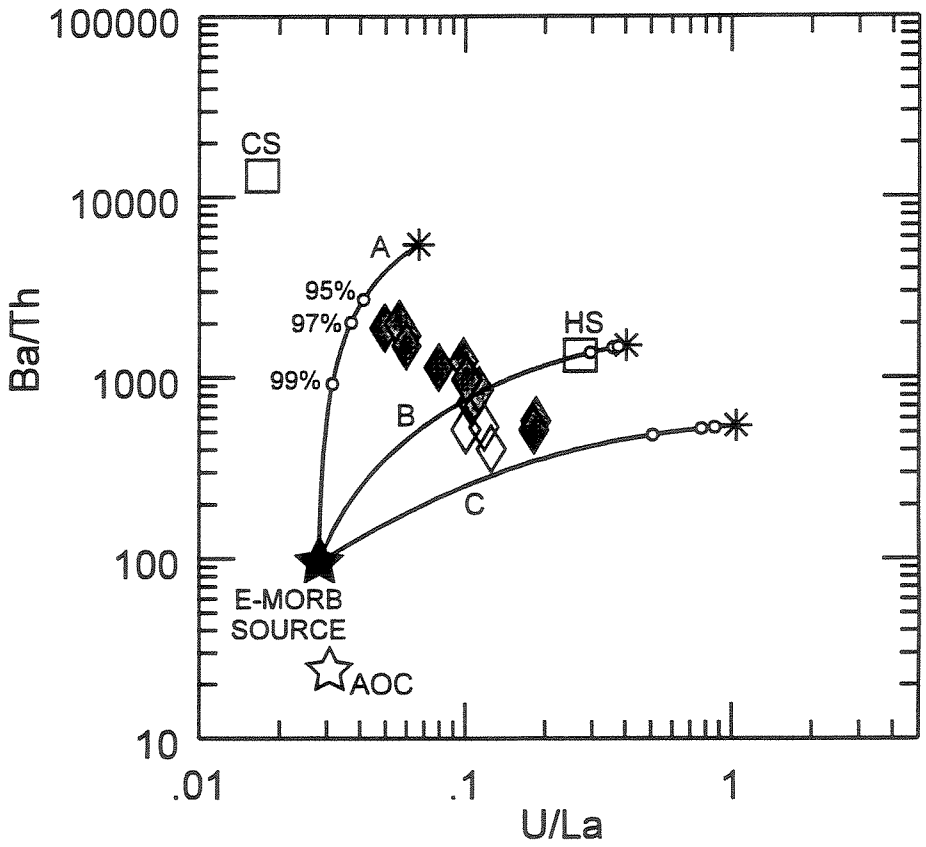


Figure 5-9 Mixing lines between EMORB mantle and various slab fluids. The small circles represent 95, 97, and 99% EMORB mantle. Mixing line A reproduces the chemical characteristics of the carbonate-rich lavas from Central America. This line was created by mixing EMORB mantle with a mixed fluid (80% fluid from altered oceanic crust, AOC, and 20% fluid from the carbonate sediments, CS). Lines B and C represent the mixing of EMORB mantle with mixed fluid (80% F-AOC + 20% F-CS) and melt derived from the hemipelagic sediments. The fluids and melts for lines A and B were the product of complete dehydration of the amphibole, whereas those for line C result from the breakdown of some of the amphibole. Line B has a Ba/Th ratio that is too high to reproduce the composition of the hemipelagic-rich lavas from Central America. Allowing some amphibole to be left after the production of fluids and/or melts, as in case C, lowers Ba/Th.

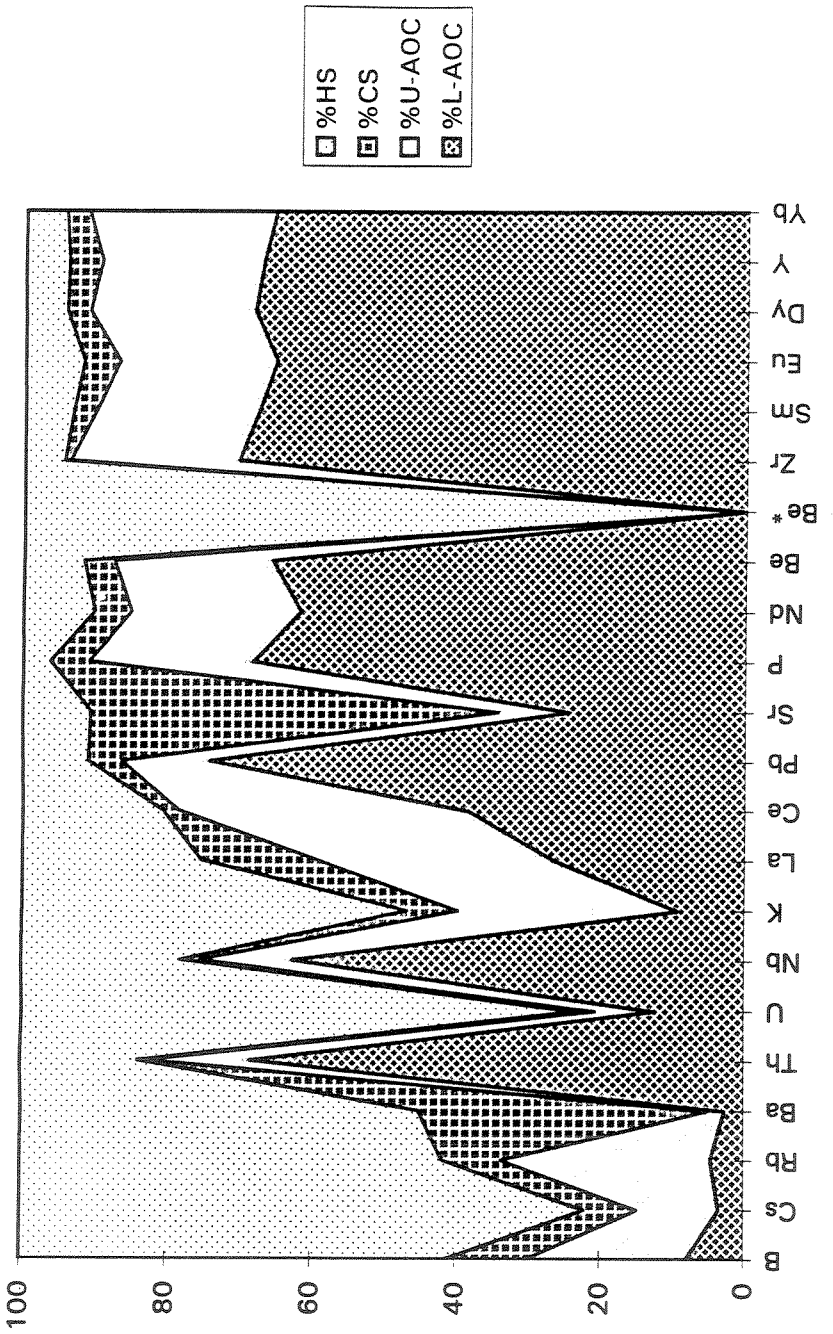


Figure 5-10 Percentage input from the different units of the subducting slab; the size of the areas are proportional to the contribution from each unit. The hemipelagic sediments (HS) contribute all of the ^{10}Be (Be*) and most of the B, Cs, Rb, Ba, U, and K. The carbonate sediments (CS) contribute most of the Sr and some of the Ba. The composition of the altered oceanic crust is not well constrained, but up to date information indicates that the upper altered oceanic crust (U-AOC) contributes more B, Cs, Rb, and K than the lower hydrothermally altered oceanic crust (L-AOC). The lower oceanic crust contributes most of the Pb. The reservoir of Th is poorly constrained.

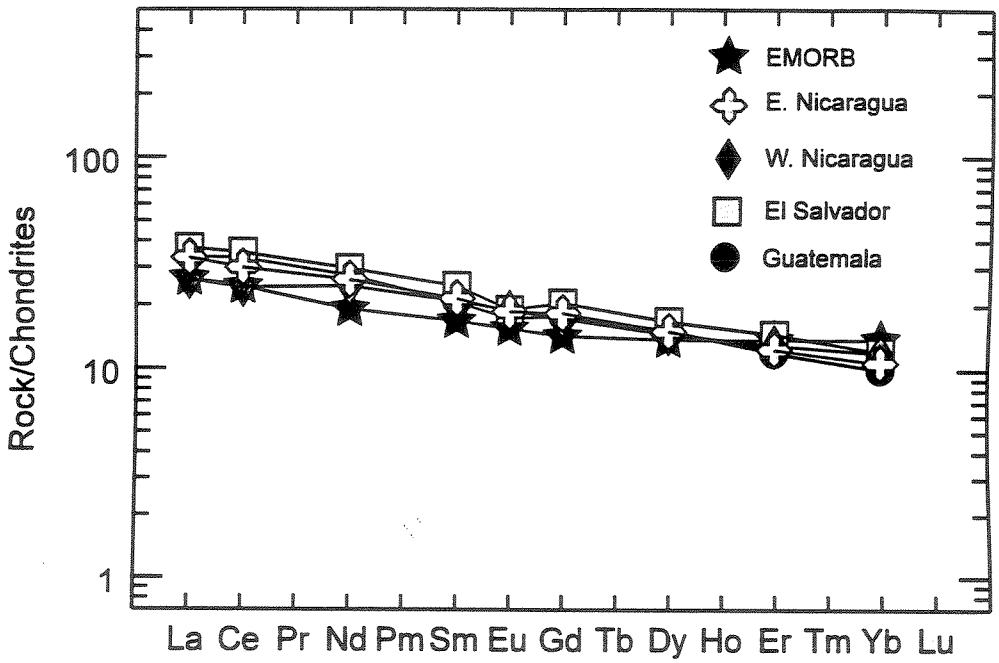


Figure 5-11 REE patterns for EMORB and mean lavas from W. Nicaragua, Eastern Nicaragua, El Salvador, and Guatemala. The lavas are assumed to have originated from a mantle that has a similar composition to the source of EMORB. See text for details

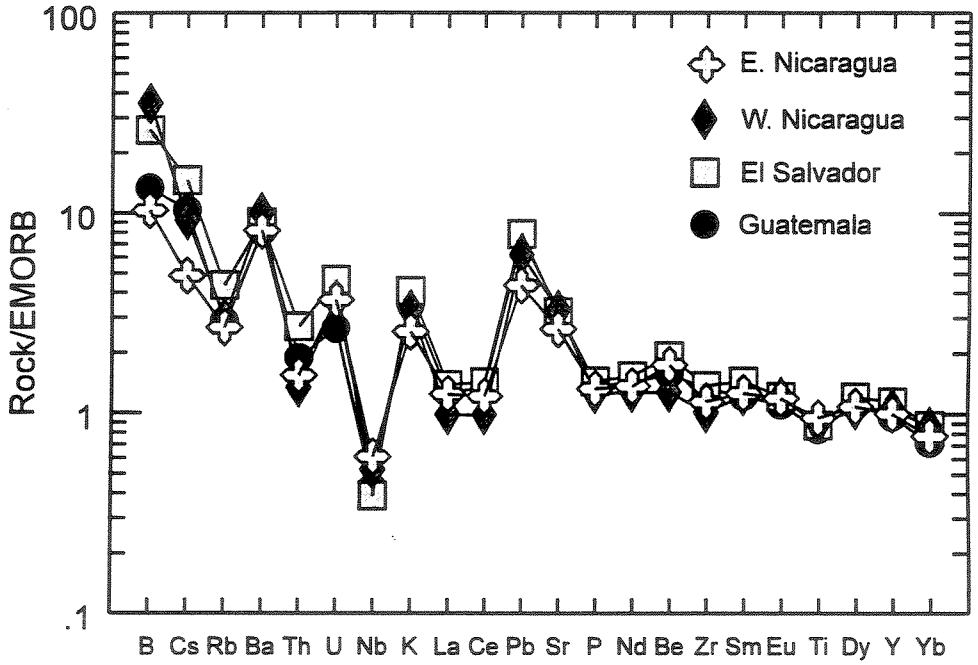


Figure 5-12 EMORB normalized diagram for the mean lavas from W. Nicaragua, E. Nicaragua, El Salvador, and Guatemala. All the lavas have very similar patterns, typical of arc related lavas, that is enriched in LILE and depleted in HFSE.

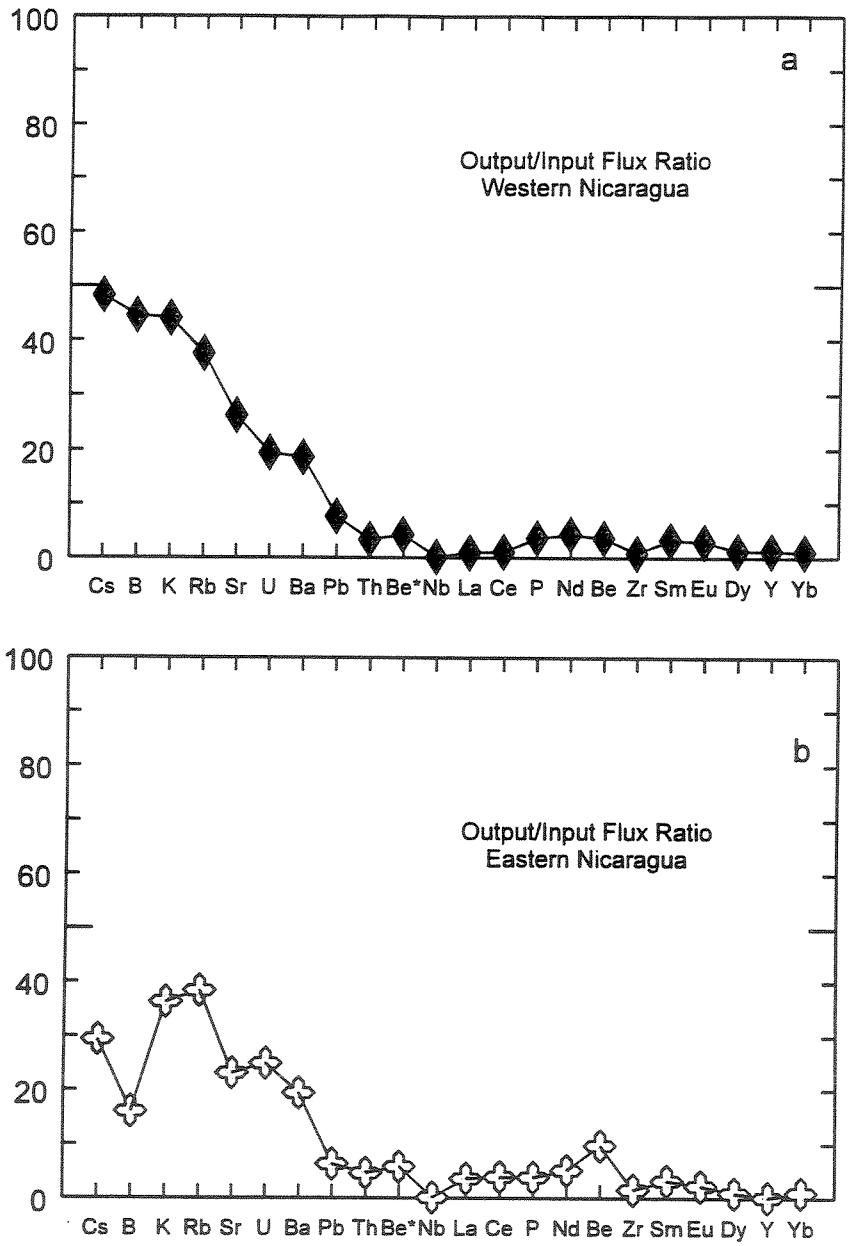


Figure 5-13 Recycling efficiency plots for western Nicaragua (a) and eastern Nicaragua (b); these results are calculated assuming that the thickness of the altered oceanic crust is 2 km. The elements are arranged based on the output/input flux ratios for western Nicaragua. The major difference between the recycling efficiency in western Nicaragua (a) and the other segments of the arc (5-13b, c, d) is the recycling efficiency of boron. In figures 5-13b, c, and d boron has a similar recycling efficiency to Sr, Ba, and U.

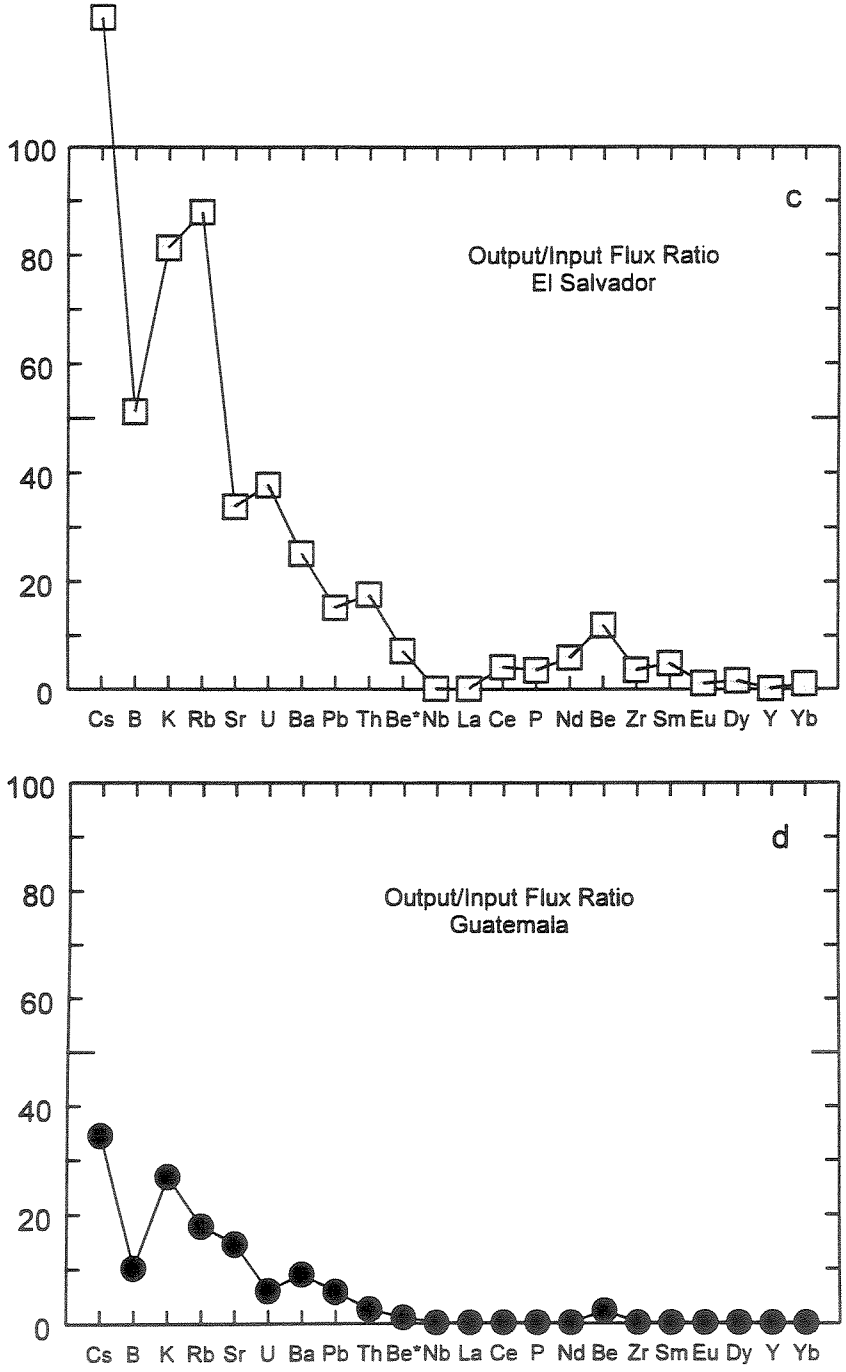


Figure 5-13 cont. Recycling efficiency plots for El Salvador (c) and Guatemala (d); these results are calculated assuming that the thickness of the altered oceanic crust is 2 km. The scale for the recycling efficiency in El Salvador indicates that the scaling of the output/input flux ratios is not appropriate, as no element could be recycled with an efficiency greater than 100%. The conclusions drawn from these diagrams are based on the relative arrangement of the elements.

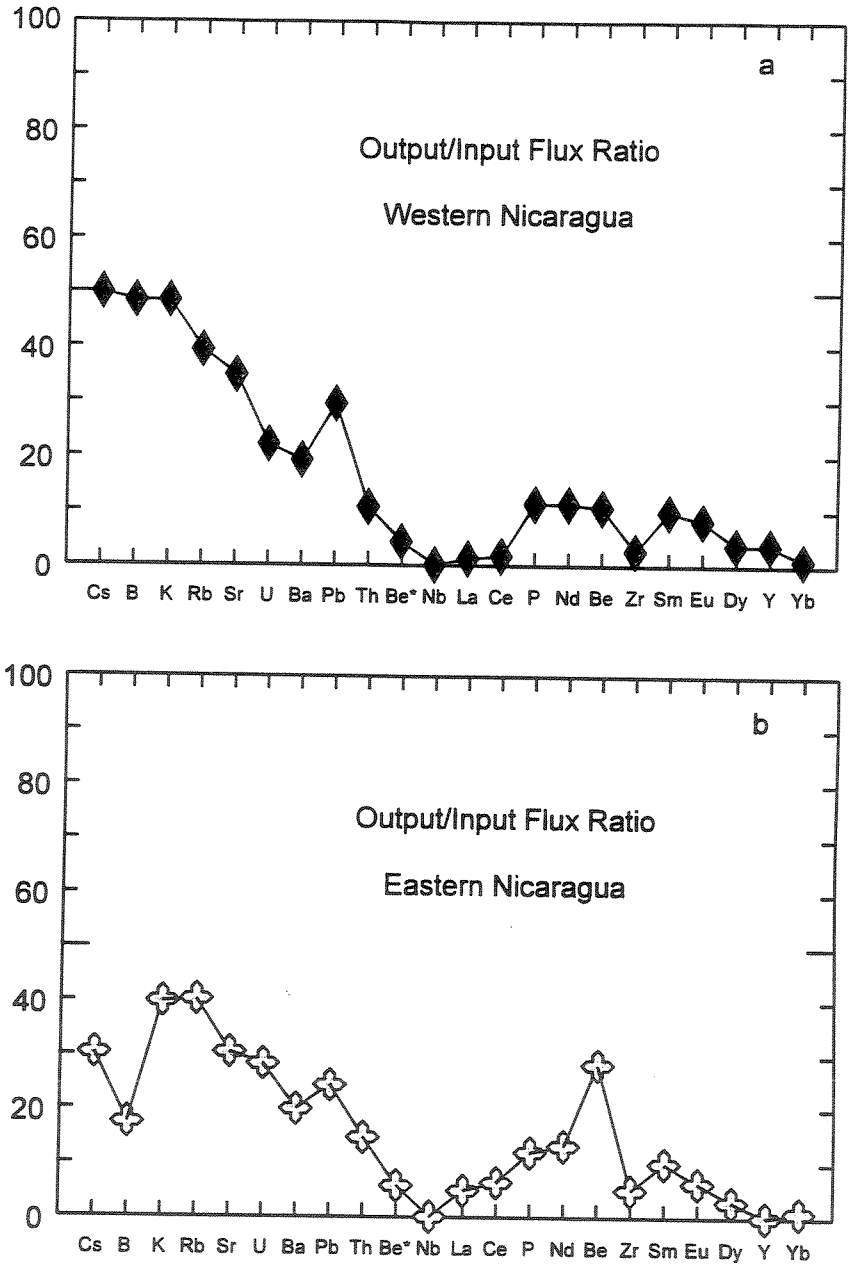


Figure 5-14. Similar efficiency recycling plots to those from figure 5-13; however, the results for this figure are calculated assuming that the thickness of the altered oceanic crust is 0.5 km. Western Nicaragua (a) and eastern Nicaragua (b). The most remarkable differences from the plots on figure 5-13 are the increased efficiencies for Pb, Th, and Be.

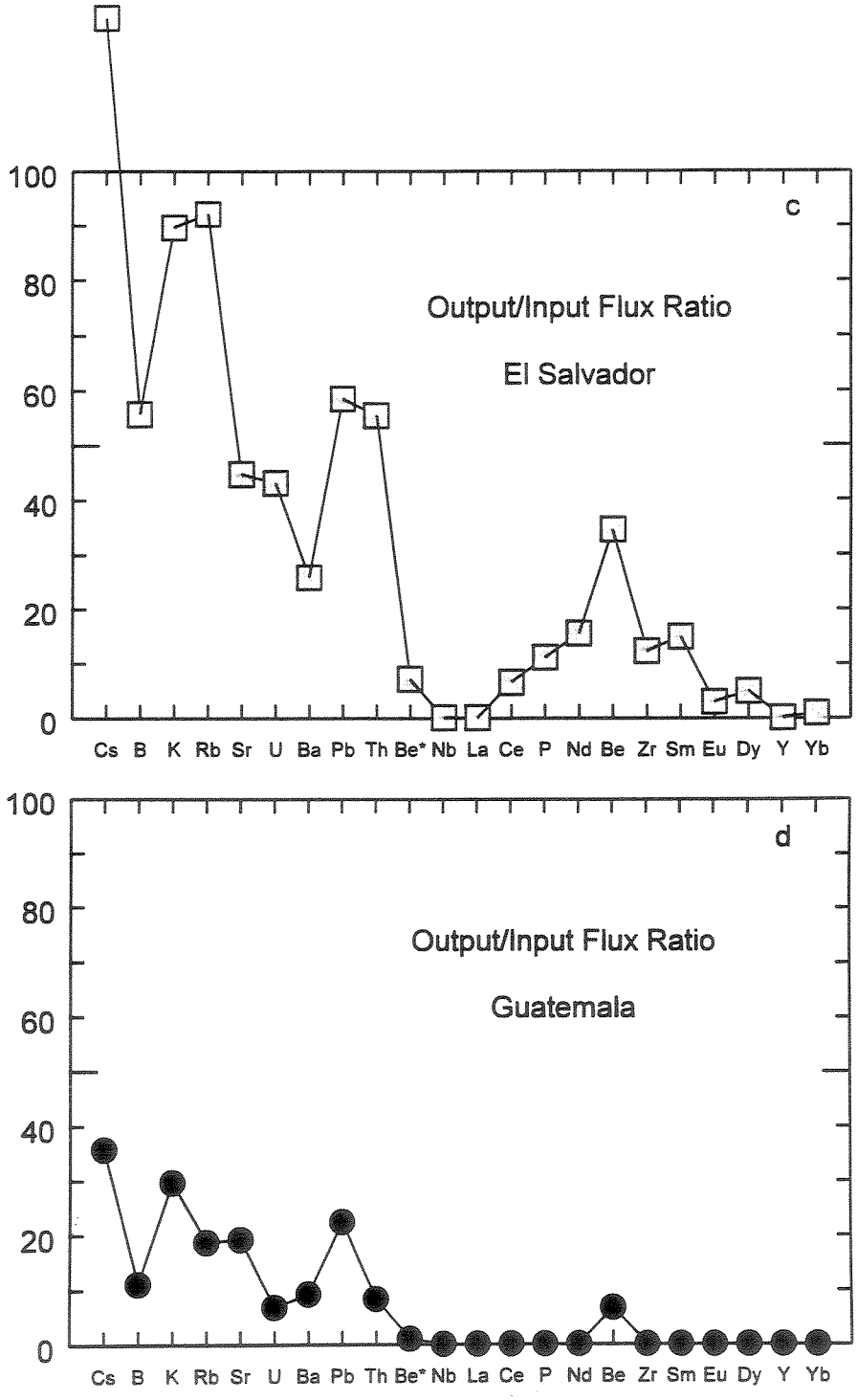


Figure 5-14 cont. Similar efficiency recycling plots to those from figure 5-13; however, the results for this figure are calculated assuming that the thickness of the altered oceanic crust is 0.5 km. El Salvador (c) and Guatemala (d). For the two segments of the arc, the efficiency with which Pb, Th and Be are recycled also increases relative to that observed in the models from figure 5-13.

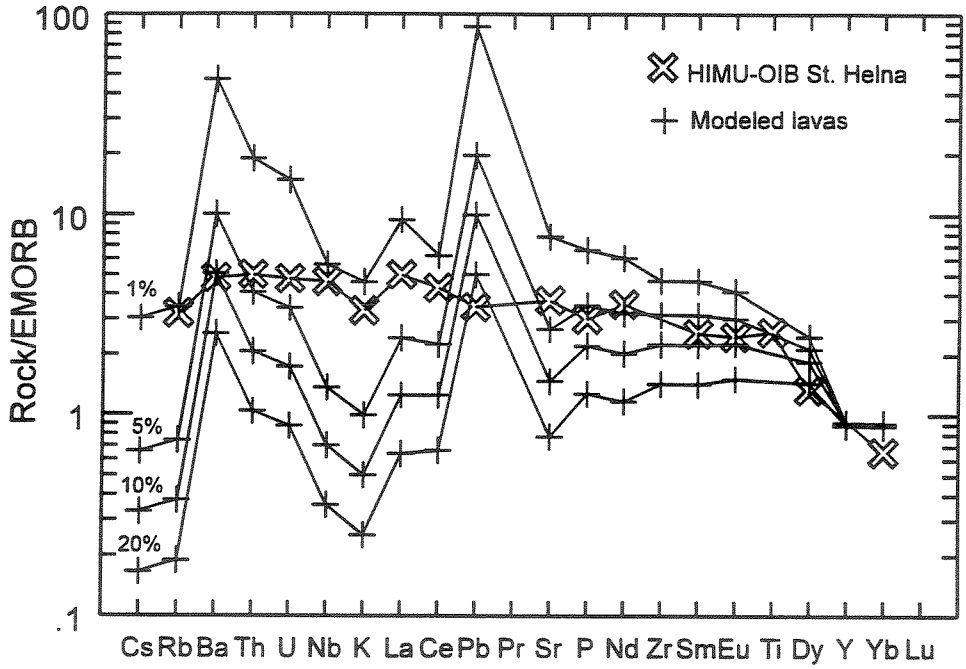


Figure 5-15. EMORB normalized diagram of HIMU-OIB from St. Helena and melts from modified N-MORB mantle. The N-MORB mantle was mixed with residual subducted slab (97:3). Based on the results of the output/input flux model for western Nicaragua, the mixed mantle melts have higher Ba and Pb content than OIB. Thus, the residual oceanic crust is not a likely modifier of the mantle to generate HIMU OIB lavas. The normalizing factors, as well as the N-MORB and St. Helena concentrations are from Sun & McDonough (1989).

VI. REFERENCES

Abratis M, Wörner G (1997) Subduction of the aseismic Cocos Ridge displaced magma sources beneath the Cordillera de Talamanca, Costa Rica. Seventh Annual Goldschmidt Conference, p 1.

Albrecht A, Hall GS, Herzog GF (1992) Determination of trace element concentrations in meteorites by Inductively Couple Plasma-Mass Spectrometry. J. Radioanal-Nucl. Chem 164(1):13-22.

Alt JC, Laverne C, Vanko DA, Tartarotti P, Teagle DAH, Bach W, Zuleger E, Erzinger J, Honnorez J, Pezard PA, Becker K, Salisbury MH, Wilkens RH (1996): Hydrothermal alteration of section of upper oceanic crust in the eastern equatorial pacific: a synthesis of results from site 504 (DSDP legs 69,70, and 83, and odd legs 111,137,140, and 148). Proceedings of the ODP, Scientific Results, 148,417-433.

Arculus RJ (1994) Aspects of magma genesis in arcs. Lithos 33:189-208.

Bach W, Erzinger J, Alt JC, Teagle DAH (1996): Chemistry of the lower sheeted dike complex, hole 504B (leg 148): influence of magmatic differentiation and hydrothermal alteration. Proceedings of the Ocean Drilling Program Scientific Results, 148, 39-55.

Bailey EH, Ragnarsdottir KV (1994) Uranium and thorium solubilities in subduction zone fluids. EPSL 124:119-129.

Balzer V, Plank T, Carr MJ (1996) Sediment recycling through time in Nicaragua. AGU Fall Meeting V21A-02.

Bebout GE, Ryan JG, Leeman WP (1992) B-Be systematics in subduction-related metamorphic rocks: Characterization of the subducted component. Geochim et Cosmochim Acta 57:2227-2237.

Bennett EA (1990) Niobium contents of Central American Lavas. Master Thesis, Rutgers University.

Berger WH.(1970): Biogenous deep-sea sediments: fractionation by deep-sea circulation. Geological Society of America Bulletin, 81, 1385-1402.

Bishop JKB (1988): The barite-opal- organic carbon association in oceanic particulate matter. Nature, 332, 341-343.

Brenan JM, Shaw HF, Ryerson FJ, Phinney, DL (1995) Mineral-aqueous fluid partitioning of trace elements at 900°C and 2.0 GPa: Constraints on the trace element chemistry of mantle and deep crustal fluids. Geochim et Cosmochim Acta 59:3332-3350.

Brown GC (1982) Calc-alkaline intrusive rocks: their diversity, evolution and relation to volcanic arcs in Andesites ed. Thorpe. John Wiley & Sons, pg. 437-461.

Carr MJ (1984) Symmetrical and segmented variation of physical and geochemical characteristics of the Central American volcanic front. J Volc and Geoth Res 20:231-252.

Carr MJ, Feigenson MD, Bennett EA (1990) Incompatible element and isotopic evidence for tectonic control of source mixing and melt extraction along the Central American Arc. Contrib Mineral Petrol 105:369-380.

Carr MJ, Stoiber RE (1977) Geologic setting of some destructive earthquakes in Central America. Geol Soc Am Bull 88:151-156.

Carr MJ, Stoiber RE (1990) Volcanism. In The Geology of North America, The Caribbean Region. Geol Soc Am H:375-391.

Cheatham MM, Sangrey WF, White WM (1993) Sources of error in external calibration ICP-MS analysis of geological samples and an improved non-linear drift correction procedure. Spectrochimica Acta 48B:E487-E506.

Condomines M, Sigmarsson O (1993) Why are so many arc magmas close to ^{238}U-^{230}Th radioactive equilibrium? Geochim et Cosmochim Acta 57:4491-4497.

Coulbourn WT, Hesse R, Azema J, Shiki T (1982) A summary of the sedimentology of DSDP leg 67 sites: the Middle America trench and slope off Guatemala - an active margin transect. Initial Reports DSDP 67: ed.: J. Aubouin et al 67:759-774.

Davies JH, Stevenson DJ (1992) Physical model of source region of subduction zone volcanics. J Geophys Res 97:2037-2070.

DeMets C, Gordon RG, Argus DF, Stein S (1990) Current plate motions. Geophys. J. Int. 101:425-478.

Domanik KJ, Holloway JR (1996) The stability and composition of phengitic muscovite and associated phases from 5.5 to 11 GPa: implications for deeply subducted sediments. Geochim Cosmochim Acta 60(21):4133-4150.

Edwards CM, Morris JD, Thirlwall MF (1993) Separating mantle from slab signatures in arc lavas using B/Be and radiogenic isotope systematics. Nature 362:530-533.

Elderfield H (1988) The oceanic chemistry of the rare earth elements. Phil. Trans. Roy. Soc. London 325A:105-126.

Ellam RM, Hawkesworth CJ (1988) Elemental and isotope variations in subduction related basalts: evidence for a three component model. Contrib Mineral Petrol 98:72-80.

Elliott T, Plank T, Zindler A, White W, Bourdon B (in press) Element transport from subducted slab to juvenile crust at the Mariana arc.

Farrell JW, Raffi I, Janecek TR, Murray DW, Levitan M, Dadey KA, Emeis KC, Lyle M, Flores JA, Hovan S (1995): Late Neogene sedimentation patterns in the eastern equatorial Pacific Ocean. Proceedings of ODP, Scientific Results, 138, 717-753.

Feigenson MD, Carr MJ (1985) Determination of major trace and rare-earth elements in rocks by DCP-AES. Chem Geol 51:19-27.

Feigenson MD, Carr MJ (1993) The source of Central American lavas: inferences from geochemical inverse modeling. Contrib Mineral Petrol 113:226-235.

Feigenson MD, Carr MJ, Maharaj S (in review): Lead isotopes in Central America: insights into sediment recycling and the nature of the mantle wedge. EPSL

Gill JB, Morris JD, Johnson RW (1993) Time scale for producing the geochemical signature of island arc magmas: U-Th-Po and Be-B systematics in recent Paupa New Guinea lavas. Geochim. et Cosmochim. Acta 57:4269-4283.

Govindaraju K (1994) Compilation of working values and sample description for 383 geostandards. Geostandards Newsletter, special issue 18:1-158.

Harrison WE, Hesse R, Gieskes JM (1982): Relationship between sedimentary facies and interstitial water chemistry of slope, trench, and Cocos Plate sites from the Middle America Trench transect, active margin off Guatemala, Deep Sea Drilling Project Leg 67. Initial Reports DSDP 67: ed.: J. Aubouin et al 67:603-613.

Hawkesworth SP, Turner SP, McDermott DW, Peate DW, Calsteren P (1997) U-Th isotopes in arc magmas: implications for element transfer from the subducted crust. Science 276:551-555.

Hawkesworth CJ, Gallagher K, Hergt JM, McDermott F (1994): Destructive plate margin magmatism: Geochemistry and melt generation. Lithos 33:169-188.

Hochstaedter AG, Ryan JG, Luhr JF, Hasenaka T (1996) On B/Be ratios in the Mexican Volcanic belt. Geochim Cosmochim Acta 60(4):613-628.

Hole MJ, Saunders AD, Marriner GF, Tarney J (1984): Subduction of pelagic sediments: implications for the origin of Ce-anomalous basalts from the Mariana Islands. J. Geol. Soc., 141, 453-472.

Holloway JR (1997) Generation of subduction zone magmas: experimental constraints. Seventh Annual Goldschmidt Conference, p 96.

Hoogewerff JA, Bergen MJ, Vroon PZ, Hertogen J, Wordel R, Sneyers A, Nasution A, Varekamp JC, Moens HL, Mouchel D (1997) U-series, Sr-Nd-Pb isotopes and trace-element systematics across an active island arc-continent collision zone: implications for element transfer at the slab-wedge interface. Geochim et Cosmochim Acta 61(5):1057-1072.

Ishikawa T, Nakamura E (1990) Suppression of boron volatilization from a hydrofluoric acid solution using a boron-mannitol complex. Anal. Chemistry 62:2612-2616.

Ishikawa T, Nakamura E (1992) Boron isotope geochemistry of the oceanic crust from DSDP/ODP Hole 504B. Geochim et Cosmochim Acta 56:1633-1639.

Ishikawa T, Nakamura E (1994) Origin of the slab component in arc lavas from across-arc variation of B and Pb isotopes. Nature 370:205-208.

Karl SM, Wandless GA, Karpoff AM (1992): Sedimentological and geochemical characteristics of leg 129 siliceous deposits. Proceedings of the Ocean Drilling Program Scientific Results, 129, 31-79.

Kenison Falkner K, Klinkahmmer GP, Ungerer CA, Christie DM (1995) Inductively coupled plasma mass spectrometry in geochemistry. Annu Rev Earth Planet Sci 23:409-429.

Kennett J (1987): Marine Geology, Prentice-Hall, Inc.

Kepezhinskas P, Defant MJ, Drummond MS (1996) Progressive enrichment of island arc mantle by melt-peridotite interaction inferred from Kamchatka xenoliths. Geochim et Cosmochim Acta 60:1217-1229.

Kepezhinskas P, McDermott F, Defant MJ, Hochstaedter A, Drummod MS, Hawkesworth C, Koloskov A, Maury RC, Bellon H (1997) Trace element and Sr-Nd-Pb isotopic constraints on a three-component model of Kamchatka arc petrogenesis. Geochim et Cosmochim Acta 61:577-600.

Keppler H, Wyllie PJ (1990) Role of fluids in transport and fractionation of uranium and thorium in magmatic processes. Nature 348:531-533.

Klinkhammer GP, Palmer MR (1991): Uranium in the oceans: Where it goes and why. Geochimica et Cosmochimica Acta, 55, 1799-1806.

Langmuir CH (1994) Water in the solid earth. Nature 369:704-705.

Ledbetter MT (1985) Tephrachronology of marine tephra adjacent to Central America. Geol Soc Am Bull 96:77-82

Leeman WP, Carr MJ, Morris JD (1994) Boron geochemistry of the Central American volcanic arc: constraints on the genesis of subduction-related magmas. Geochim et Cosmochim Acta 58:149-168

Lin PN. (1992): Trace element and isotopic characteristics of western Pacific pelagic sediments: Implications for the petrogenesis of Mariana Arc magmas. Geochimica et Cosmochimica Acta, 56, 1641-1654.

Longerich HP, Jenner GA, Fryer BJ, Jackson SE (1990) Inductively coupled plasma-mass spectrometric analysis of geological samples: A critical evaluation based on case studies. Chem Geol 83:105-118.

Lyle M, Dadey KA, Farrell J (1995): The late Miocene (11-8 MA) Eastern Pacific carbonate crash: evidence for reorganization of deep-water circulation by the closure of the Panama gateway. Proceedings of the Ocean Drilling Program Scientific Results, 138, 821-838.

Masuzawa T, Takada J, Matsushita R (1992): Trace- element geochemistry of sediments and sulfur isotope geochemistry of framboidal pyrite from site 795, leg 127, Japan Sea. Proceedings of the Ocean Drilling Program Scientific Results, 127/128, 705-717.

Maury RC, Defant MJ, Joron JL (1992) Metasomatism of the sub-arc mantle inferred from trace elements in Philippine xenoliths. Nature. 360:661-663.

McCullock MT, Gamble JA (1991) Geochemical and geodynamical constrains on subduction zone magmatism. EPSL 102:358-374.

McLennan SM, Taylor SR, McCulloch MT, Maynard JB (1990): Geochemical and Nd-Sr isotopic composition of deep-sea turbidites: Crustal evolution and plate tectonic associations. Geochimica et Cosmochimica Acta, 54, 2015-2047.

Miller DM, Langmuir CH, Goldstein SL, Franks AL (1992) The importance of Parental Magma Composition to Calc-Alkaline and Tholeiitic Evolution: Evidence from Umnak Island in the Aleutians. JGR 97:321-343.

Minai Y, Matsumoto R, Watanabe Y, Tominaga T (1992): Geochemistry of rare earths and other trace elements in sediments from sites 798 and 799, Japan Sea. Proceedings of the Ocean Drilling Program Scientific Results, 127/128, 719-737.

Mitchell JG, Terrell DJ (1985): Downhole variation of potassium, inter gas abundance and apparent K-Ar age in basalts from the Costa Rica rift, Hole 504B, leg 83, DSDP, in Initial Reports DSDP 83 eds RN Anderson et al. 305-312.

Moran AE, Sisson VB, Leeman, WP (1992) Boron depletion during progressive metamorphism: Implications for subduction processes. EPSL 111:331-349.

Morris JD (1991) Applications of cosmogenic ^{10}Be to problems in the earth sciences. Annu. Rev. EPS 19:313-350.

Morris JD, Leeman WP, Tera F (1990) The subducted component in island arc lavas: constraints from Be isotopes and B-Be systematics. Nature 344:31-36.

Murray RW, Buchholtz ten Brink MR, Gerlach D, Price Russ III G, Jones DL (1992) Interoceanic variation in the rare earth, major, and trace element depositional chemistry of chert: Perspectives gained from the DSDP and ODP record. Geochim et Cosmochim Acta 56: 1897-1913.

Nakamura E, Ishikawa T, Birck JL, Allègre CJ (1992) Precise boron isotopic analysis of natural rock samples using a boron-mannitol complex. Chem Geol 94:193-204.

Nelson BK (1995) Fluid flow in subduction zones: evidence from Nd- and Sr-isotope variations in metabasalts of the Franciscan complex, California. Contrib. Mineral Petrol. 119:247-262.

Noll PD, Newsom HE, Leeman WP, Ryan JG (1996) The role of hydrothermal fluids in the production of subduction zone magmas: Evidence from siderophile and chalcophile trace elements and boron. Geochim et Cosmochim Acta 60:587-612.

Othman DB, White WM, Patchett J (1989): The geochemistry of marine sediments, island arc magma genesis, and crust-mantle recycling. Earth and Planetary Science Letters, 94, 1-21.

Palmer MR (1991) Boron-isotope systematics of Halmahera arc (Indonesia) lavas: Evidence for involvement of the subducted slab. Geology 19:215-217.

Patino LC, Carr MJ, Feigenson MD (in press) Cross-arc geochemical variations in volcanic fields in Honduras, CA: progressive changes in source with distance from the volcanic front. Contrib Mineral Petrol

Peacock SM (1991) Numerical simulation of subduction zone pressure-temperature-time paths: constraints on fluid production and arc magmatism. Phil Trans R Soc Lond A335:341-353.

Pearce JA, Peate DW (1995) Tectonic implications of the composition of volcanic arc magmas. Annu. Rev. Earth Planet. Sci. 23:251-285.

Peterson LC, Murray DW, Ehrmann WU, Hempel P (1992): Cenozoic carbonate accumulation and compensation depth changes in the Indian Ocean. Scientific Drilling in the Indian Ocean Geophysical Monograph, 70, 311-333.

Plank T, Langmuir CH (1993) Tracing trace elements from sediment input to volcanic output at subduction zones. Nature 362:739-742.

Plank TA (1993) Mantle melting and crustal recycling in subduction zones. Ph.D. thesis, Columbia University.

Plank T, Ludden JN (1992): Geochemistry of sediments in the Argo abyssal plain at site765: a continental margin reference section for sediment recycling in subduction zones. Proceedings of the Ocean Drilling Program Scientific Results, 123, 167-189.

Plank T, Johnson M (1997) Experimental study of trace-element partitioning in fluids and melts generated during sediment subduction. Seventh Annual Goldschmidt Conference, p 164.

Plank T, Langmuir CH (1988): An evaluation of the global variations in the major element chemistry of arc basalt. Earth Planet. Sci. Lett. 90:349-370.

Price RC, McCulloch MT, Smith IEM, Stewart RB (1992) Pb-Nd-Sr isotopic compositions and trace element characteristics of young volcanic rocks from Egmont Volcano and comparisons with basalts and andesites from the Taupo Volcanic Zone, New Zealand. Geochim et Cosmochim Acta 56:941-953.

Protti M, Guendel F, McNally K (1995) Correlation between the age of the subducting Cocos Plate and the geometry of the Wadati-Benioff zone under Nicaragua and Costa Rica, in Mann P., ed. Geologic and Tectonic development of the Caribbean Plate boundary in southern Central America. Geological Society of America special paper 295:309-326.

Puchelt (1972) Barium in Wedephol KH ed. Handbook of geochemistry. New York-Heidelberg (Springer-Verlag) Vol II-3.

Reagan MK, Morris JD, Herrstrom EA, Murrell MT (1994) Uranium series and beryllium isotope evidence for an extended history of subduction. Geochim et Cosmochim Acta 58:4199-4212.

Ryan JG, Langmuir CH (1993) The systematics of boron abundances in young volcanic rocks. Geochim et Cosmochim Acta 57:1489-1498.

Ryan JG, Morris J, Tera F, Leeman WP, Tsvetkov A (1995) Cross-Arc geochemical variations in Kurile arc as a function of slab depth. Science 270:625-627.

Shaw DM (1970) Trace element fractionation during anatexis. Geochim Cosmochim Acta 34:237-243.

Schiano P, Clocchiatti R, Shimizu N, Maury RC, Jochum KP, Hofmann AW (1995): Hydrous, silica-rich melts in the sub-arc mantle and their relationship with erupted arc lavas. Nature 377, 595-600.

Schmidt MW. (1995): Lawsonite: Upper pressure stability and formation of higher density hydrous phases. American Mineralogist 80, 1286-1292.

Shibata T, Nakamura E (1997) Across-arc variations of isotope and trace element compositions from Quaternary basaltic volcanic rocks in northeastern Japan: implications for interaction between subducted slab and mantle wedge. JGR 102:8051-8064.

Shipboard Scientific Party (1982) Site 495: Cocos Plate - Middle America trench outer slop. Initial Reports DSDP 67:79-142.

Smith HJ, Spivack AJ, Staudigel H, Hart SR (1995) The boron isotopic composition of altered oceanic crust. Chem Geol 126:119-135.

Staudigel H, Davies GR, Hart SR, Marchant KM, Smith BM (1995): Large scale isotopic Sr, Nd and O isotopic anatomy of altered oceanic crust: DSDP/ODP sites 417/418. EPSL, 130, 169-185.

Stern CR, Wyllie PJ (1973): Melting relations of basalt-andesite-rhyolite-H_2O and a pelagic red clay at 30 kb. Contrib. Mineral and Petrol. 42:313-323.

Stolper E, Newman S (1994) The role of water in the petrogenesis of Mariana trough magmas. EPSL 121:293-325.

Stolz AJ, Jochum KP, Spettel B, Hofmann AW(1996): Fluid- and melt related enrichment in the subarc mantle: Evidence from Nb/Ta variations in island-arc basalts. Geology 24(7):587-590.

Sun S, McDonough WF (1989): Chemical and isotopic systematics of oceanic basalts: implications for mantle composition and processes, in Magmatism in the Ocean Basins eds: AD Saunders and MJ Norroy, Geological Society Special Publications 42:313-345.

Tatsumi Y, Hamilton DL, Nesbitt RW (1986) Chemical characteristics of fluid phase released from a subducted lithosphere and origin of arc magmas:

Evidence from high-pressure experiments and natural rocks. J Vol and Geoth Res 29:293-309.

Taylor RS, McLennan SM (1985) The Continental Crust: its composition and evolution. An examination of the geochemical record preserved in sedimentary rocks. Blackwell Scientific Publications, p. 28.

Tera, F; Brown, L; Morris, J; Sacks, SI; Klein, J; Middleton, R (1986): Sediment incorporation in island arc magmas: Inferences from Be-10. Geochim Cosmochim Acta 50:636-660.

Thirlwall MF, Graham AM, Arculus RJ, Harmon RS, Macpherson CG (1996) Resolution of the effects of crustal assimilation, sediment subduction, and fluid transport in island arc magmas: Pb-Sr-Nd-O isotope geochemistry of Grenada, Lesser Antilles. Geochim Cosmochim Acta 60(23):4785-4810.

Toyoda, K; Nakamura, Y.; Masuda, A (1990): Rare earth elements of Pacific pelagic sediments. Geochimica et Cosmochimica Acta, 54, 1093-1103.

von Breymann, MT.; Emeis, KC; Camerlenghi, A (1990): Geochemistry of sediments from the Peru upwelling area: results from sites 680, 682, 685, and 688. Proceedings of the Ocean Drilling Program Scientific Results, 112, 491-503.

von Huene, R; Shipboard Scientific Party (1982): Site 495: Cocos Plate - Middle America trench outer slope. Initial Report. DSDP 67, 79-141.

Walker JA, Carr MJ, Patino LC, Johnson CM, Feigenson MD, Ward RL (1995) Abrupt change in magma generation processes across the Central American arc in southeastern Guatemala: flux-dominated melting near the base of the wedge to decompression melting near the top of the wedge. Contrib. Mineral. Petrol. 120:378-390.

Weaver BL (1991) Trace element evidence for the origin of ocean-island basalts. Geology 19:123-126.

Williams H, McBirney AR (1969) Volcanic history of Honduras. University of California press, 101 p.

Woodhead JD (1989) Geochemistry of the Mariana arc (western Pacific): Source composition and processes. Chem Geol 76:1-24.

Woodhead JD, Johnson RW (1993) Isotopic and trace-element profiles across the New Britain island arc, Paupa New Guinea. Contrib Mineral Petrol 113: 479-491.

Wright JD, Miller KG, Fairbanks RG (1992) Early and middle Miocene stable isotopes: implications for deepwater circulation and climate. Paleoceanography 7:357-389.

Yogodzinski GM, Kay RW, Volynets ON, Koloskov AV, Kay SM (1995) Magnesian andesite in the western Aleutian Komandorsky region: Implications for slab melting and processes in the mantle wedge. GSA Bulletin 107:505-519.

APPENDIX - ANALYSES OF BORON BY DCP-AES

A. Uses of Boron in arc geochemistry

Boron has been used in geochemical studies of arc related lavas as a tracer of the input from the subducting slab. In general, arc related lavas have higher boron concentrations than basalts from other tectonic settings (Ryan and Langmuir, 1993). The authors report that the boron content of MORB and OIB ranges from 1 to 5 ppm. For Central American lavas, Leeman et al. (1994) report that boron ranges from 2.1 (GR-5) to 46 (Cos9a). The enrichment of boron in arc lavas is caused by input from the subducting slab.

Due to the interaction of the oceanic crust with sea water, boron concentrations of altered oceanic crust and marine sediments are higher than the concentrations in pristine, mantle derived material. Moran et al. (1992) show that altered oceanic crust has a highly variable boron content, 0.5 to 200 ppm. In Site 504B, boron content correlates with depth, as well as the type of alteration. Therefore, the abundance of B in altered oceanic crust depends on the type of alteration (Ishikawa and Nakamura, 1992). The basaltic oceanic crust that was affected by low temperature alteration has higher boron concentrations than the deeper, hydrothermally altered oceanic crust. Furthermore, the behavior of boron in altered oceanic crust is similar to the behavior of other elements like Cs, K, and ^{18}O (Palmer, 1991 and Smith et al., 1995). The other source of boron in subducting slabs is the sediment pile deposited on the oceanic crust. Moran et al. (1992) report that pelagic clays and pelagic carbonates have high boron concentrations of ~230 ppm and ~55 ppm, respectively.

The isotopic composition of boron in altered oceanic crust and marine sediments is different; thus the isotopic composition of boron can be used to distinguish the source of this element in arc related lavas (Ishikawa and Nakamura, 1994). The altered oceanic crust is enriched in ^{11}B, with a $\delta^{11}B$ ranging from +2 to +9‰, whereas pelagic sediments have a $\delta^{11}B$ between -12 and -6‰. Using the differences in the B isotopic composition,

Ishikawa and Nakamura (1994) conclude that the slab component for the lavas from the Izu arc is 99 wt.% derived from the altered oceanic crust and 1 wt.% from the sediments.

In addition to using boron to trace the slab input, boron has also being used to infer the process that transfers material from the subducting slab to the mantle wedge. High concentrations of boron have been found in veins of metamorphic rocks associated with old subduction zones (Bebout et al., 1992). Based on this observation the authors conclude that boron was mobilized by the fluid that generated the veins. Thus, boron has been used as tracer of the transfer of hydrous fluids from the slab to the mantle wedge during arc magmatism (e.g. Morris et al., 1990; Ryan and Langmuir, 1993; Ryan et al., 1995).

B. Sample preparation

There are three common techniques for measuring B in arc lavas: prompt-gamma neutron activation, alkali fusion, and acid digestion using mannitol (e.g. Leeman et al., 1994; Ryan and Langmuir, 1993; and Ishikawa and Nakamura, 1994). For a study of lavas from Central America, Leeman et al. (1994) use nondestructive prompt-gamma neutron activation to determine boron concentrations. The authors report the accuracy to be 5% for samples with concentrations >10 ppm and 20% when the concentration is ~ 2 ppm. I did not use this technique because one of the objectives of my work was to develop a procedure to analyze boron in-house, and we do not have ready access to a prompt-gamma neutron activation reactor.

Ryan and Langmuir (1993) have successfully analyzed boron using atomic emission spectrometers, like the DCP-AES available at the Geology department of RU. They (1993) dissolved igneous rocks from different tectonic settings using various alkali fusions (Na_2CO_3 and K_2CO_3 or Na_2CO_3 alone). The authors report a precision of 5% for > 10 ppm, 10% for 1-10 ppm and 20-25% for < 1 ppm. This statistics are better than those reported by Leeman et al. (1994) for prompt-gamma neutron activation. However,

the use of fluxes to prepare the samples results in blanks that have high boron contents. For example, as much as 500 ng of boron can be added to the sample by Na_2CO_3.

One of the major problems in preparing geological samples for boron analyses is that the commonly used acid digestions often result in loss of boron due to its volatility. Ishikawa and Nakamura (1990) report that boron in HF and HCl forms gaseous boron fluoride and/or boron chloride with a very low boiling temperature. However, Ishikawa and Nakamura (1990) demonstrate that the volatilization of boron during HF-HCl digestions is suppressed in the presence of mannitol, as long as the mannitol/boron mole ratio is more than one. Moreover, mannitol does not incorporate large amounts of boron as the alkali fluxes do, and so does not appreciably increase the blank. Nakamura et al. (1992) report blanks of 4 ng B using mannitol.

In an attempt to analyze boron at the Department of Geological Sciences, Rutgers University, two sample preparations were tested: slurries and acid digestions using mannitol. The two techniques will be discussed in detailed in the following sections.

1. Slurry

One hundred milligrams of powdered sample were soaked with 10 ml of a 1% triton solution, used as a dispersing agent to avoid the agglutination of the powder particles. The samples were shaken before the peristaltic pump took the solution to the nebulizer. However, it was observed that the slurry did not have a homogenous distribution of solid particles in the pump tubing. In order to increase the homogeneity of the solution going into the nebulizer, the bottle that contains the slurry solution was placed in an ultrasonic bath as the solution was being taken by the peristaltic pump. The purpose of the ultrasonic bath was to maintain a homogenous slurry solution. Before using the ultrasonic bath, a magnetic strirrer was used, but the distribution of the solid particles was not uniform in the solution and a lot of turbulence was created in the center of the beaker.

One of the major problems found with analyzing slurries was contamination between samples. It was difficult to clean the intake system (peristaltic pump tubing)

because residual particles would stick in the tubing. The poor cleaning between samples created significant contamination problems and erratic results. Another common problem when analyzing slurries was the clogging of the nebulizer. The diameter of the orifice through which the sample enters the nebulizer is very small, and this small hole was easily obstructed by the solid particles of the slurry.

The results from the experiments that used a slurry solution were of poor accuracy and poor precision (Table A-1). New powders of some of the analyzed samples were processed, assuming that finer grain size would create more homogenous slurries and improve the results. However, the results were not conclusive. The results for the slurry experiments listed in table A1 were obtained using standard addition calibration.

2. Acid digestion with mannitol

Retaining the boron in the sample during acid digestion using mannitol was a major improvement on sample preparation, but it is not a technique free of problems. Ishikawa and Nakamura (1990) and Nakamura et al. (1992) indicate that it is important to separate the boron from major cations that can interfere in its analysis. In order to clean the sample the authors suggest the use of cation and ion exchange chromatography. The interference effects are specially problematic when analyzing boron by atomic emission spectrometry. There is a direct spectral interference between iron, a major element in geological material, and boron at a wavelength of 2497.73 Å. A solution that contains 500 ppm of Fe gave 92 counts above background on the same wavelength that a 0.14 ppm of B solution gave only 69 counts above background. Thus, it would be very difficult to determine low concentrations of boron in the presence of iron.

Therefore, the solutions obtained from the acid digestion were processed through cation exchange columns to separate boron from iron. The boron-mannitol complex behaves like an anion (Ishikawa and Nakamura, 1990). Thus, it is not retained in the cation exchange column if water is used as an elutant, whereas iron and other cations will be retained. The resin used was Bio-Rad analytical grade cation exchange resin AG®

50W-X8, 200-400 mesh in hydrogen form. Before loading the resin into the polypropylene columns (1.5 x 12 cm), the resin was rinsed with H_2O several times to clean it and to let it expand. Initially a resin volume of 15 ml was used, but significant Fe was detected in the eluted boron solutions. Therefore, 20 ml of resin were used and the iron concentrations were lowered to the point that only a small signal was detected at the wavelength of interest.

a. Sample Preparation using mannitol

The following sample preparation is an adaptation from Nakamura et al. (1992) and Tera (personal communication). Before describing the sample preparation, it is important to emphasize that all glassware should be avoided during the sample preparation. Most glassware is made of borate silicate glass, and is thus a major source of boron contamination.

1. Weigh 1 gm of powder sample into a 23 ml Savillex beaker. Make sure that the powder has not been contaminated with $LiBO_2$. If you are not sure that the powder is free of boron contamination, prepare a new powder. Tungsten carbide mills can be used to prepare the powders. If there is powder prepared from leached rock chips, this powder can be used to prepare the sample for boron analysis. Ryan (personal communication) indicates that using powders from leached samples should not be a problem because most of the boron is structurally bound in silicates.

2. Add 1 ml of 5% mannitol solution, 2 ml of 6N HCl, 2 ml H_2O. Shake the sample gently to disperse the sample.

3. Add four (4) milliliters of hydrofluoric acid (48-51%) very slowly (add 1 ml at a time, letting the sample sit for one minute before adding the next milliliter) to avoid volatilization of boron when the hydrofluoric acid reacts with the silicates. After all the acid is added to the sample cap the beaker tightly.

4. Place the beaker in an ultrasonic bath until no particles are observed (it could take up to 4 hours). This step is very important because all of the particles of the sample must be in contact with the acids.

5. After no particles are observed, place the beaker on a hot plate overnight at a temperature no greater than 70°C (the lowest setting of the hot plate). Keep the beaker tightly capped.

6. Take the beaker off the hot plate, and let it cool to room temperature.

7. Transfer the contents of the beaker to a 12 ml Nalgene High-Speed centrifuge tube (keep the beaker to be rinsed in step 9). Centrifuge for 15 minutes at 8500 rpm. Nakamura et al. (1992) show that the precipitates from this step, fluorides, have very little boron. The authors indicate that there is a 99.3% recovery of boron in the supernatant.

8. Transfer the supernatant to a clean 23 ml Savillex beaker, a beaker that containing 0.2 ml 5% mannitol.

9. Rinse the dirty beaker (the one used through step 7) with 1 ml HF, and then transfer this solution to the centrifuge tube that contains the fluoride residue from the previous centrifuge step. Rinse the residue well by shaking the tube. Centrifuge as before, and then transfer the new supernatant to the beaker from step 8. Repeat this step.

10. Place the beaker that contains the supernatant, uncapped, on the hot plate and evaporate the solution. The temperature should remain lower than 70°C to avoid the volatilization of boron. Do not let the solution dry completely, and take the sample off the hot plate when the bottom is still a little wet.

11. Add 1 ml 6N HCl and evaporate without drying completely ($T < 70°C$). Again taking the sample off the hot plate when a little acid remains. The beaker should be uncapped to allow the acid to evaporate.

12. Add 1 ml 0.1N HCl, tightly cap the beaker and place it on the hot plate for two hours ($T < 70°C$). After two hours take the capped beaker off the hot plate and let it cool down.

b. Cation Exchange Chromatography

The resin in the cation exchange columns is cleaned and preconditioned before loading the samples. To clean a column after a sample has been processed through, elute 50 ml of 4.5 N HCl through the column. After cleaning, the column is preconditioned by eluting 30 ml of H_2O.

13. Transfer the solution of digested sample (from step 12) to a small centrifuge tube (set aside the beakers to be cleaned in step 15), and centrifuge for 15 minutes.

14. Load supernatant into the preconditioned cation exchange column.

15. Rinse the beakers from step 13 with 0.5 ml of H_2O, add rinse to the residue from the centrifuge from step 13, and centrifuge again for 15 minutes.

16. Add the supernatant to the column.

17. Repeat steps 15 and 16.

18. Elute 5 ml of H_2O through the columns. Add 1 ml at a time, and wait for it to go through.

19. Collect the next 5 ml of H_2O. Again add 1 ml at a time. This stock solution contains the boron with a dilution factor of 5 (1 gm in 5 ml). Figure A-1 shows the elution curve for boron.

To run in the DCP-AES, the samples should be diluted depending on their boron content. Samples that have less than 5 ppm of boron can be run with a dilution factor of 10, and those that have more than 5 ppm should be diluted by a factor of 20.

One of the greatest difficulties when analyzing boron is to avoid contamination. There are two major places were extra boron can be added to the sample. The first possibility is if the sample was powdered earlier and this powder has been used to prepare samples for major element analysis using lithium metaborate. There is a large probability that the powdered sample could have been contaminated with the lithium metaborate powder. The other place where the sample can be contaminated is when powdering the sample. Extra care must be taken so that there is no contamination between samples and

that no borate glass contaminates the sample. This second contamination is more difficult to avoid, but whenever the results are suspicious, a new powder of the sample should be prepared.

Besides avoiding contamination before and during sample preparation, the analyst should be sure that the intake system for the DCP-AES (the nebulizer, the mixing chamber, waste collector, and other parts of the instrument that are in contact with the sample) are as clean as possible. To minimize the contamination during analysis, separate tubing for the peristaltic pump was used. The other parts of the instrument that are in contact with the sample were acid-cleaned by soaking in warm (70°C) 10% HNO_3 overnight. Other parts were soaked in water overnight. If samples prepared with $LiBO_2$ were run prior to the boron run, water samples should be checked for low boron contents. If water gives a high boron signal, the cleaning procedure should be repeated.

c. DCP-AES Settings

The DCP-AES (direct current plasma - atomic emission spectrometer) was warmed up for at least 20 minutes. After the warm up period the peak for 10 ppm B solution was found at a wavelength of 2497.73 Å. Usually the 10 ppm B solution produces at least 1500 counts when the time was set at 15 and the voltage at 5. The position of the peak, as well as the background levels, were checked by doing background profiles of water and a standard solution that contains at least 0.3 ppm B. If the back ground levels were high, the nebulizer, mixing chamber and other parts needed were further cleaned. If the peak was not well centered, the 10 ppm B solution was introduced again and the correct peak position was found.

One of the most persistent problems that I had when running boron was the poor accuracy of samples that had low concentrations of boron (<5 ppm). After doing several background profiles of the samples (Figure A-2), it was concluded that the problem was caused by high background levels, likely due to matrix effects. Therefore, a background correction was established and the low B samples were run successfully.

Based on the background profiles in figure A-2, the spectral window where the background should be measured was determined to be LO2 and HI2. To set the window move the thumbwheels labeled LOW WAVELENGTH and HIGH WAVELENGTH in the front of the DBC panel to 2 for each wavelength. Then select the channel (channel 1) on the multichannel chassis. Turn on the BCKGRD switch. Select the type of background correction using the keyboard on the control panel, and then press SET BCKGRD push-button. For the boron analyses, the selected background corrections was # 4. This type of correction is based on the high and low wavelength absolute corrections, i.e. it is a weighted average correction.

After setting the instrument for background corrections, the instrument was auto ranged as it is done for regular runs. The selected time of integration was 9 seconds, and the readings were repeated 2 times. Usually, the integrations are last 5 seconds and are repeated 3 times. However, when doing background corrected data acquisition, longer times are more adequate. The samples were run only 2 times because of volume limitations.

d. Results

The boron concentrations determined so far are listed in table A-2; also listed are the boron concentrations for some of the same samples obtained by Leeman et al. (1994). The new concentrations were calculated using standard solutions. The new boron analyses of most of the samples agree, within the published error, with the values of Leeman et al. (1994). There is only one sample, PP9, that is consistently higher than the value obtained by Leeman et al. (1994). This sample has been run several times and new powders have been prepared. But the high values persist.

Four samples from Honduras were analyzed to determine their boron concentrations. The results show that boron, as other subducting slab tracers, decreases with increasing distance from the trench. Figure A-3 shows the positive correlation between Ba/La and B/La in back arc lavas from Honduras. Ba/La has been used to infer

slab input in front and back arc lavas in Central America (Carr et al., 1990 and Patino et al., in press). The positive correlation observed in figure A-3 agrees with previous conclusions that indicate that a slab component is present in the generation of lavas from Zacate Grande. Furthermore, the relatively low B/La and high Ba/La ratios in the sample from Tegucigalpa implies that there is a subducted component present in the generation of this lava as well, but most likely the composition of the slab component has changed with increasing distance from the front. This conclusion agrees other across arc studies (e.g. Ryan et al., 1995).

The new boron values for the samples that had not been run previously follow the general trends described by the rest of the Central American arc samples (Fig. A-4). The boron analysis for Te-114, from western Nicaragua, confirms previous conclusions for this segment of the arc. In chapters 4 and 5, it was concluded that the lavas from western Nicaragua had unusually higher fluxes from the subducting slab. The B/La ratio for Te-114 is higher than any other arc sample, except those from western Nicaragua (Fig. A-4).

Table A-1

	Slurry with 1% triton Boron		Leeman boron *
	Coarse	Fine	
PP8	2.5	12.52	2.4
NE202	3.96	8.56	2.9
IZ108	6.2	23.14	18.8
IZ112	3.38	15.9	17.1
TE1	11.66	18.85	36
COS9A	38.21	42	46

* data from Leeman et al. (1994)

Table A-1. Boron results when using slurry solutions

Table A-2

	RU boron[1]	Leeman boron[2]	Consen. boron[3]
E1	8.86	8	
IZ108	19.4	18.8	
ZA2	11.34		
ZA7	12.56		
COS9A	47	46	
TE114	17.72		
PP8	2.3	2.4	
PP9	5.86	2.7	
GUC303	2.91	2.4	
HONC118	9.2		
YO10	3.5		
RGM-1	31.8		28
BIR-1	0.51		0.33

[1] Acid digestion with mannitol
[2] Data from Leeman et al. (1994)
[3] Data from Govidaraju (1994)

Table A-2. Results of boron analyses when using acid digestion and mannitol to prepare the solutions.

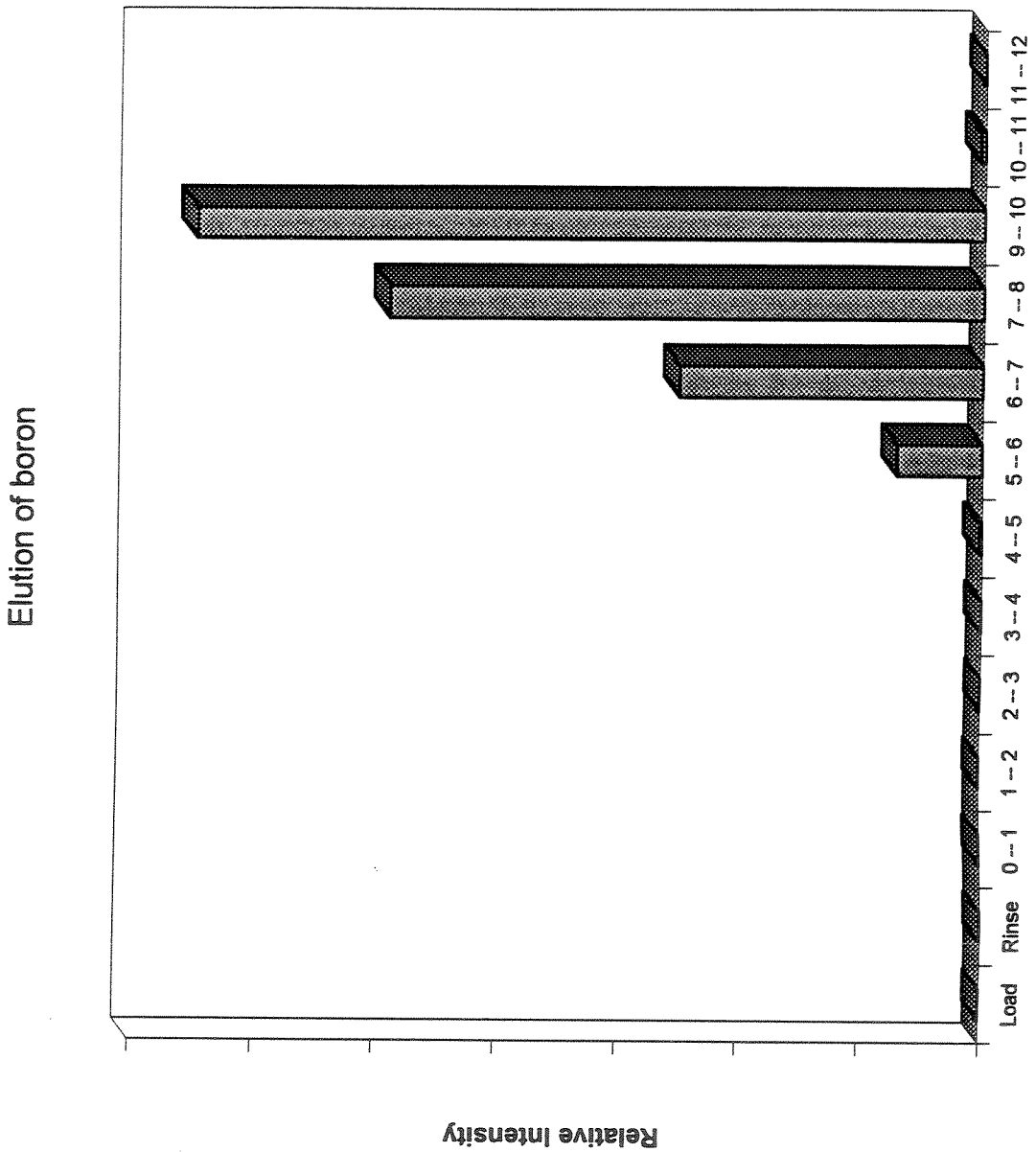


Figure A-1. Elution curve for B from a column that has 20 ml of resin. See text for details on the type of resin. The collection of B started after the initial 5 ml of H_2O were eluted. Most of the boron comes out after 9 ml of H_2O have been added, and then the boron content of the elutant decreases to background levels.

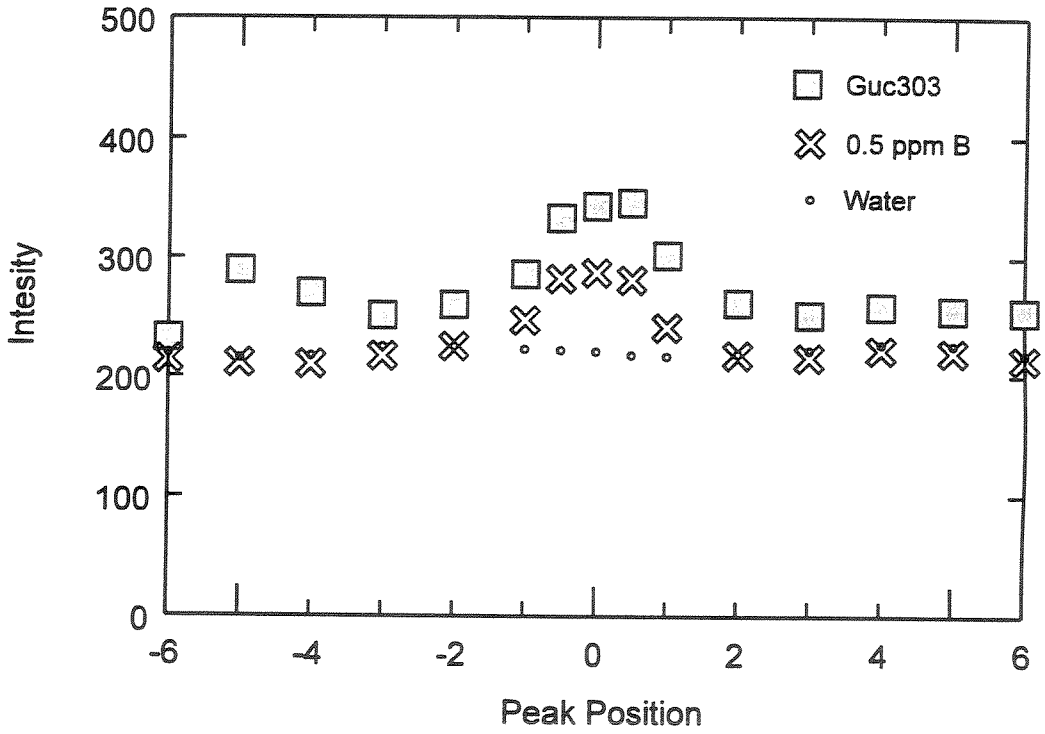


Figure A-2. Background profile for boron in the DCP-AES. The 0.5 ppm B standard solution has the same background as water. However, the rock solution (Guc303) has higher background than the water. Thus, the need to collect background corrected data when analyzing B in the DCP.

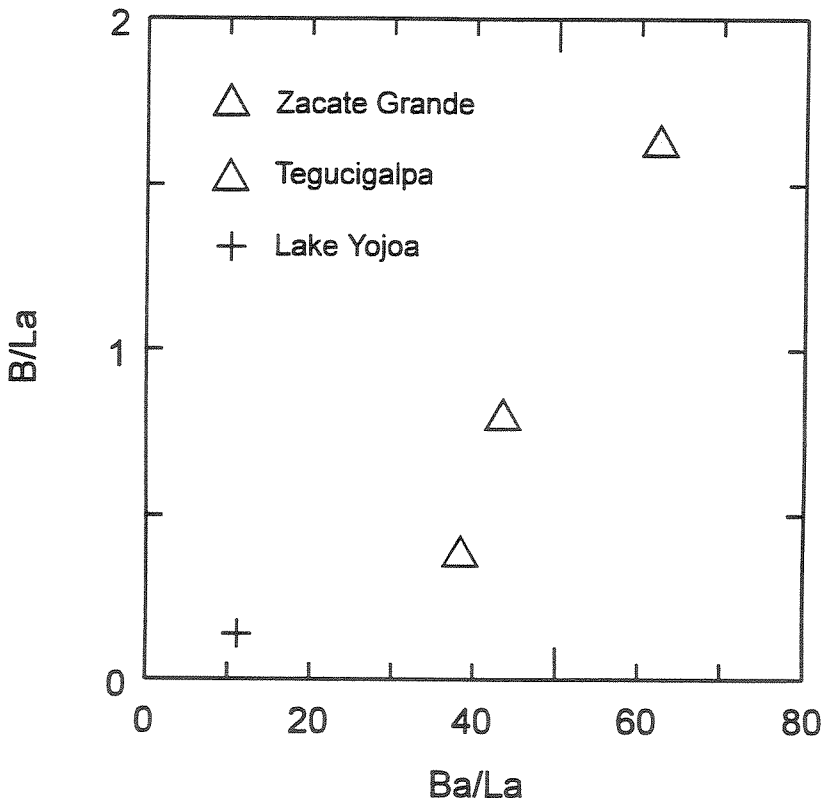


Figure A-3. Ba/La vs. B/La for samples from back arc volcanic fields in Honduras. B/La decreases, as Ba/La, with increasing distance from the trench.

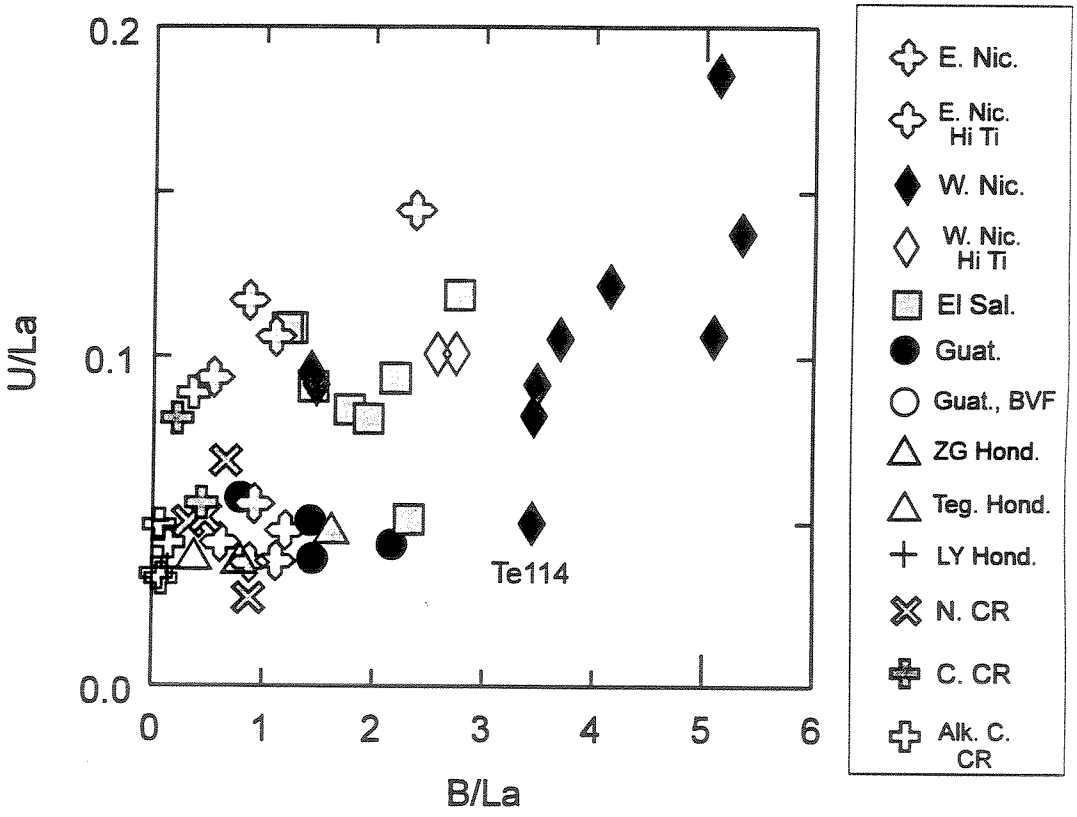


Figure A-4. B/La vs. U/La for lavas from Central America. Most of the boron concentrations are from Leeman et al. (1994). The new boron data agrees well with previous results. The majority of samples from western Nicaragua are characterized by B/La > 3, whereas the lavas from the rest of the arc have lower ratios.

VITA

LINA C. PATINO

EDUCATION

Ph.D., Geological Sciences, October 1997
Rutgers University, New Brunswick, NJ.
Dissertation: "Geochemical Characterization of Central American Subduction Zone System: Slab input, Output from the Volcanoes, and Slab-Mantle Interactions"

M.S., Geological Sciences, May 1993
Rutgers University, New Brunswick, NJ.
Thesis: "Geochemical traverse across Honduras."

B.S., Geological Sciences, January 1990
Rutgers University, Cook College, New Brunswick, NJ.
Honors Project: "Rare Earth Element Study of South-East Guatemala Basalts."

County College of Morris, Randolph, NJ 07869 1986-1987.

Universidad EAFIT, Medellín, Colombia 1984-1985.

EXPERIENCE

-*Geochemical Analyst,* 1989 - 1997
Department of Geological Sciences, Rutgers University, New Brunswick, NJ

- Preparation of samples for major, trace element and isotope analyses using different techniques such as fluxes, acid attack, and ion exchange chromatography.
- Implementation of sample preparation for ^{10}Be and Boron analyses.
- Operation of DCP-AES and ICP-MS.
- Interpretation and publication of analyzed data.
- Assist undergraduate and graduate students and visitors in sample preparation and analyses.

-*Assistant to the Director of the Center for International Faculty & Student Services,* 1991 - 1996
Rutgers University, New Brunswick, NJ

- Liaison between student organizations and the staff of the center.
- Assist in the organization of orientation for new international students.
- Volunteer Coordinator during orientation for new international students.
- Organize multicultural discussion/support groups.
- Plan extracurricular activities to enhance participation of the international community

-*Teaching Assistant*, Jan. 1991 - present.
Geological Sciences Dept., Rutgers University, New Brunswick, NJ.
- Lab instructor for: Introductory Geology
  Mineralogy
  Metamorphic and Igneous Petrology
- Responsible for the lab preparation, presentation and assistance to undergraduate students at the introductory and advance levels.

PUBLICATIONS

"Geochemical traverse across Honduras."
Contributions of Mineral Petrology, in press, 1996 by L.C. Patino, M.J. Carr, M.D. Feigenson.

"Constraints on partial melting imposed by REE variations in Mauna Kea basalts."
Journal Geophysical Research, in press, by M.D. Feigenson, L.C. Patino, M.J. Carr.

"Abrupt change in magma generation processes across the Central American arc in southeastern Guatemala: flux-dominated melting near the base of the wedge to decompression melting near the top of the wedge."
Contributions to Mineral Petrology 120:378-390, 1995 by J.A. Walker, M.J. Carr, L.C. Patino, C.M. Johnson, M.D. Feigenson, R.L. Ward.